U.S. Department
of Transportation
**National Highway
Traffic Safety
Administration**

DOT HS 807 956
Final Report

June 1992

Vehicle Dynamic Stability And Rollover

This report contains an extensive amount of statistical analysis carried out by traditional multiple linear regression methods. These methods are not as powerful as newer logistic regression methods which have recently been used within the Department of Transportation for a significant amount of rollover analysis.

Technical Report Documentation Page

1. Report No.	2. Government Accession No.	3. Recipient's Catalog No.
DOT HS 807 956		

4. Title and Subtitle	5. Report Date
VEHICLE DYNAMIC STABILITY AND ROLLOVER	June 1992
	6. Performing Organization Code
7. Author(s) R. Wade Allen, Henry T. Szostak, David H. Klyde, Theodore J. Rosenthal, Keith J. Owens	8. Performing Organization Report No. STI - TR-1268-1
9. Performing Organization Name and Address SYSTEMS TECHNOLOGY, INC. 13766 South Hawthorne Blvd. Hawthorne, CA 90250	10. Work Unit No. (TRAIS)
	11. Contract or Grant No. DTNH22-88-C-07384
12. Sponsoring Agency Name and Address U.S. Department of Transportation National Highway Traffic Safety Administration Washington, DC 20590	13. Type of Report and Period Covered Final Report
	14. Sponsoring Agency Code

15. Supplementary Notes

Lloyd H. Emery, Contracting Officer's Technical Representative

16. Abstract

This report considers ground vehicle lateral/directional stability which is of primary concern in traffic safety. Lateral/directional dynamics involve yawing, rolling and lateral acceleration motions, and stability concerns include spinout and rollover. Lateral/directional dynamics are dominated by tire force response which depends on horizontal slip, camber angle and normal load. Vehicle limit maneuvering conditions can lead to tire force responses that result in vehicle spinout and rollover. This report describes accident analysis, vehicle testing and computer simulation analysis designed to give insight into basic vehicle design variables that contribute to stability problems.

Field test procedures and results for twelve test vehicles are described. The field test results were used to validate a simulation model which was then analyzed under severe maneuvering conditions to shed light on dynamic stability issues associated with spinout and/or rollover. Vehicle parameter measurements for an additional 29 vehicles are also included that, when combined with the twelve field test vehicles, illustrate the distribution of stability relevant characteristics for a wide range of cars, light trucks and utility vehicles. Simulation analysis for selected vehicles is used to show the relationship between vehicle characteristics and lateral/directional stability problems.

The results of vehicle testing and simulation analysis indicate that a vehicle that has both a relatively low ratio of track width to center of gravity height and is equipped with tires which have a relataively high peak coefficient of friction will have a propensity to rollover during steering maneuvers on a flat surface. Vehicle testing and computer simulation analysis also indicate that directional stability is significantly influenced by the relationship between vehicle weight distribution and lateral load transfer distribution that is greater than or equal to the percent weight on the front axle. Two of the test vehicles which had relatively low front axle lateral load transfer distribution were found to have a spinout tendency, and simulation analysis showed that directional stability can be directly influenced by shifting the lateral load transfer distribution between the front and rear axles.

17. Key Words	18. Distribution Statement
Dynamic Stability, Rollover Vehicle Testing, Computer Simulation	Document is available to the public through the National Technical Information Service, Springfield, Virginia 22161

19. Security Classif. (of this report)	20. Security Classif. (of this page)	21. No. of Pages	22. Price
None	None	298	

TABLE OF CONTENTS

TABLE OF CONTENTS (Concluded)

LIST OF FIGURES

LIST OF FIGURES (Continued)

LIST OF FIGURES (Continued)

LIST OF FIGURES (Continued)

LIST OF FIGURES (Continued)

LIST OF FIGURES (Continued)

LIST OF FIGURES (Concluded)

LIST OF TABLES

SECTION I

INTRODUCTION

This report describes work carried out to examine the relationship between vehicle lateral/directional stability and control characteristics and loss of control accidents which result in vehicle rollover. The overall study employed a range of research approaches, including accident and vehicle parameter statistical analysis, vehicle parameter measurements and field testing, and computer simulation analysis of vehicle dynamic stability characteristics. The general intent of this composite approach was to develop validated models of vehicle dynamic response characteristics that could be used to establish the relationship between vehicle parameters and dynamic stability. Given stability critical parameters, vehicle characteristics would then be related to accident rates using statistical analysis procedures.

Over the years there have been numerous attempts to relate vehicle characteristics to accident experience. Accident rate has been related to vehicle weight (Ref. 1) and more recently to center of gravity location (Refs. 2, 3). This report describes research including vehicle field test and computer simulation analysis designed to give insight into the relationship between vehicle stability and accident experience, particularly involving vehicle rollover propensity. The research approach involves vehicle parameter measurement and vehicle testing to provide a validated vehicle dynamics computer simulation which is then used to analyze vehicle stability in limit performance maneuvering up to and including spinout and rollover.

Earlier versions of the computer simulation used herein have been described previously (Refs. 4, 5). Field test and validation efforts in the current work have exposed the need for further vehicle simulation model developments to adequately represent the complexities of lateral/directional and longitudinal dynamics. Procedures have also been evolved in collaboration with another research group for comprehensive validation of vehicle simulation maneuvering characteristics, including both steady state and dynamic attributes of lateral/directional and longitudinal properties (Ref. 6).

This project was conducted in two phases. The first phase included shop and field testing of 12 passenger cars, vans, light trucks and utility vehicles, including limited tire testing. This effort involved validation of a vehicle

dynamics computer simulation against field test data under steadystate, transient and sinusoidal steer maneuvering conditions. For safety reasons, vehicle testing was not designed to induce loss of control or rollover, although two vehicles experienced spinouts. The validated computer simulation was used to explore vehicle limit performance maneuvers which would induce loss of control and/or rollover. The second phase involved parameter testing and estimation for 29 additional passenger cars, vans, light trucks and utility vehicles that were selected to represent a broad range of design characteristics. Basic characteristics of the 29 phase two vehicles were then compared with the phase one vehicles to obtain a broad view of the potential stability characteristics of the vehicle fleet.

The next section reviews some background on vehicle stability characteristics under steering and braking conditions that are relevant to the analyses and testing undertaken in this project. Section III includes analysis of vehicle rollover parameters and their relationship to recently published vehicle rollover accident data (Ref. 3), and vehicle selection for this project is examined in the light of past rollover analyses. Sections IV and V summarize testing methods, including shop measurements and estimation procedures and field test techniques. Section VI considers validation of the computer simulation against field test data under steadystate, transient and frequency response conditions and summarizes the characteristics of all test vehicles and implications for dynamic stability. Section VII explores simulation analysis of limit performance maneuvering (i.e., steering and braking), how this relates to the basic characteristics of the 12 field test vehicles, and implications for the remaining 29 test vehicles. Recent rollover accident data for the vehicle population considered herein is related to measured vehicle characteristics in Section VIII. A summary of the work described herein and conclusions regarding vehicle dynamic stability are finally given in Section IX. Several appendices describe the computer simulation vehicle dynamic model and parameter measurement and estimation procedures.

SECTION II

BACKGROUND

A. OVERVIEW

Vehicle handling stability is dominated by tire force response characteristics. Lateral acceleration (i.e., steering) and longitudinal acceleration (i.e., speed control) must derive from tire forces. Lateral acceleration stems from steering inputs which lead to tire side slip angles with respect to the vehicle velocity vector which then result in tire side forces. Engine and brake torques cause tire longitudinal slip with respect to the road surface which then leads to longitudinal forces. The tire composite forces (lateral and longitudinal) at the front and rear axles result in linear accelerations which influence translational motions and moments which affect angular motions. Tire forces result in complex interactions with vehicle dynamics because, in addition to responding to driver inputs (i.e., steering, throttle and braking), they also respond to resultant vehicle motions (Ref. 5 and references therein provide the background for this review).

The interaction of tire/wheel response with vehicle dynamics is summarized in the Fig. 1 block diagram which is based on the vehicle dynamics model summarized in Appendix A. Tire forces are dependent on tire slip relative to the road surface. Lateral forces arise from tire side slip and camber angle while longitudinal forces which provide acceleration and braking depend on longitudinal slip of the tire/wheel unit. Tire forces are also a direct function of normal load which results in an interaction with load transfer as will be discussed subsequently. A component of tire lateral slip is due to steer angle relative to the body axis, and both front and rear axle steer can derive from several inputs including steering wheel angle, body roll angle, and compliance effects due to forces and moments developed from the tire/road interaction. These wheel steer effects result in significant interactions with the vehicle steering system which in turn result in significant effects on the vehicle response dynamics (e.g., Refs. 4, 5).

In the range of linear tire force response corresponding to low to moderate maneuvering accelerations (i.e., below 0.5 g) vehicle handling characteristics remain relatively stable. At higher maneuvering accelerations, tire force

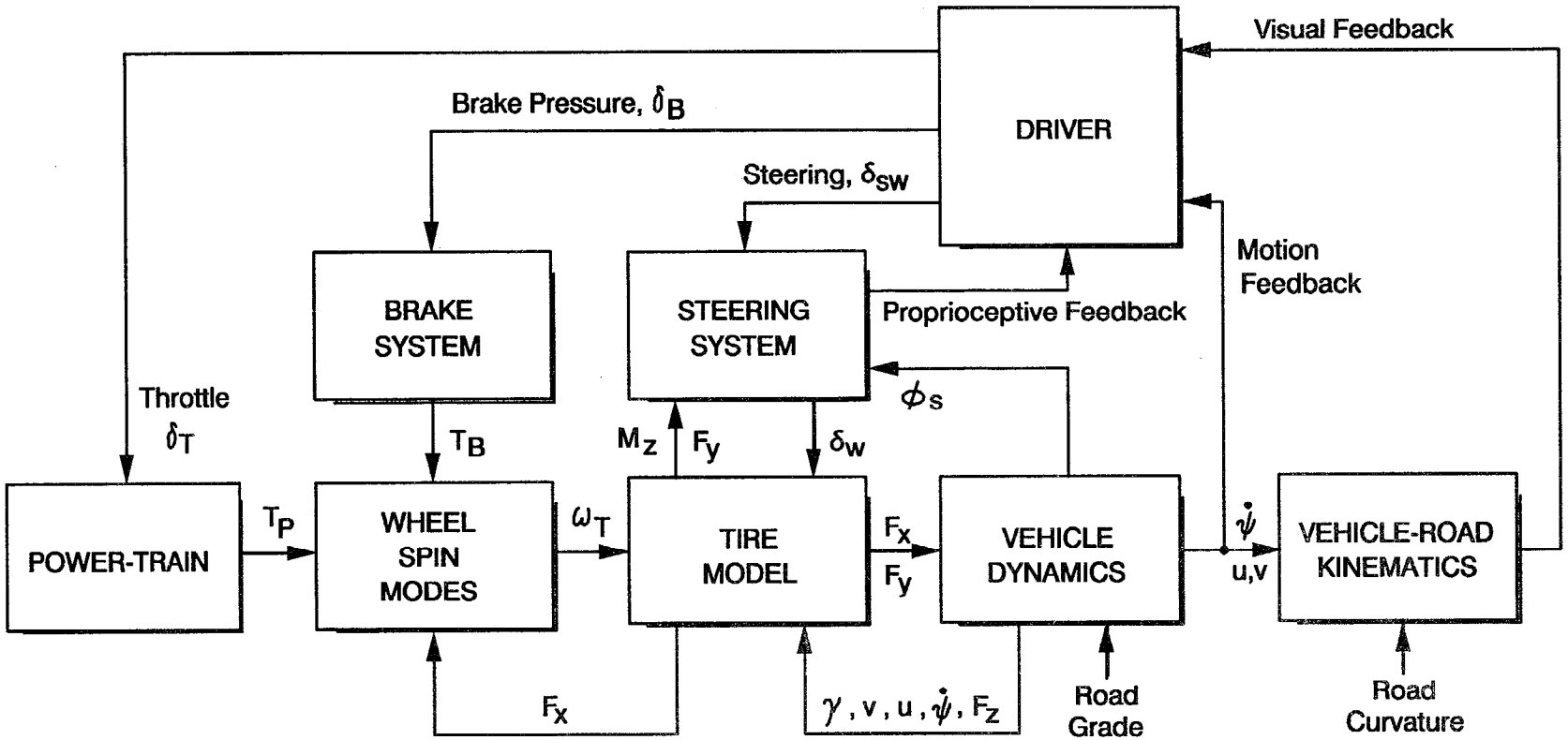

F_x, F_y, F_z = x, y, z forces from or on tire

M_z = Aligning moment from tire

ω_T = Wheel spin velocity

v, u = Vehicle side and forward velocities

δ_{SW}, δ_w = Steering and road wheel angles

ϕ_s, γ = Body roll and wheel camber angles

$\dot{\psi}$ = Vehicle yaw rate

note that tire side slip = $\alpha = f(v, u, \dot{\psi}, \delta_{SW})$

tire longitudinal slip = $S = f(\omega_T, u)$

Figure 1. Vehicle Dynamics Block Diagram Based on Appendix A Dynamic Model

response begins to saturate. This results in changes to vehicle steady state and dynamic characteristics. As summarized in Fig. 2, based on a tire model developed in Ref. 5, a typical highway vehicle tire has a limit force response defined in terms of a coefficient of friction. Composite force cannot exceed this friction "ellipse," and, as the limit is approached, there is a reduced ability to change tire forces with respect to lateral slip angle and longitudinal slip ratio. This reduction in tire force change sensitivity generally influences vehicle dynamics. Note also in Fig. 2 that tire response characteristics, including the limit coefficient of friction, change as a function of normal load which makes the effect of load transfer important.

Consideration of driver control of vehicle dynamics, as illustrated in Fig. 1, is important in order to maintain some perspective of the vehicle dynamics effects that are of consequence in crash avoidance maneuvering. The basic yawing and rolling modes are central to the issues considered in this report. Tire saturation basically limits driver control of steering and braking in addition to reducing the responsiveness of the vehicle dynamics and changing understeer /oversteer characteristics (Ref. 5). Thus, under limit performance conditions, the driver's control capability is reduced and the response dynamics of the vehicle degrade which makes tire saturation characteristics of paramount importance to driver control. The dynamics of the wheel spin mode under light braking conditions are high frequency and of no real consequence to the driver. Under severe braking conditions wheel lockup is an issue as it can lead to complete tire force saturation which eliminates directional stability and steering control.

The steering system has high frequency dynamics (the shimmy mode) which are not of direct importance in driver control. The steering dynamics do induce an effective lag in the steering response, which does contribute to the vehicle directional dynamics. Similarly, the tires have a side force delay (Refs. 5, 7) which also contributes to the vehicle directional dynamics. The importance of these steering and tire delays decrease, however, as the tires go into saturation under limit performance maneuvering. Concerning the brake system, front to rear proportioning and booster saturation are of significant importance to the driver. The responsiveness of the power train could have some influence on the driver's maneuvering ability, but has not been considered in this project.

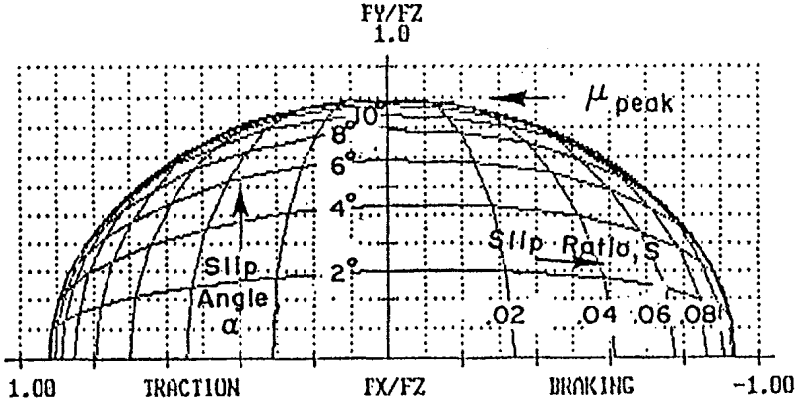

a) Tire Friction Ellipse

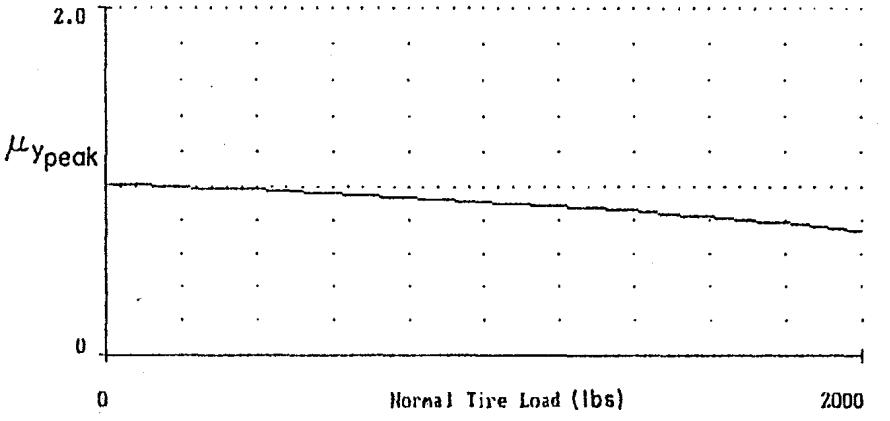

c) Peak Coefficient of Friction

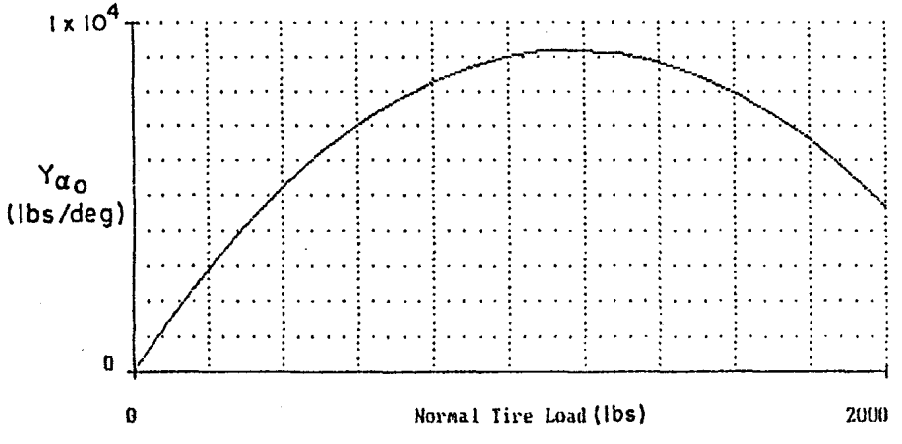

b) Side Force Coefficient ($\partial F_y / \partial \alpha$)

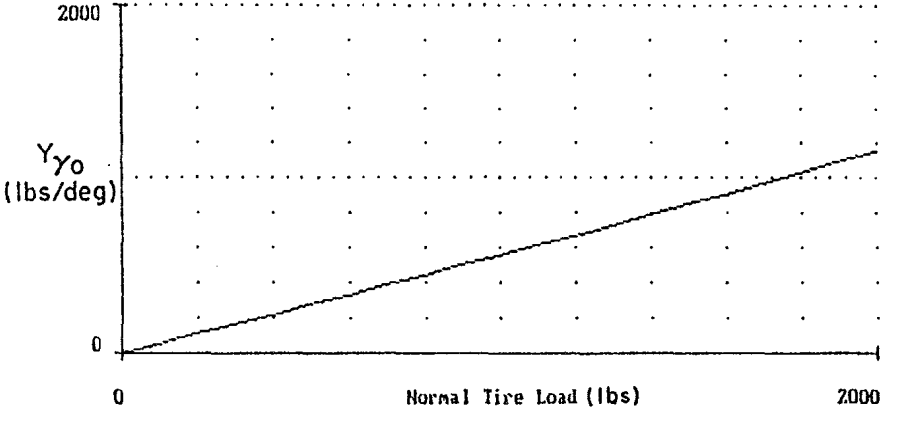

d) Camber Force Coefficient ($\partial F_y / \partial \gamma$)

Figure 2. Tire Horizontal Force Response Characteristics

Finally, it should be noted that driver steering and braking inputs provide the primary initial excitation for vehicle directional dynamics during crash avoidance maneuvering. The amplitude and timing of steering and/or braking inputs determine the severity of vehicle motions. The extreme nonlinearities associated with tire limit performance make handling and stability sensitive to the detailed amplitude and timing of large amplitude steering and braking profiles. The influence of control input profiles will be considered further here, although a complete nonlinear analysis of the influence of control input characteristics on vehicle stability is beyond the scope of this project.

B. DIRECTIONAL STABILITY

Directional (i.e., yaw or heading) stability depends on the horizontal plane moments applied to the vehicle under various maneuvering conditions due to the composite tire forces. Under accident avoidance conditions these forces typically result from steering and/or braking and are heavily influenced by load transfer. As summarized in Fig. 3, steering (cornering) causes normal load to be transferred from the inside to outside tires which decreases the force generating capacity of the inside tire and increases the outside tire force generating capacity since a tire's lateral force capacity is basically proportional to the normal load on the tire. However, as shown in Fig. 2b, because of a tire's normal load sensitivity, the ratio of the lateral force capacity to normal load is not constant and it decreases with increasing normal load. Eventually when the normal load gets high enough, usually near a tire's rated normal load capacity, the lateral load capacity of a tire actually decreases with increasing normal load. As such, as more load is transferred from the inside tire to the outside tire on an axle, the average lateral force capacity of the two tires on that axle decreases. As the lateral force capacity of the tires on an axle decrease with increasing lateral load transfer and the lateral force demands of the cornering maneuver increase with increasing lateral acceleration, the tires on an axle can saturate.

If the front tires saturate first the vehicle understeers and plows out in the limit. If the rear tires saturate first the vehicle oversteers and can spin out. Lateral load transfer is generally influenced by the ratio of center of gravity height to track width as indicated in Fig. 3. The saturation of the front relative to the rear axle can be controlled by adjusting the relative load

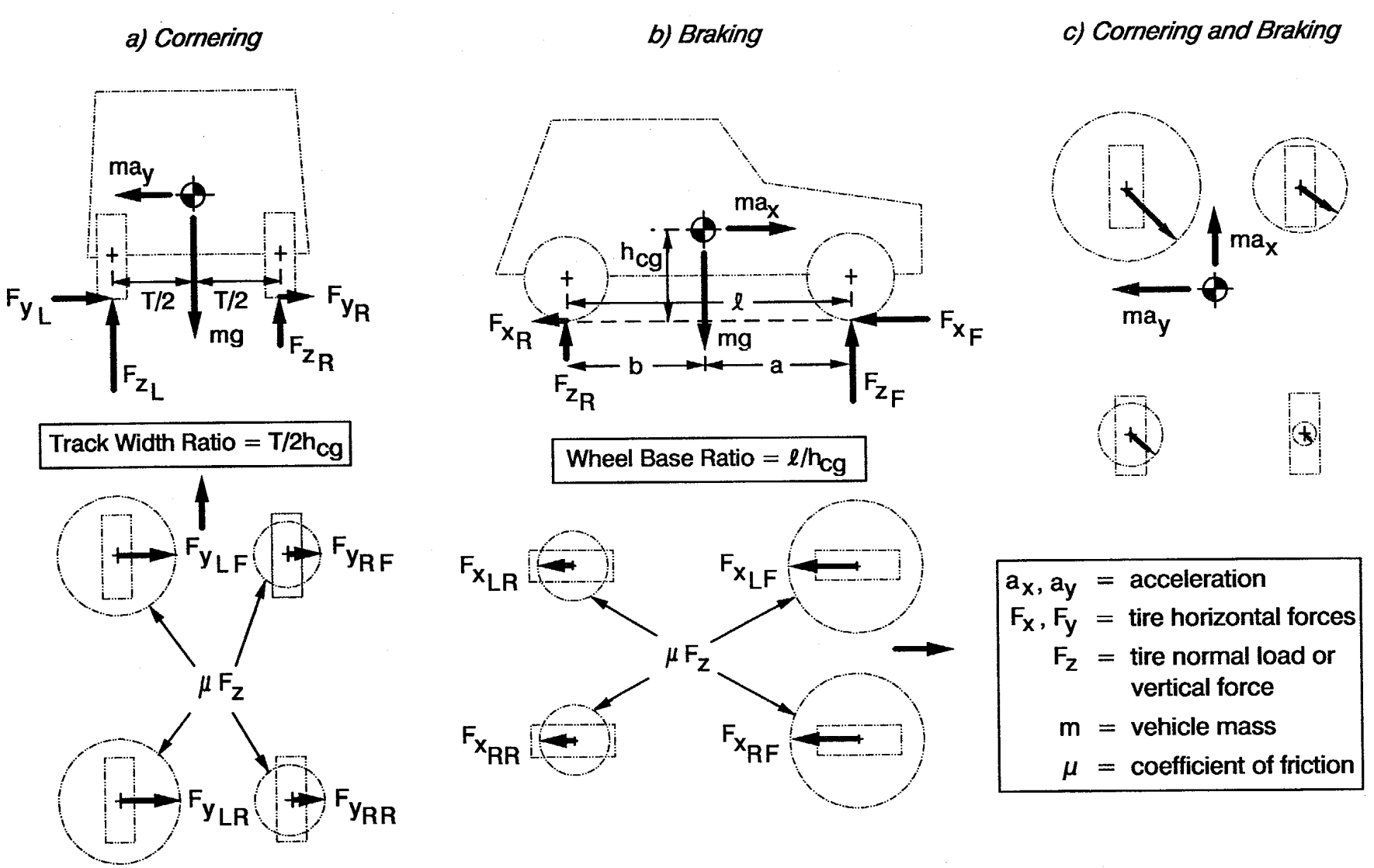

Figure 3. Maneuvering Induced Load Transfer Effects on Tire Horizontal Force Response Capacity

transfer between the two axles. This is accomplished by setting the relative roll stiffness at the front and rear axles with antiroll torsion bars which are typically designed to give limit understeer (under lower g cornering conditions, understeer also derives from roll and compliance steer effects).

Braking conditions cause load transfer from the rear axle to the front axle as indicated in Fig. 3. Under hard braking conditions the rear axle is lightly loaded which greatly restricts the rear axle braking force capacity relative to the front axle. To avoid rear axle lockup under these conditions, nonlinear brake pressure proportioning valves are used to reduce rear brake torque under hard braking conditions as summarized in Fig. 4 (Ref. 5).

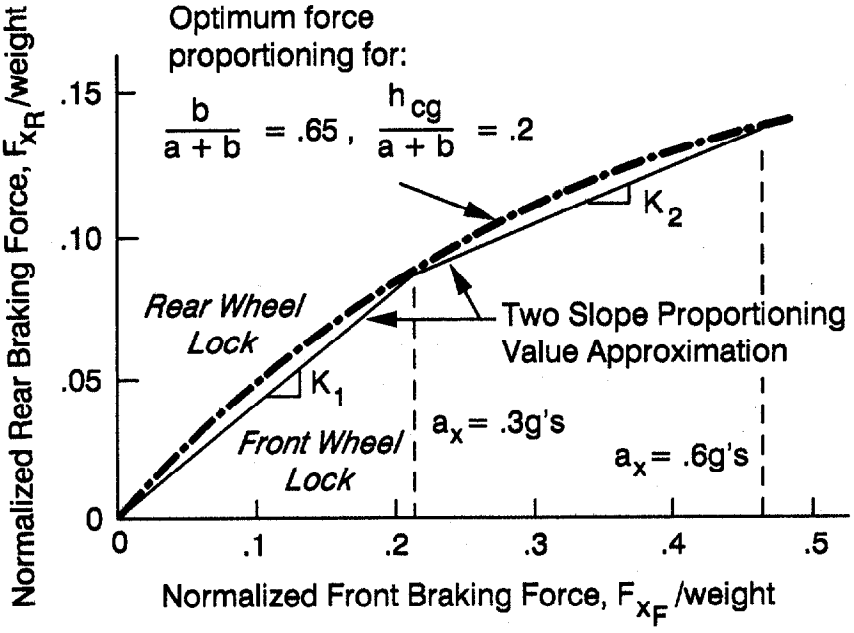

Figure 4. Optimum Braking Forces and Nonlinear Proportioning Valve Characteristics (adapted from Ref. 5)

Longitudinal load transfer depends on the ratio of center of gravity height to wheel base as indicated in Fig. 3, which is the main factor in setting optimal brake proportioning as indicated in Fig. 4. Brake proportioning depends on brake pad frictional properties which can be quite variable due to in-use factors and quality control of after-market components. Measurement of the brake proportioning of in-use vehicles indicates variability on the order of 20% or more (Ref. 8) which makes this characteristic one of the most variable parameters influencing handling and stability.

Combined cornering and braking produces the most severe handling condition as suggested in Fig. 3. With load shifting to the front axle and outside tires, the inside rear tire can be seriously unloaded and subject to lockup in the absence of an antilock system. Previous analysis (Refs. 4, 5) has shown that braking in a turn can lead to significant oversteer and directional instability. The severity of this condition is related to load transfer which in turn is related to the ratio of center of gravity height to wheel base and track width as summarized in Fig. 3. Directional stability characteristics are directly related to these ratios, as will be discussed further on.

C. ROLLOVER STABILITY

Rollover requires elevating the c.g. (center of gravity) over the wheels on one side of the vehicle. As illustrated in Fig. 5 rollover might be accomplished under severe lateral maneuvering conditions given sufficient tire side force capability, or result from a lateral tripping mechanism. The distinction between tire side force and a tripping mechanism becomes somewhat blurred as we consider increased surface friction and soft shoulder conditions where tires plow into the surface material so that side force develops from soil shear rather than tire/surface friction. During cornering, the tire side force and inertial (centrifugal) force due to lateral acceleration result in a roll moment. Simple analysis indicates that for this roll moment to be sufficient to roll over the vehicle, the lateral acceleration must be greater than one half the vehicle track width divided by the center of gravity height as indicated in Fig. 5. Peak lateral acceleration maneuvering capability of light passenger vehicles is on the order of 0.6-0.8 g due to tire and load transfer characteristics, while the "track width ratio" defined in Fig. 3 is typically near or above unity for passenger cars, vans, pickups and light utility vehicles.

Since tire side force characteristics do not have a high enough coefficient of friction to roll a typical light passenger vehicle under steady state conditions on an average flat, paved surface, additional conditions must contribute to rollover. Vehicle transient maneuvering might excite the vehicle roll mode in such a manner as to contribute to rollover (Ref. 9). Higher effective coefficient of friction conditions can result if a vehicle intrudes on a soft shoulder where tires dig into the surface material resulting in high side forces given sufficient slip angle. One limiting condition results from a vehicle

a) Center of Gravity Elevation

$$\Delta h = \sqrt{y_{cg}^2 + h_{cg}^2} - h_{cg}$$

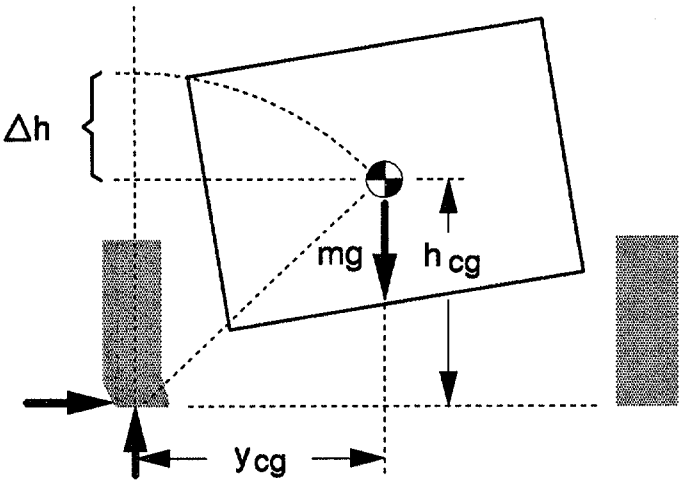

b) Tire Side Forces at Rollover

$$ma_y h_{cg} = mgy_{cg}$$

or

$$\frac{a_y}{g} = \frac{y_{cg}}{h_{cg}}$$

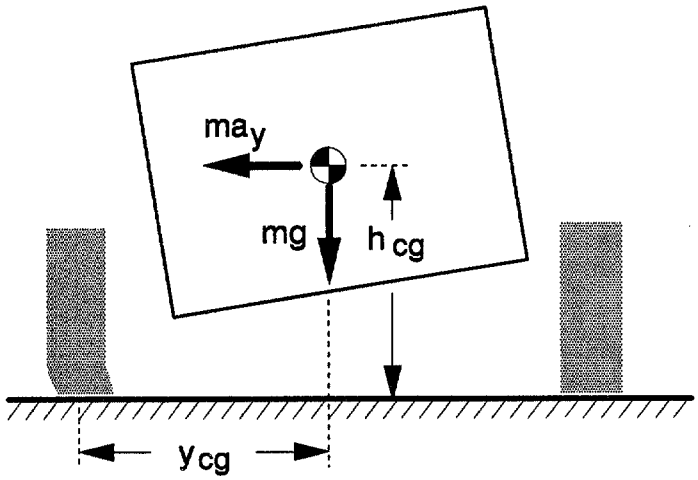

c) Tripping

$$\dot{y}_c^2 \cong 86 \bullet \Delta h \bullet \left[1 + \frac{y_{cg}^2}{h'^2}\right]$$

(see Table 1)

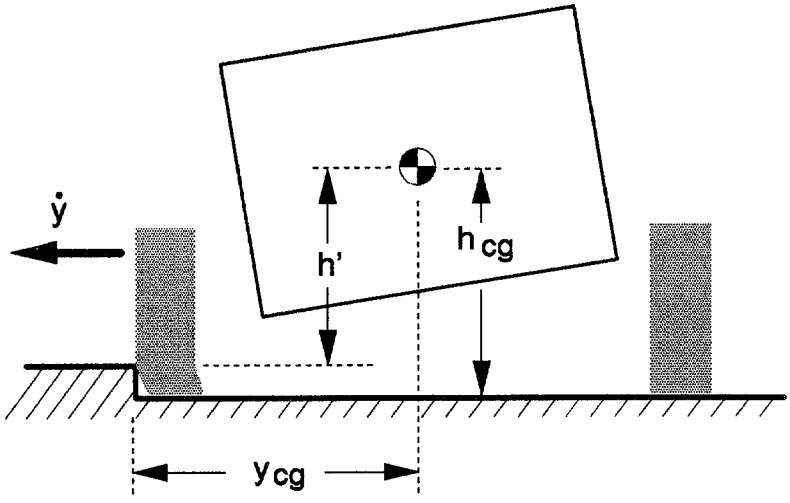

Figure 5. Conditions Leading to Rollover

sliding into a curb with sufficient velocity such that its translational momentum is translated into sufficient angular momentum to cause rollover as illustrated in Fig. 5 (e.g. Refs. 10, 11). Sliding on paved surfaces into curbs or off onto shoulders or into ditches may imply a loss of directional stability as a precursor to rollover.

As summarized in Table 1, tripped rollover can be related to track width ratio and the c.g. elevation required for rollover by making a simple assumption about the relationship between vehicle dimensions and mass and moment of inertia. Given this assumption, the critical lateral velocity for tripped rollover derived by Jones (Ref. 10) can be expressed approximately in terms of track width ratio and the c.g. elevation required for rollover. This approximation is important for two reasons. First, it illustrates that tripped rollover can be related to simple vehicle dimensional properties which also determine a vehicle's rollover sensitivity to lateral maneuvering conditions. Second, the vehicle parameters are easily established from routinely published data if we allow for one additional approximation for vehicle c.g. height. As described elsewhere (Refs. 5, 12) c.g. height for light passenger vehicles can be expressed as a relatively constant proportion (.36-.42) of roof height which also is routinely published.

Rollover rates for large tractor-semitrailer trucks involved in single vehicle accidents (SVA) has been shown to be strongly related to a rollover threshold metric which includes track width ratio reduced by suspension and tire compliance effects (Ref. 13). SVA rollover rates for light passenger vehicles have also been shown to be significantly related to track width ratio (Ref. 2) and a combination of track width and wheel base (Refs. 3, 14). In these analyses rollover rate is inversely proportional to both track width ratio and wheel base. The last two analyses also accounted for driver age and found minor effects (i.e., younger drivers have higher rollover rates).

TABLE 1. LATERAL VELOCITY FOR TRIPPED ROLLOVER
(ADAPTED FROM JONES, Ref. 10)

$$\dot{y}_c^2 = \frac{2g\, I_o}{m\, h'}\left[\sqrt{1 + \frac{y_{cg}^2}{h'^2}} - 1\right]$$

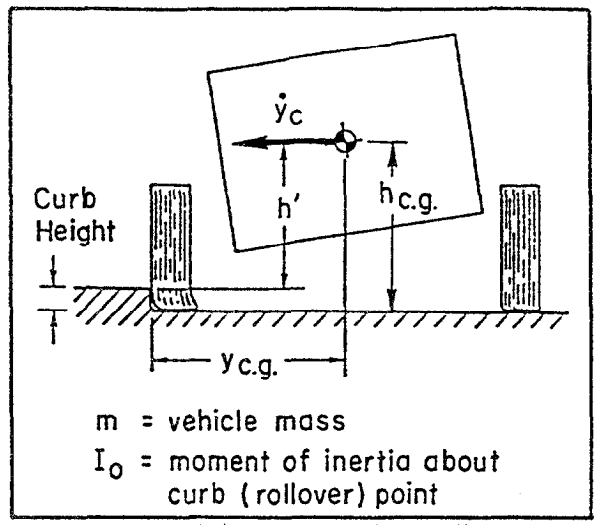

where

$$I_o = I_\phi + m(y_{cg}^2 + h'^2)$$

Roll inertia approximation

$$I_\phi = \frac{m}{12}(W^2 + H^2) \qquad \text{where} \quad W \doteq 2y_{cg}, \quad H \doteq 2h'$$

$$\therefore\ I_o = \frac{m}{12}(4y_{cg}^2 + 4h'^2) + m(y_{cg}^2 + h'^2) = \frac{4m}{3}(y_{cg}^2 + h'^2)$$

and

$$\dot{y}_c^2 = 86h'\left[1 + \frac{y_{cg}^2}{h'^2}\right]\left[\sqrt{1 + \frac{y_{cg}^2}{h'^2}} - 1\right] = 86\Delta h\left[1 + \frac{y_{cg}^2}{h'^2}\right]$$

where

$$\Delta h = \sqrt{h'^2 + y_{cg}^2} - h' = h'\left[\frac{\sqrt{1 + y_{cg}^2}}{h'^2} - 1\right]$$

SECTION III
ACCIDENT ANALYSIS AND VEHICLE SELECTION

A. OVERVIEW

It was desired to select vehicles for this project that had a range of characteristics that might be related to dynamic stability and rollover. Common characteristics such as track width ratio and wheel base that have previously been related to SVA (single vehicle accident) rollover rates were considered as primary variables, along with other classification variables such as vehicle class (passenger car, light truck, utility vehicle), size (subcompact, compact, mid size) and drive type (front wheel drive, rear wheel drive, four wheel drive). Vehicles were selected in two phases on this project. In the first phase, twelve test vehicles were selected for parameter and field testing, based on rollover rate analyses and engineering judgement. The test vehicles were selected to span the range of potential parameters that could serve to influence directional control and/or rollover. In the second phase, vehicles were selected by the NHTSA for parameter testing that spanned the range of passenger vehicle characteristics and market classes.

This section reviews the preliminary rollover rate accident analysis that assisted in vehicle selection, then summarizes selected test vehicle characteristics for a variety of parameters. As will be noted, vehicle parameters tend to be strongly related to basic vehicle size, and it is difficult to obtain independent variation of parameters such as track width ratio, wheel base, and c.g. (center of gravity) elevation required for rollover. The correlation of these parameters for the selected vehicles will be examined.

B. ROLLOVER RISK FACTORS

A recent analysis of rollover risk in single vehicle accidents has considered a range of vehicle, driver and accident factors (Ref. 3). Using logistic regression analysis of a data base of 40 vehicles, which included passenger cars and utility vehicles and excluded vans and pickup trucks, it was found that the track width ratio is by far the most influential vehicle variable in predicting the rollover rate (i.e., percentage of all single vehicle accidents that resulted in rollover) of passenger cars and utility vehicles. Some influence of wheelbase was found; however, that influence was not nearly as strong as that for the track width ratio.

When the statistical model was used to predict rollover involvement at the accident level, i.e., predicting whether a particular single vehicle crash will result in a rollover, a variable representing whether the crash occurred in a rural or urban environment was found to exhibit a similar level of significance as that of the track width ratio. Although the urban/rural variable exhibited similar importance in the accident level prediction of rollover, its exclusion from the model had little effect on the coefficient of the track width ratio, i.e., the amount of predicted influence of a given change in track width ratio on rollover involvement was the same whether or not the urban/rural variable was included in the model. The urban/rural variable did not, however, seem to exhibit as strong an influence when predicting rollover involvement at the make/model level, e.g., predicting the rollover per single vehicle accident rate (RO/SVA) for a given make/model of vehicle. This result is not unexpected. For example, when all the crashes, both urban and rural, for a given vehicle make/model are aggregated to predict its rate, the influence of the urban/rural variable could be lost if the "urban/rural" influence is similar for the different vehicle make/models.

Other non-vehicle factors in Ref. 3, i.e., driver age, driver sex, and road condition, did not affect the strong influence found for the track width ratio; however, several were found to be "statistically significant." In order to facilitate further discussion of the results of the Ref. 3 analysis, linear regression techniques were performed using the same data. Basic Vehicle characteristics and rollover rates taken from Reference 3 were entered into a Lotus 1-2-3© spread sheet along with other published data for the specified vehicles in the data base. The spread sheet allowed composite vehicle stability parameters, as discussed in Section II above, to be easily computed and plotted, and subjected to regression analysis.

The relationship between rollover rate taken as the dependent variable and track width ratio and wheel base taken as independent variables for the Ref. 3, passenger car and utility vehicle data base, is illustrated in Fig. 6 along with regression analysis results. Vehicles are subdivided into reasonably well established classes based on size, weight and intended use. Utility vehicles and small cars tend to have the highest rollover rates, with medium, large and sport cars having the lowest rates. The squared correlation coefficient (i.e., r^2 or "r squared") for the Fig. 6 data is quite high and statistically significant ($P<.001$) and comparable with the correlations reported in Reference 3. The regression

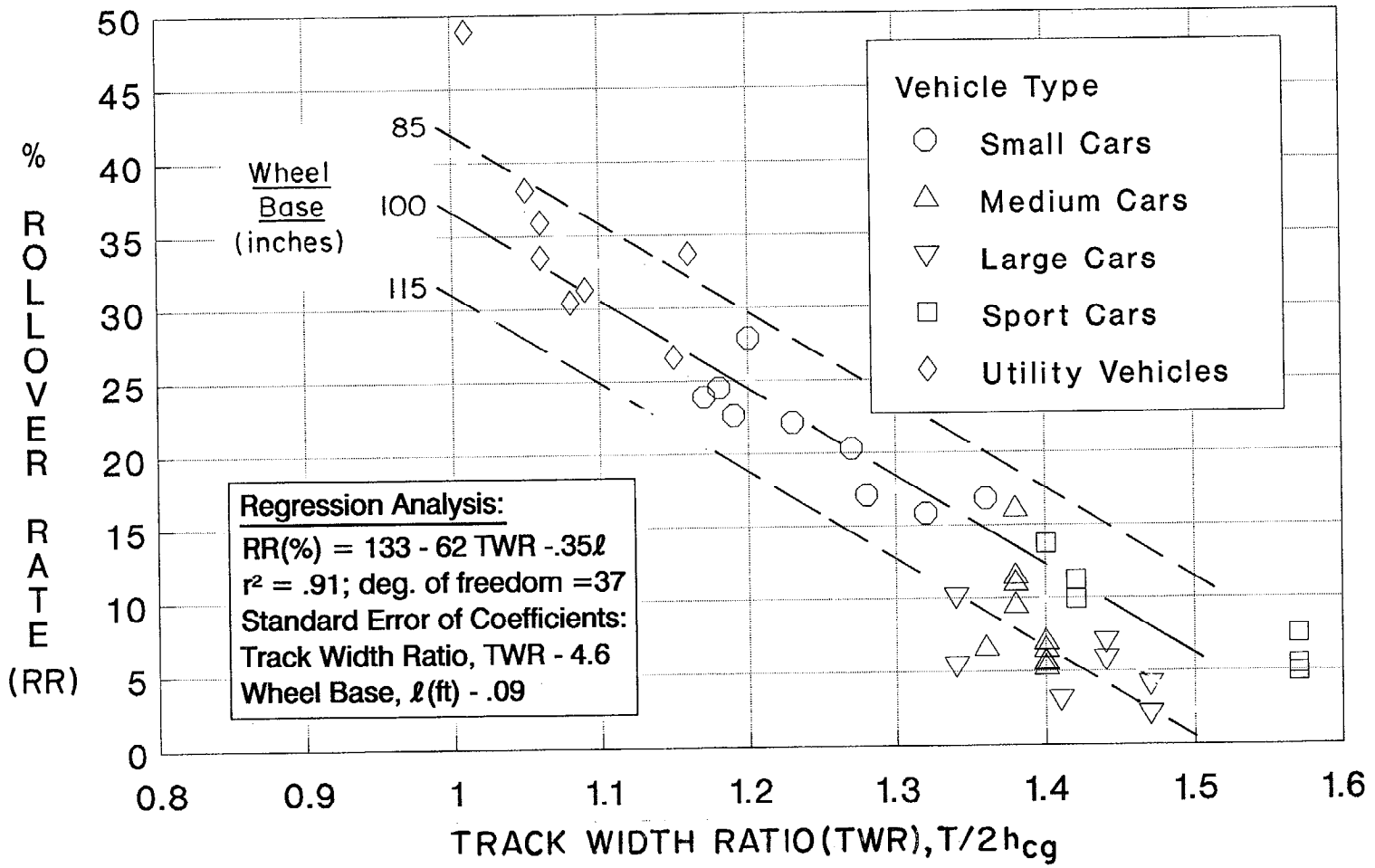

Figure 6. Relationship Between Rollover Rates in Single Vehicle Accidents and Vehicle Characteristics (data adapted from Ref. 3)

analysis in Reference 3 also showed that wheelbase had a small but consistent relationship with rollover rate, and the authors suggested that this effect was due to the collinearity between track width ratio (referred to as "stability factor") and wheelbase. As noted in Fig. 7, the correlation between these variables is low but is statistically significant ($P<.001$).

The regression analysis sensitivity of rollover rate to wheel base is indicated in Fig. 6, which shows rollover increasing with decreasing wheel base for passenger cars and utility vehicles. This result could have some bearing on directional stability, with longer wheel base cars having greater directional stability in extreme maneuvering conditions and thus avoiding rollover situations. The sensitivity of rollover rate to wheel base is small, however, when compared to the sensitivity with track width ratio. The wheel base range from 85 to 115 inches gives a change in rollover rate according to the regression relationship of about 12%, while the track width ratio range of 1 to 1.5 gives a change of about 36%. These ranges cover the majority of the vehicles in the Reference 3 analysis, as noted in Fig. 6.

The relationship between rollover rate and the critical lateral velocity required for tripped rollover, as calculated from the Table 1 formula for the Ref. 3 data, is shown in Fig. 8. As noted, the regression is statistically significant ($P<.001$), but with a lower correlation than the relationship of Fig. 6. When wheel base was added to the tripped velocity regression analysis, its contribution was found to be statistically insignificant for passenger cars and utility vehicles. The general trends for the various vehicle classes are roughly the same in Figs. 6 and 8, which is not surprising since tripping velocity is a strong function of track width ratio (Table 1). It should also be noted that the tripping velocities required for rollover are fairly low (i.e., 8-14 mph). Tripping does imply lateral skidding, however, which must be preceded by loss of directional control.

C. TEST VEHICLE SELECTION

Vehicles were selected for two phases of this project. A first group of twelve vehicles were selected in phase 1 by project personnel in collaboration with NHTSA for purposes of field testing and simulation. A second larger set of 29 vehicles were selected by NHTSA personnel in phase 2 for parameter measurement only. Characteristics of all test vehicles are summarized in Appendix E. It was desired to select vehicles for field testing and simulation analysis that spanned the range

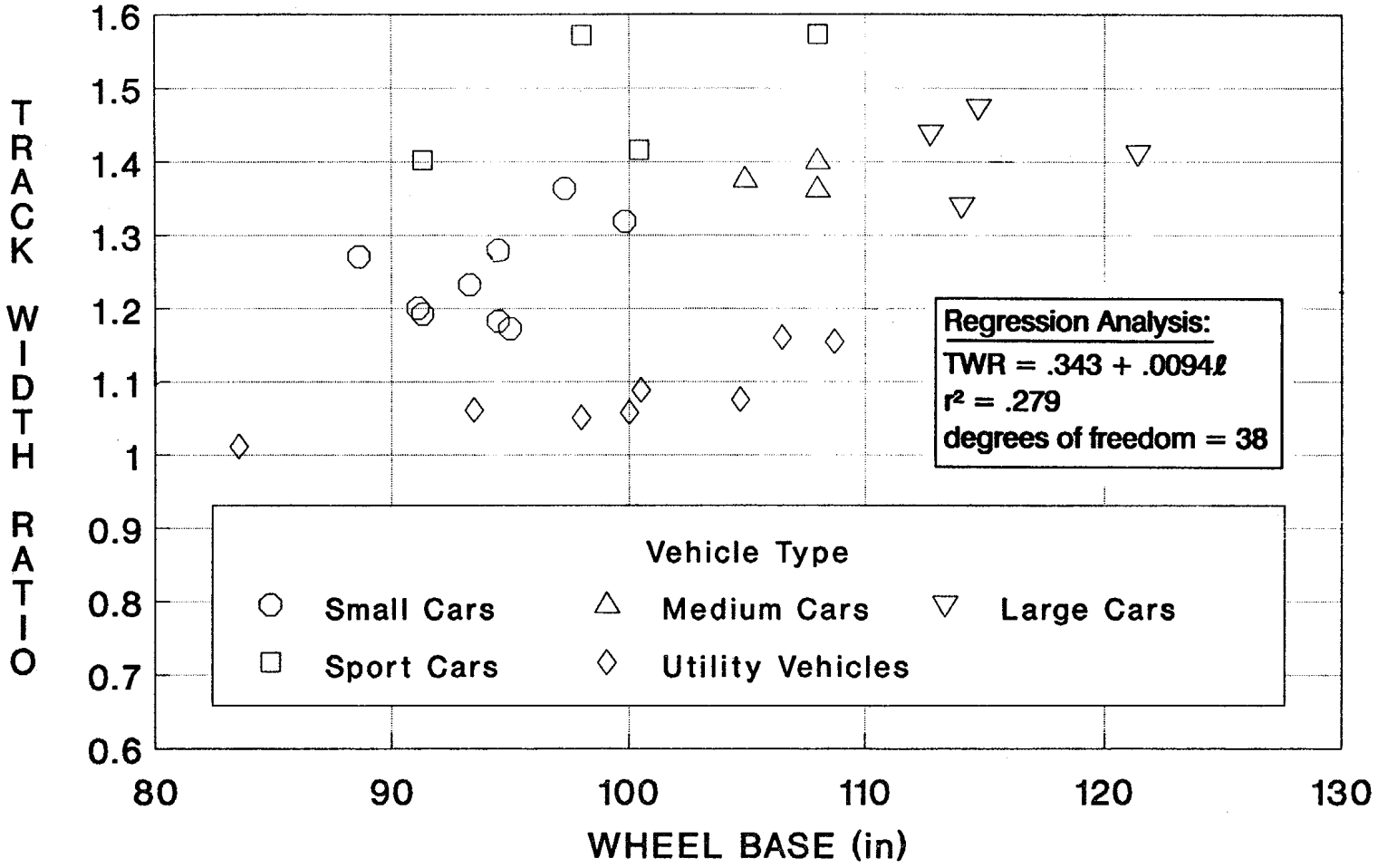

Figure 7. Track Width Ratio (T/2hcg) as a Function of Wheel Base (data adapted from Ref. 3)

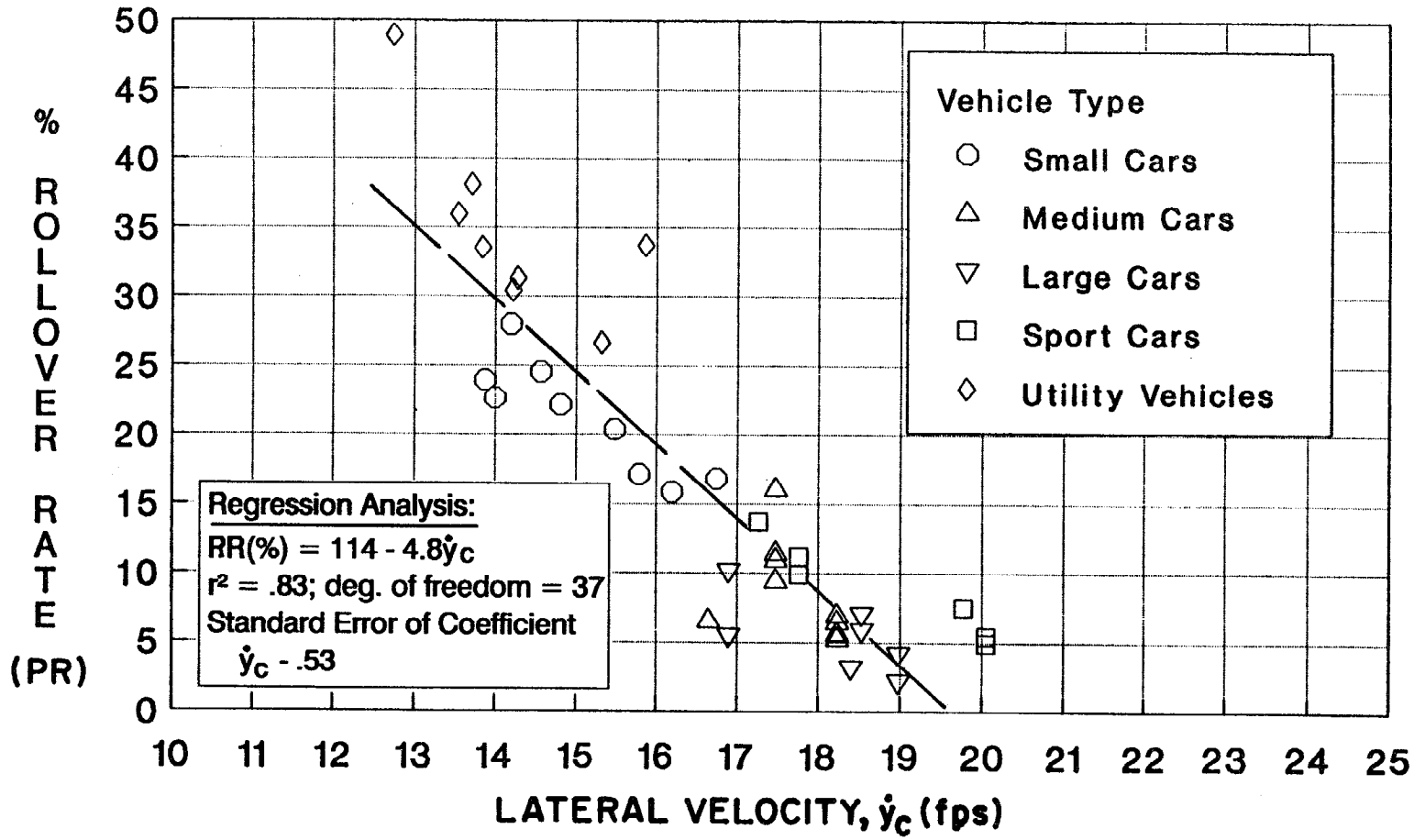

Figure 8. Relationships Between Rollover Rates in Single Vehicle Accidents and Lateral Velocity Required for Tripped Rollover

of rollover propensity as defined by the stability parameters discussed previously. Vehicles selected for the field testing phase of this project are summarized in Table 2.

TABLE 2. PHASE 1 TEST VEHICLE CHARACTERISTICS

REF. #	VEHICLE TYPE	Weight (lbs)	Wheel Base (ft)	TWR	WBR
1	Small FWD Pass. Car	2550	7.85	1.26	4.29
6	Small FWD Pass. Car	2035	7.84	1.33	4.58
8	Small FWD Pass. Car	2015	7.58	1.33	4.51
10	Small RWD Pass. Car	2110	7.86	1.23	4.54
16	Medium RWD Pass. Car	3355	8.70	1.33	4.73
17	Large RWD Pass. Car	3830	9.67	1.40	5.28
18	Pass. Van FWD	3572	9.90	1.19	4.66
19	Pass. Van RWD	3622	9.92	1.11	4.35
23	Small Pickup 4x4	3240	9.23	1.09	4.35
34	Small Utility 4x4	2135	6.67	1.12	3.48
37	Medium Utility RWD	3650	8.37	1.12	4.02
40	Medium Utility 4x4	3520	7.85	1.00	3.24

As mentioned earlier, the previous analysis (Ref. 3) of rollover risk in single vehicle crashes did not include any vans or pickup trucks. In order to examine whether the influence of various vehicle stability parameters on rollover involvement found for other classes of vehicles, i.e., passenger cars and utility vehicles, are also seen for van and pickup truck class vehicles, nearly 40% of the phase 1 and phase 2 vehicles selected for this study are vans and pickup trucks.

In Fig. 9, the relationship of wheel base ratio to track width ratio for the selected test vehicles is compared with the vehicles from the data base used in

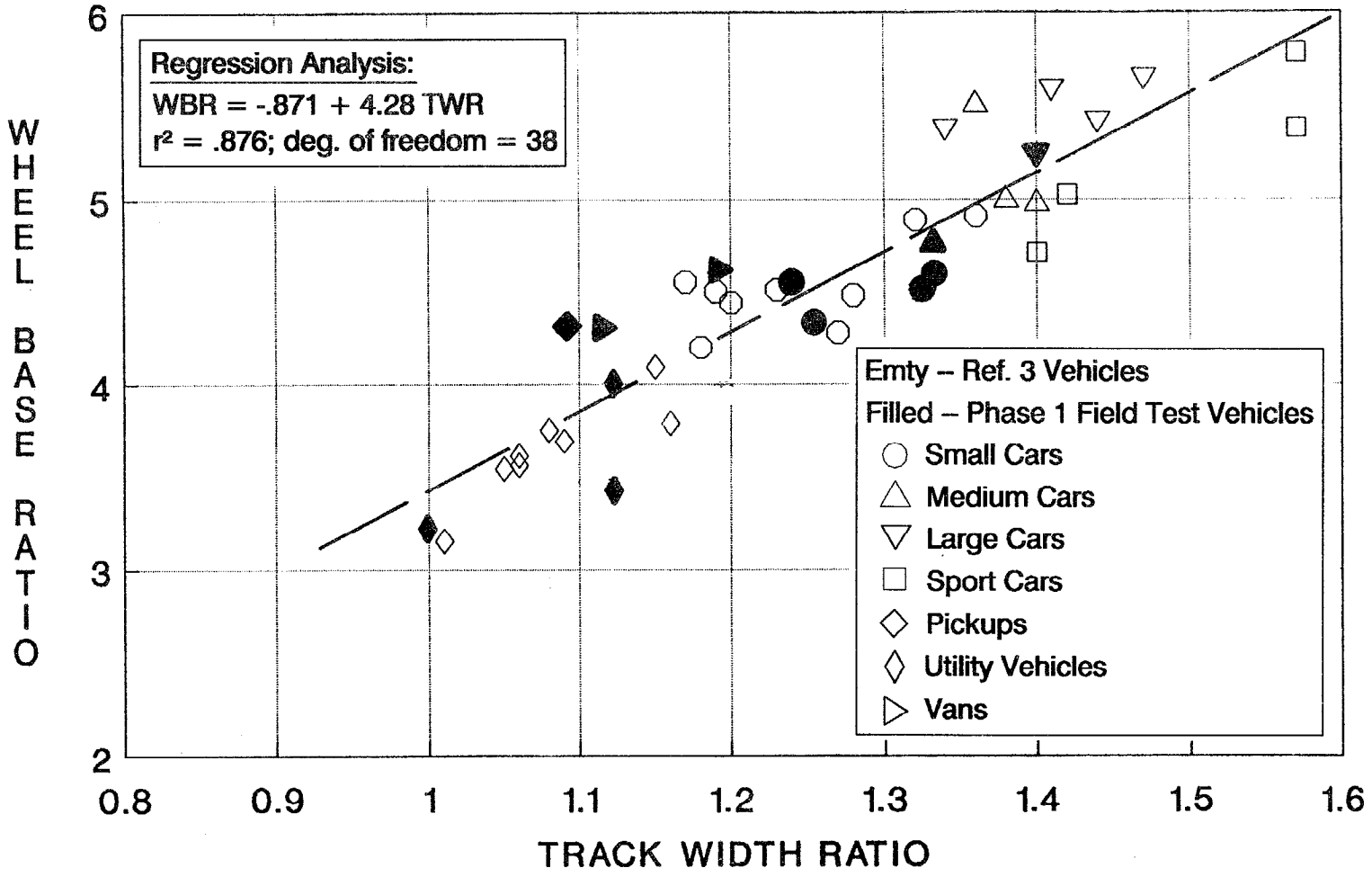

Figure 9. Wheel Base Ratio vs. Track Width Ratio for Reference 3 Vehicles as Compared with Phase 1 Vehicles Selected Herein for Field Testing

Reference 3. Here we see that wheel base ratio and track width ratio are highly correlated ($P<.001$), and the selected test vehicles encompass a reasonable span of the previous data base (Ref. 3). We previously noted that absolute wheel base had a low correlation with track width ratio (Fig. 7), and it is the wheel base ratio with respect to c.g. height that results in the high correlation with track width ratio. Recall from previous discussion that wheel base ratio relates to load transfer under braking conditions (a potential factor in directional stability), while track width ratio relates to lateral load transfer and rollover propensity. The Fig. 9 data show that these two stability related metrics are highly correlated, which is basically a vehicle size covariation, so that directional and rollover stability may be confounded to a significant degree.

In Fig. 10, the relationship between wheel base and c.g. height change required for rollover is shown for the selected field test vehicles as compared with the Reference 3 data base. These variables relate to lateral and longitudinal size and are somewhat less dependent on each other than the Fig. 9 variables. The selected test vehicle characteristics span the range of the Reference 3 data set in Fig. 10.

In many cases, the various relationships between vehicle stability related parameters above show significant correlation. Parameters that relate to directional stability (i.e., wheel base ratio) and rollover propensity (i.e., track width ratio) co-vary in a manner that should generally degrade vehicle stability. Based on the previous rollover rate analysis, as a class, light utility vehicles have the poorest characteristics and small subcompact vehicles span a wide range of intermediate stability. The vehicles selected for field testing, as discussed in subsequent sections, span the major portion of the range of stability parameter characteristics, as analyzed in the data set adapted from Ref. 3, as well as the phase 2 vehicles selected herein for parameter measurement. Field test measurements and simulation analysis can now be used to give further insight into the stability characteristics of these vehicle classes, as discussed subsequently.

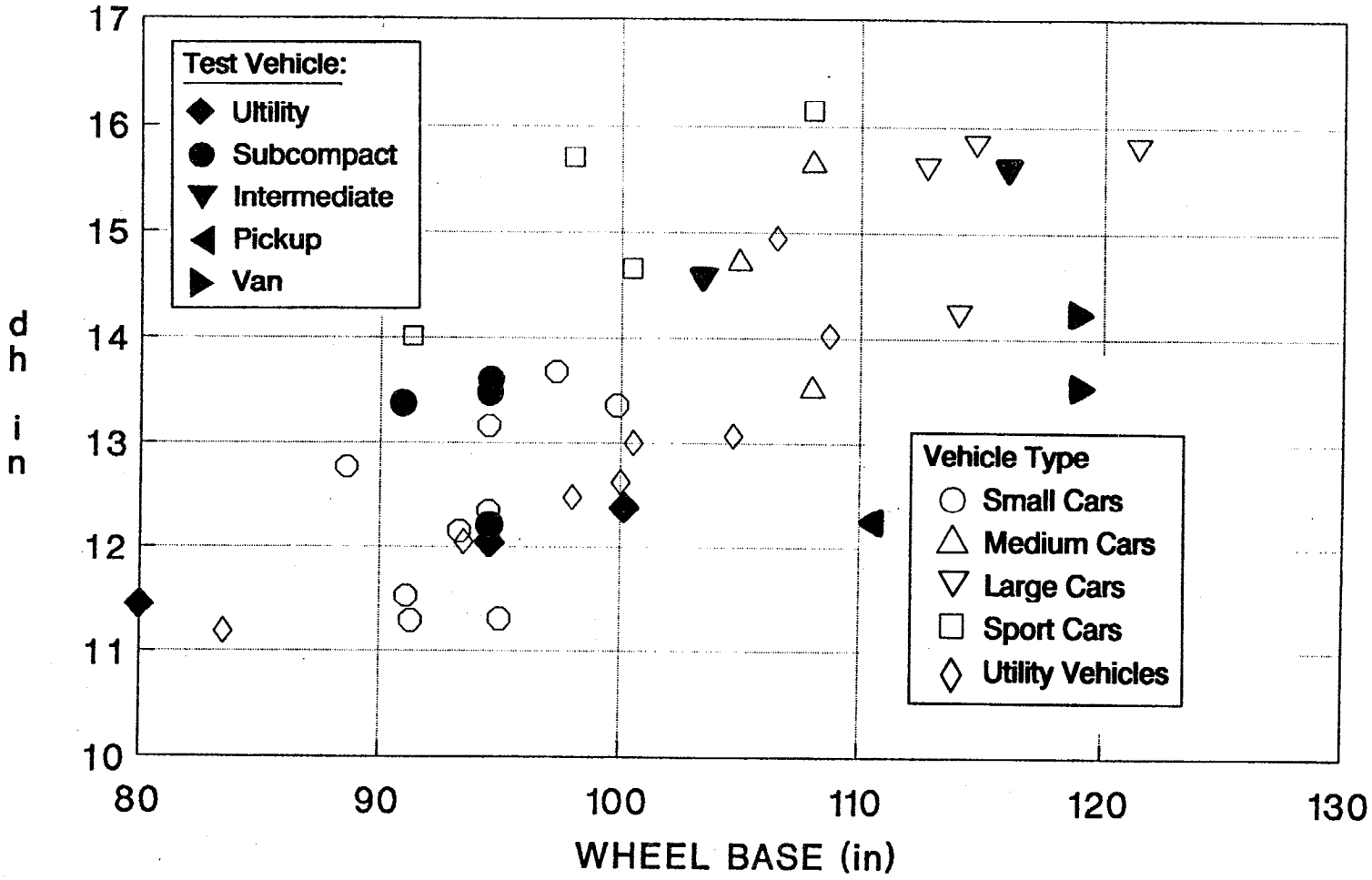

Figure 10. Wheel Base vs. C.G. Elevation Required for Rollover for Reference 3 Vehicles as Compared with Phase 1 Vehicles Selected herein for Field Testing

SECTION IV

VEHICLE PARAMETER IDENTIFICATION

A. OVERVIEW

The objectives of the overall vehicle testing program were threefold: 1) collect dynamic model parameters to be used in a vehicle dynamic analysis simulation; 2) to obtain direct measures of vehicle rollover stability; 3) to measure vehicle behavior for use in validating the vehicle dynamics simulation. The original twelve phase 1 vehicles were subjected to all of these procedures, which has resulted in fairly complete validation of simulation models for use in handling and stability analysis. Stability and parameter measurements were carried out for an additional twentynine vehicles in phase 2, but no field test validation data was obtained for these vehicles. The goal for the twelve phase 1 vehicles was to obtain validated computer simulation models that could be used to analyze handling and stability properties under limit performance maneuvering conditions. This section discusses results from vehicle and tire parameter measurement, and the side pull metric for rollover stability. Vehicle field testing is covered in Section V and simulation validation and analysis are carried out in Sections VI and VII.

B. VEHICLE PARAMETER MEASUREMENT AND ESTIMATION

The vehicle parameters required for analysis and computer simulation were obtained through a combination of shop testing and estimation. The complete list of parameters required for the computer simulation program are summarized in Appendix A. Measured vehicle properties summarized in Table 3 include vehicle dimensions, weight distribution and c.g. (center of gravity) location, suspension geometry, steering system gain and aligning torque compliance, roll gradient and roll stiffness. Suspension geometry parameters are used to compute composite deflection steer, camber and side force jacking properties as discussed in Appendices A and C. Vehicle dimensions and mass distributions are used to compute moments of inertia as discussed in Appendix B. Roll damping was estimated to give a heave damping ratio of between .25 and .40 depending on the estimated ride quality stiffness (i.e., soft = .25 – .30; firm = .30 – .35; stiff = .35 – .40). The steering system natural frequency and damping were set to

TABLE 3. VEHICLE PARAMETER IDENTIFICATION

MEASURED

Mass and weight distribution
Vehicle geometry (trackwidth, wheelbase, etc.)
Center of gravity location
Spring rates, roll stiffness
Suspension geometry
Steering ratio and compliance
Tire parameters (phase 1 vehicles)

ESTIMATED

Moments of inertia
Heave damping
Steering system natural frequency and damping
Tire parameters (phase 2 vehicles)

typical values respectively of 12 Hz and 0.5. A listing of measured and vehicle characteristics is summarized in Appendices B and C.

The longitudinal c.g. location is obtained directly from normal load (weight) measurements at the four wheels using vehicle weight scales. The height of the c.g. was obtain by a pitching tilt method as discussed in Appendix D. It has been shown in the past that c.g. height is a direct function of vehicle roof height (Refs. 4 and 12) and the data trends for the test vehicle population herein are shown in Figure 11 for the combined phase 1 and phase 2 vehicle populations. Vehicles are designated by number as defined in Appendix E. Passenger cars (numbers 1-17) tend to have c.g. height to roof height ratios that are slightly higher than the utility/pick up/van categories. Pickups (numbers 23-33) and soft top utility vehicles (numbers 34,35 and 41) tend to have lower c.g. height to roof height ratios because they have less sheet metal above the window line. The longitudinal c.g. location relative to the wheel base is plotted in Figure 12 as a function of vehicle wheel base for the test vehicle population. The twelve phase 1 field test vehicles span the range of vehicle c.g. location and size aside from the longer wheel base pickups, vans and utility vehicles. The front wheel drive cars typically have a more forward c.g. location, while the midengine sport car (vehicle #11) has the most rearward c.g. location.

The track width ratio (static rollover stability ratio or ratio of c.g. height to track width) has a direct physical relationship to vehicle rollover

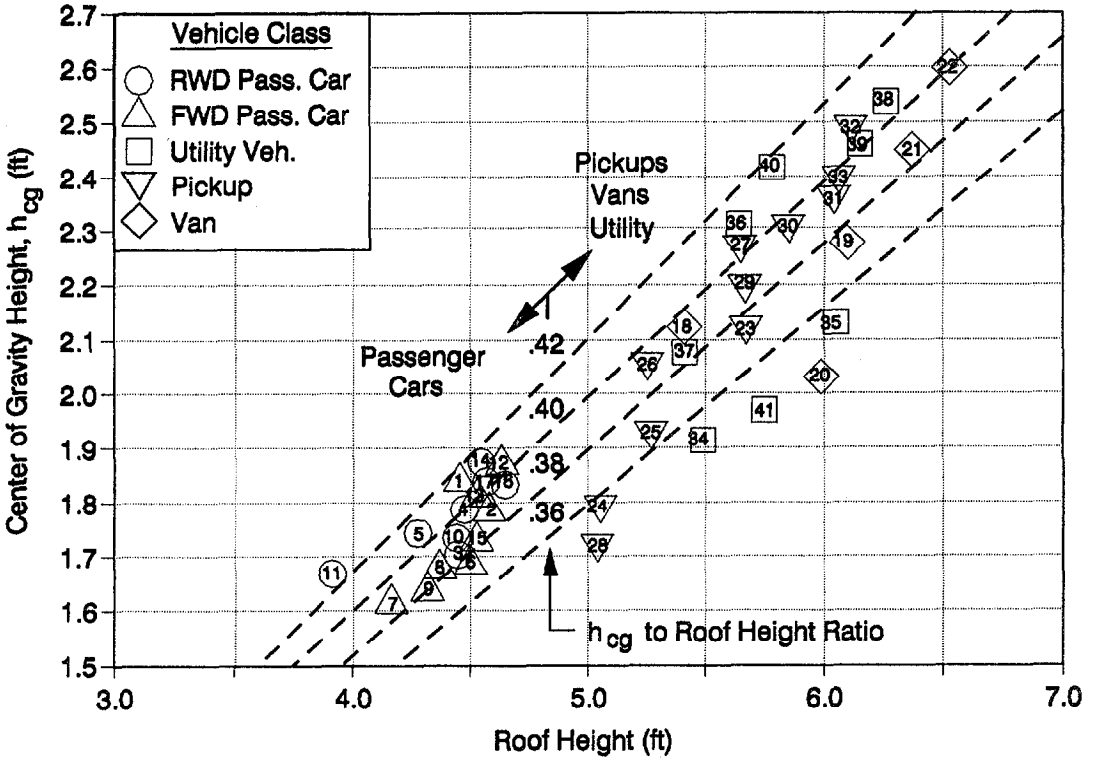

Figure 11. Center of Gravity (c.g.) Height as a Function of Roof Height for all Phase 1 and Phase 2 Test Vehicles.

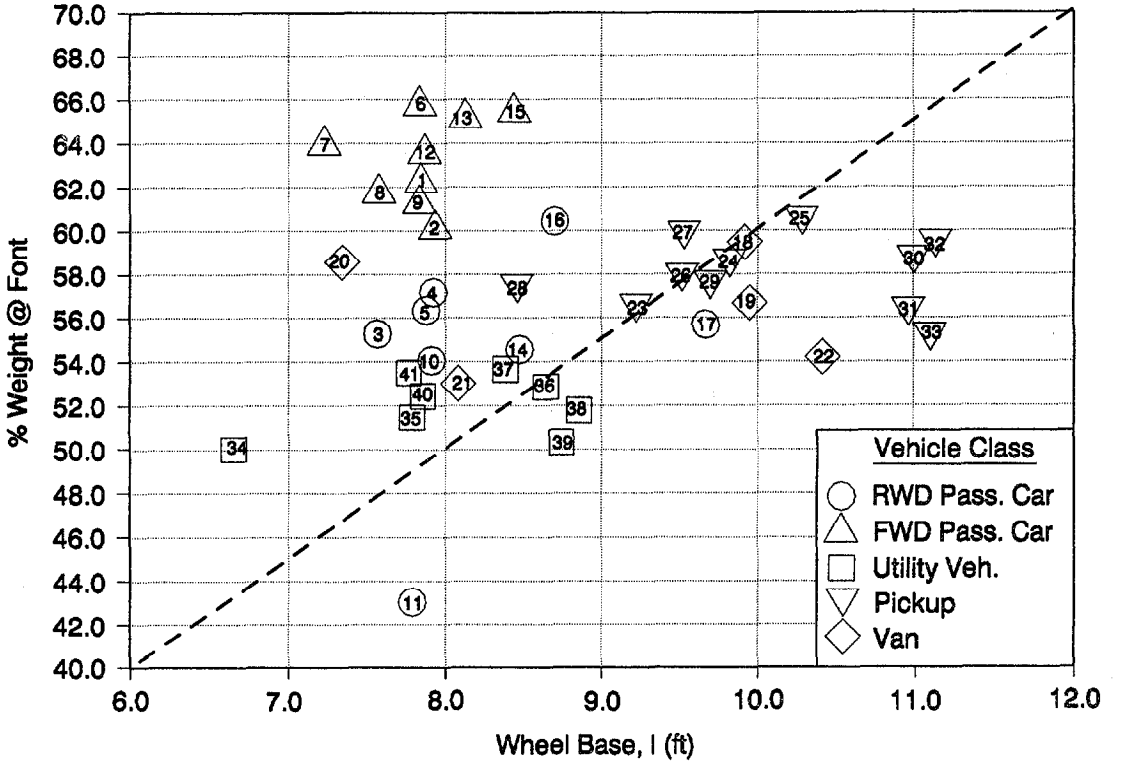

Figure 12. Weight Distribution as a Function of Wheel Base for all Phase 1 and Phase 2 Test Vehicles.

propensity as discussed previously. Track width ratio is plotted as a function of wheel base (a metric of vehicle size) in Figure 13. There is no clear trend here, and the phase 1 field test vehicles represent a reasonable sample from the overall test vehicle population. Wheel base ratio (the ratio between wheel base and c.g. height) is plotted against track width ratio in Figure 14. Both of these variables are measures of maneuvering induced load transfer (as suggested in Fig. 3), with smaller values giving higher load transfer and potentially worse handling and stability problems. The relationship in Figure 14 basically represents a covariation of wheel base with track width, so that there is a strong trend for simultaneous degradation of directional and rollover stability with vehicles in the lower left hand corner being particularly vulnerable. The phase 1 field test vehicles represent a reasonable sample of the Figure 14 characteristics.

As noted in Section II, roll stiffness at the front and rear of vehicles is used to adjust understeer/oversteer characteristics over the range from normal to limit performance handling. Generally it is necessary to have understeer to avoid directional instability. Understeer can be realized over the full maneuvering range with more cornering load transfer at the front axle relative to the rear axle, which in turn can be achieved by making the front roll stiffness higher than the rear. In Figure 15 roll stiffness distribution is plotted as a function of weight distribution for the test vehicle population. Here we see that roll stiffness is generally biased towards the front axle. Aside from the group of front wheel drive passenger cars, (designated by the Δ symbol) there is a slight trend for roll stiffness distribution to shift towards the front axle with increasing front axle weight distribution. Front drive cars tend to understeer and plow due to power application, so presumably they require less front roll stiffness for a given front weight distribution.

Changes in tire side force characteristics that lead to understeer are strongly influenced by overall load transfer distribution (LTD). The roll stiffness distribution discussed above is only one component of LTD as analyzed in Appendix F, the other factors involve the front and rear roll axis heights and the sprung and unsprung mass distributions. When all of these factors are taken into account per the Appendix F equations, then the relationship between LTD and weight distribution for the test vehicle population is as indicated in Figure 16. Here we see that LTD is generally biased towards the front axle which

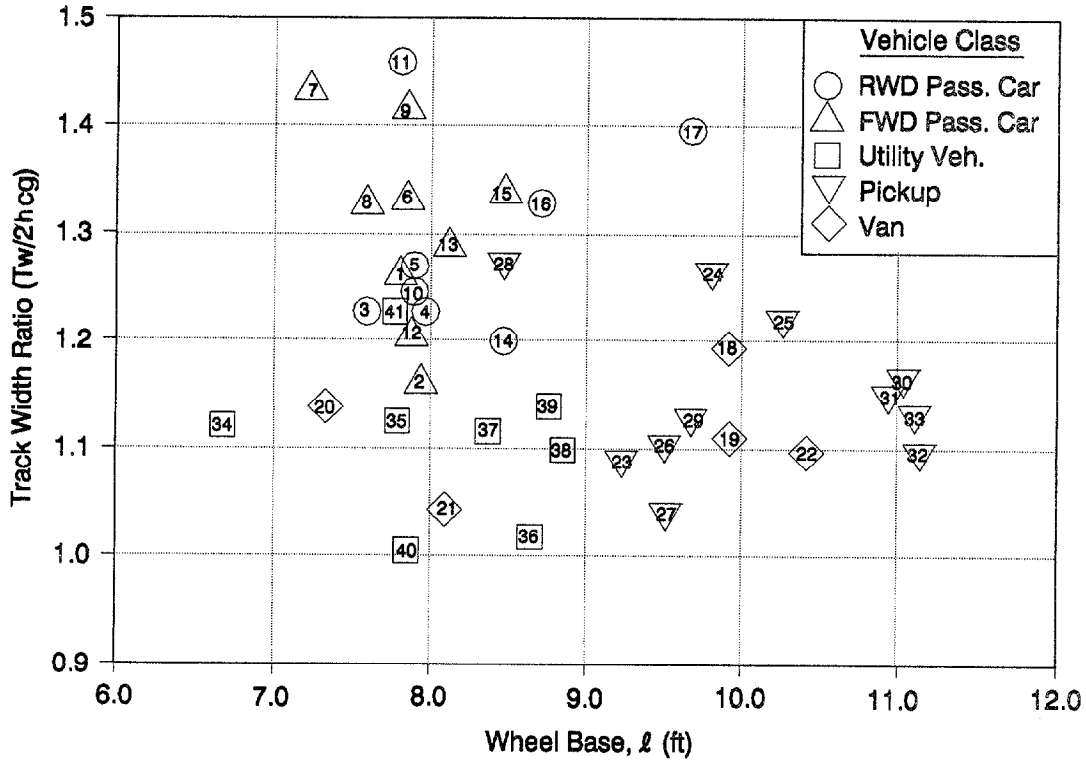

Figure 13. Track Width Ratio as a Function of Wheel Base for all Phase 1 and Phase 2 Test Vehicles.

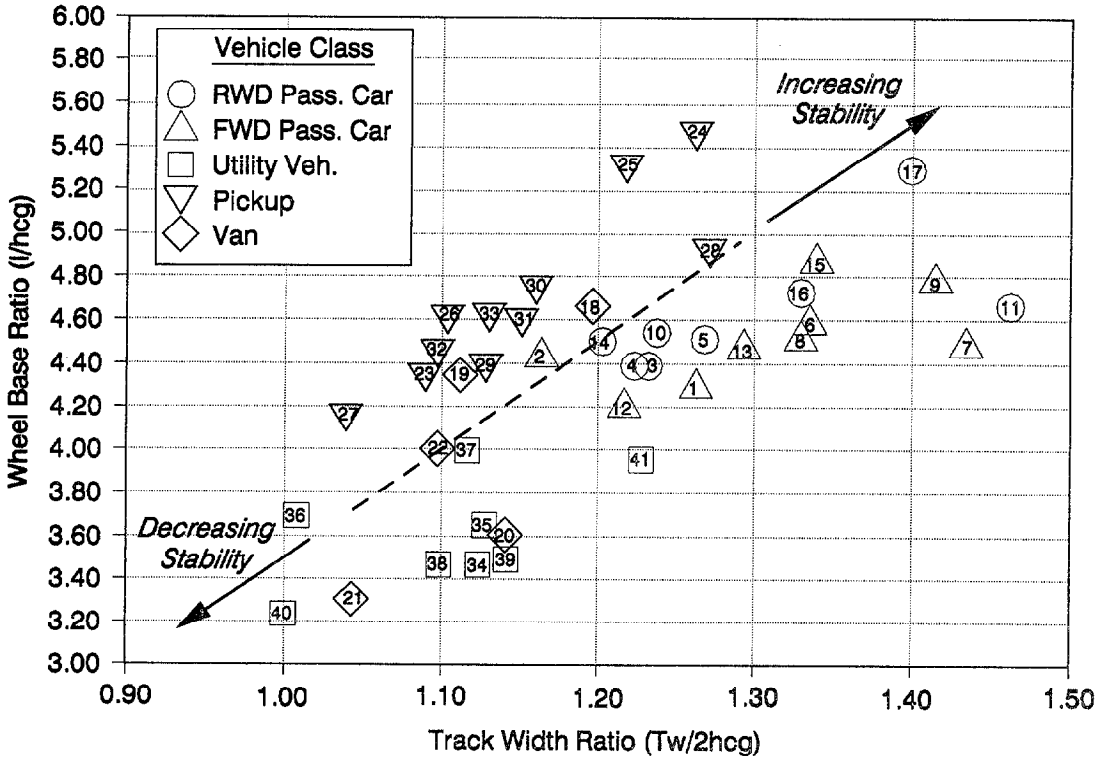

Figure 14. Wheel Base Ratio (Wheel Base Divided by c.g. Height) as a Function of Track Width Ratio (Half Track Width Divided by c.g. Height) for all Phase 1 and Phase 2 Test vehicles.

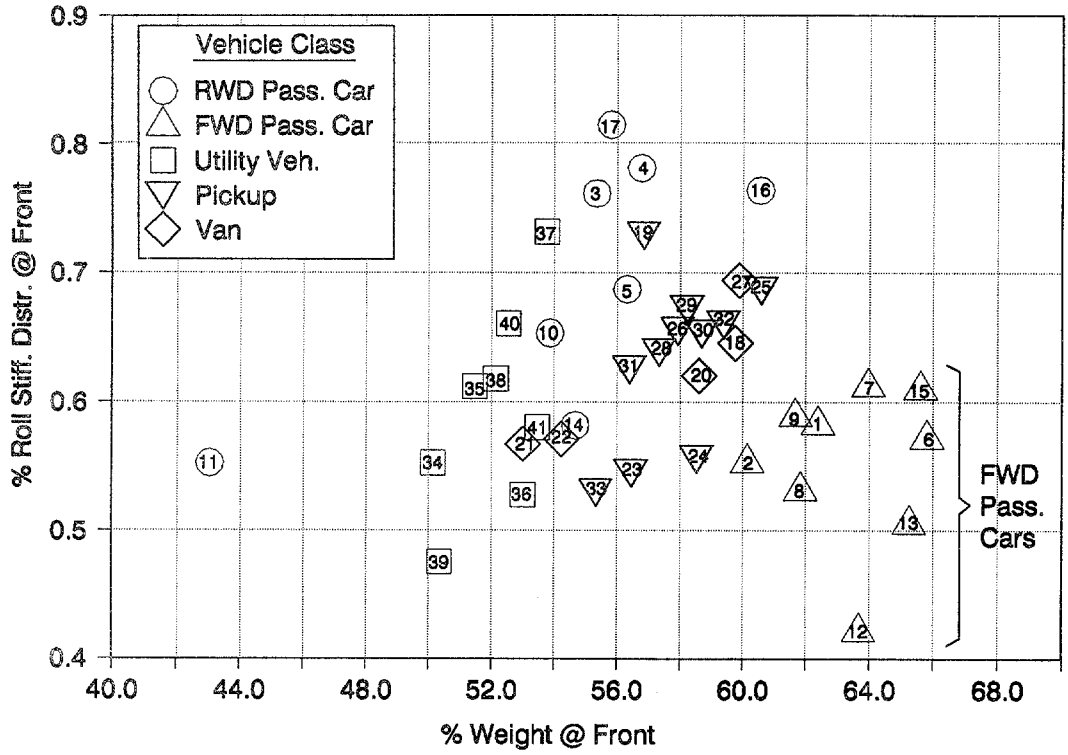

Figure 15. Roll Stiffness Distribution (% Front Axle) as a Function of Weight Distribution (% Front Axle) for all Phase 1 and Phase 2 Test vehicles.

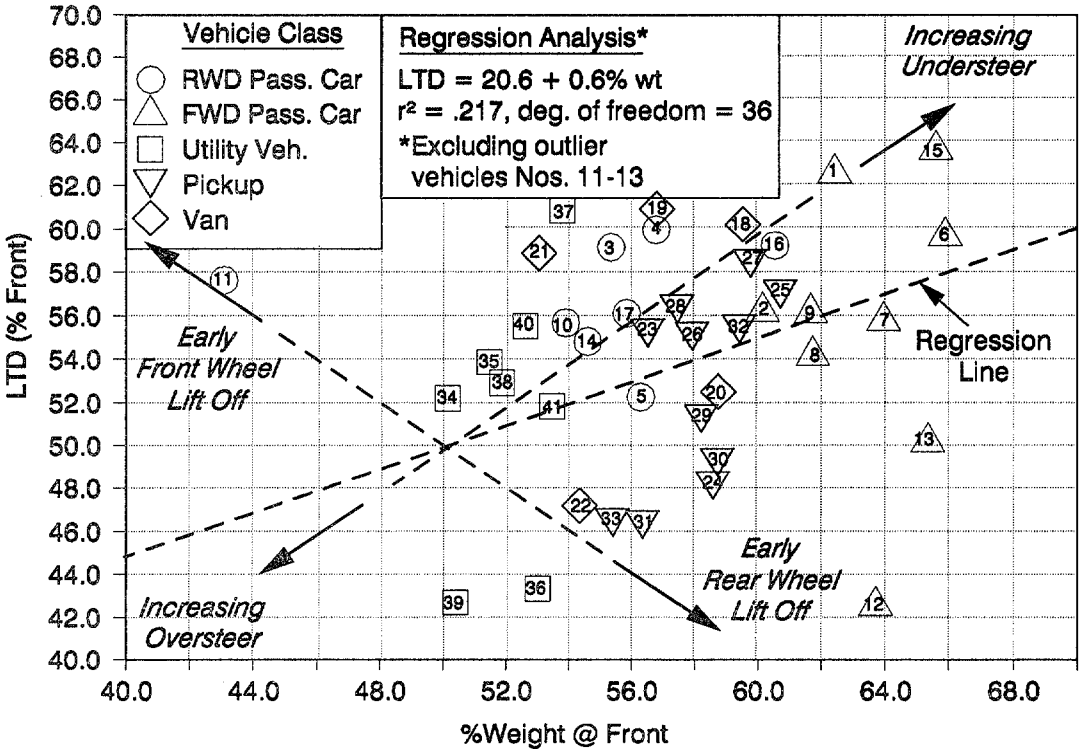

Figure 16. Lateral Load Transfer Distribution (LTD) as a Function of Weight Distribution for all Phase 1 and Phase 2 Test Vehicles.

is consistent with achieving understeer. LTD also generally varies directly with front weight distribution. The trend here is more consistent then that in Fig. 15, with the small front wheel drive passenger cars now consistent with the general trend.

The Figure 16 data do not imply a very precise relationship between LTD and weight distribution, but there are some interesting trends that can be cited as we move along the diagonals. Moving along the diagonal from the lower left to upper right corners implies increasing understeer as the front axle tires are increasing in saturation due to both increased weight and increased load transfer during cornering. Moving along the opposite diagonal away from the 50% diagonal point implies early wheel liftoff at the axle indicated. Note that several small front wheel drive passenger cars are situated in the direction of early rear wheel liftoff which is typically observed with the cornering of these vehicles. It is interesting to note here that when wheel lift off does occur, load transfer at that axle remains constant with increased cornering severity, while the outside tire of the other axle takes the brunt of load transfer thereafter. There are other factors that contribute to limit oversteer and dynamic instability, including bump stops, suspension lift, wheel camber and tire characteristics, so the Figure 16 diagram gives only a part of the story. Further results from field testing and simulation analysis will be shown to be consistent with some of the Figure 16 implications.

C. TIRE CHARACTERISTICS

As noted previously, tire characteristics have an extremely important influence on vehicle handling and stability as discussed in Section II and analyzed in some detail in Reference 5. Tires provide the maneuvering forces for lateral and longitudinal acceleration. Sufficient lateral acceleration can induce rollover and premature rear tire force saturation can induce directional instability. Tire characteristics are critical to the computer simulation used for stability analysis herein, and appropriate camber thrust saturation effects are essential for rollover situations. Past simulation work (Refs. 4, 5) has been accomplished using Calspan tire test data (Refs. 15, 16) since the simulation tire model was originally set up to be specified directly in terms of standard Calspan coefficients (Ref. 15).

A majority of the test vehicle population tire characteristics in this project were described directly from published Calspan data. Additional on-road testing was undertaken as part of this effort, however, to meet two key objectives:

- to obtain on-road asphalt surface data as a cross check and validation of tire machine data obtained on the Calspan TIRF facility
- to obtain camber sweep data up to large camber angles typical of rollover conditions

The second objective was critical to the overall goal of this project of obtaining a better understanding of rollover conditions. As rollover proceeds, tire camber increases which acts to relieve tire side force and thus reduce the basic source of rollover moment. At high tire slip conditions, required to generate the high side forces necessary to induce rollover, the camber side force relieving effect must saturate in a manner similar to the side force saturation effect occurring at high slip angles and slip ratios if a sustained rollover moment is to be maintained.

Collection of validation data for camber saturation effects required sweeping camber angle at high side slip conditions in order to obtain data under conditions that approximate rollover. To accomplish this a special apparatus was constructed at the University of Maryland Department of Mechanical Engineering that permitted simultaneous large steer and camber angle operating conditions (Ref. 22). The truck mounted apparatus, permitted tires to be tested under actual road surface conditions. Steer and camber angle and brake force were controlled hydraulically, and resulting forces and moments were measured with a series of load cells placed in the constraining structure mounted to the truck test bed. Test runs on eight tires (seven were the same brand and type found on phase 1 field test vehicles) were conducted at approximately 10 mph in a parking lot at the University of Maryland. Tests were conducted over a range of normal loads nominally at 50%, 100% and 150% of operating loads on the test vehicles involved in this project.

The testing included steer angle, camber angle and braking sweeps required to obtain Calspan coefficients (Ref. 15) that describe tire force response characteristics and are used directly in the tire model of the computer simulation described in Appendix A and References 4 and 5. Raw force response data

was smoothed and fitted with Calspan coefficients using regression analysis procedures. A test tire found on one of the phase 1 field test vehicles (the #34 utility vehicle) had also been tested by Calspan for research conducted at the NHTSA Vehicle Research Test Center (VRTC) in Ohio. Calspan tire machine measurements are compared with University of Maryland field measurements in Table 4, and the following correspondences are noted:

TABLE 4. COMPARISON OF CALSPAN AND UNIVERSITY OF MARYLAND (UMCAR) TIRE TEST COEFFICIENTS: BRIDGESTONE SF-405 P205-70R15 @ 25 PSI

FZ LB.	Yalpha CALSPAN lb./deg	Yalpha UMCAR lb./deg	Ygamma CALSPAN lb./deg	Ygamma UMCAR lb./deg	S%slip CALSPAN lb./%sl	S%slip UMCAR lb./%sl
390	135.7	137	10.1	7	–	147
650	199.3	195	11.6	10.1	–	125
910	231	228	13.2	11.3	–	162
1170	234.7	242	15.5	19	–	312
FZ LB.	μypeak CALSPAN –	μypeak UMCAR –	α@μypk CALSPAN deg	α@μypk UMCAR deg	μxpeak UMCAR –	%sl@μxp UMCAR –
390	1.06	1.14	10.3	6	1.05	5
650	1.01	1.05	6.8	7.5	–	–
910	0.95	0.97	8.3	9	0.9	7
1170	0.91	0.86	12.4	9.5	0.84	5

- Side force response to steer angle - this variable, denoted as Yalpha herein and as Calpha by Calspan, has significant influence on vehicle handling under low g steering maneuvering conditions. The absolute magnitude and change with normal load are quite comparable.

- Side force response to camber angle - this variable, denoted as Ygamma herein and as Cgamma by Calspan, has minor influence on vehicle handling under low g cornering conditions, and significant influence under rollover conditions which result in large camber angles. The Calspan and U. of Md. measurements are comparable at nominal normal loads, but the U. of Md. measures show much more load sensitivity at low and high loading extremes.

- Maximum coefficient of friction - this variable influences limit performance maneuvering. Peak values and the steer angle at which the peak occurs are comparable at nominal

loads. The U. of Md. measurements show more load sensitivity for the peak coefficient of friction and less sensitivity in the steer angle at which the peak occurs at extreme low and high loads.

The above comparison does not indicate any serious disagreement between tire machine and field test measurements. As discussed above, the field test apparatus used here was also capable of large camber sweeps so that data on camber side force saturation could be observed. Camber sweep data from 0 to 30 degrees were collected over a range of constant slip angle operating conditions. The data were then reduced via regression analysis to give camber stiffness coefficients at each slip angle operating condition. A summary plot of the camber side force response at various steer angles is shown in Figure 17. The relationship between slip angle and camber angle effects in Figure 17 are the same as occur during rollover, where increasing slip angle causes increasing side force and increasing camber angle in response to the steer induced side force reduces the total side force. Here we see that as slip angle is increased the camber side force sensitivity decreases, and that in the region of slip angle saturation camber angle sensitivity approaches zero. Thus, as tires saturate due to high cornering slip angles, camber angle has minimal influence on the side force response.

Figure 18 summarizes additional tire measurement characteristics obtained through regression analysis for the phase 1 field test vehicle tires. Cornering stiffness (Fig. 18 a)and peak side force coefficient of friction (Fig. 18 b) show a very consistent decline with normal load for all tires. The utility vehicle #34 has one of the most aggressive tires, which when combined with a low track width ratio makes this vehicle quite vulnerable to rollover under limit maneuvering conditions. Traction stiffness (Fig. 18 c)and peak coefficient of friction (Fig. 18 d) show some limited load dependency, but with considerably less consistency across tires than for the side force characteristics. The slide coefficient of friction (Fig. 18 e) shows fairly consistent load dependency, with values that are on the order of 20% below the peak coefficient of friction values. Load normalized camber coefficient (Fig. 18 f) does not show very much load variation consistency across tires, and on a per degree basis camber angles result in only about 10% of the side force developed from slip angles. Thus camber effects exert only a small influence on total tire side force output.

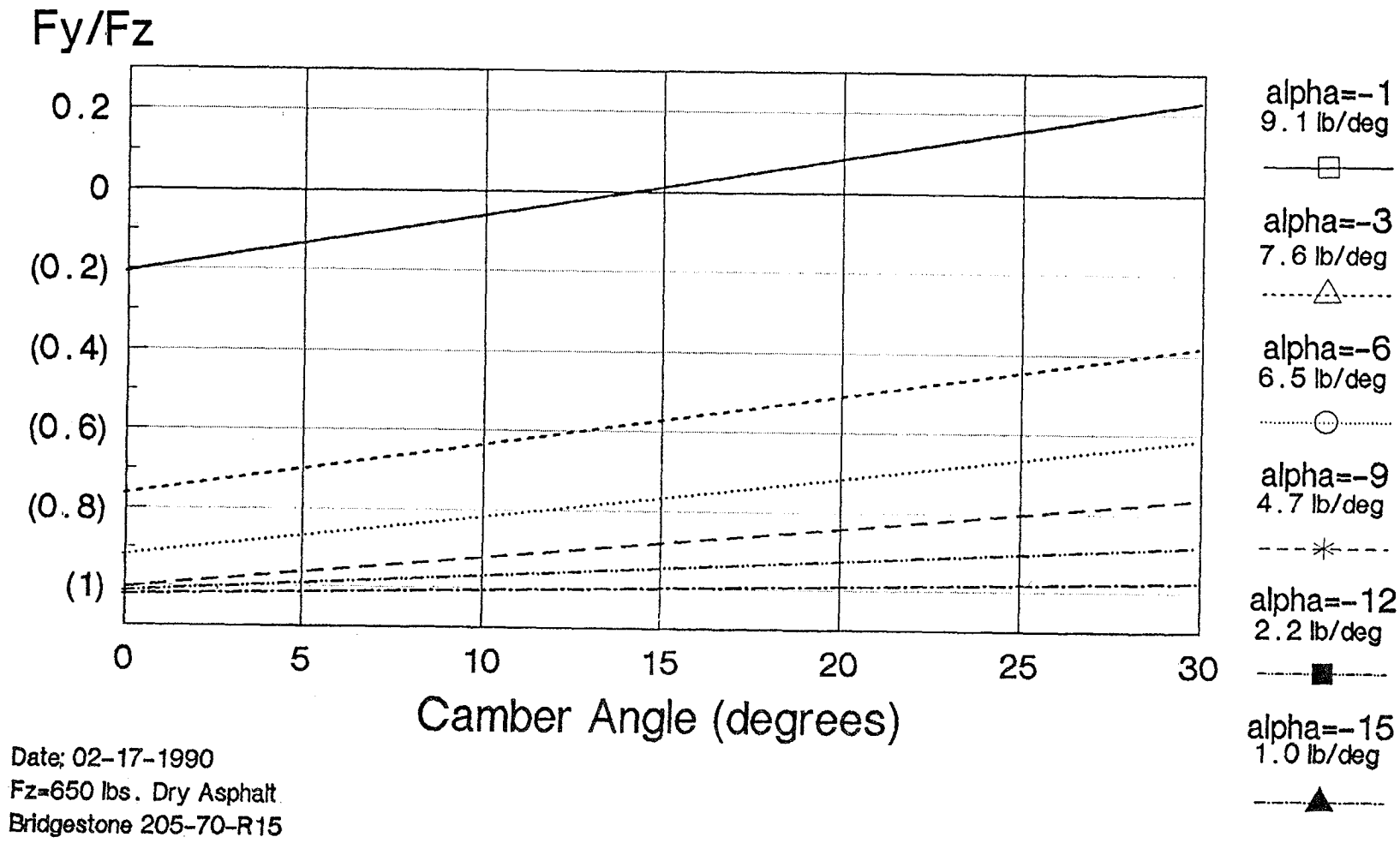

Figure 17. Camber Side Force Response over a Range of Side Slip Conditions

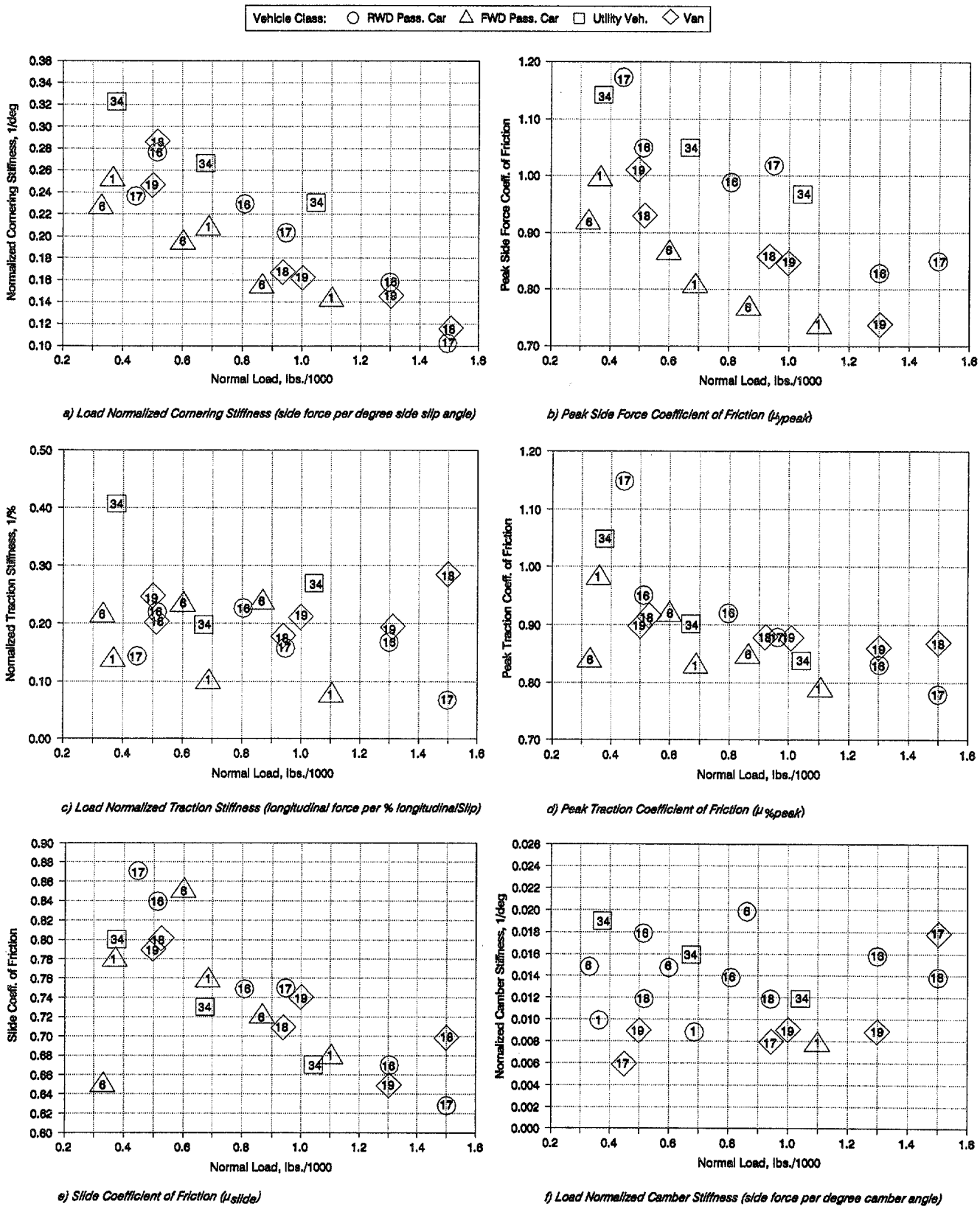

Figure 18. Measured Tire Response Characteristics for Phase 1 Field Test Vehicles (Table 2).

D. SIDE PULL TEST

The rollover sensitivity of all Phase 1 and Phase 2 test vehicles in this project was characterized by the sidepull test shown schematically in Figure 19. The purpose of this test is to simulate the lateral inertial forces acting on a vehicle that occur due to lateral acceleration, e.g. during cornering. The side pull force is directed through the vehicle c.g. (center of gravity), parallel to the horizontal plane and normal to the vehicle longitudinal centerline. The side pull force required to cause rollover is generally related to the track width ratio, but several other factors come into play as indicated in Figure 19. As the vehicle sprung mass rotates about the roll axis, the sprung mass center of gravity moves closer to the outside wheel rollover axis. Furthermore, due to tire and suspension compliance, the outside wheel rollover axis and the center of gravity are brought even closer together, so that the resulting effective track width at rollover is significantly narrower than the basic static level. The sprung mass center of gravity can also translate vertically because of the suspension response to the side forces and suspension kinematics as discussed in Appendices A and C. Some vehicles squat which improves rollover resistance while other vehicles jack up which reduces rollover resistance. Details of the side pull test procedures are given in Appendix G.

As indicated in Figure 19, the side pull force required for rollover can be expressed as an equivalent lateral acceleration in g (acceleration due to gravity) units when divided by the vehicle weight. This equivalent lateral acceleration is a measure of the effective track width to c.g. height ratio for the vehicle at tip over. This effective ratio is compared to the static track width ratio for the test vehicle population in Figure 20. Slopes have also been indicated in Figure 20 that relate the equivalent tip over acceleration to a percentage of the static track width ratio. This percentage is referred to as an efficiency factor, with higher efficiency indicating a higher rollover resistance at a given track width ratio. Aside from one pickup, passenger cars are noted to have amongst the lowest efficiency factors, while trucks, vans and utility vehicles tend to have higher efficiency. The vehicles with the worst rollover tendencies would be found at the bottom of Figure 20, which includes trucks, vans, utility vehicles and one passenger car (#2). Two passenger cars (#'s 2, 9), a sport car (#11), a pickup (# 28) and a utility vehicle (#41) have

$$\frac{a_{y_{RO}}}{g} = \frac{\text{Side Pull Force}}{\text{Vehicle Weight}} \; ; \; \text{Rollover Condition} -- ma_{y_{RO}} h_{cg} = mgy_{cg}$$

$$\text{or} \quad \frac{a_{y_{RO}}}{g} = y_{cg}/h_{cg}$$

$a_{y_{RO}}$ = equivalent lateral acceleration required for rollover
c.g. = center of gravity
g = acceleration due to to gravity
m = total vehicle mass
x_{cg} = effective half track width
y_{cg} = c.g. height

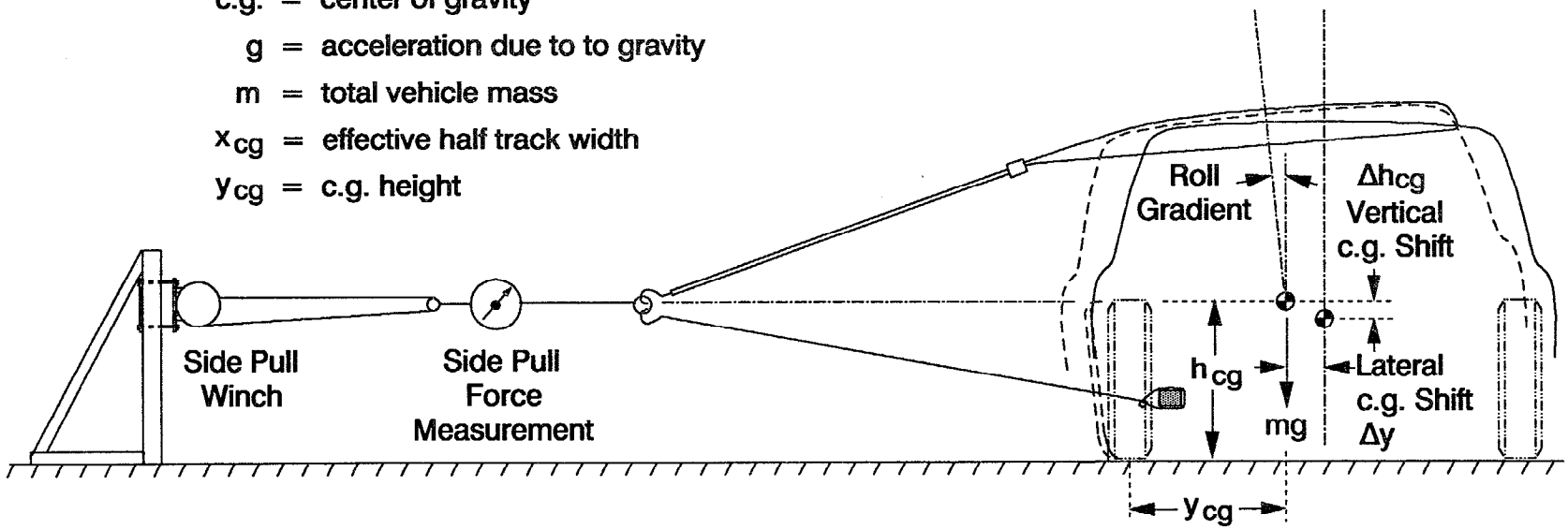

Figure 19. Side Pull Measurement and Variables Related to Rollover

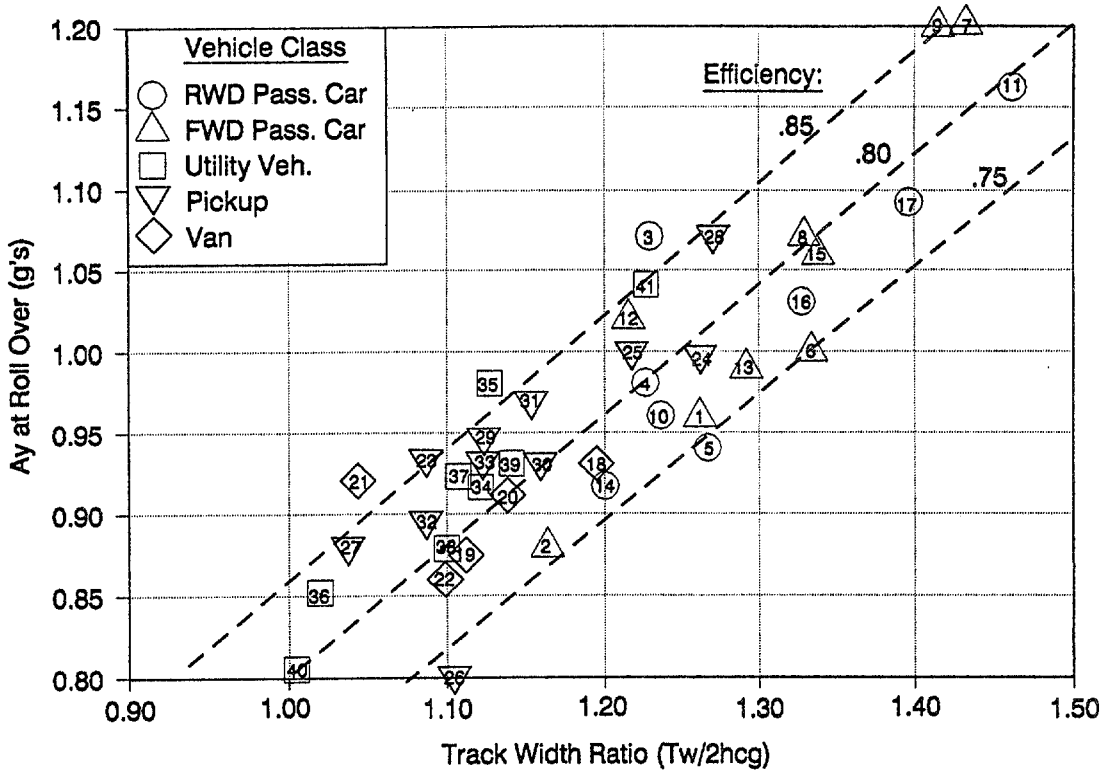

Figure 20. Side Pull Test Results: Equivalent Lateral Acceleration Required for Rollover as a Function of Track Width Ratio for all Phase 1 and Phase 2 Test Vehicles.

notably high rollover resistance values compared to other members of their vehicle classes.

The factors contributing to the rollover efficiency factor were explored using regression analysis. Independent variables considered were the roll gradient, which accounts for the lateral c.g. shift due to roll angle, the change in c.g. vertical location at rollover, which accounts for suspension squat/lift effects, and the change in track width which accounts for tire and suspension compliance effects. The results are summarized in Figure 21 where the rollover efficiency factor is plotted as a function of roll gradient. On a simple correlation basis the most important explanatory variable is roll gradient followed by c.g. height and track change, with the majority of the effect explained by the combination of roll gradient and c.g. height change (52%). Although statistically significant, the regression analysis indicates that only 56% of the variance in rollover efficiency factor is explained by the independent variables which suggests the involvement of additional unexplained factors. Figure 22 shows the relationship between rollover efficiency factor and c.g.

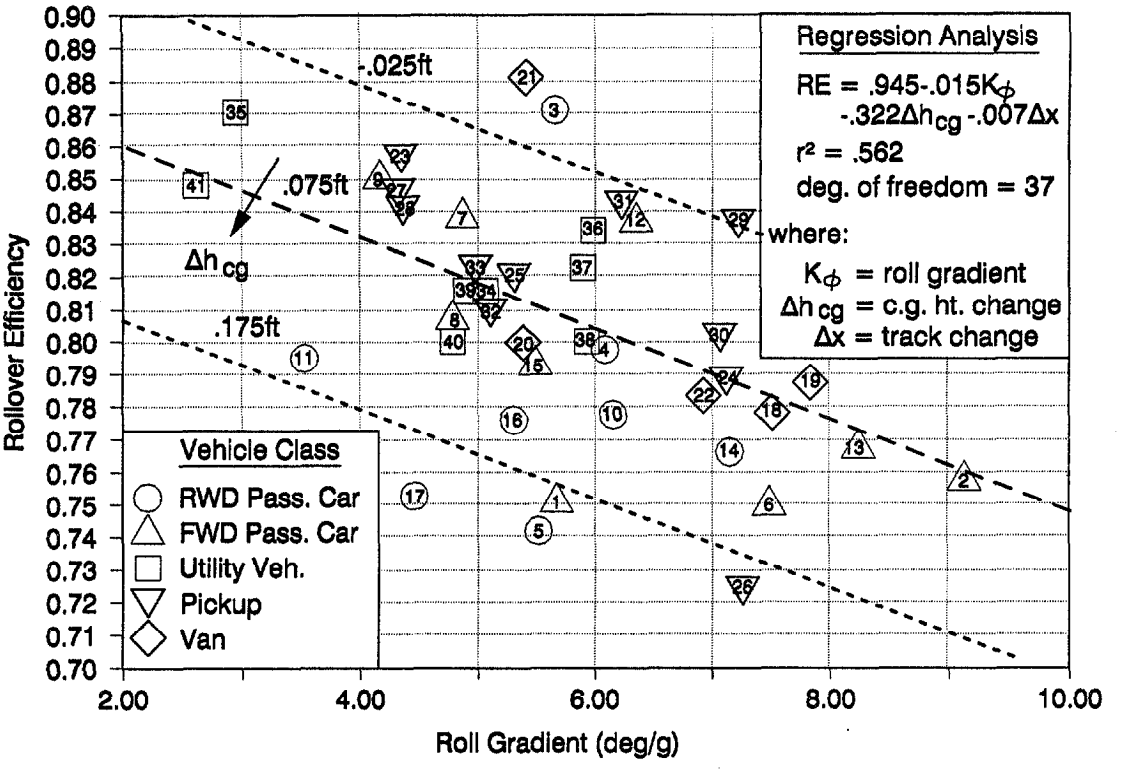

Figure 21. Influence of Vehicle Roll Gradient on Rollover Efficiency for all Test Vehicles

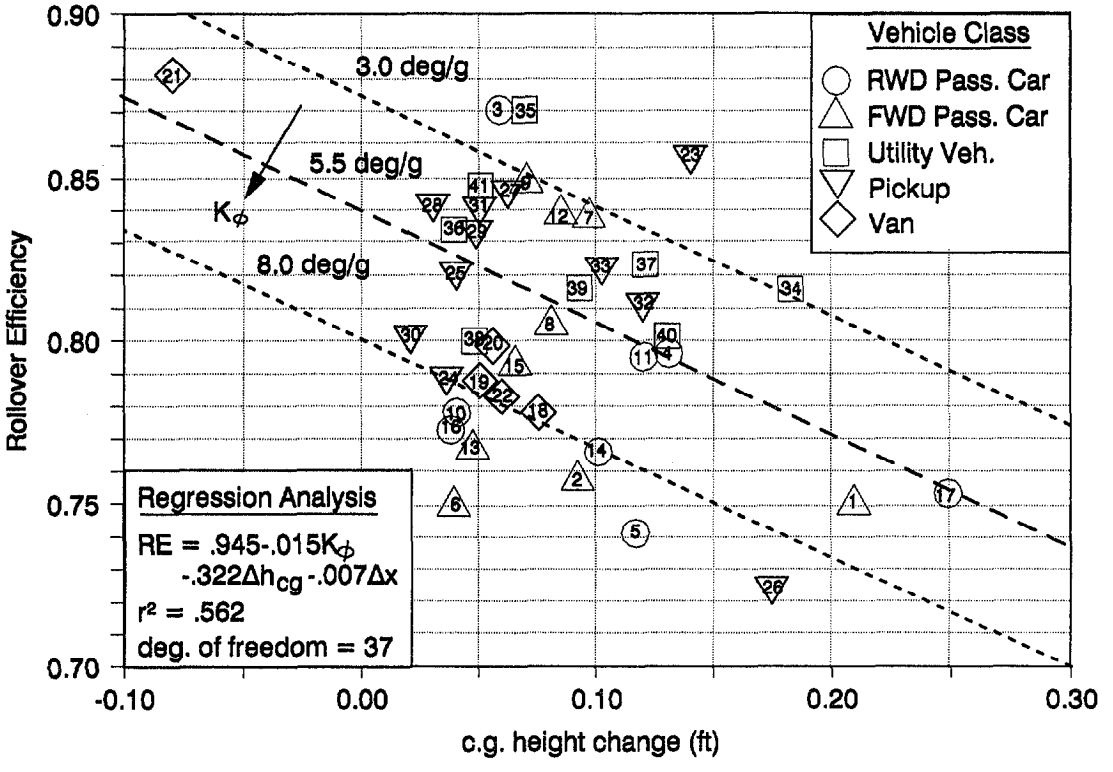

Figure 22. Influence of Vehicle Center of Gravity Height change at Wheel Liftoff on Rollover Efficiency Factor for all Test Vehicles

height change. Note that the largest c.g. height changes are on the order of 3 inches (.25 ft.) which are associated with a small and large passenger car. The majority of vehicles have c.g. height changes on the order of one inch.

For on road maneuvering, the rollover sensitivity of a vehicle depends not only on the lateral acceleration metric discussed above, but also the aggressiveness of the tires which supply the maneuvering force capability. Furthermore, it is the effective maneuvering capacity of the tires on the vehicle, accounting for composite load transfer effects, that is critical. For the twelve phase 1 field test vehicles a steady state cornering test was conducted, as described in the next section, that along with a validated simulation model, allowed maximum cornering capacity to be determined. Table 5 compares the lateral acceleration required for tip over with the cornering capacity determined from field test measurements and computer simulation analysis. This table is very revealing as it illustrates that for vehicles with low rollover lateral acceleration requirements such as 4 X 4 pickups, vans and utility vehicles, tires play a significant role in rollover potential. This also raises a more general issue, that by changing tires and rims (which can influence track width and c.g. height), vehicle rollover potential can be seriously affected. Many sport and recreational vehicles are sold with a variety of tire/wheel options, and vehicle owners have a significant after market selection of options. Thus, rollover potential is not a simple matter of single factory design conditions.

An independent study of vehicle side pull characteristics has been carried out by NHTSA (Ref. 25) using a much more sophisticated apparatus than employed here. Differences in measurements on identical vehicles were found between the STI and NHTSA procedures due to hysteresis, the tire restraining lip, etc. These differences have been identified and accounted for in Ref. 25. The measurements in Figures 20 -22 and Appendix E of this report are felt to be internally consistent for the purposes of this project and appropriate for the conclusions that are drawn.

TABLE 5. PHASE 1 FIELD TEST VEHICLE SUMMARY OF ROLLOVER PROPENSITY METRICS

Vehicle No. Class (App. E)	Side Pull $A_{y_{R0}}$ (g's)	Tire Cornering Capacity (g's)	Steady State Rollover Propensity Margin (g's)
1 Small FWD* Pass. Car	.99	.71	.29
6 Small FWD Pass. Car	1.00	.65	.35
8 Small FWD Pass. Car	1.07	.72	.35
10 Small RWD† Pass. Car	.96	.70	.26
16 Medium RWD Pass. Car	1.03	.69	.34
17 Medium RWD Pass. Car	1.05	.74	.31
18 FWD Van	.93	.72	.21
19 RWD Van	.88	.62	.26
23 Light 4 x 4 Pick up	.93	.78	.15
34 Light Utility Vehicle	.92	.81	.11
37 Light Utility Vehicle	.92	.65	.27
40 Light Utility Vehicle	.81	.68	.13

*FWD = Front Wheel Drive † = Rear Wheel Drive

SECTION V

FIELD TESTING

A. OVERVIEW

Detailed field test procedures and results will be described in this section for three phase 1 vehicles that are representative of the range of test vehicle characteristics. Data for all twelve phase 1 test vehicles can be found in Appendix H. Basic characteristics of the three representative test vehicles are summarized in Table 6. The light utility vehicle (test vehicle #34, Appendix E) is basically characterized by a short wheel base and high center of gravity which imply significant load transfer under high performance maneuvering conditions. The light utility vehicle also has aggressive tires (high coefficient of friction) which means it can sustain higher maneuvering accelerations which will aggravate rollover stability problems under emergency maneuvering conditions. At the other extreme the intermediate sized sedan (test vehicle #17, Appendix E) has high track width and wheel base ratios and moderate tire characteristics

TABLE 6. BASIC CHARACTERISTICS OF EXAMPLE TEST VEHICLES

Parameter			Utility, #34	Sub Compact, #1	Intermediate Sedan, #17
Mass		m(slugs)	72	84	125
Yaw Moment of Inertia		I_z(ft.lb/sec^2)	865	1135	3000
C.G. LOC.	Front Axle	a(ft)	3.33	2.9	4.1
	Rear Axle	b(ft)	3.33	4.95	5.57
	Height	h_{cg}(ft)	2.05	1.83	1.83
Track Width		T(ft)	4.3	4.61	5.1
Wheel Base		1(ft)	6.66	7.85	9.67
Track Width Ratio		$T/2h_{cg}$	1.05	1.26	1.39
Wheel Base Ratio		$1/h_{cg}$	3.25	4.3	5.28

which should represent modest handling and stability characteristics. The small subcompact vehicle (test vehicle #1, Appendix E) has intermediate track width and wheel base ratios and the least aggressive tires of the three representative test vehicles.

The main objective of the field test program was to obtain data for validating the computer simulation model as discussed in Section VI. To this extent we did not obtain large amounts of repetitive field test data from which to empirically describe vehicle characteristics. The emphasis was on obtaining clean data on a small number of runs that would allow model validation over several types of operating conditions. The overall objective of this project was to study vehicle stability problems, although it was never intended to carry vehicle testing to spinout or rollover conditions for safety reasons. Nonetheless, vehicle tests were carried as close to limit performance conditions as safety would permit, and in two cases vehicle spinouts were unintentionally encountered.

Vehicle testing procedures were designed to assess various aspects of vehicle performance, particularly under limit performance conditions, that would allow broad validation of the computer simulation model. Differential tire saturation effects between the front and rear axles are the main cause of directional stability problems, and it was considered essential to include near limit saturation test conditions. Lateral/directional testing included steady state turn circle and transient steer tests carried out as close to vehicle cornering capacity limits as possible. Dynamic response tests using sinusoidal steer frequency sweeps were carried out under low lateral acceleration conditions where tire effects are linear, but input frequencies were carried out to well beyond the vehicle's directional response mode in order to obtain a complete frequency response description of vehicle linear lateral/directional response dynamics.

Braking response tests were also carried out to limit performance brake lockup conditions. Brake characteristics were found to be reasonably well balanced on all vehicles, except for one utility vehicle that did not have a nonlinear brake proportioning valve. Because brake proportioning can vary by 20% or more between vehicles of a given year and model (Ref. 8), braking characteristic analysis for the individual test vehicles was deemphasized relative to lateral/directional properties.

B. INSTRUMENTATION

Vehicle field testing involved steady state and transient braking and steering tests designed to reveal dynamic response and limit performance capabilities of each vehicle. Vehicle instrumentation was set up to allow specification of lateral/directional and longitudinal dynamics. The layout, an expanded set of that used in earlier work (Ref. 17), is shown in Figure 23. An inertial measurement unit (IMU) mounted near the vehicle center of gravity sensed lateral and longitudinal accelerations, and roll and yaw rates. An inertially balanced fifth wheel trolley mounted on the rear bumper measured forward speed, body roll angle and side slip angle. Tachometers were mounted on each wheel to sense rotational rate. Steering angle was sensed with a potentiometer and front and rear axle brake pressure were obtained with pressure transducers. The sensor signals were amplified and filtered with signal conditioning electronics. A laptop computer was used to sample and store the data and provide on-line display or immediate replay of test results to permit monitoring of data quality and test conditions (Ref. 18). Photographs of instrumented vehicles are shown in Figure 24.

The above instrumentation suite was designed to give fairly comprehensive measurements of vehicle lateral/directional and longitudinal motions that could be used to provide validation for a vehicle dynamics computer simulation. The lateral/directional dynamics are characterized by steering input and yaw rate, roll rate and lateral acceleration response. Steady state slip angle of the rear axle can be derived from the fifth wheel trolley side slip angle to give some information on rear axle composite side force response. Lateral acceleration results in inertial forces which stimulate the vehicle roll dynamics as measured by the IMU roll rate gyro and fifth wheel roll potentiometer. The longitudinal dynamics are characterized by brake pressure input and longitudinal acceleration response. The front and rear brake pressure transducers allow measurement of nonlinear brake proportioning valve characteristics. Forward speed and wheel rotational rate tachometers are used to derive tire longitudinal slip ratios which relate to braking tire forces.

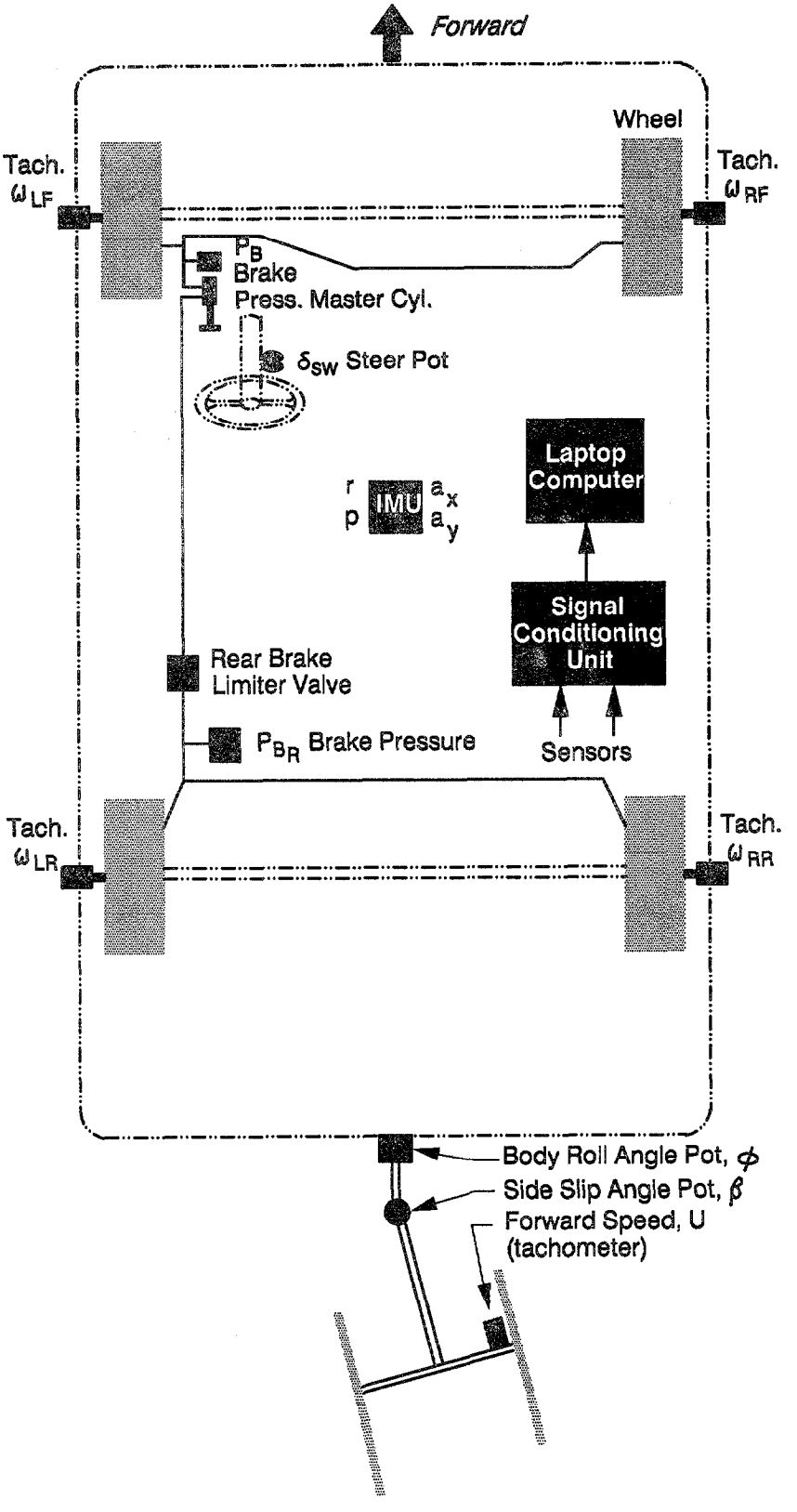

Figure 23. Instrumentation Layout

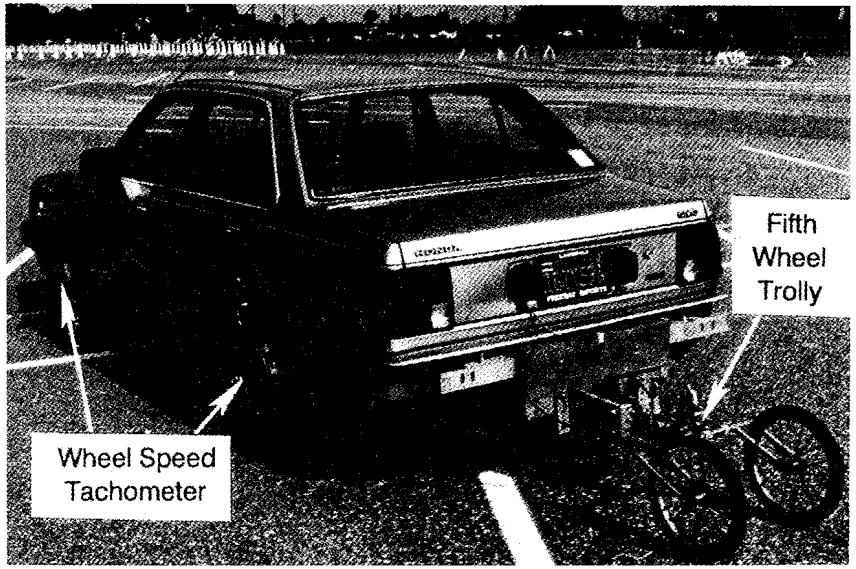

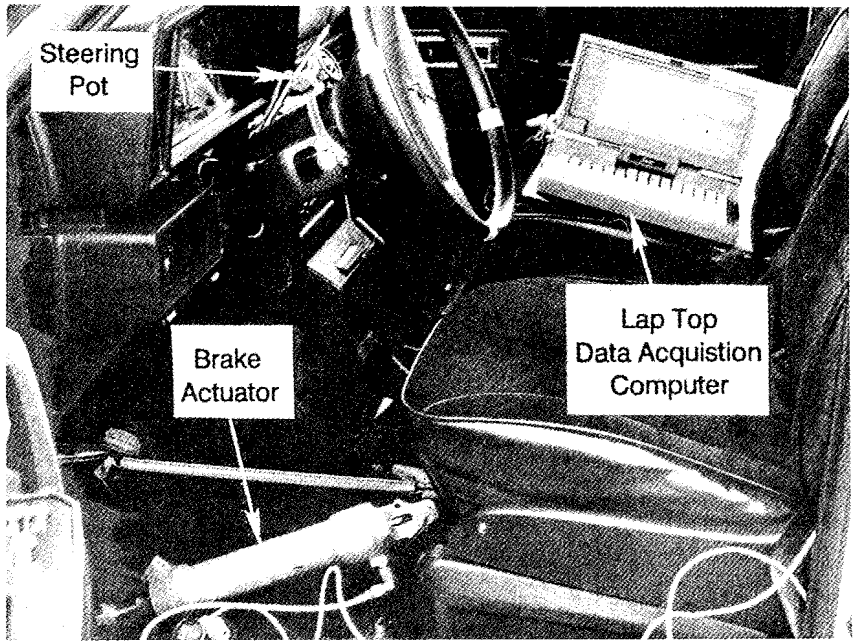

c) Front Seat Instrumentation

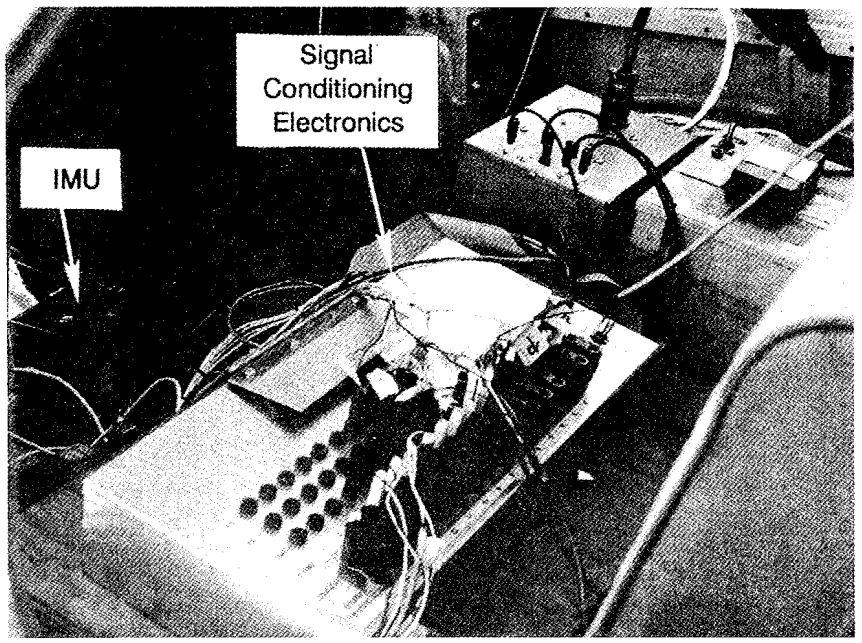

d) Rear Seat Mounted Sensors and Electronics

Figure 24. Vehicle Instrumentation

C. STEADY STATE STEERING RESPONSE

Test maneuvers were specified to adequately exercise vehicle steady state and dynamic response. Steady state steering characteristics are determined by driving around a constant radius circle. The maneuver is started at a low speed (i.e., less than 5 mph) and speed is increased slowly up to the limit understeer condition. This test results in a measure of vehicle steering and slip angle response as a function of lateral acceleration (Ref. 11). Lateral acceleration increases with speed on the turn circle which requires increasing tire side force response. This test basically measures changes in steady state cornering characteristics and roll response as a function of lateral acceleration. These changes result from the composite effect of roll steer, steering compliance and tire force saturation at the front and rear axles due to slip angle and load transfer effects.

Typical steady state turn circle results (computer data cross plots) are shown in Figure 25 for the light utility vehicle (vehicle #34, Appendix E). The steering response indicates a typical understeer characteristic compared to the Ackerman steer required for the 75 foot circle used in these tests. The linear understeer effect at low and moderate g cornering is due to roll and compliance steer effects. At higher g cornering levels the nonlinear understeer effect is due to the front axle tire side force saturation. The slope of the side slip angle versus lateral acceleration characteristic in Figure 25b) permits computing the composite rear axle side force coefficient (differential change in side force with respect to slip angle). The slope is constant at low and moderate cornering g's (the linear tire force response regime) and falls off at higher cornering g levels due to tire saturation. Finally, the roll angle response as a function of lateral acceleration in Figure 25c) basically defines the vehicle's roll gradient. Taken as a whole, the Figure 25 data provide a composite view of the test vehicle's steady state steering response characteristics, which must be exhibited by the computer simulation model as one factor in validation procedures as will be discussed subsequently.

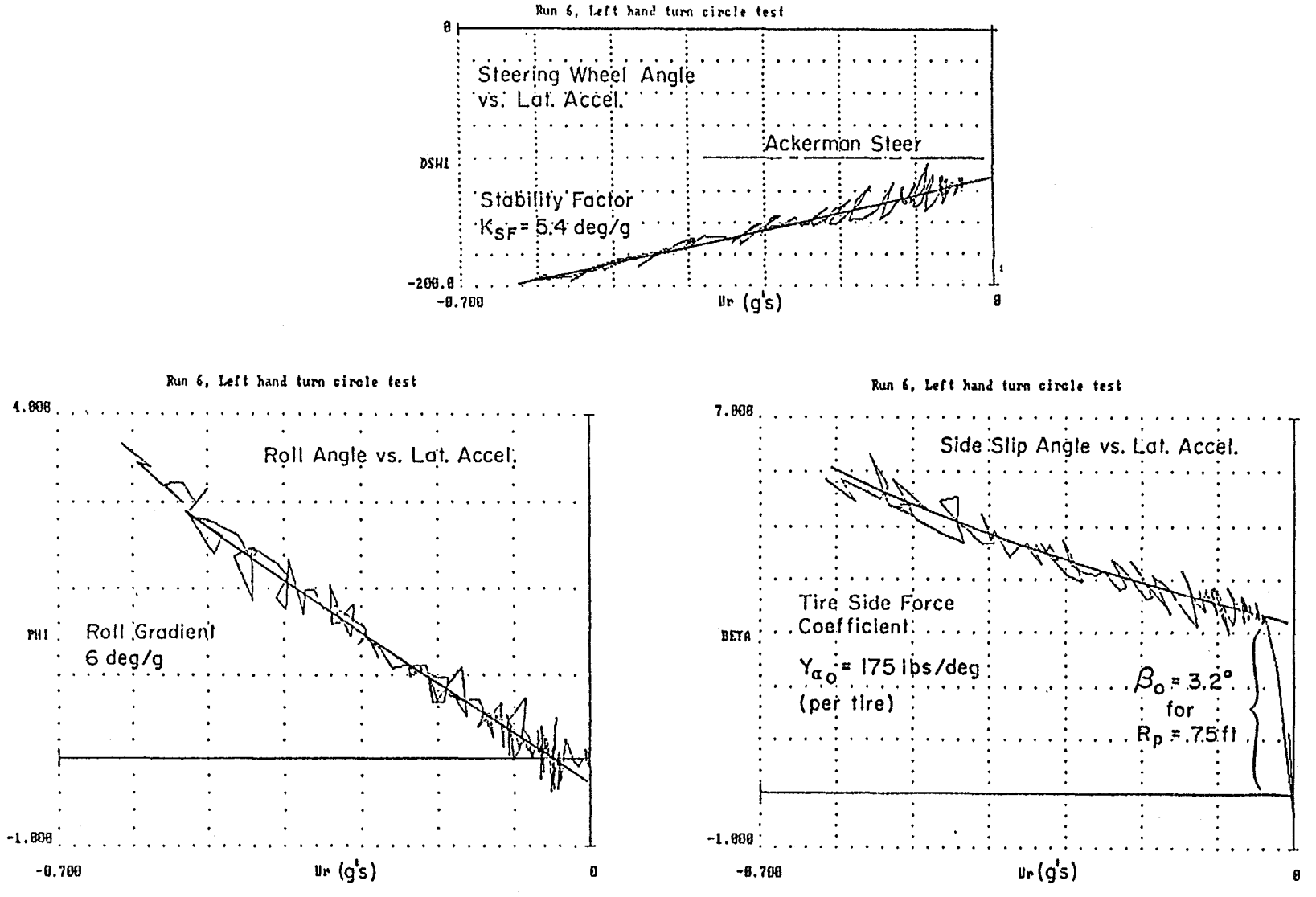

Figure 25. Example Steady State Test Results for a Light Utility Vehicle (Vehicle #34, Appendix E)

D. BRAKING RESPONSE

Vehicle braking response characteristics were analyzed with constant brake pressure and ramp brake pressure runs. Constant brake pressure runs were conducted at increasingly higher pressures to determine the points at which the front and rear axles lock up. Given the longitudinal acceleration and wheel slip ratio, front and rear brake pressure measurements permit computing the proportioning of front and rear axle braking forces. Given these forces over a range of longitudinal acceleration values then permits the brake proportioning diagram to be prepared as shown in Figure 26. The ideal curve is obtained by assuming front and rear axle longitudinal slip ratios which are proportional to braking

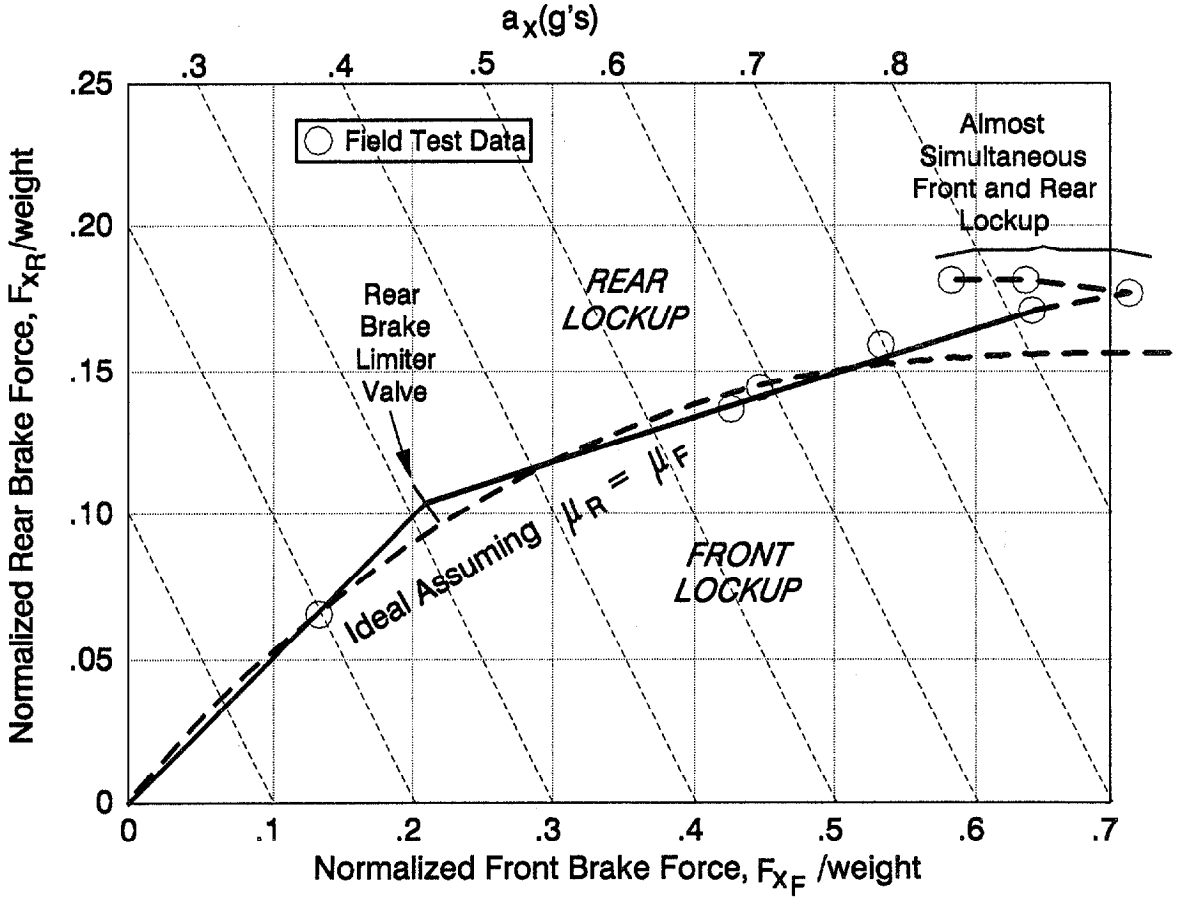

Figure 26. Example Brake Proportioning Diagram for a Small Passenger Car (#1, Appendix E)

force normalized by axle load (Figure 4 and Ref. 5). Because of longitudinal load transfer as dictated by the wheel base ratio (i.e., wheel base divided by c.g. height) brake force proportioning must shift to the front axle at higher braking g levels. If the measured brake proportioning falls off of the Figure 26 ideal curve then the vehicle can be front or rear biased in its braking characteristics. The Figure 26 data show reasonably balanced braking characteristics.

The braking response data in Figure 27 derived from ramp brake stops are the longitudinal equivalent of the steady state steering response curves in Figure 25. During these runs the test driver ramps up pedal pressure to wheel lockup just prior to stopping in order to achieve quasi steady state braking conditions over the full deceleration range. Vehicle deceleration is a relatively linear function of front axle brake pressure and slip ratio as shown in Figure 27 a). The front and rear axle pressure versus slip ratio characteristics also shows relatively linear characteristics because of the braking force response characteristic of the tires. The relationship between the front and rear brake pressures shows the effect of the nonlinear proportioning valve.

Because of the brake proportioning variability that exists between vehicles of a given model year due to a variety of in-use factors (Ref. 8), identification of braking characteristics was not emphasized. Vehicles with nonlinear proportioning valves showed reasonably well balanced braking characteristics. One notable example (vehicle #40, Appendix E) did not have a nonlinear proportioning valve. The vehicle had rear biased brake proportioning at the dry pavement traction limits, and exhibited some spinout tendency under hard braking. Serious front brake bias would exist for stopping on low coefficient surfaces.

E. DYNAMIC RESPONSE

The basic lateral/directional dynamics of the test vehicles were measured with a sinusoidal steer test. During this test the driver produces a sinusoidal steering input that starts at low frequency and is increased to the maximum that can be generated. As shown in Figure 28 the steering input produces sinusoidal vehicle motion responses. Fast Fourier transform (FFT) procedures are then applied to the steering input and motion responses to give power spectra, describing functions and coherence (Ref. 24 analogous to the linear correlation coefficient) as illustrated in Figure 29. Describing functions give the

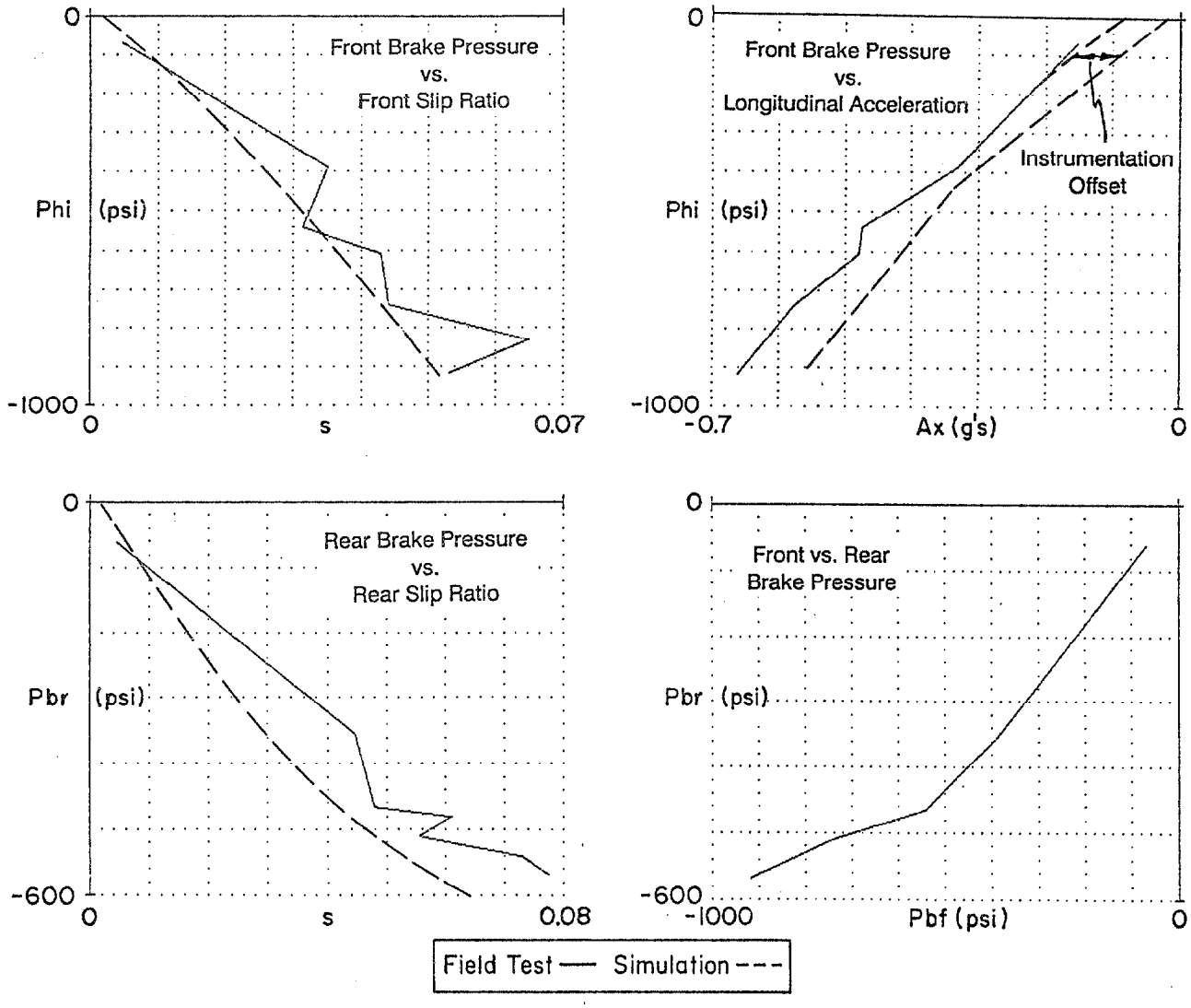

Figure 27. Example Ramp Brake Test Date for a Light Utility Vehicle (Vehicle #34, Appendix E)

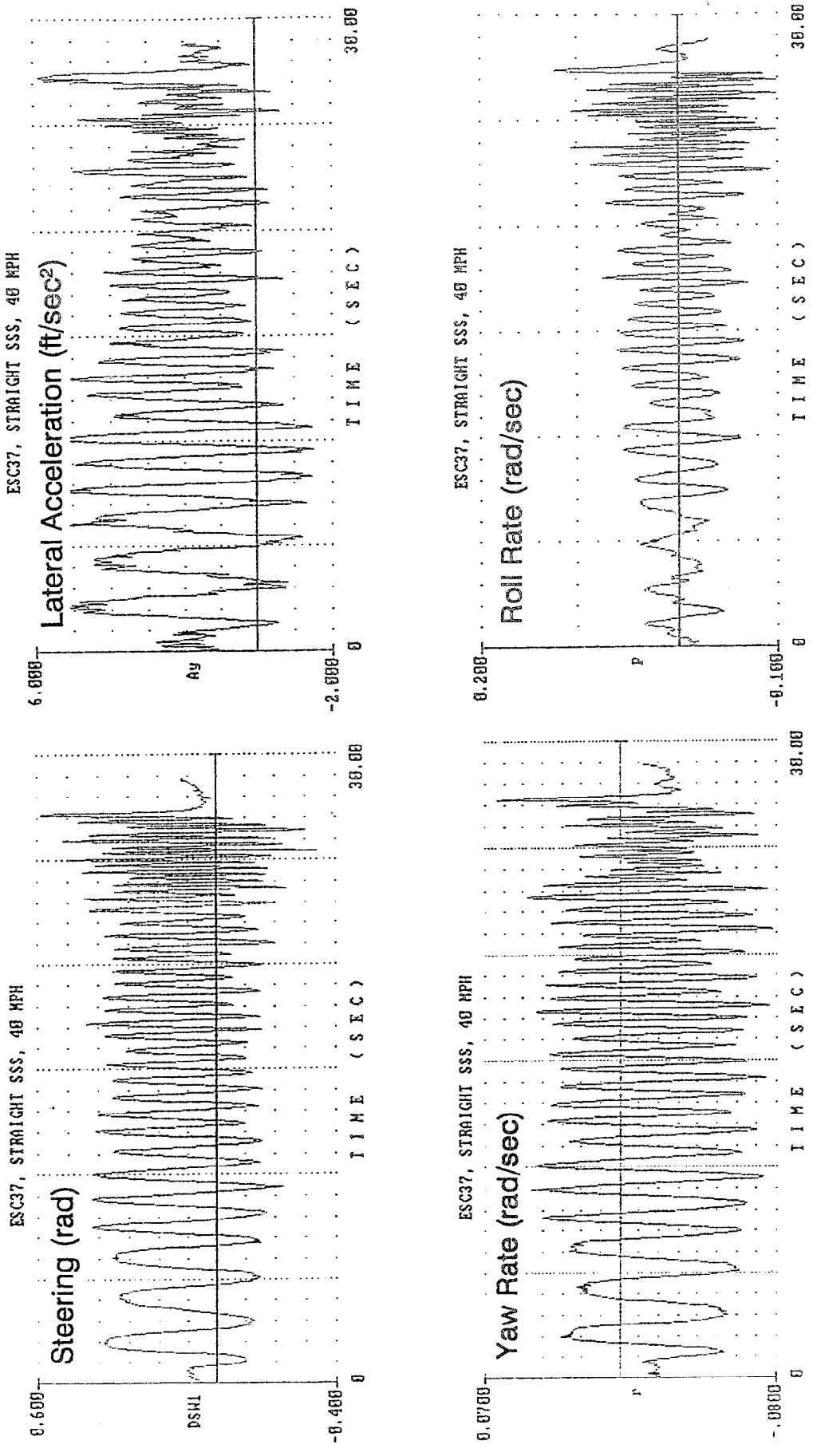

Figure 28. Example Sinusoidal Steer Date for a Small Passenger Car (#1, Appendix E)

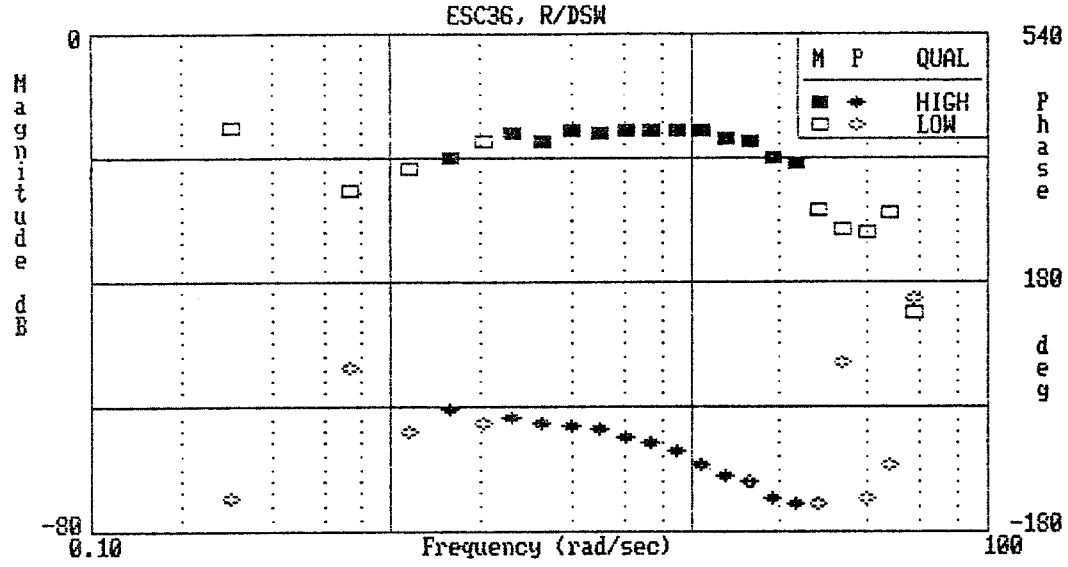

a) Transfer Function

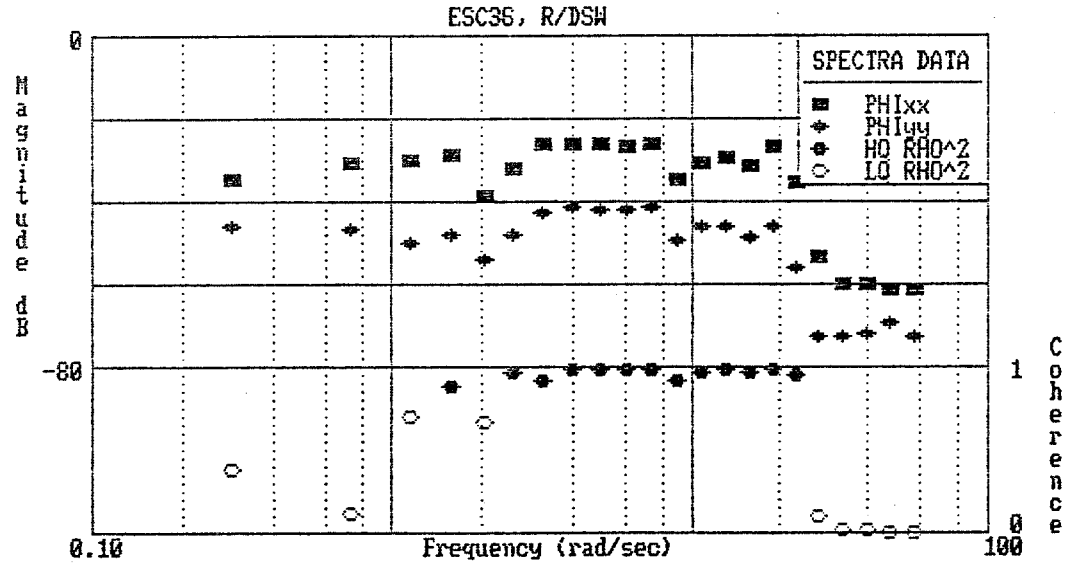

b) Power Spectra and Measurement Coherence

Figure 29. Example Steering to Yaw Describing Function Data for a Small Passenger Car (#1, Appendix E)

frequency response between steering input and vehicle motion variables. The motion variables of interest here for the purposes of computer simulation validation include yaw rate, roll rate and lateral acceleration.

Typical describing functions are shown in Figure 30. The yaw rate describing function is typified by an upper bandwidth limit that is a function of vehicle tire and steering characteristics and yaw moment of inertia. The lateral acceleration describing function shows the typical null response at mid frequencies where the vehicle rotates about the c.g. and produces little measurable lateral translation. Lateral acceleration provides the inertial force input to the roll dynamics, and the roll describing function exhibits some effect of the null response mode. Describing functions were run over a range of speeds as illustrated in Figure 31. Note that the high frequency phase lag changes very little as a function of forward speed. This is consistent with previous analysis (Refs. 5 and 19) which showed that tire lag decreases with speed while vehicle inertial dynamic lags increase with speed and these two effects tend to cancel over a fairly wide speed range important in handling and stability.

F. TRANSIENT RESPONSE

The final test maneuver involved a severe transient steering input designed to reach maximum cornering capability and provide significant roll mode stimulus. Although this maneuver is intended to reproduce limit transient steering effects, some caution was observed when testing vehicles with significant rollover propensity (i.e., low track width ratio or roll stability parameter). The maneuver amounted to a hard turn towards one side of the test course, a hard turn in the opposite direction, then a return to the center line. Typical results for the transient steering maneuver are shown in Figure 32. This run resulted in a measured peak body referenced lateral acceleration of nearly 0.9 g, which amounts to a lateral acceleration on the order of 0.8 g when a 10% body roll correction is accounted for. The side slip measure shows significant side slip indicating significant tire saturation effects.

The transient response maneuver was intended to be near limit performance, but stable. Some care was taken in testing the phase 1 field test vehicles described in Appendix E that were known to have low rollover propensity margins in order to avoid rollover. Since the primary objective of the field testing was to provide data for computer simulation validation, safety devices such as

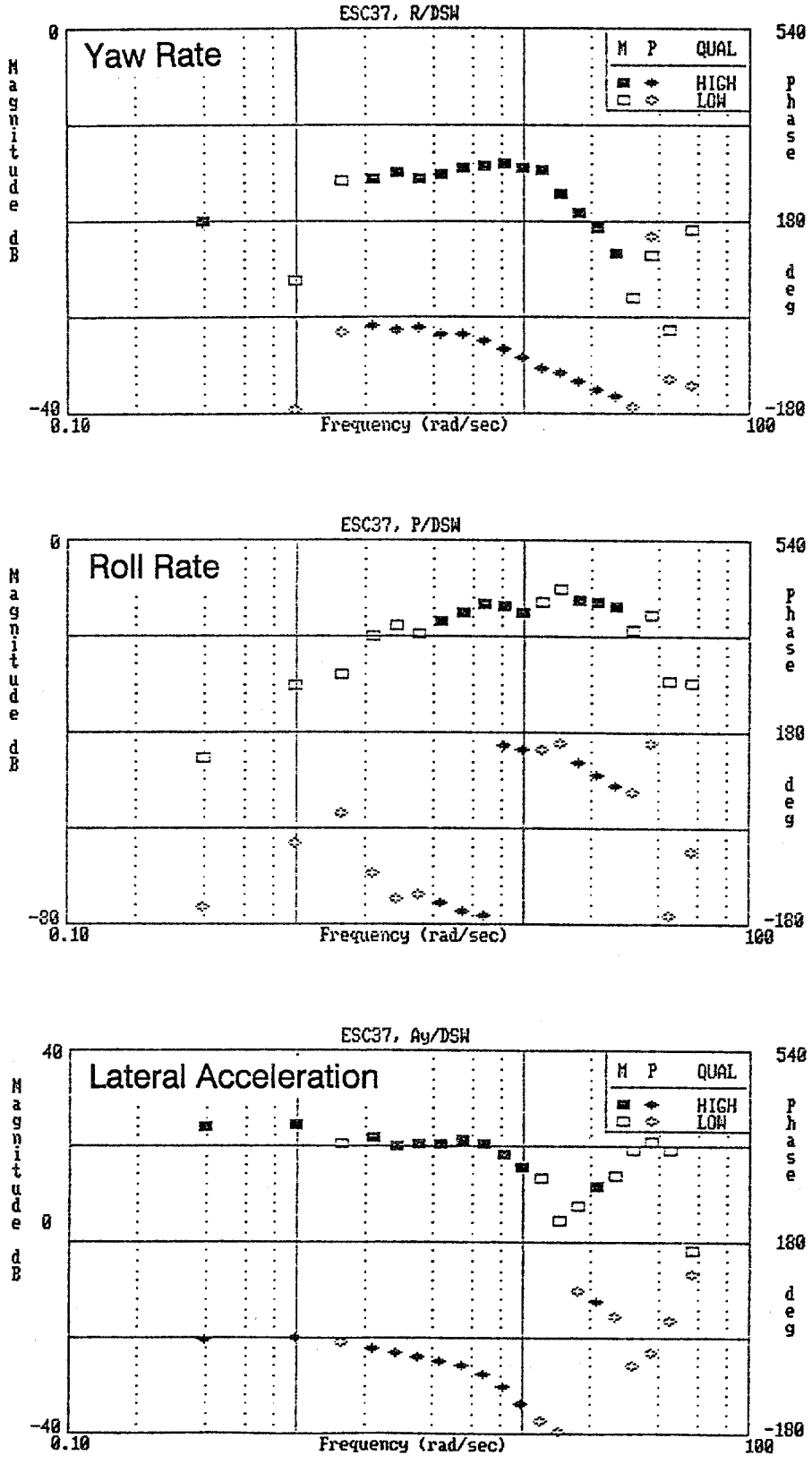

Figure 30. Example Steering Input to Vehicle Response Describing Functions for a Small Passenger Car (#1, Appendix E)

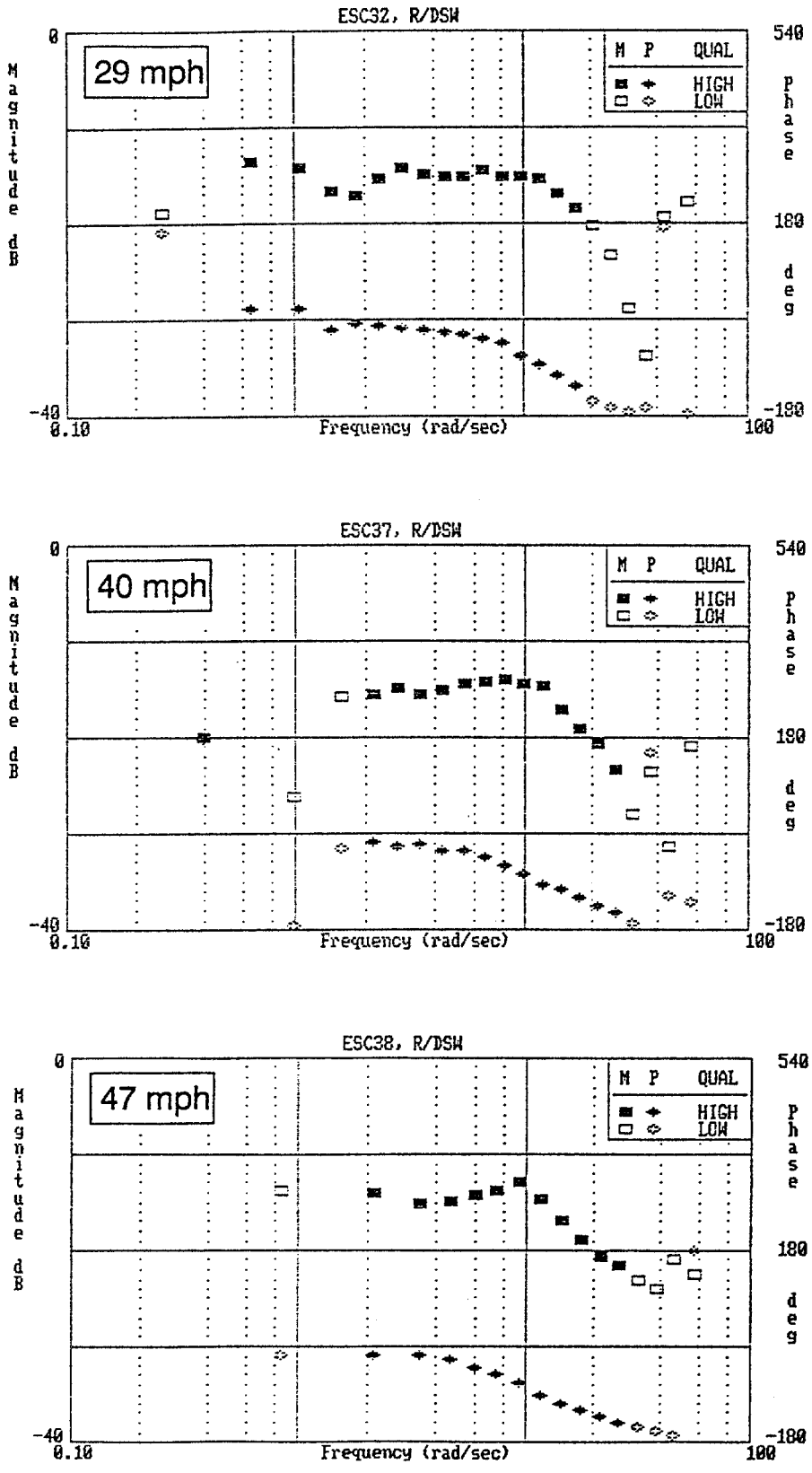

Figure 31. Example Yaw Rate Describing Functions at Several Speeds for a Small Passenger Car (#1, Appendix E)

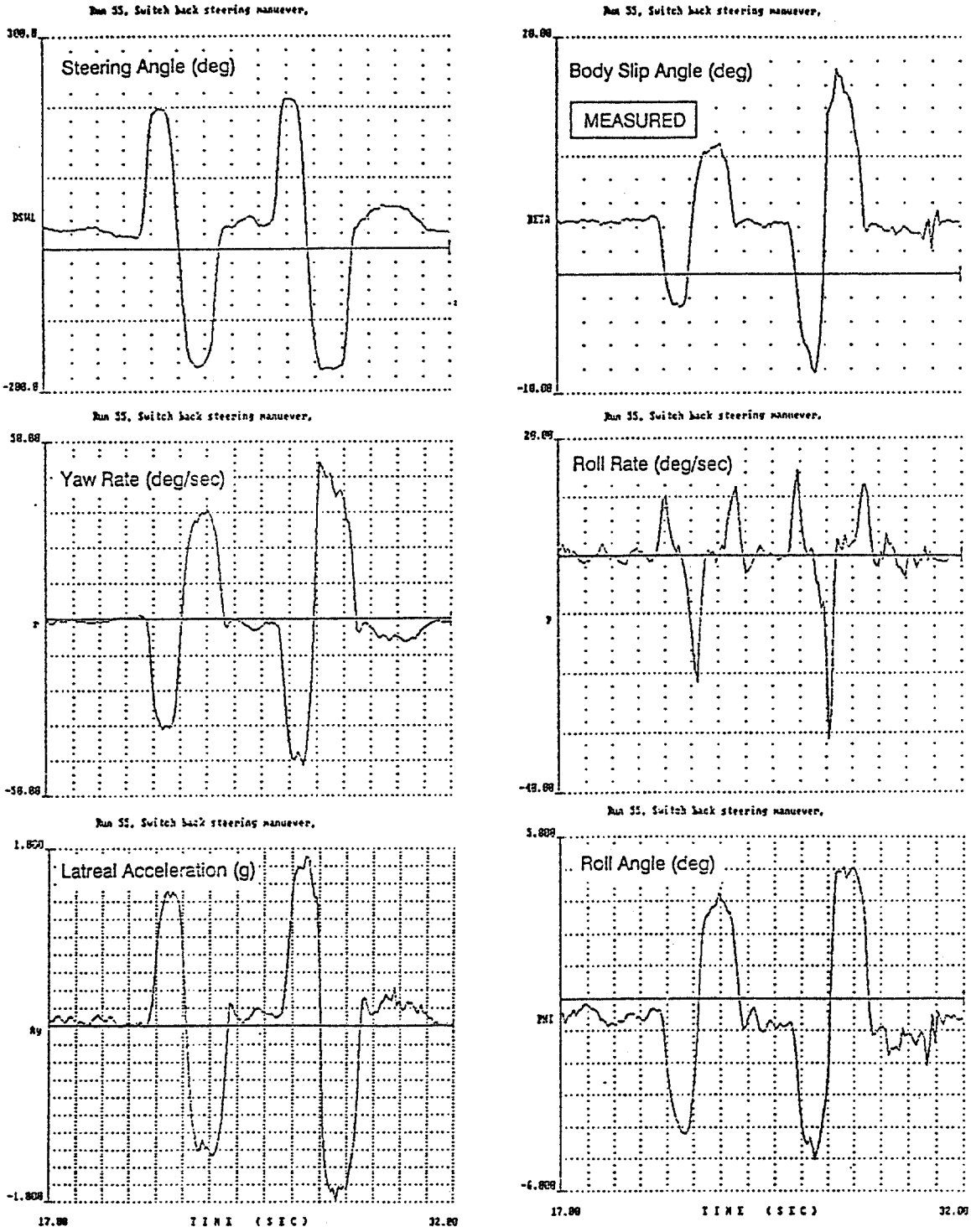

Figure 32. Example Transient Response Steering Data for a Light Utility Vehicle (includes instrumentation offsets) (Vehicle #34, Appendix E)

outriggers were not used in order to avoid changing vehicle response characteristics as little as possible. Nonetheless, two vehicle spinouts were experienced during the field testing. Data from these tests are shown in Figure 33. The subcompact sedan spins out on the second reversal while the pickup spins out on the first reversal. In each case the spinout occurs when the body slip angle exceeds about 0.3 radians (on the order of 17 degrees) which would have clearly saturated the rear axle. Because the steering wheel was returned to near zero, the front axle side slip is probably somewhat less than saturated, which results in an unbalanced yawing moment that causes the spinout. The sequence of events leading up to a spinout will be explored in more detail in Section VII with computer simulation analysis.

G. SUMMARY OF FIELD TEST MEASUREMENTS

A general summary of the results for the field tests measurements on the twelve phase 1 vehicles is given in Table 7. The steady state turn circle test basically allows identification of the vehicles' low to moderate g understeer and roll gradient characteristics, and the limit performance cornering capability. The understeer characteristics vary from a low of 1.7 deg/g to a high of 7.1 deg/g with a median in the range of 3.5 to 3.8 deg/g. The lowest understeering vehicle (a small front wheel drive sedan, also experienced a spinout during testing. The second vehicle that experienced a spinout (a light 4 wheel drive pickup) had the second highest understeer. Referring to the turn circle test data for this pickup (vehicle #8, Appendix H) shows that although the low g understeer is high, under limit cornering conditions the front and rear axles limit almost simultaneously. Roll gradients show nominal values with the two vans and one small front wheel drive car having the highest values. The utility vehicles tend to have smaller roll gradients due to stiff suspensions, while the passenger cars in general have intermediate values. The cornering limit capacity ranges from a low value of .62 g's for a rear wheel drive van to a high of .81 g's for a small utility vehicle. Both of these vehicles have low rollover stability metrics, and subsequent analysis will show that the aggressive tires on the utility vehicle give it a significant rollover tendency.

The dynamic response testing (i.e., FFT analysis of sinusoidal steer inputs) is summarized in terms of the phase lag characteristics of the steering input to yaw rate output transfer function. Previous research has shown that the yaw rate

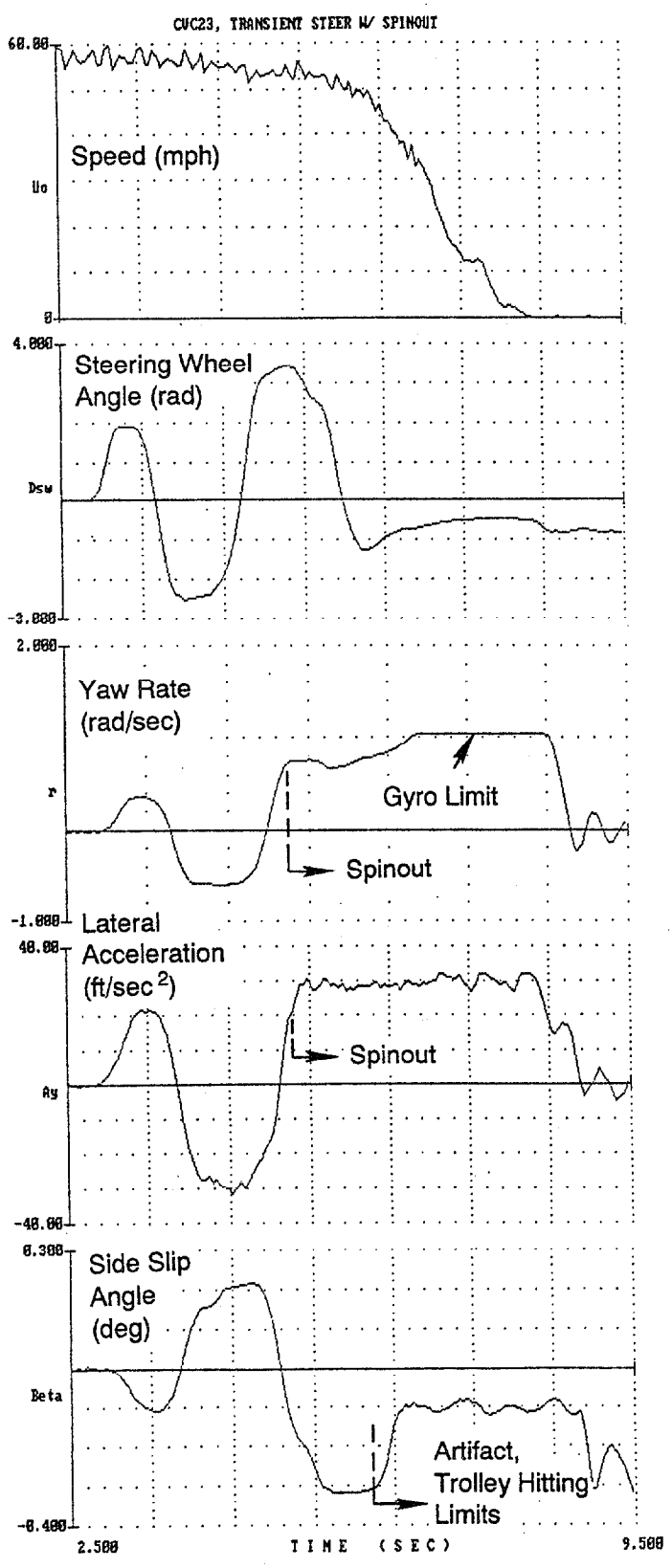

a) Subcompact Sedan (Veh. no. 8, App. E)

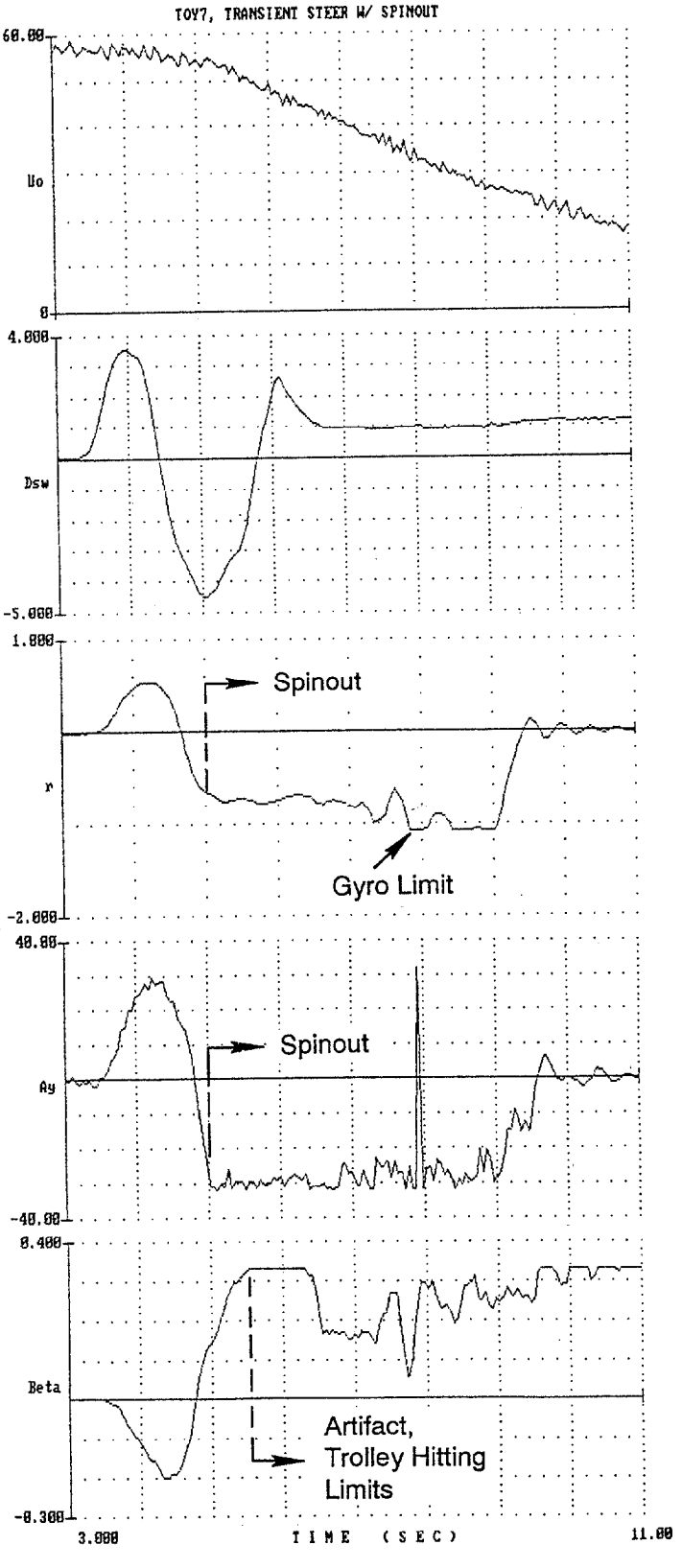

b) Pickup (Veh. no. 23, App. E)

Figure 33. Transient Maneuver Spinout Cases

TABLE 7. FIELD TEST MEASUREMENT SUMMARY

Vehicle Ref.No. (App.E)	Type	Steady State Test			Dynamic Response Test[3] (Yaw Rate TF)		Straight Line Braking Tests First Lockup
		Understeer (deg/g	Roll Gradient (deg/g	Cornering Limit (g's)	Freq.@ 45° Phase Lag (rad/sec)	Freq.@ 90° Phase Lag (rad/sec)	
1	Small FWD Car	3.8	6.9	.71	6.9	11.7	Right Side/Rear
6	Small FWD Car	3.2	9.2	.65	7.1	12.7	Front
8	Small FWD Car[1]	1.7	6.5	.72	6.9	13.1	Front
10	Small RWD CAr	3.4	6.8	.70	8.0	13.8	Rear
16	Medium RWD Car	3.5	5.3	.69	6.15	11.6	Slight Rear
17	Large RWD Car	5.6	6.0	.74	4.2	10.2	Rear
18	FWD Van	2.5	8.6	.72	6.9	11.5	Rear
19	RWD Van	4.0	8.5	.62	6.8	11.0	Rear
23	Light 4WD Pickup[1]	6.3	7.5	.78	5.0	9.8	Slight Rear
34	Small 4WD Util. Veh.	7.1	5.8	.81	8.1	13.3	Rear
37	Med. RWD Util. Veh.	4.3	6.5	.65	7.8	11.0	Rear
40	Med. 4WD Util.Veh.	2.8	5.0	.68	7.0	11.5	Left Rear/Rear[2]

[1]Spinout during transient response testing
[2]Spinout tendency in straight line braking
[3]Relatively constant over a range of speeds

transfer function can be simply characterized by a yaw rate bandwidth given by the frequency at which the phase lag equals 45 degrees. The inverse of this bandwidth then gives an equivalent time constant for the vehicle's yaw response to steering inputs. In Figure 31 the phase lag characteristic over a range of speeds was relatively constant, which is consistent with previous analysis (Ref. 5). The frequency points for both 45 degree and 90 degree phase shift was determined for each vehicle for a range of speeds and found to be relatively constant, with the average results given in Table 7 for each test vehicle. The 90 degree phase lag frequency includes the basic vehicle yaw rate band width plus higher frequency effects due steering system and tire side force lags. The basic vehicle yaw rate bandwidth results (i.e., the 45 degree phase shift point) range from a high of 8.1 rad/sec (or a time constant of about .12 seconds) to a low of 5.0 rad/sec a time constant of .20 seconds). The light four wheel drive utility vehicle (#34) with the aggressive tires gave the highest bandwidth, while a large rear wheel drive car (#17) gave the lowest bandwidth. The yaw rate bandwidth is a measure of how fast a vehicle will respond to steering inputs. Higher bandwidths may allow the driver to induce rollover more easily in a vehicle with a poor track width ratio and aggressive tires such as #34.

Results from the straight line braking test in Table 7 show some tendency for rear bias, and perhaps some left to right asymmetry. One vehicle, a medium four wheel drive utility vehicle that did not have a nonlinear proportioning valve (vehicle #40, Appendix E) exhibited a spinout tendency under hard braking. As has been noted previously, vehicle brake proportioning within a given model vehicle can vary by as much as 20% (Ref. 8) so the single vehicle results in this project must be taken with some caution.

SECTION VI

COMPUTER SIMULATION VALIDATION

A. OVERVIEW

Validation of the computer simulation for the purposes of handling and stability analysis must consider dynamic response which is determined by vehicle inertial, damping and compliance characteristics as well as the basic nonlinear response of the tires at significant maneuvering accelerations. The nonlinear tire effects can be characterized under steady state maneuvering conditions (Ref. 17), whereas the vehicle dynamic characteristics must be stimulated with time varying control inputs. While complete validation may not be obtained for all aspects of each maneuvering condition discussed below, the overall intent of the validation is to obtain computer simulation models for each of the twelve phase 1 test vehicles that are appropriate for conducting limit performance transient maneuvers.

B. TIRE CHARACTERISTICS

The simulation tire model uses Calspan parameters that map directly into the key tire performance characteristics as a function of load, including:

- low slip cornering, traction and camber stiffness
- peak and slide coefficient of friction

For the limit performance conditions considered here, the main issue is the manner in which camber thrust interacts with and saturates as a function of tire slip conditions. Large camber angles are typically associated with rollover conditions. For on-road limit maneuvering conditions which might lead to rollover, the tires must generate high side force due to large (near saturation) slip angles. Furthermore, cambering due to rollover would tend to reduce tire side force thus alleviating rollover tendency. Calspan coefficients do not deal with the interaction of side slip angle on camber thrust characteristics.

The original simulation tire model (Refs. 4,5) assumed an interaction which has been updated as indicated in Table 8 for the current analysis herein. The side force due to camber, $F\gamma$, is assumed to be given by a camber coefficient times camber angle modified by a saturation function:

TABLE 8. SUMMARY OF BASIC TIRE MODEL EQUATIONS
(Adapted from Refs. 4,5)

1. Composite slip

$$\sigma = \frac{\pi a_p^2}{8\mu_o F_z}\sqrt{K_s^2\tan^2\alpha + K_c^2\left\{\frac{S}{1-S}\right\}^2}$$

2. Force Saturation Function

$$f(\sigma) = F_c/\mu F_z = \frac{c_1\sigma^3 + c_2\sigma^2 + (4/\pi)\sigma}{c_1\sigma^3 + c_3\sigma^2 + c_4\sigma + 1}$$

3. Normalized Side Force

$$* \quad F_y/\mu F_z = \frac{f(\sigma)K_s \tan\alpha}{\sqrt{K_s^2\tan^2\alpha + K_c'^2 S^2}} + F_{y_\gamma}/\mu F_z$$

4. Normalized Longitudinal Force

$$F_x/\mu F_z = \frac{-f(\sigma)K_c' S}{\sqrt{K_s^2\tan^2\alpha + K_c' S^2}}$$

5. Aligning Torque

$$M_z = \frac{K_m a_p^2 \tan\alpha}{(1 + G_1\sigma^2)^2}\left[\frac{K_s}{2} - G_2 K_c \frac{S}{1-S}(2 + \sigma^2)\right]$$

6. Slip to Slide Transition

$$K_c' = K_c + (K_s - K_c)\sqrt{\sin^2\alpha + S^2\cos^2\alpha}$$

$$* \quad F_\gamma = Y_\gamma \gamma \left\{1 - K_\gamma[f(\sigma)]^2\right\}$$

$$\mu = \mu_o\left[1 - K_\mu\sqrt{\sin^2\alpha + S^2\cos^2\alpha}\right]$$

*Modified from Refs. 4 and 5

$$F_\gamma = y_\gamma \gamma \left\{1 - K_\gamma [f(\sigma)]^2\right\}$$

The camber saturation function $1 - K_\gamma[f(\sigma)]^2$ is based on the composite slip saturation function $f(\sigma)$ with an added saturation parameter $K\gamma$. The above saturation relationship has the effect of reducing the effective camber coefficient with increasing composite slip (i.e., cornering and/or braking conditions).

Tire test data in Figure 17 discussed in Section IV.C clearly showed that camber stiffness declines with increasing side slip angle. Figure 34 shows tire camber stiffness coefficient as a function of side slip angle for both test data and the simulation model. Note that the simulation model camber stiffness saturates much more quickly than the actual tire test response. The tire model camber stiffness is expressed as a function of the model's composite slip saturation function, and the data in Figure 34 suggest that a less aggressive function determines camber saturation. The current tire model is still adequate for rollover analysis, however, as camber saturation is appropriate out in the high side slip regions where high tire side forces can contribute to rollover. Also, the total camber thrust force is a small proportion of the total side force, so differences between the actual tire response and tire model are probably not critical as suggested by the tire model side force response plot shown in Figure 35.

C. STEADY STATE RESPONSE

Steady state simulation response was determined with a constant radius turn circle maneuver with slowly increasing speed similar to the field test maneuver. The results for each test vehicle are shown in Figure 36 along with field test comparison data obtained from the turn circle field test. The effect of tire side force saturation is reflected in Figure 36 where the cornering acceleration reaches a limit. The field test data goes out to about 80-90% of the limit and shows good agreement over the measurement range. The Figure 36 steering angle results basically exhibit front axle roll and compliance steer effects under low g conditions and side force saturation effects under high g conditions. Body slip angle relates to similar rear axle effects.

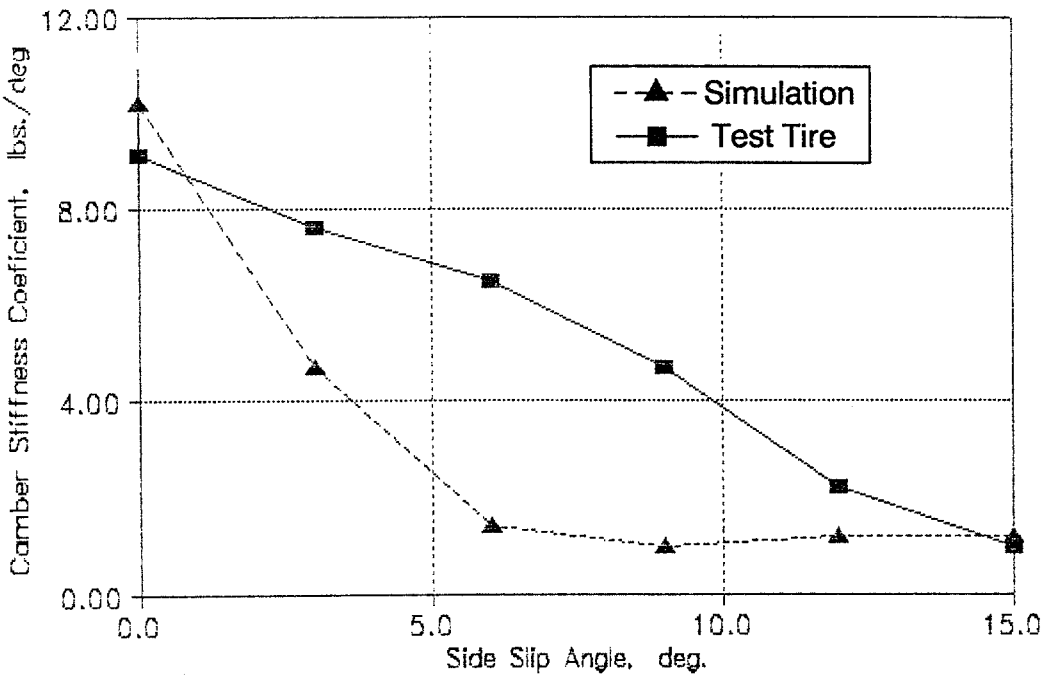

Figure 34. Comparison of Camber Stiffness Coefficient Saturation Between a Test Tire (Table 4 & Fig. 17) and Simulation Tire Model (Table 8)

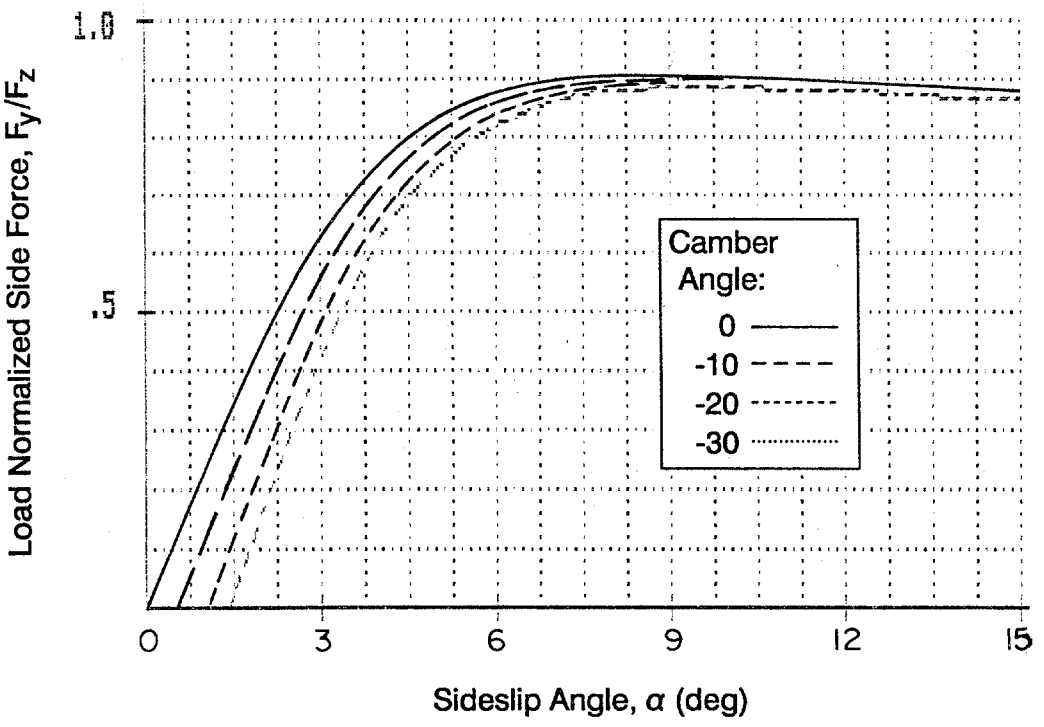

Figure 35. Camber Saturation Effect on Simulation Tire Model Side Force Response (Table 4 Test Tire, K_γ = 0.90)

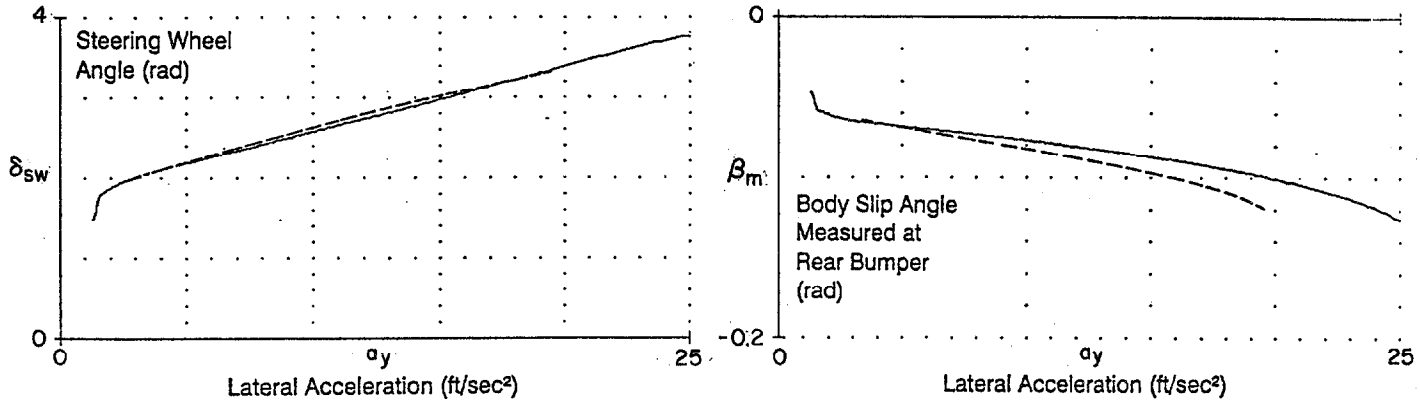

a) Light Utility Vehicle (No. 34)

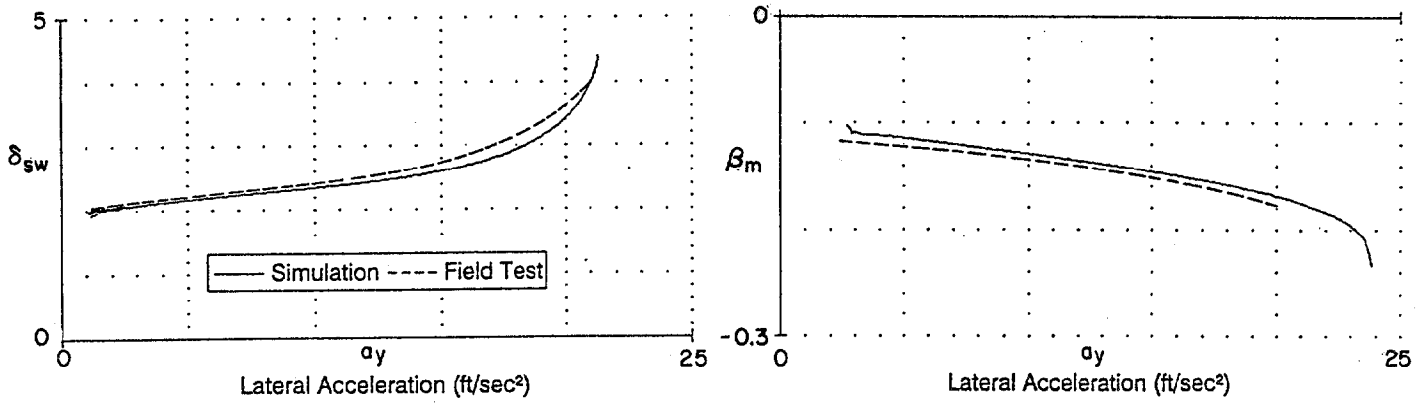

b) Subcompact (No. 1)

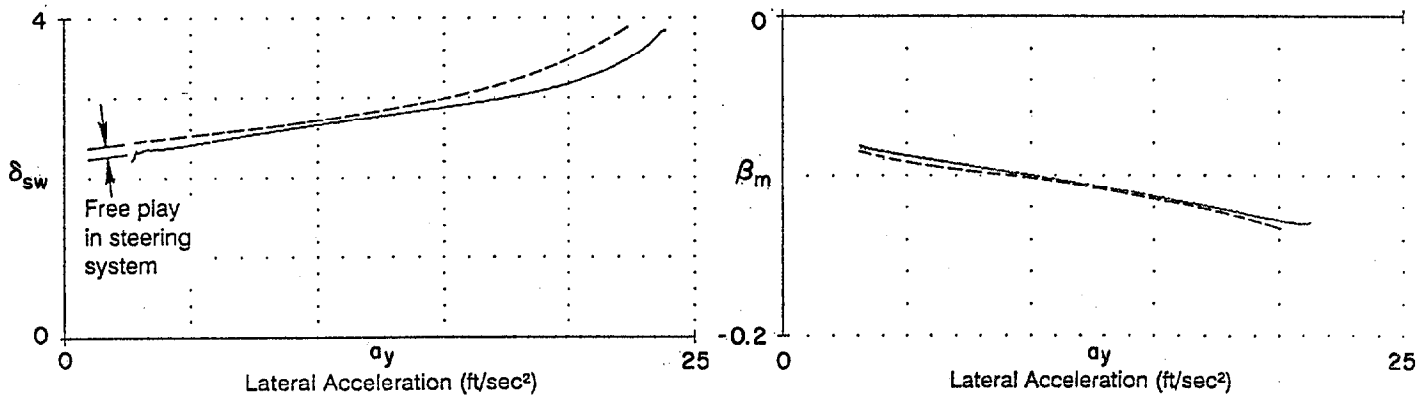

c) Intermediate Sedan (No. 17)

Figure 36. Steady State Validation Plots

The intermediate and subcompact test vehicles show a gradual transition to limit understeer in Figure 36, while the light utility vehicle shows relatively neutral steer up to the limit region. The reason for this is evident when the front and rear axle side force coefficients calculated by the computer simulation, are examined in Figure 37 (the interpretation of composite side force coefficients is discussed in some detail in Refs. 4 and 5). Here we see that the front axle side forces clearly saturate first for the subcompact and intermediate sized cars, while for the light utility vehicle the front and rear axles saturate simultaneously at the cornering limit. The passenger cars have front axle antiroll bars which give added roll stiffness to the front axle and cause the combined front tire side force to saturate before the rear axle thus leading to limit understeer. The light utility vehicle has an equal weight distribution and roll stiffness between the front and rear axles thus leading to the simultaneous front and rear side force saturation property.

D. DYNAMIC RESPONSE

The basic lateral/directional dynamic characteristics of the computer simulation were validated by taking describing functions of yaw rate, lateral acceleration and roll rate response to sinusoidal steering inputs. The simulation permits the specification of a sinusoidal steering input with increasing frequency throughout the run as illustrated in Figure 38. The time traces in Figure 38 clearly show the effects of yaw rate attenuation at high frequencies, and roll rate resonance and lateral acceleration attenuation at mid frequencies. Fast Fourier transforms (FFT) were taken of these simulation runs and compared with field test data as illustrated in Figure 39. Relatively good comparisons in response amplitude and phasing are noted for the directional and roll modes for all three example vehicles. Matches for the other test vehicles are summarized in Appendix H. These data comparisons show that the computer simulation dynamics give a reasonable match to the field test vehicles under low lateral acceleration dynamic conditions (i.e., less than 0.3 g's) where the tire side force characteristics are in their linear range. The describing function data basically validate the combined effect of vehicle inertial dynamics and linear tire side force characteristics. Larger transient inputs are needed to validate the limit performance capability of the computer simulation as discussed next.

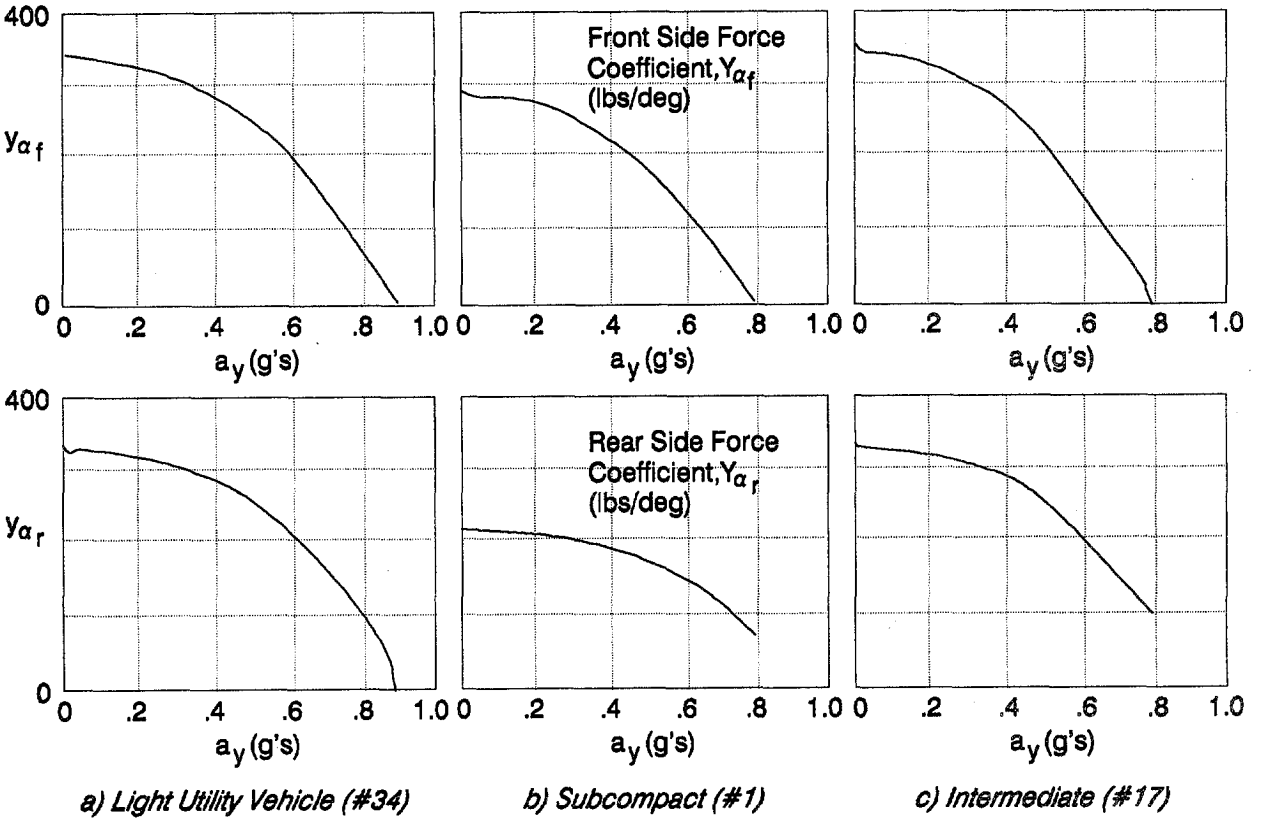

Figure 37. Simulation Side Force Coefficient Plots

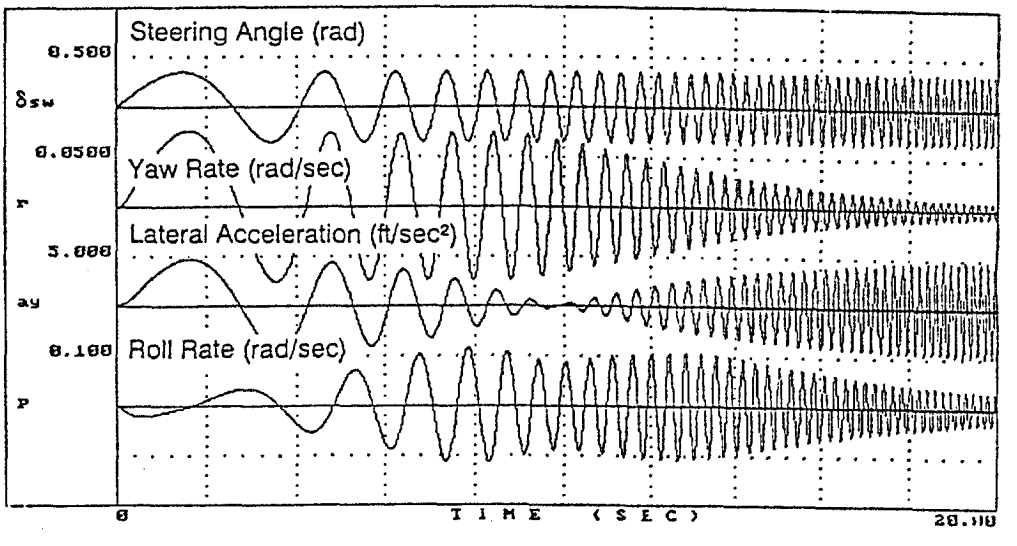

Figure 38. Simulation Sinusoidal Steer Inputs

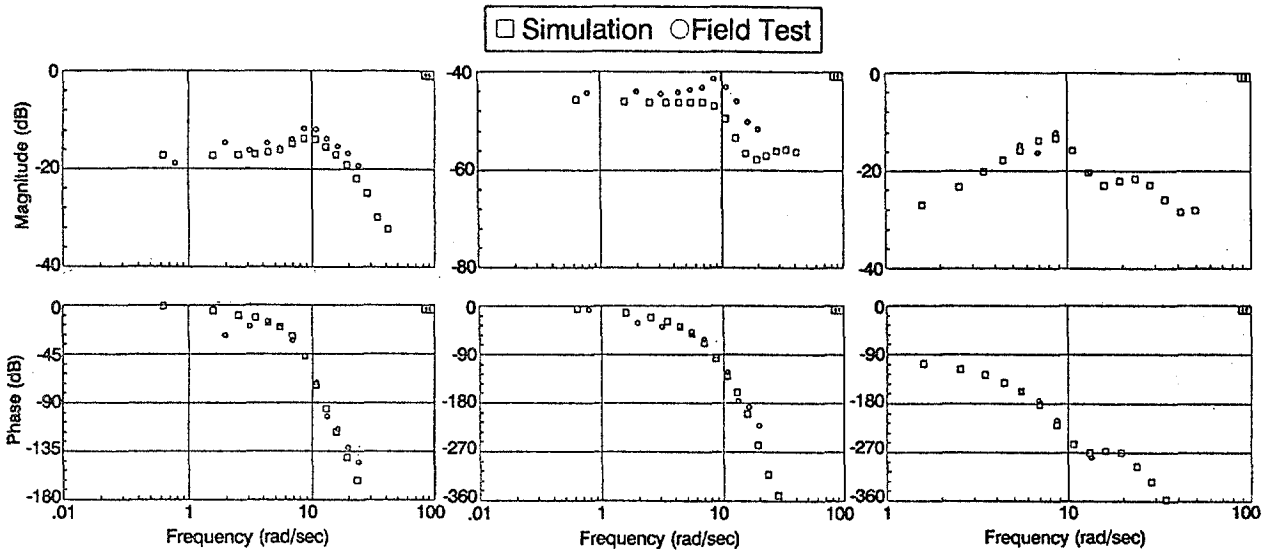

a) Light Utility Vehicle, No. 34 (speed = 64 ft/sec)

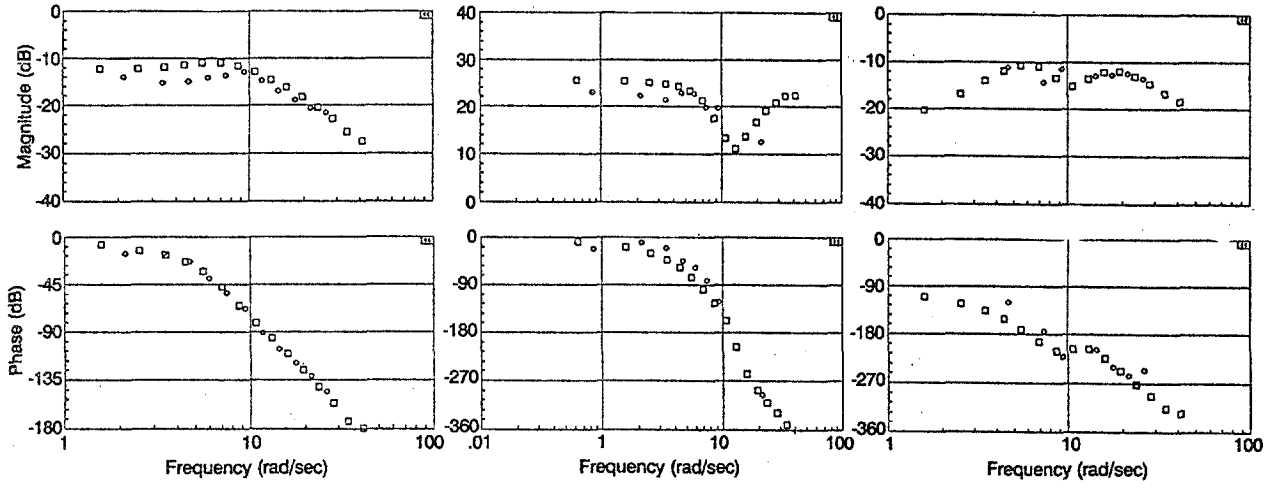

b) Subcompact, No. 1 (speed = 64 ft/sec)

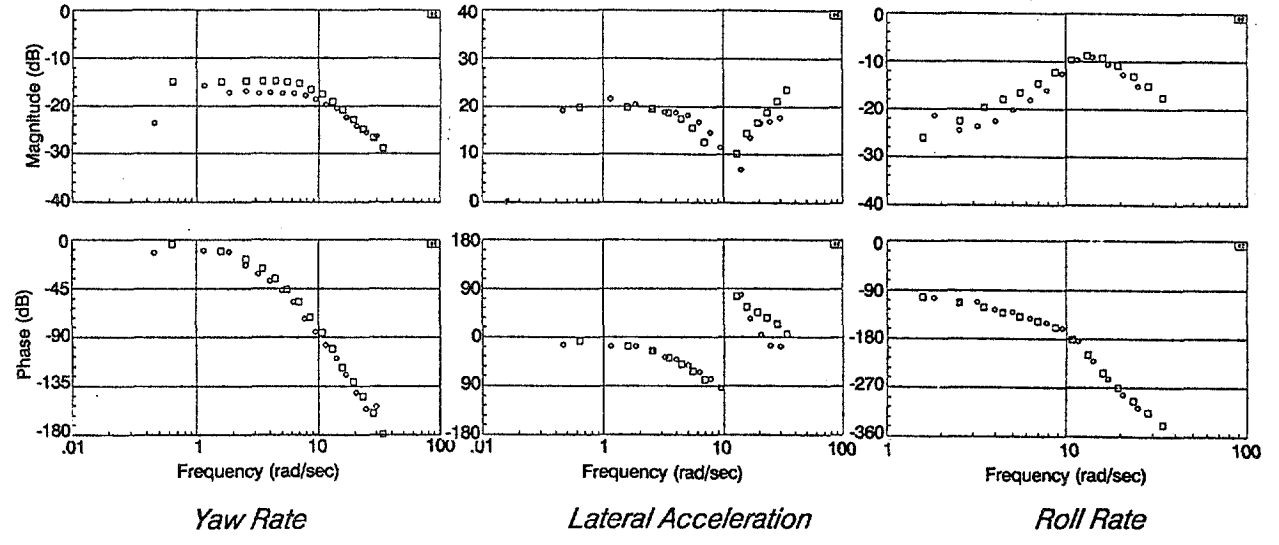

Yaw Rate *Lateral Acceleration* *Roll Rate*

c) Intermediate Sedan, No. 17 (speed = 51 ft/sec)

Figure 39. Simulation Transfer Function Validation

E. TRANSIENT RESPONSE AND DIRECTIONAL INSTABILITY

The limit performance capability of the simulation was validated with large transient steering responses. The steering time profiles obtained in field test runs were used as inputs to the computer simulation and the subsequent time response of various variables were compared for each vehicle as shown in Figure 40. The transient test conditions in Figure 40 represent maneuvering conditions up into the lateral acceleration regime of 0.8 g's which should encompass significant tire side force saturation. Reasonable matches are noted across vehicles and response variables in Figure 40 and Appendix H for all twelve phase 1 field test vehicles for the normal transient steer tests.

Validation attempts for the two spinout cases were not initially successful and were found to require some extra consideration in tire modeling. The spinouts imply loss of rear axle traction, and the exponentially increasing yaw rate and body slip angle conditions during the spinouts indicate a yawing moment that is increasing with slip angle. The yawing moment arises from the differential effect of the front and rear axle side forces, and a spin out case implies a loss of rear axle traction that would otherwise act to stabilize the vehicle directional mode. Using tire parameters that were adequate for successful validations of stable transient maneuvers would not result in a computer simulation directional instability for the spinout case steering inputs.

Because the two vehicles with spinouts had lightly loaded rear axles, it was hypothesized that some mechanism had resulted in an effective reduction in rear tire adhesion that could be modelled as a reduction in rear tire/road coefficient of friction. The effective coefficient of friction reduction was modelled by reducing the tire model Calspan parameter B_3 which is the constant term for the coefficient of friction load function (Ref. 5). Attempts were made to achieve a spinout of the small 4 door sedan (veh. #8) computer simulation model by reducing the rear tire coefficient of friction. A reduction of 15% in the effective rear tire coefficient of friction, combined with a dropped throttle at the end of the reversal steer, was found to be required to make the small four door sedan directionally unstable given the field test steering input that resulted in the spinout. Simulation and field test time histories are compared in Figure 41 a). Here we see that the vehicle follows the first steering reversal in a stable manner. Directional stability is lost during the second

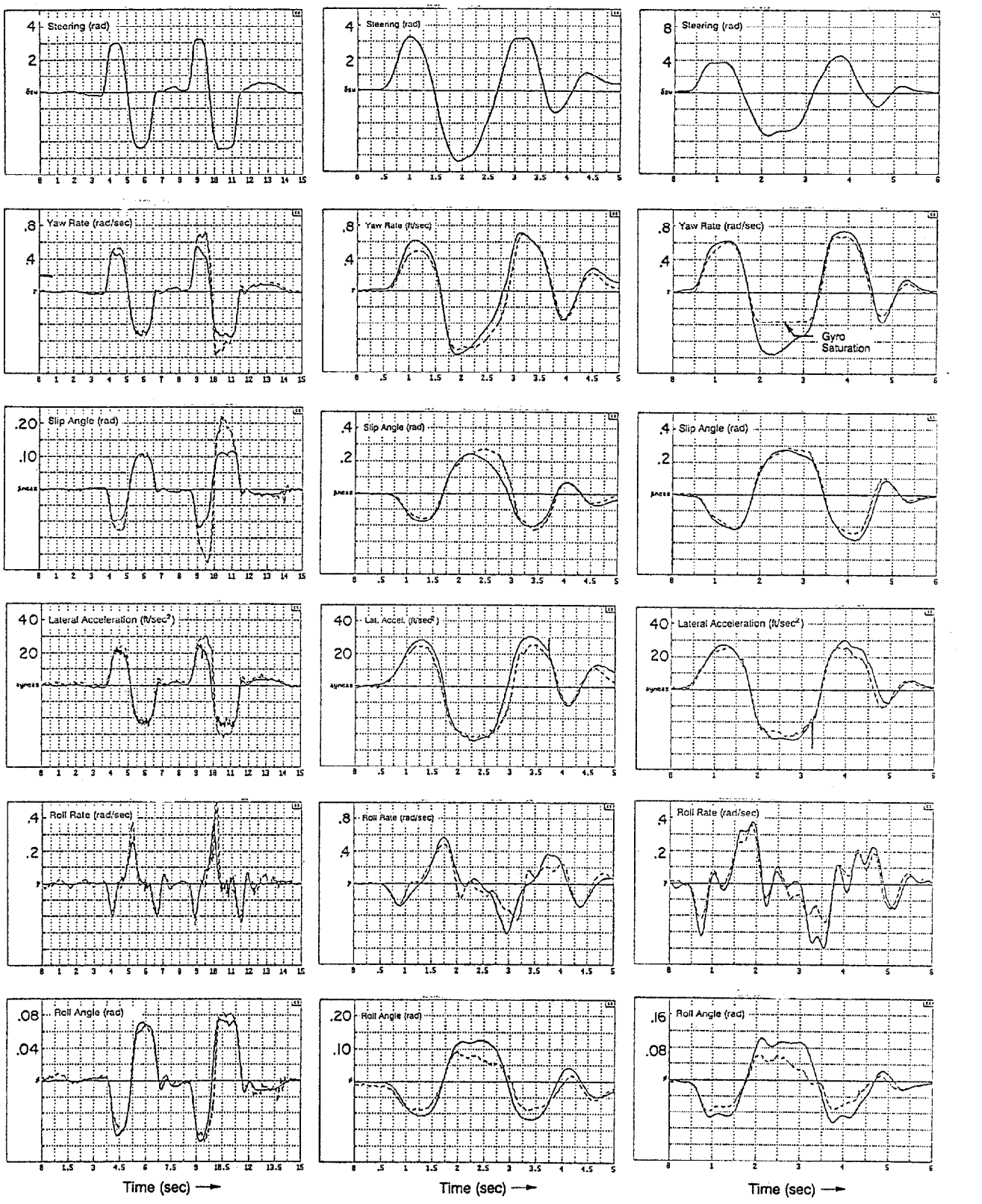

a) Light Utility Vehicle, No. 34 (speed = 40 ft/sec) *b) Subcompact, No. 1 (speed = 50 ft/sec)* *c) Intermediate Sedan, No. 17 (speed = 47 ft/sec)*

Figure 40. Transient Response Validation Examples

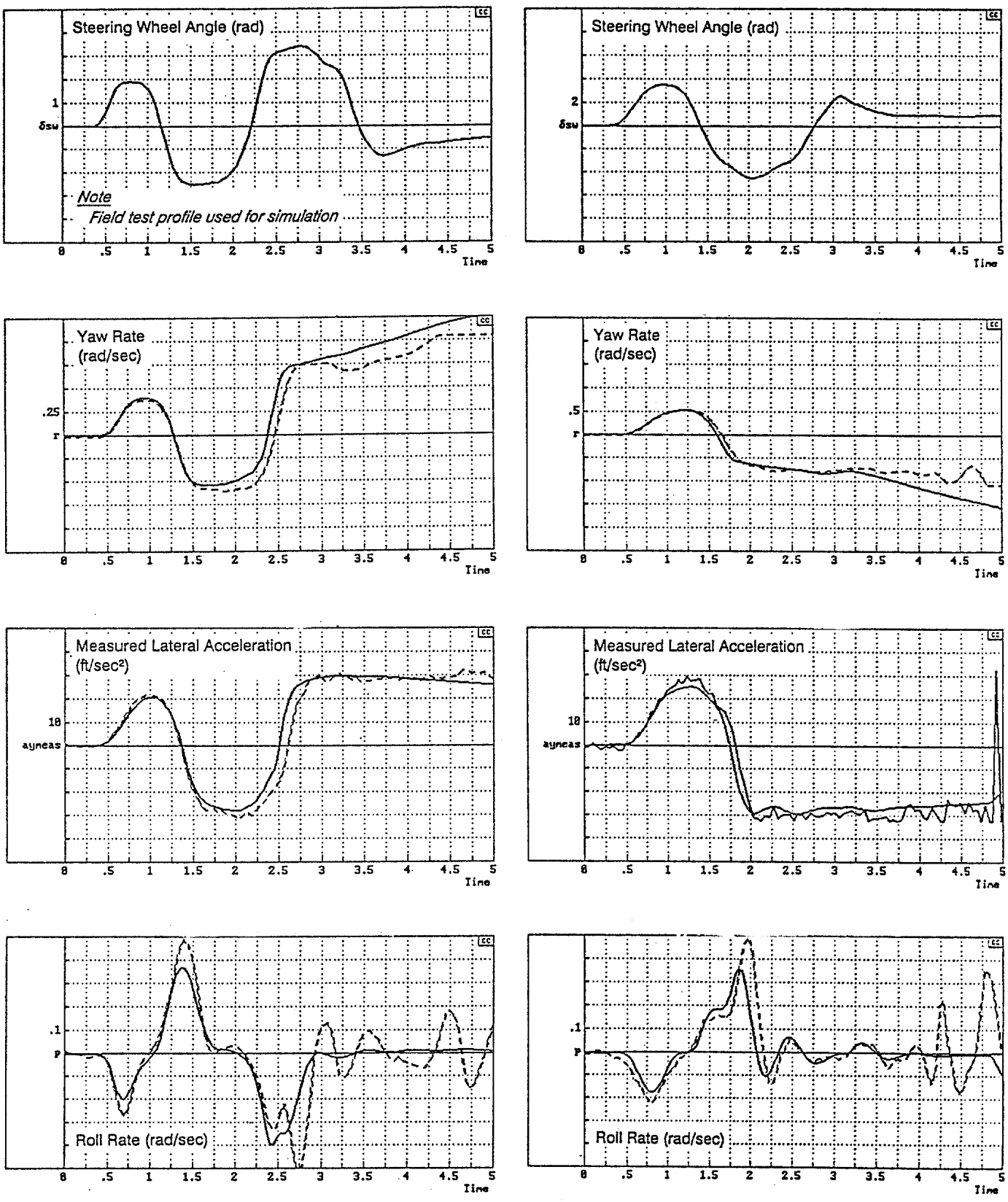

a) Small FWD Sedan (Veh. # 8, App. E)

b) Light 4 × 4 Pickup (Veh. # 23, App. E)

Figure 41. Computer Simulation Validation of Field Test Spinout Cases (_____ Simulation; ------- Field Test)

reversal, and the spinout instability is noted to be quite similar for the simulation and field test time histories.

Although the throttle position was not measured during the field testing, the small four door sedan was found to have a significant oversteer response to a dropped throttle during cornering. Also, the test driver felt that he dropped the throttle when the vehicle began sliding during the second steer reversal. Given the field test steering input, the vehicle was found to be stable with constant throttle. The dropped throttle has such a significant effect because it changes the saturation characteristics of the front axle of the front drive sedan. Power application in a front drive vehicle contributes to front axle saturation and is a component of understeer. When the throttle is dropped, the front axle picks up some side force capability which leads to oversteer.

A 15% reduction in coefficient of friction was applied to the 4 X 4 pickup (veh. #23) rear tires, and simulation and field test time histories for the spinout case are compared in Figure 41 b). The pickup spins out with a constant throttle setting, and will not spin out with a dropped throttle for the spinout steering profile. Because the pickup is rear wheel drive, dropping the throttle tends to strengthen the side force capacity at the rear axle which has a stabilizing understeer effect.

The rationale for reduction of rear tire coefficient of friction was considered in some detail. The general rationale is a combination of various vehicle characteristics that would contribute to rear axle hop. These factors include:

- forward weight distribution that results in a light rear axle loading, typical of front wheel drive vehicles and pickups
- stiff rear axle springs such as on pickup trucks
- large unsprung to sprung mass ratio such as with solid rear axle units on rear wheel drive vehicles
- small static tire deflection which increases the likelihood of load alleviation under hop conditions

In general, axle hop leads to a variation in rear axle loading, with low loadings resulting in loss of adhesion under hard cornering conditions. Ideally, the reduced rear axle coefficient of friction should be simulated by the computer

simulation model with an accurate rear axle hop mode that is excited by road roughness. This model would most likely have to include nonlinear tire vertical deflection stiffness, nonlinear shock damping and suspension stiction effects. This is an area of potential future expansion of the current model, but does imply additional parameter identification problems.

Given the steady state and dynamic response validation noted above, the transient comparisons suggest a valid computer simulation that can be used for near limit performance maneuvering analysis as presented in the next section.

SECTION VII

SIMULATION ANALYSIS

A. OVERVIEW

Given the above validation the computer simulation described in Appendix A can now be used to analyze near limit performance maneuvering conditions that lead to loss of vehicle stability. Lateral/directional instability includes both spinout and rollover. Both of these conditions can occur under limit performance maneuvering conditions involving high tire side forces. Spinout occurs when rear axle tire adhesion limits are exceeded while the front axle still has some side force capacity available. Spinout may be superseded by roll instability in vehicles with low rollover stability limits. The analysis in this section will attempt to determine the vehicle characteristics and maneuvering conditions that play a primary role in spinout and rollover.

B. MANEUVERING CONDITIONS AND DIRECTIONAL STABILITY

Vehicle dynamics are extremely nonlinear in the region of limit performance, due to the way tire saturation interacts with maneuvering conditions. Therefore, computer simulation solutions are highly dependent on the input conditions including steering, braking and power application. A relevant example to be considered here is the light pickup truck discussed in the last section that spun out during the field testing portion of this research project. The maneuver for this computer simulation analysis was an idealized version of the Figure 41b) field test steering profile. As noted by the Figure 42a) body slip angle trace, the light pickup truck spins out under a reversal steer profile at a speed of 60 feet/second (41 mph) where the second peak in the profile is slightly longer by 0.25 seconds than the first steering peak. The spinout can be averted by modifying maneuvering conditions, either by shortening the length of the second steer peak by 0.25 seconds in Figure 42b), or by reducing the speed to 50 feet/second in Figure 42c). In the case of the early steering return (Figure 42b) spinout is averted because lateral acceleration is reduced slightly and the rear axle side force capacity is able to recover. In the lower speed case, lateral acceleration is lower and the rear axle side force capacity is never saturated.

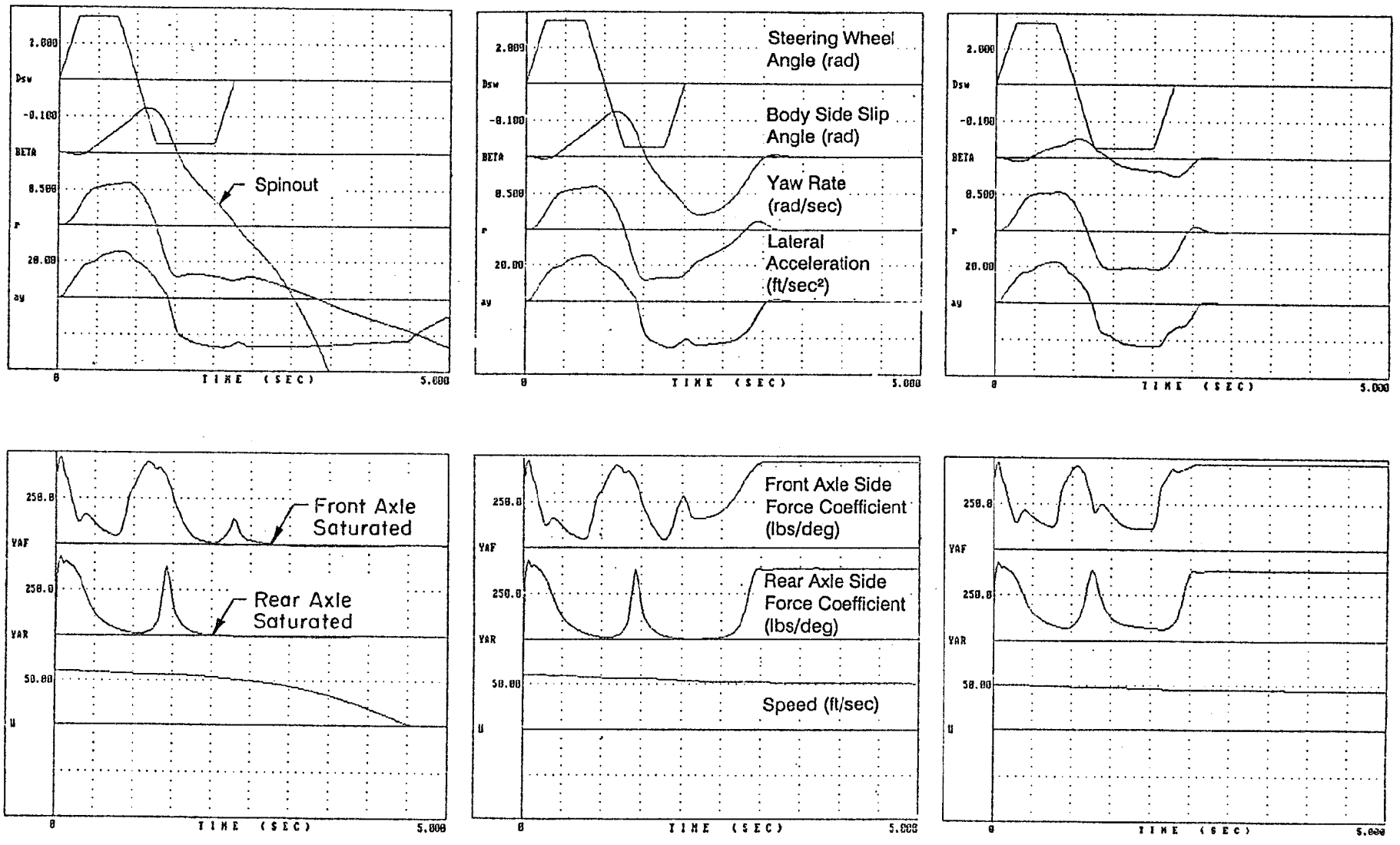

a) Spinout *b) Stable (reduced steering input)* *c) Stable (reduced speed)*

Figure 42. Computer Simulation Analysis of the Effects of Maneuvering Condition on the Yaw Stability of a Light Pickup Truck (Vehicle #23, Appendix E)

In the example above directional instability or spinout results from rear axle side force saturation. Another example is given in Figure 43 which compares dropped and constant throttle conditions for an idealized reversal steer maneuver with the compact four door sedan that spun out during field testing (Figure 41a). In the dropped throttle case power was removed over the interval from 0.7 to 0.8 seconds and at about 1.75 seconds the vehicle begins to spin out compared to the constant throttle case. The constant throttle case reaches a significant body slip angle but eventually recovers. The removal of front axle traction force due to the dropped throttle condition causes subtle changes in the yawing moments under hard maneuvering which leads to spinout.

C. DIRECTIONAL INSTABILITY TIME CONSTANT

The basic nature of the directional instability shown in Figures 42 and 43 is that yaw rate increases with increasing body slip angle due to loss of rear axle adhesion, while for the stable cases yaw rate decreases with increasing body slip angle. The relationship of yaw rate and body slip angle can be conveniently portrayed in crossplots as shown in Figure 44. For the stable cases, the yaw rate and body slip angle return to zero as the vehicles stabilize after the reversal steer maneuvers. For the unstable cases both yaw rate and body slip angle increase as the vehicle spins out.

The severity of directional instability can be characterized by the time constant of the diverging directional variables. A true dynamic instability is represented by an exponential increase in all the derivatives of a variable. Given a directional instability starting at some operating condition defined by a body slip angle, β_0, the exponential increase is then given by,

$$\beta-\beta_0 = \Delta\beta = ae^{t/\tau_\beta}$$

Assuming that yaw rate, r, is approximately the derivative of body slip angle, then diverging yaw rate is given by

$$r-r_0 = \Delta r \approx \frac{d\beta}{dt} = \frac{a}{\tau_\beta}e^{t/\tau_\beta}$$

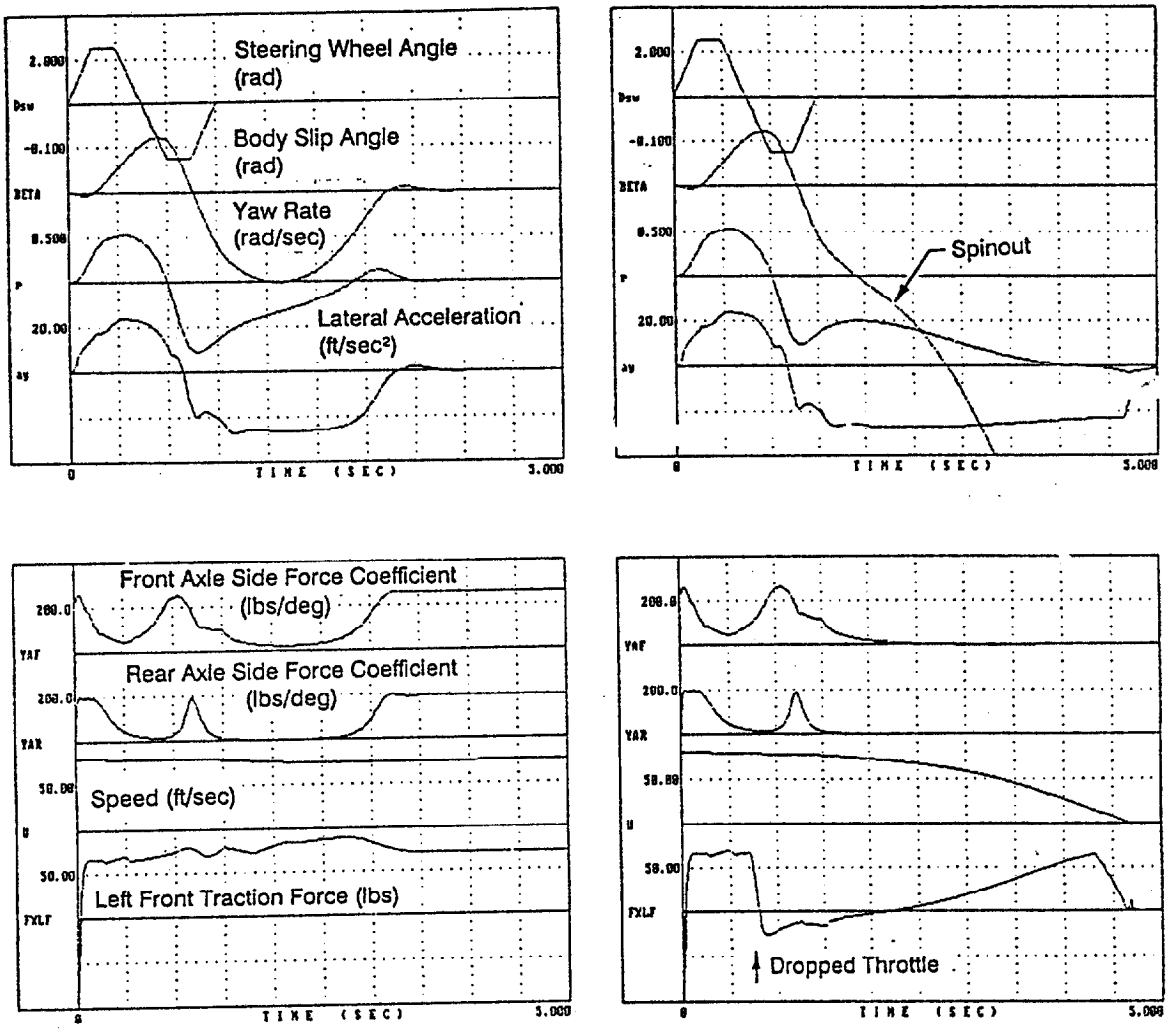

Figure 43. Computer Simulation Analysis of Maneuvering Condition on the Yaw Stability of a Small Front Wheel Drive Sedan (Vehicle #8, Appendix E)

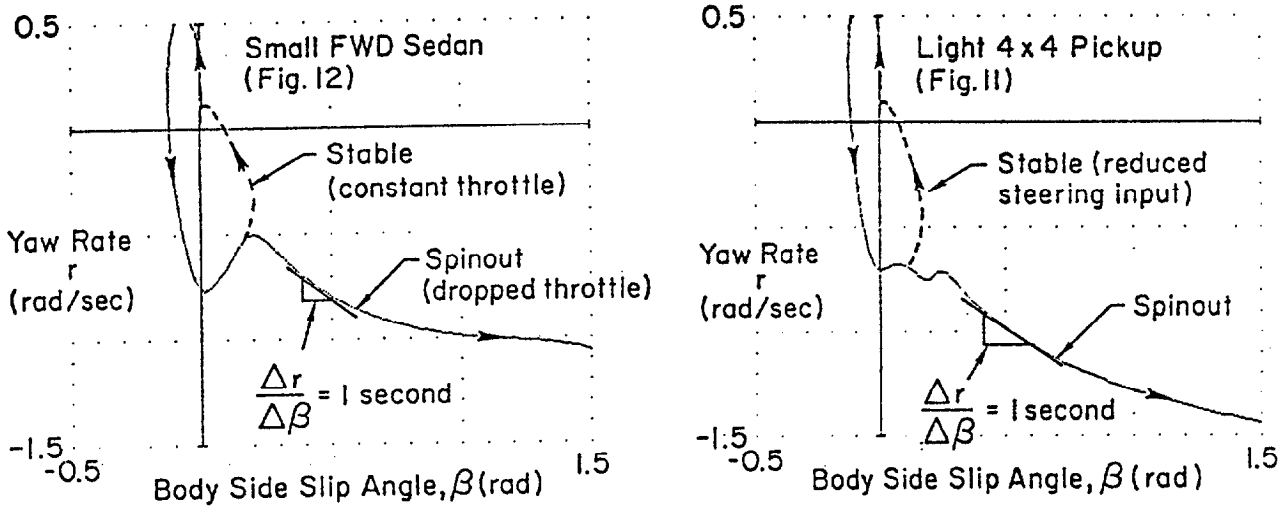

Figure 44. Body Slip Angle vs. Yaw Rate Crossplots for Stable and Spinout Computer Simulation Maneuvers in Fig. 42 and 43.

Now, if we take the ratio of the above two equations, then the unstable divergence time constant is given by

$$\frac{\Delta r}{\Delta \beta} = \tau_{\beta}$$

This ratio is basically the slope of the Figure 44 cross plots. Slopes in Figure 44 at the beginning of the spin outs indicate time constants on the order of 1.0 second. This time constant is slower than the 0.3 second magnitude shown for rear biased braking spinouts on low coefficient surfaces analyzed in Reference 21.

D. VEHICLE CHARACTERISTICS INFLUENCING DIRECTIONAL STABILITY

Further analysis was undertaken to determine vehicle design conditions that are spin out prone. Previous discussion centered on how LTD (load transfer distribution) between the front and rear axles controls side force saturation and determines understeer/oversteer tendencies. Vehicles from the phase 1 test program herein were analyzed with the computer simulation to determine how changes in LTD influenced understeer/oversteer. Load transfer distribution was modified by changing each vehicle's auxiliary roll stiffness as provided by anti-roll bars. The simulation maneuver used was a double reversal steer, which was accompanied by dropped throttle for front drive vehicles.

Some sample transient response results are shown for a compact front wheel drive vehicle in Figure 45. This vehicle was part of the phase 1 field test vehicle population, and simulation analysis has shown it to be quite directionally stable. Figure 45a) shows the stable response of the vehicle to a double steer reversal maneuver in its tested LTD configuration with constant power application (best case). Figure 45b) shows the vehicle spinning out under dropped throttle conditions (worst case) with the LTD shifted towards the rear which results in prematurely saturating the rear axle side forces. The effects between the two Figure 45 cases are subtle as evidenced by the inertial motions and tire side slip angles and forces. During the first and second steer profile peaks, the rear axle slip angles in the spinout case clearly go further into the saturation region (as reflected in the side force coefficient traces), and this result starts before the throttle is dropped. The high slip angle sequence in the spinout case also

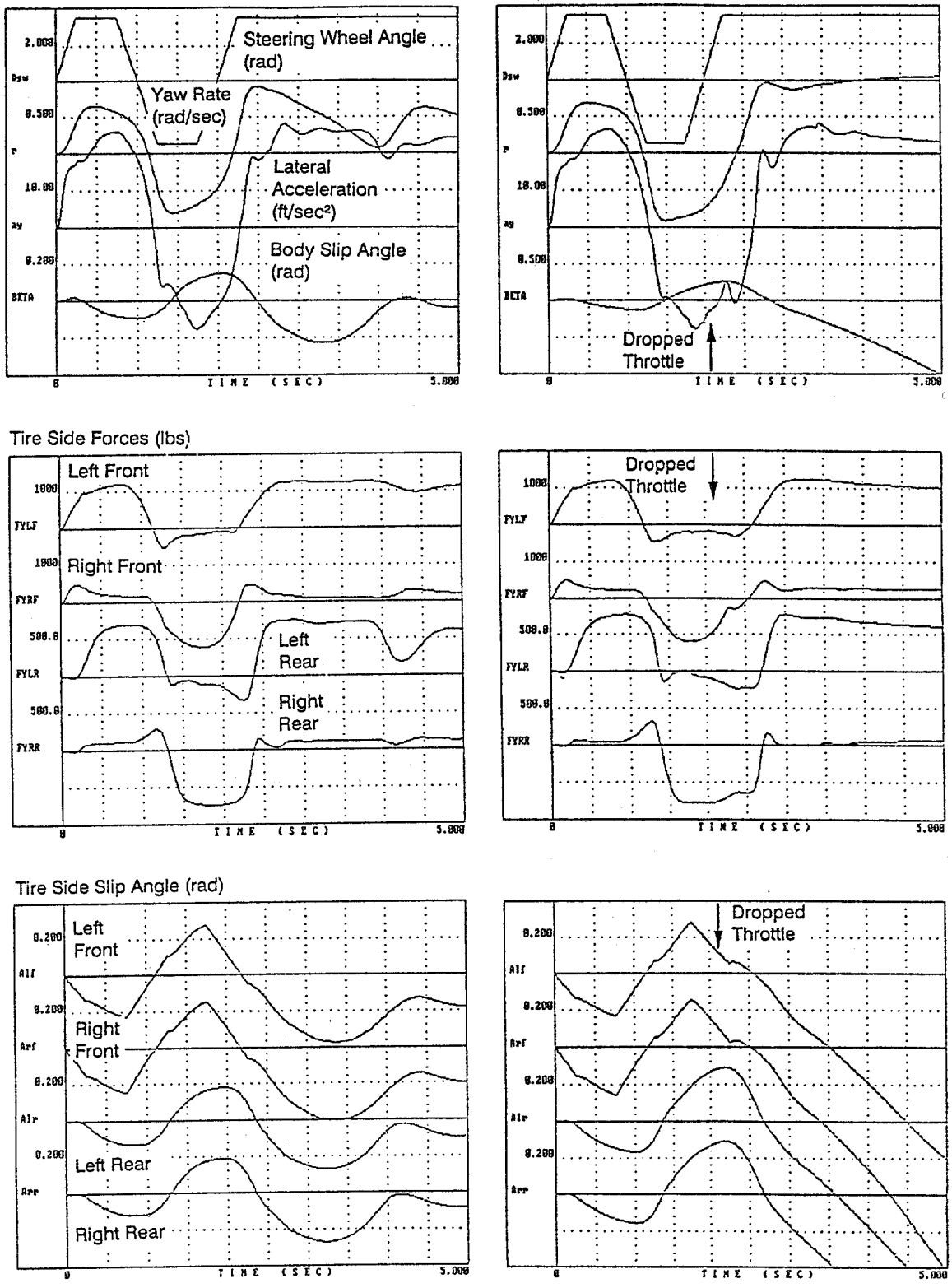

a) Constant Throttle, LTD = 63.5%

b) Dropped Throttle, LTD = 57.5%

Figure 45. Computer Simulation Analysis of the Effect of a Rearward Shift in LTD (Lateral Load Transfer Distribution, Appendix F) on the Directional Stability of a Small Sedan (Vehicle #1, Appendix E)

is preceded by a larger yaw rate than the stable case which is associated with the inside rear wheel lifting off the ground.

The influence of the shift in LTD can be further interpreted by considering the effect on the axle side force coefficients which represent the change in side force with respect to slip angle. The results illustrated in Figure 46 were computed by having driver feedbacks (References 5 and 19) control the computer simulation in a steady state turn circle maneuver as described in Section V. Under the normal LTD configuration the front axle saturates well before the rear axle which gives limit understeer. Shifting the LTD to the rear causes a subtle shift in axle side force capability, with minor gains at the front axle and minimal loss at the rear axle (because it is lightly loaded) which moves the vehicle towards oversteer. The increase in front axle side force coefficient under the rearward LTD condition is consistent with the larger vehicle motion response compared to the standard LTD condition. These larger motions then result in more rear axle saturation which subsequently leads to spinout. The subtle effect of LTD changes on axle side force coefficients apparently has a nonlinear multiplying effect on directional stability near the performance limit of the tire/wheel combination.

The results of the above and similar analyses are summarized in the LTD vs. weight distribution plot of Figure 47 which follows from Figure 16 and related discussion. Three light, front wheel drive vehicles from the Phase 1 field test program were considered. These vehicles included the compact four door sedan discussed above that had experienced a spinout during field testing and was shown to be directionally unstable in subsequent simulation analysis, and two that were shown to be directionally stable based on simulation analysis. The results in Figure 47 show the change in LTD required to alter the directional stability characteristics of the three small front wheel drive vehicles. Additional simulation analysis was also carried out for vehicles 12 and 13 from the phase 2 parameter test group. These vehicles proved to be directionally unstable which is consistent with their low front LTD values relative to the other front wheel drive vehicles in Figure 47. Vehicles 12 and 13 would require a significant increase in LTD to achieve directional stability under limit performance maneuvering conditions.

Results for three heavier vehicles from the phase 1 field test, two vans and a utility vehicle, are also indicated in Figure 47. Simulation analysis showed all of these vehicles to be directionally stable in their original configuration

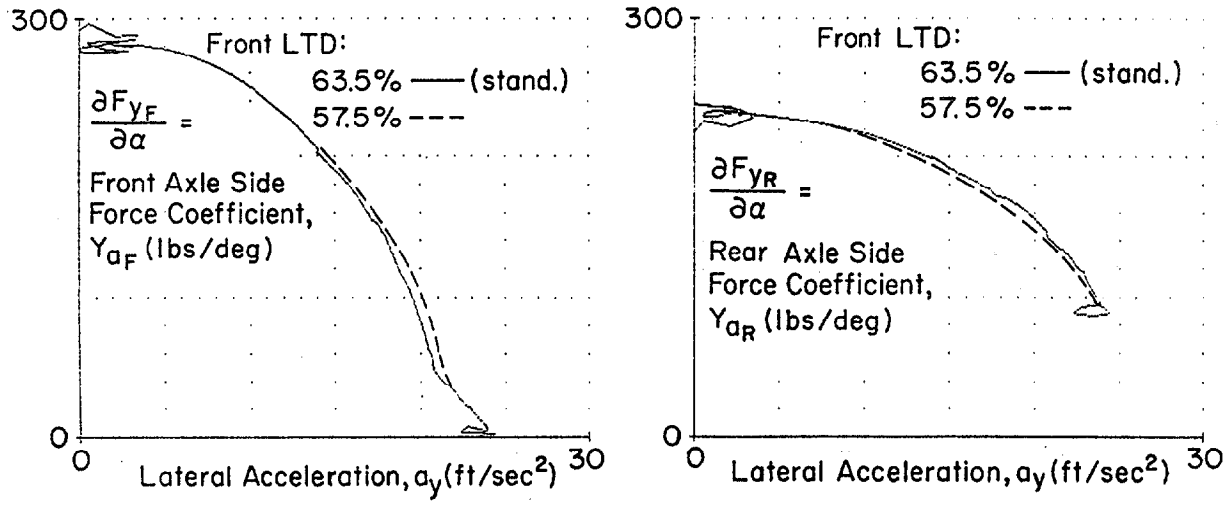

Figure 46. Effects of a Rearward Shift in LTD on the Computer Simulation Axle Side Force Coefficients for a Small Sedan (Vehicle #1, Appendix E)

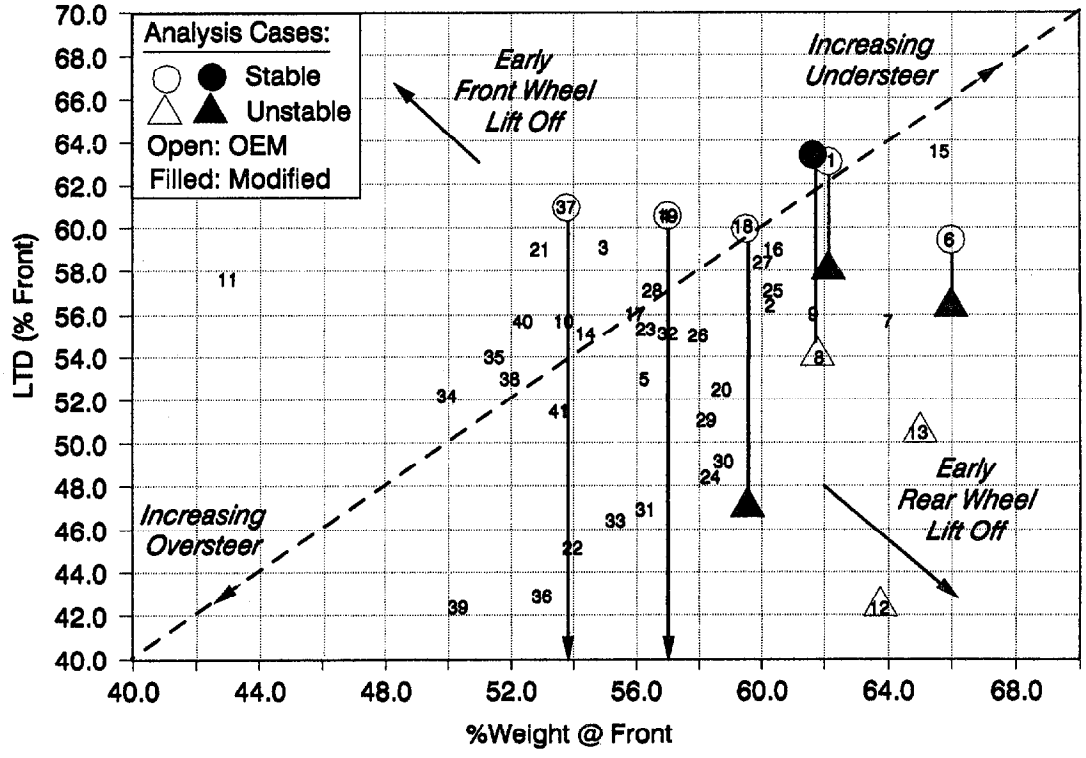

Figure 47. Lateral Load Transfer Distribution Shifts Required to Change Vehicles from Limit Understeer to Directional Instability

as tested. The utility vehicle requires a large change in LTD before it becomes directionally unstable. When LTD is changed towards the unstable direction for the two vans, (vehicles 18 and 19) they experience significant rear inside wheel lift and vehicle 19 rolls over rather than spinning out. Both of the vans have a higher roll gradient than the utility vehicle, and when the LTD is shifted towards the rear, the rear inside tire experiences early lift off which causes two effects. First, at wheel lift off no additional weight transfer can occur at the rear axle which prevents rear axle side force saturation if it had not occurred before wheel lift off. Second, the center of gravity rises due to the rear wheel lift off, which can then lead to roll over. This result for the vans shows an interesting interaction between directional and rollover stability which is discussed next.

E. INFLUENCE OF VEHICLE CHARACTERISTICS AND MANEUVERING CONDITIONS ON ROLLOVER

The interaction of maneuvering conditions and vehicle characteristics can also have a significant effect on rollover potential. Figure 48 shows the response of three vehicles to a limit step steer input. Both passenger cars initially go into front axle side force saturation or limit understeer for a brief transient period. Both the front and rear axle side forces of the light utility vehicle saturate for a much longer period of time during which the vehicle's side slip angle exceeded 30 degrees (i.e., over 0.55 radians). Roll angle and wheel normal load traces show that neither of the passenger cars are close to rollover. However, wheel normal load traces for the light utility vehicle show a transient period where the right (inside) wheels are off the ground. As noted previously (Figure 14) the light utility vehicle # 34 has low track width and wheel base ratios relative to c.g. height which lead to significant load transfer effects. The Figure 48 results show significant yaw and roll stability effects related to these design characteristics.

A reversal steer maneuver is sufficient to roll over the light utility vehicle on a flat surface as shown in Figure 49 while the passenger cars prove to be quite stable. Normal wheel loads show that the intermediate sized car is never near rollover, while the subcompact picks up the left rear wheel for an instant during the roll mode transient. The left side tires of the utility vehicle leave the ground shortly after the steering transient is completed. Note also that the maximum steering amplitude for the utility vehicle rollover run is

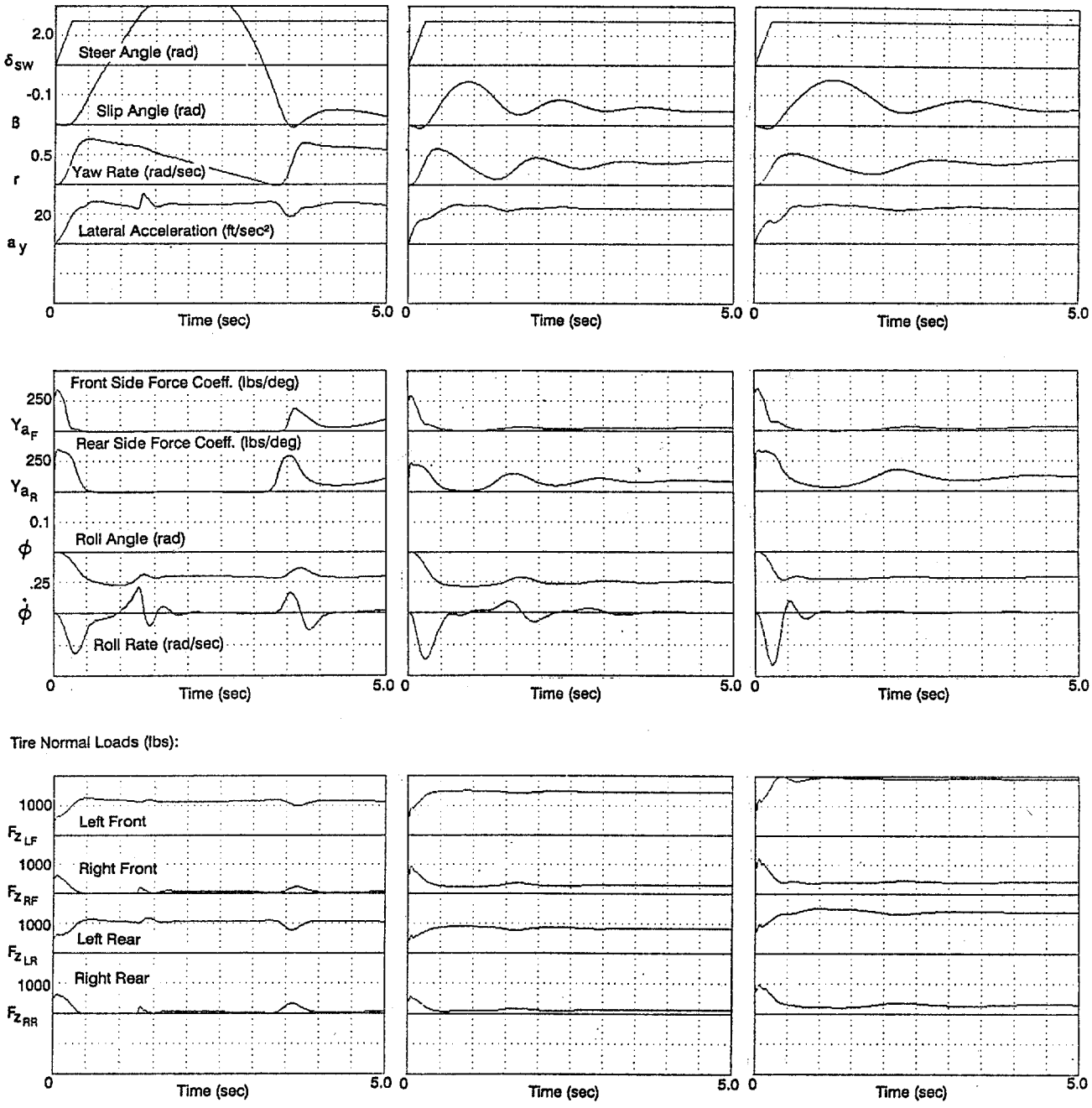

a) Light Utility Vehicle (no. 34, App. E) *b) Subcompact (no. 1, App. E)* *c) Intermediate Sedan (no. 17, App.E)*

Figure 48. Computer Simulation Analysis of the Step Steer Response of Three Vehicles at a Speed of 80 ft/sec

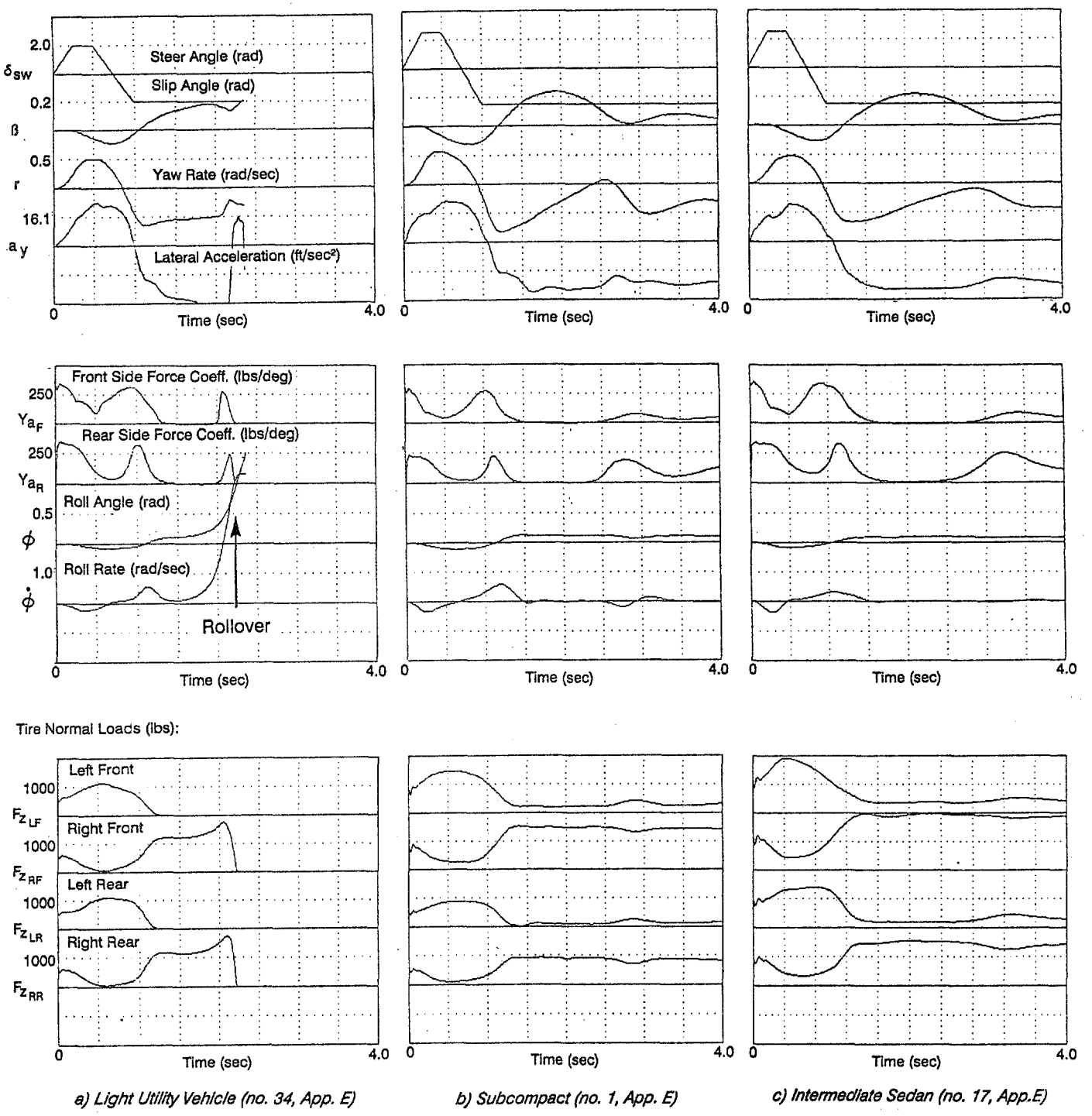

a) Light Utility Vehicle (no. 34, App. E) *b) Subcompact (no. 1, App. E)* *c) Intermediate Sedan (no. 17, App.E)*

Figure 49. Computer Simulation Analysis of the Reversal Steer Response of Three Vehicles at a Speed of 80 ft/sec

only two thirds the amplitude of the Figure 48 step steer which did not cause rollover. The steering reversal in Figure 49 excites the utility vehicle roll mode to a sufficient extent to cause rollover (untripped on a flat surface).

The light utility vehicle can also be induced to roll over if braking is combined with a step steer maneuver as shown in Figure 50. The step steer levels in Figure 50 are the same as in Figure 48 and a pulse brake application has been added with a duration on the order of 1.5 seconds and an amplitude sufficient to give on the order of 0.6 g deceleration. The load transfer due to deceleration lifts the rear wheel of the light utility vehicle for a significant interval while the subcompact inside rear wheel shows only a very brief transient lift off. The intermediate sedan wheels remain in solid contact with the ground throughout the brake in a turn maneuver similar to the previous two maneuvers.

The directional stability of the light utility vehicle is most significantly disturbed during the brake in a turn maneuver with side slip angle reaching twice the magnitude of the passenger cars prior to rollover. The subcompact incurs a side slip transient response during recovery from braking that is as large as the response during the braking pulse. The intermediate sedan shows the greatest directional stability, with minimal side slip response beyond the braking episode.

Referring to Table 5 discussed in Section IV, two utility vehicles in the phase 1 field test population were noted to have the lowest rollover propensity margins (i.e., #34 and #40). It was demonstrated above that a reversal steer maneuver was required to rollover Vehicle #34. Simulation analysis in Figure 51 shows that utility vehicle #40 will rollover with a simple step steer maneuver. Referring back to Figure 20 in Section IV, note that vehicle #40 has the lowest track width ratio of the entire test vehicle population in this project. Further simulation analysis not included here has shown that vehicles with track width ratios in the region of 1.1 and below and equivalent lateral accelerations for rollover (side pull test) in the region of .90 and below are prone to rollover under severe maneuvering conditions. These boundaries are somewhat vague, however, and depend on other factors such as tire cornering capacity that have been discussed previously.

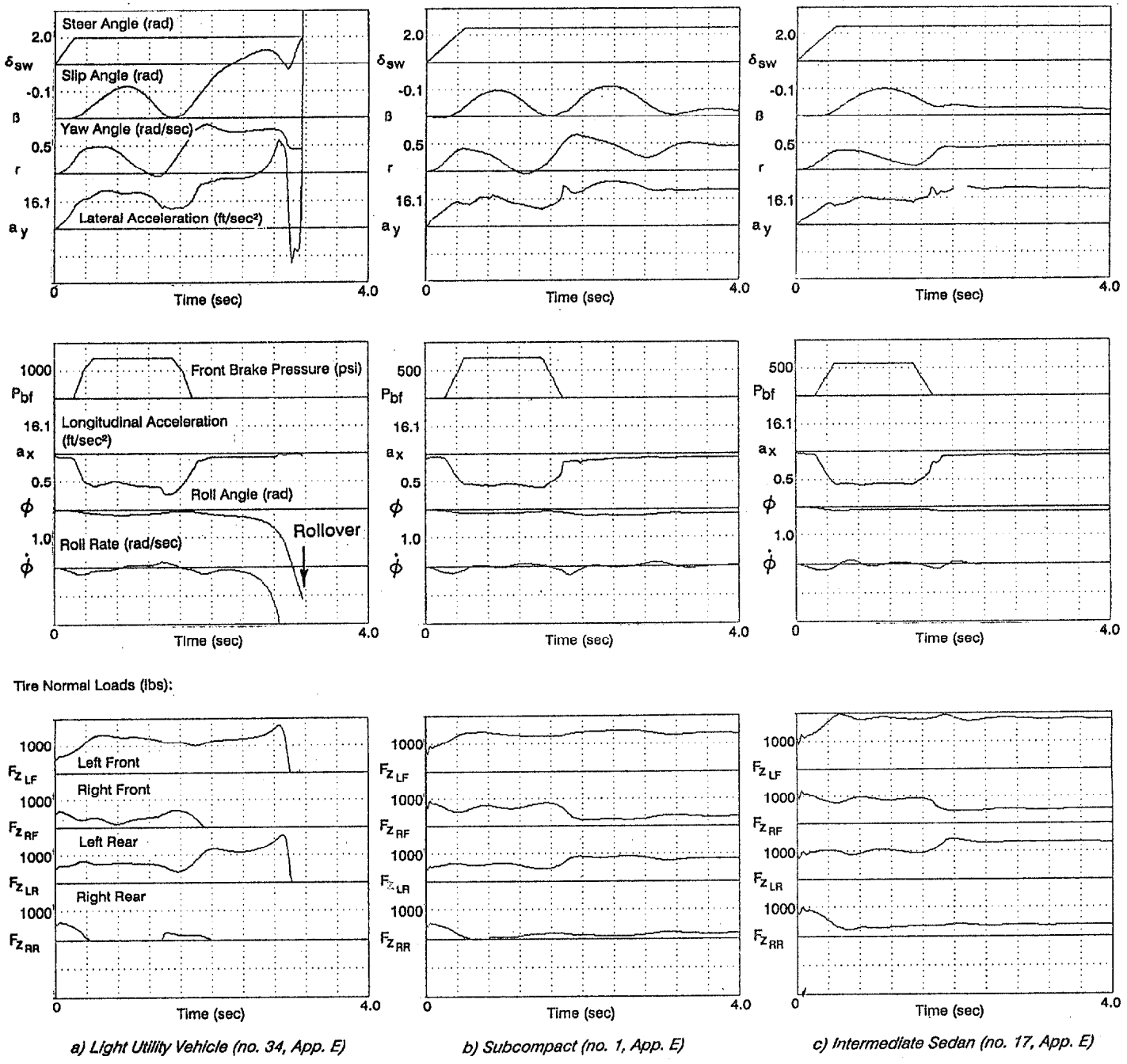

a) Light Utility Vehicle (no. 34, App. E) *b) Subcompact (no. 1, App. E)* *c) Intermediate Sedan (no. 17, App. E)*

Figure 50. Computer Simulation Analysis of the Response of Three Vehicles to a Brake-in-a-Turn Maneuver at a Speed of 80 ft/sec

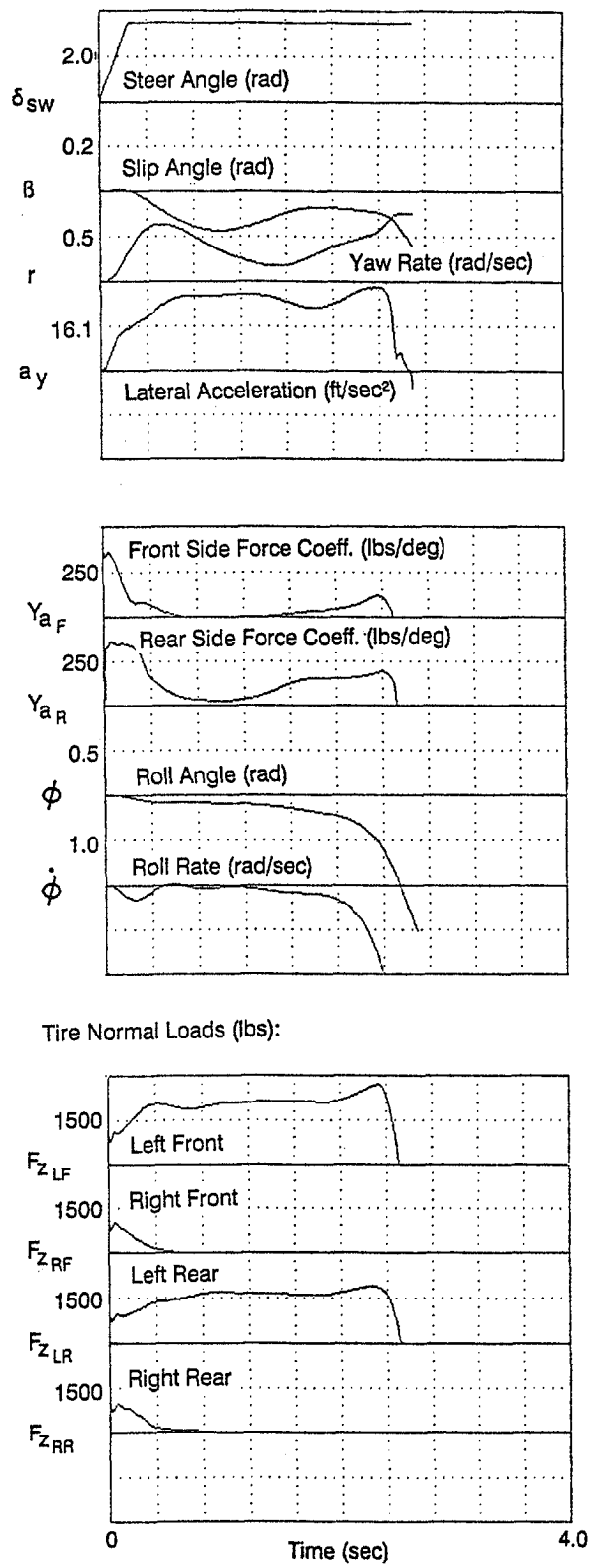

Figure 51. Computer Simulation Analysis of the Step Steer Response of Utility Vehicle #40 at a Speed of 80 ft/sec

F. ROLLOVER STABILITY

The utility vehicle rollover events in Figures 49-51 suggest a relatively simple rollover stability model. Note that in each case after the inside wheels have lifted off the normal loads increase in an exponential manner which is accompanied by an exponential increase in lateral acceleration, roll angle and roll rate. This effect is in contrast to the utility vehicle response in Figure 48 under step steer conditions where even under inside wheel lift off conditions outside wheel normal loads and lateral acceleration decline. These results suggest a simple instability model due to a rollover moment that increases with roll angle. Under dynamic conditions that result in sufficient roll rate, normal loads are increased at the outside wheels. At a given side slip condition the increased normal load leads to increased side forces that are sufficient in combination with angular momentum effect, to cause rollover.

The unstable exponential increase in roll rate in the rollover events of Figures 49-51 is evidenced by the fact that the magnitude doubles about every 0.15 seconds. This is a rapid roll divergence, and the overall rollover sequence goes to completion in on the order of one second which would not allow for significant driver corrective response (in Reference 21 it is demonstrated that drivers have a difficult time in reacting to directional mode divergence time constants on the order of .3 seconds). The cross plots of roll angle vs. roll rate illustrated in Figure 52 also show the effect of the divergent rollover sequences of Figures 49 and 50. In Figure 52 we see part of the sequence that represents stable roll response, but then at some point the operating conditions are such that the roll mode diverges.

The relationship between roll angle and roll rate for a dynamic instability are similar to the directional mode above. An unstable roll angle divergence beyond some constant operating point, ϕ_0, is given by an exponential function,

$$\phi - \phi_0 = \Delta\phi = be^{t/\tau_\phi}$$

Roll rate is then given by

$$\frac{d\Delta\phi}{dt} = \dot{\phi} = -\frac{b}{\tau_0} e^{t/\tau_\phi}$$

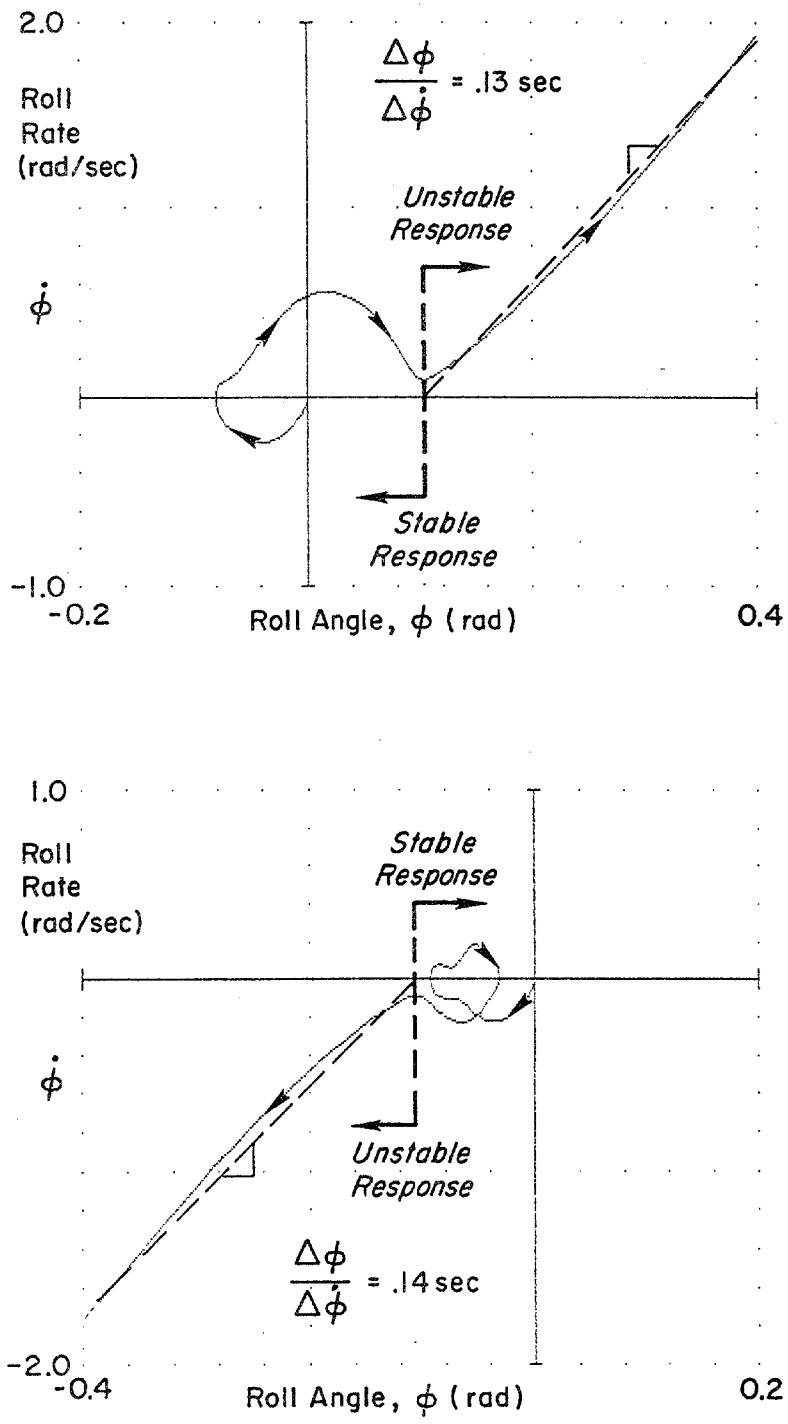

Figure 52. Cross Plots of Roll Angle and Roll Rate for the Light Utility Vehicle Rollover Events of Fig. 49 and 50.

and the ratio of the above two expressions then gives the rollover divergence time constant

$$\frac{\dot{\phi}}{\Delta\phi} = \tau_{\phi}$$

For both maneuvers note that, as indicated in Figure 52, the light utility vehicle has a roll divergence time constant of about .13 to .14 seconds (about six times as fast as a typical directional mode divergence discussed above).

The point at which the roll mode goes unstable in Figure 52 represents a critical operating condition where the roll rate begins to increase with roll angle. This operating condition is very sensitive to the initial steering input magnitude as illustrated in Figure 53 where roll responses are compared for several amplitude conditions with timing of the reversal steer profile held constant at the Figure 49 condition. Note that a difference of only about 1.3% in steering amplitude separates stable and unstable roll responses (i.e., 1.950 and 1.975 radians). This system response sensitivity represents a bifurcation point in system stability that is extremely sensitive to initial conditions. The reason for this operating condition sensitivity is illustrated in Figure 54 which portrays the composite force acting on the vehicle center of gravity due to vehicle weight and the inertial force due to lateral acceleration. If the composite force vector lies inside the rollover axis at the tire patch then the roll response is stable while if the vector falls outside of the rollover axis then sufficient roll moment is generated to cause rollover.

The exponential divergence in the roll mode instability arises from two main effects which cause the composite roll moment to increase with roll angle. First, the side force at the outside tires increases with increased normal load due to suspension and tire compression. This normal load is not relieved significantly by the sprung mass vertical response because of the rapidity of the rollover divergence. Second, as rollover progresses, c.g. height goes up which increases the lateral inertial force moment arm, and the c.g. moves towards the outside wheels which reduces the restoring moment of the vehicle weight. The composite effect of these changes is to give a roll moment that increases with roll angle thus producing a classical dynamic instability. This rollover instability is much more dramatic than directional instability, however, as evidenced by the relative difference in divergence time constants.

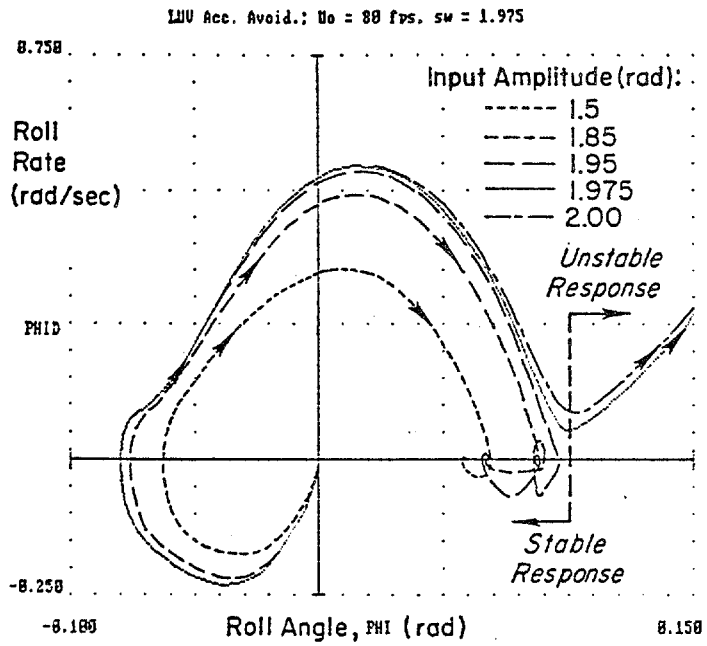

Figure 53. Rollover Phase Plane Plots for a Light Utility Vehicle at Several Input Amplitudes Showing a Bifurcation Point Between Stable and Unstable Maneuvering Conditions

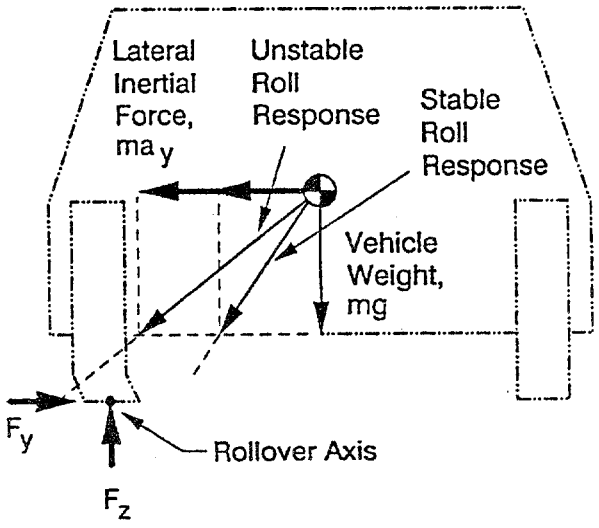

Figure 54. Rollover Model for Defining the Bifurcation Point Between Stable and Unstable Response

SECTION VIII

ROLLOVER ACCIDENT ANALYSIS FOR THE TEST VEHICLE POPULATION

A. BACKGROUND

Rollover accident analysis was addressed in Section III based on previously published data (i.e., Reference 3). For the vehicle population used in this research project (Appendix E), the NHTSA has carried out an accident analysis of an accident data base for the states and years summarized in Table 9. Using Vehicle Identification Numbers (VINs) NHTSA has identified single vehicle accidents (SVAs), the subset involving rollovers, and the ratio of rollovers to SVAs for each test vehicle make and model listed in Appendix E. The rollover rate data was then combined into the Appendix E spread sheet data tables, and univariate and multivariate linear regression analyses were carried out to identify the vehicle parameters that correlate with rollover accidents.

B. ROLLOVER RISK FACTORS

The spreadsheet program QUATRO PRO© was used to explore the dependence of SVA rollover rates on various vehicle parameters. Variables that relate to rollover propensity and directional stability were tested using univariate linear regression, as summarized in Table 10. Of the variables relating to rollover propensity, Track Width Ratio (i.e., TWR or ratio of half track width to c.g. height) and a_{yRO} or equivalent lateral acceleration for rollover have the highest correlations. Surprisingly, TWR has a significantly higher correlation than a_{yRO}, indicating that the efficiency factor variables do not contribute in a significant way to rollover rates. The correlation between efficiency factor and rollover rate is noted to be not significantly different from zero.

When multivariate linear regressions were used to consider a combination of variables, including rollover propensity parameters and directional stability parameters in Table 11, TWR and wheel base are noted to have significant regression parameters, with all other parameters being nonsignificant according to the Students 't' test. In Section III, wheel base was also found to have a significant correlation with rollover rate when considered in combination with TWR, and in Table 11, this is noted to be true with the current test vehicle population. The regression coefficients for the current test vehicle population

TABLE 9. STATE AND YEARS FOR ACCIDENT ANALYSIS

Georgia:	1987 – 88
Maryland:	1986 – 88
Michigan:	1986 – 88
New Mexico:	1986 – 88
Utah:	1986 – 88

TABLE 10. VARIABLES ANALYZED FOR CORRELATION WITH ROLLOVER RATES FOR SINGLE VEHICLE ACCIDENTS

	Correlation coeff. (r)	P
ROLLOVER PROPENSITY:		
Track Width Ratio - TWR	.769	<.001
Equivalent Lateral Acceleration – A_{yR0}	.629	<.001
Efficiency Factor	.303	NS
Roll Gradient – K_ϕ	.032	NS
DIRECTIONAL STABILITY		
Wheel Base – l	.000	NS
Lateral Load Transfer Distribution – LTD	.126	NS
Weight Distribution – wt.	.241	NS

TABLE 11. MULTIPLE REGRESSION ANALYSIS BETWEEN ROLLOVER RATE AND SEVERAL ROLLOVER PROPENSITY AND DIRECTIONAL STABILITY PARAMETERS

VARIABLE	COEFF.	STD. ERR.	't'	p
Track Width Ratio	-79.0	10.8	7.31	<.001
Wheel Base	-2.18	.912	2.39	<.025
Efficiency	7.45	33.2	0.22	NS*
Load Transfer Dist.	.0538	.197	0.27	NS
Weight Dist.	.221	.251	0.88	NS
Roll Gradient	-.927	.981	0.94	NS

r^2 = .679 ; Degrees of Freedom = 34

*NS = Not Statistically Significant

are also comparable to the coefficients shown in Fig. 6 for an earlier data base (i.e., Reference 3). A cross plot of rollover rates for the current test vehicle data base as a function of Track Width Ratio is given in Figure 55. Several vehicles are noted to have low rollover rates for their TWRs, including vans as a vehicle class. Also note that the passenger car, pickup and utility vehicle classes each span a relatively wide range of TWRs and the rollover sensitivity with TWR seems to hold up within each class.

The statistical significance of the influence of wheel base on rollover rate in the Table 11 regression analysis seems to be inconsistent with the zero correlation given in Table 10. The simple correlation coefficient between wheel base and track width ratio is about .106, so there is a small correlation between these two independent variables. The statistical significance of wheel base when considered in combination with track width ratio in the Table 11 regression analysis is probably due to the interaction of these two independent variables, and deserves more thorough investigation in future work.

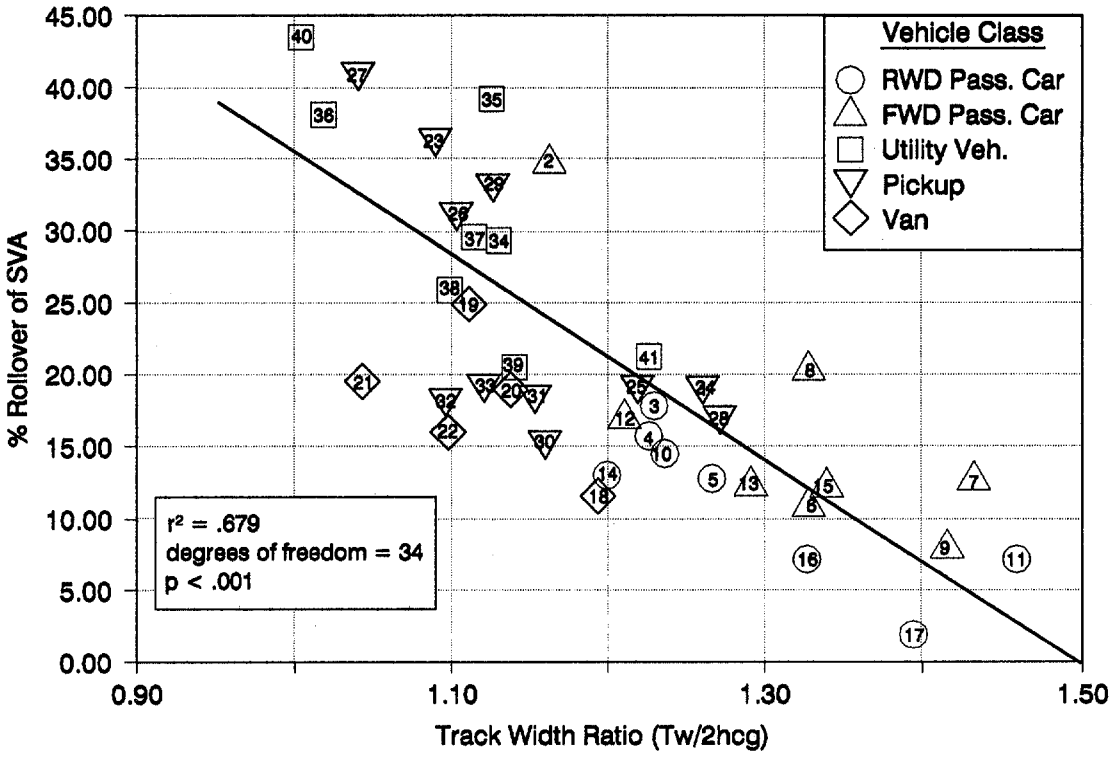

Figure 55. Relationship Between Rollover Rates in Single Vehicle Accidents and Vehicle Characteristics for the Current Test Vehicle Population (Appendix E)

SECTION IX

CONCLUSIONS AND RECOMMENDATIONS

Statistical analysis has shown that vehicle track width ratio (referred to elsewhere as a rollover 'stability factor') is strongly related to the single vehicle accident rollover rate of a large range of vehicles. Regression analysis shows some additional influence of wheel base on rollover rate. A computer simulation has been validated with field test data that can permit analysis of the effect of vehicle characteristics on directional stability and rollover propensity. Twelve vehicles were tested that span the range of rollover related parameters, and computer simulation of these vehicles in limit performance maneuvers was conducted in an attempt to rank directional stability and rollover propensity. A low track width ratio (the ratio of half track width to c.g. height) is clearly related to the propensity for rollover based on both accident data base statistical analysis and computer simulation analysis. Directional stability was shown to be related to the relationship between lateral load transfer distribution and weight distribution.

Many stability related parameters discussed herein co-vary such that vehicle stability could be compromised by several variables simultaneously. Track width ratio and wheel base ratio influence load transfer under maneuvering conditions, and load transfer can have a significant influence on directional stability as indicated by computer simulation analysis. The low track width ratios of pickups and utility vehicles that contribute to rollover propensity also lead to high lateral load transfer characteristics during cornering. Track width ratio and wheel base ratio are highly correlated so that vehicles with high lateral load transfer during cornering also experience high longitudinal load transfer during braking. During combined cornering and braking the pickup truck and utility vehicle categories exhibit significantly lower levels of stability compared with passenger cars. Also, due to high longitudinal load transfer during braking, stability during braking is more sensitive, to brake proportioning so that in-use vehicles may become more prone to rear brake lockup during transient braking conditions and when brake proportioning shifts to rear biasing due to in-use wear characteristics.

Directional stability is determined basically by the side force operating points at the front and rear axles under a given maneuvering condition. When the

rear axle saturates first, then the vehicle becomes directionally unstable. Under limit performance maneuvering conditions, both front and rear axles are near saturation, so the instability may be marginal and result in a slide-out (constant yaw rate) rather than spinout (divergent or exponentially increasing yaw rate). Minimum yaw divergence time constants observed here in the region of 1.0 second are not particularly dramatic compared to rear biased braking on low coefficient surfaces. However, during emergency limit performance maneuvering, the driver may not be prepared to effectively control this spinout condition.

The above analyses indicate that directional stability is influenced by lateral load transfer distribution (LTD) which can have significant influence on vehicle controllability, particularly under emergency limit performance maneuvering. The results indicate that vehicles whose LTDs are near to or greater than vehicle weight distribution exhibited stable vehicle responses. However, many vehicles whose LTDs are significantly less than their vehicle weight distribution also exhibited stable directional responses indicating that other considerations (e.g., wheel camber, tire characteristics) probably have significant influence. The results also suggest an influence of LTD on rollover stability. As center of gravity location is increased relative to track width and weight distribution moves significantly fore or aft, wheel lift off can result, having a negative influence on both directional and rollover stability, and balancing LTD becomes a critical problem.

All of the above results point to maintaining vehicle center of gravity heights as low as possible, and maintaining track width and wheel base ratios as high as possible. Four wheel drive vehicles deserve particular attention in this regard because of the chassis height required to accommodate the running gear is higher than two wheel drive models. The capability of a vehicle to achieve sufficiently high levels of lateral acceleration to initiate an untripped rollover on a flat surface is determined by the peak coefficient of friction of the vehicle's tires. Vehicles which exhibit particularly low levels of rollover stability can achieve "rollover" levels of lateral acceleration when the vehicles are equipped with "aggressive" (relatively high peak coefficient of friction) tires. Suspension designs which would tend to raise the vehicle's center of gravity when cornering, e.g., swing axle suspensions which exhibit such "jacking" effects, can reduce vehicle rollover stability. Also when tire/wheel options

raise c.g. height, an accompanying increase in track width would maintain a constant if not larger track width ratio.

Finally, further analysis work should be carried out on vehicle directional and rollover stability. There are probably yaw/roll coupling characteristics that contribute to rollover under transient conditions that have not been identified here. Directional stability and transient oversteer/spinout problems have only been touched on here and deserve additional analysis. In particular a detailed analysis of the influence of lateral load transfer distribution, maneuvering conditions and other factors leading to rear axle saturation (i.e., limit oversteer) is warranted. This analysis should include combined cornering and braking conditions, and other dynamic considerations such as suspension damping and tire properties.

REFERENCES

1. Malliaris, A.C., R.M. Nicholson, J.H. Hedlund, et al., "Problems in Crash Avoidance and in Crash Avoidance Research," SAE 830560, Feb. 1983.

2. Harwin, E.A., and H.K. Brewer, Analysis of the Relationship Between Vehicle Rollover Stability and Rollover Risk Using the NHTSA CARDfile Accident Database, Nat'l. Highway Traffic Safety Admin., 1987.

3. Mengert, P., S. Salvatore, et al., Statistical Estimation of Rollover Risk, U.S. Dept. of Trans. Nat'l. Highway Traffic Safety Admin., Report DOT-HS-807-446, Aug. 1989.

4. Allen, R.W., H.T. Szostak, and T.J. Rosenthal, "Steady State and Transient Analysis of Ground Vehicle Handling," SAE Paper No. 870495, Feb. 1987.

5. Allen, R.W., T.J.Rosenthal, and H.T. Szostak, Analytical Modeling of Driver Response in Crash Avoidance Maneuvering:

   - Vol. I: Technical Background, DOT-HS-807 270, April 1988.

   - Vol. II: An Interactive Tire Model for Driver/vehicle Simulation, DOT-HS-807 271, April 1988.

   - Vol. III: A Trim Model and Computer Program for Determining Ground Vehicle Steady State Operating Conditions and Quasilinear Stability Coefficients, DOT-HS-807 270, April 1988.

6. Heydinger, G.J., W.R. Garrott, J.P. Chrstos, et al., "Validation of Vehicle Stability and Control Simulations," SAE Paper No. 900128, Feb. 1990.

7. Loeb, J.S., et al., "Lateral Stiffness, Cornering Stiffness and Relaxation Length of the Pneumatic Tire," SAE Paper No. 900129, Feb. 1990.

8. Radlinski, R.W., "Assessment of Experimental Methods for Determining Braking Efficiency," Presented at the 12th Internat'l. Tech. Conf. on Experimental Safety Vehicles in Gothenburg, Sweden, May-June 1989.

9. Bernard, J., J. Shannan and M. Vanderploeg, "Vehicle Rollover on Smooth Surfaces," SAE Paper No. 891991, Sept. 1989.

10. Jones, I.S., The Effect of Vehicle Characteristics on Road Accidents, Pergamon Press Ltd., Headington Hill Hall, Oxford OX3 OBW, England, 1976.

11. Rosenthal, T.J., H.T. Szostak and R.W. Allen, User's Guide and Program Description for a Tripped Roll Over Vehicle Simulation, DOT-HS-807140, July 1987.

12. Garrott, W.R., M.W. Monk and J.P. Chrstos, "Vehicle Inertial Parameters-Measured Values and Approximations," SAE Paper No. 881767, Nov. 1988.

13. Gillespie, T.D. and R.D. Ervin, "Comparative Study of Vehicle Roll Stability," Report No. UMTRI-83-25, Univ. of Michigan Transportation Institute, May 1983.

14. Jones, I.S. and M.B. Penny, "Engineering Parameters Related to Rollover Frequency," SAE Paper No. 900104, SAE SP-814, pp.73-94.

15. Schuring, D.J., Tire Parameter Determination, Vol. I - Summary, NHTSA DOT HS-802 086, Nov. 1976.

16. Tapia, G.A., Extending Tire Testing, NHTSA DOT HS-806 594, Nov. 1983.

17. Allen, R.W., H.T. Szostak, T.J. Rosenthal, et al., "Test Methods and Computer Modeling for the Analysis of Ground Vehicle Handling," SAE Paper No. 861115, Aug. 1986.

18. Allen, R.W., J.R. Hogue, T.J. Rosenthal, et al., "A Data Acquisition and Analysis System Based on a Lap-Top Computer," TRB/A3B06 Midyear Meeting, Liberty Mutual Insurance Co., Hopkinton, MA, June 1988. Published in: Human Performance and Highway Visibilty: Design, Safety, & Method, Transportation Research Board, Washington, DC, TRR No. 1213, 1989 pp. 82-89.

19. Allen, R.W., H. T. Szostak, and T. J. Rosenthal, "Analysis and Computer Simulation of Driver/Vehicle Interaction," SAE Paper No. 871086, May 1987.

20. Fancher, P.S., R.D. Ervin, P. Grote, et al., Limit Handling Performance as Influenced by Degradation of Steering and Suspension Systems, Vol I, DOT HS-031-1-126, UM-HSRI-PD-72-3-1, Nov. 1972.

21. Allen R.W., J.R. Hogue and Z. Parseghian, "Manual Control of Unstable Systems," 21st Annual Conf. on Manual Control, NASA CP-2428, May 1986, pp. 32.1 – 32.18.

22. Holloway, D.C., T.J.Drach and B.Mohanty, "An Experimental Investigation of Passenger Car Tire Properties at High Slip and Camber Angles," SAE Paper No. 910233, Feb. 1990.

23. Klein, R.H., D.T. McRuer, D.H. Weir, et al., Automobile Controllability – Driver/Vehicle Response for Steering Control, Vol. I and II, NHTSA DOT HS-801 407 and NHTSA DOT HS-801 406, Feb. 1975.

24. Bendat, Julius S., and Allan G. Piersol, Measurement and Analysis of Random Data, John Wiley and Sons, Inc., NY, 1966.

25. Chrstos, J.P., An Evaluation of Static Rollover Propensity Measures, Report No. VRTC-87-0086, Transportation Research Center of Ohio, May 1991.

APPENDIX A

COMPUTER SIMULATION DYNAMICS FOR LONGITUDINAL AND LATERAL/DIRECTIONAL MODES OF GROUND VEHICLES

APPENDIX A

COMPUTER SIMULATION DYNAMICS FOR LONGITUDINAL AND LATERAL/DIRECTIONAL MODES OF GROUND VEHICLES

A. BACKGROUND AND OVERVIEW

The computer simulation dynamics described in this appendix have been adapted from an earlier automobile simulation (Ref. 14). Earlier versions of this vehicle simulation have used a fixed roll axis assumption for derivation of the equations of motion. The fixed roll axis concept has been abandoned for this version of the simulation, which instead uses a composite description of wheel/suspension motions which in effect determine the instantaneous location of the roll axis at the front and rear axles. The approach described herein was taken in order to adequately account for the response of independent suspensions to vertical terrain profiles.

The equations of motion developed herein explicitly account for all motions in the longitudinal and lateral/directional dynamics. Earlier versions of this simulation had not completely accounted for the longitudinal pitch mode which has now been specifically addressed. All wheels have separate spin modes. Tire horizontal forces are computed with the same model used previously (Refs. 2 and 13). Load transfer between tires and axles occurs due to both lateral and longitudinal acceleration.

The inertial dynamics are modeled by a variety of force and moment equations which describe the motions of the vehicle sprung mass (body, frame and power train) and wheel and suspension unsprung masses. Sprung and unsprung mass motions are kept separate in the pitch, heave, lateral and roll mode equations. The yaw and longitudinal motions are for the total vehicle mass. This approach was taken in order to provide the simplest set of equations that would adequately account for all longitudinal and lateral/directional motions. Finally, pitch and roll equations account for large angle effects so that rollover and pitchover are adequately accounted for.

B. AXIS SYSTEM AND DEGREES OF FREEDOM

The model development in this appendix divides the vehicle into three mass components, the vehicle sprung mass and the front and rear axle unsprung masses. The motions of the basic vehicle sprung mass are driven by forces developed by the tires at the roadway surface. These tire forces result from slip motions relative to the roadway surface. The slip motions in turn require specification of the motions of the tires, wheels, and other unsprung mass (suspension) components in the roadway axis system. Therefore, the unsprung mass motion variables are all set up to act in the horizontal roadway plane. The vehicle sprung mass motions then only need be modeled in the way forces react back to the unsprung masses, and to define suspension and steering effects that results from motions between the masses.

The above distinction is important, and is shown in Fig. A-1, where a "sleeve" carries and defines the unsprung masses in the horizontal roadway plane axis system. The sprung mass, and even the unsprung mass in roll-over motions, can rotate in the roll direction relative to this sleeve. This approach focuses on motions at the road surface, rather than at the sprung mass center of gravity because of the way in which tire force development is tested and modeled. All tire test data is defined as forces and moments acting in the horizontal roadway plane, in response to side slip angle, camber angle, and longitudinal slip relative to this horizontal roadway plane.

Pitch angles are assumed to be very small, with a maximum of .05 to .07 radians reached even on very bumpy road surfaces. On smooth roads, the only pitch disturbance is from longitudinal acceleration (a_x) transients, or suspension squat/lift reactions, which result in only very small pitch angles. The primary purpose for the pitch degree of freedom is to define suspension deflections which produce changes in suspension forces and steering geometry. Therefore, we are defining pitch motions to take place in the body axis system. This means that during tip-over (large ϕ_s angles), the pitch motion directions will follow the suspension as the entire vehicle rolls over. The fact that the pitch motions are extremely small, allows us to assume that most classical motion variable cross product terms can be ignored as an insignificant effect.

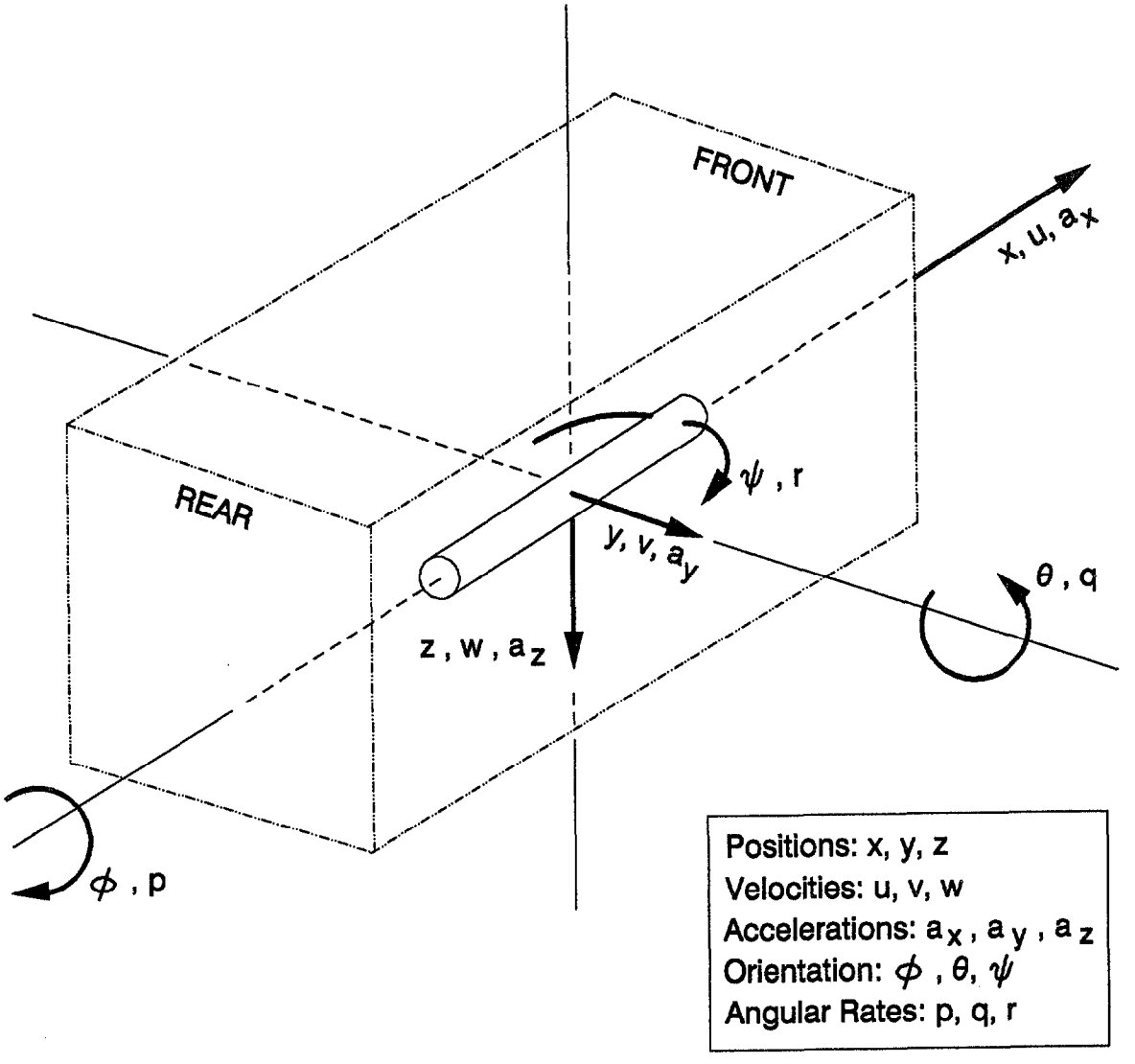

ψ ,y, v, a_y, z are fixed to a sleeve over the longitudinal body axis, which allows ψ,y, v, a_y, to stay level with the road plane, (do not rotate with ϕ), and z remain perpendicular to road plane.

Figure A-1. Vehicle Axis System

The basic vehicle model degrees of freedom described in this appendix are summarized in Table A-1. Wherever possible, we have attempted to employ composite parameter characteristics in the modeling in order to minimize the total number of parameters and give parameters (i.e., composite characteristics) that are easy to measure and/or estimate. The following features are included in the vehicle model described herein:

1. Suspension force mechanisms acting at each wheel including
   - — Springs
   - — Damping (shock absorbers)
   - — Bump stops
   - — Auxiliary roll stiffness (anti roll bars)
   - — Squat/lift forces (due to suspension geometry)

2. Steering and suspension geometry effects
   - — Wheel camber angle vs. suspension deflection and roll angle
   - — Suspension squat/lift forces due to lateral and longitudinal tire force action on suspension geometry
   - — Wheel steer as a function of
     - – Suspension deflections (roll steer)
     - – Lateral fore applied to suspension compliance
     - – Tire aligning torque applied to steering system compliance
     - – Ackerman steer geometry

3. Compliant pin joints at the roll axis between the sprung and unsprung masses to simulate real rubber bushing effects, and also avoid computational instabilities.

4. Second order lag for tire lateral force development.

5. Lateral force deflection of tire, wheel, and suspension which results in a significant loss in track width under vehicle roll over conditions.

6. Full resolution of all forces to accommodate vehicle rollover conditions.

A guide to the subsequent vehicle motion equation development was given in Fig. A-2 which shows the various model components and their interactions.

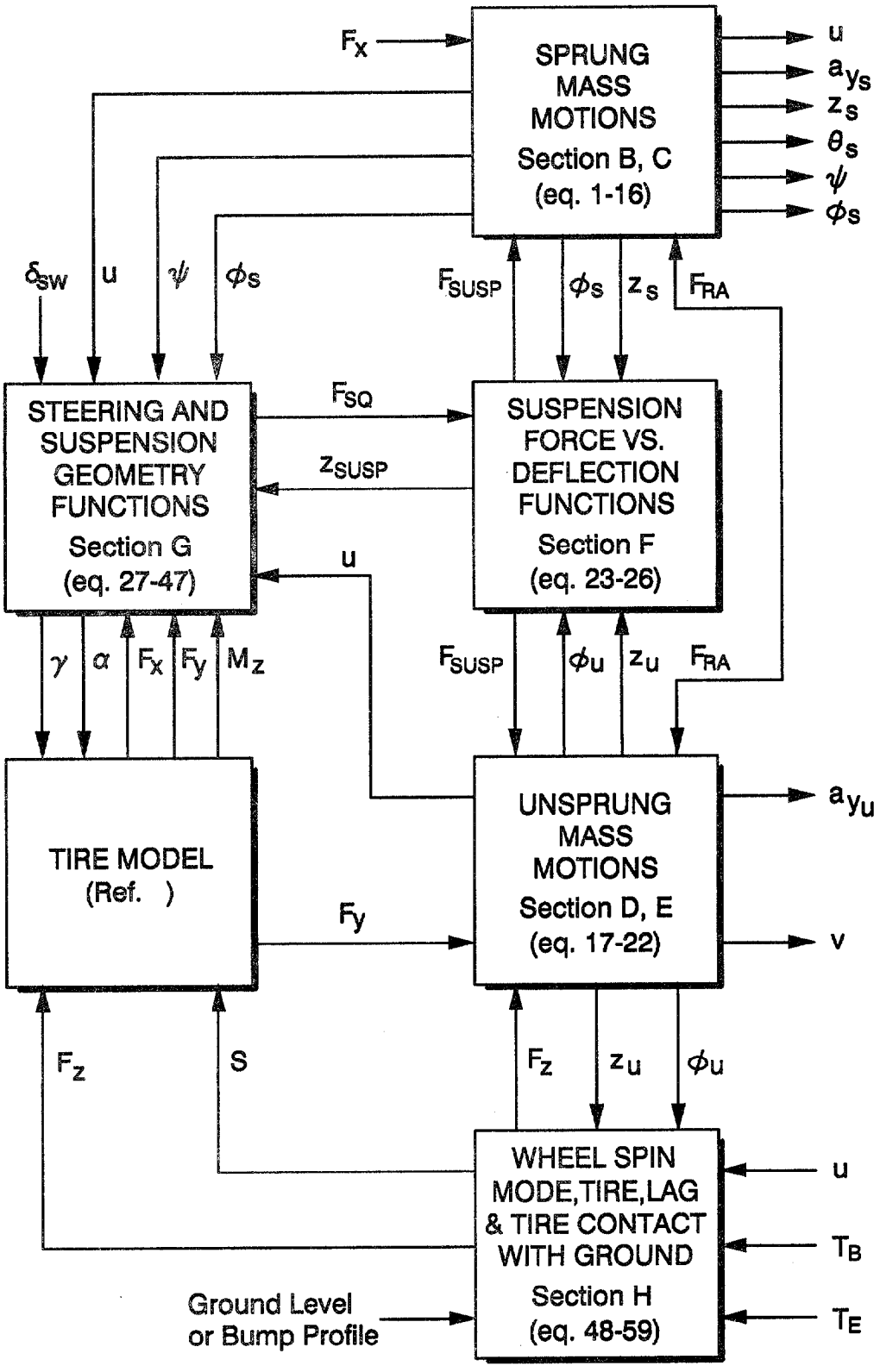

Figure A-2. Vehicle Dynamics Model Components and Their Interactions

TABLE A-1. BASIC VEHICLE MODEL DEGREES OF FREEDOM

MASS		MOTION VARIABLES	D.O.F.
Sprung Mass	(m_s)	θ_s, ϕ_s, z_s, a_{y_s}	4
Total Mass	(m)	ψ, u	2
Front Unsprung	(m_{UF})	z_{UF}, ϕ_{UF}, $a_{y_{UF}}$	3
Rear Unsprung	(m_{UR}	z_{UR}, ϕ_{UR}, $a_{y_{UR}}$	3
Wheel rotational inertia (4)	(I_W)	ω_i [spin mode, 4 wheels]	4
Wheel inertia about steer axis	(I_{FW})	δ_{WF}	1
TOTAL DEGREES OF FREEDOM			17

C. VEHICLE INERTIAL DYNAMICS

Longitudinal Force (forward velocity) — The longitudinal force equation accounts for the entire vehicle mass (see Fig. A-3).

$$m(\dot{u} - \dot{\psi}v) = \Sigma X \qquad \text{(A-1)}$$

Yawing Moment (yaw rate) — This equation is assumed to compute the angular rate of the entire vehicle mass in the horizontal plane independent of roll angle. The relationship accounts for yaw rate and roll acceleration cross coupling (see Fig. A-3).

$$I_z \ddot{\psi} - I_{xz_s} \ddot{\phi}_s = \Sigma N \qquad \text{(A-2)}$$

Sprung Mass Side Force (lateral acceleration) — Forces acting at the roll axis and at the suspension produce sprung mass lateral acceleration (see Fig. A-4).

$$m_s a_{y_s} = \Sigma Y_s \qquad \text{(A-3)}$$

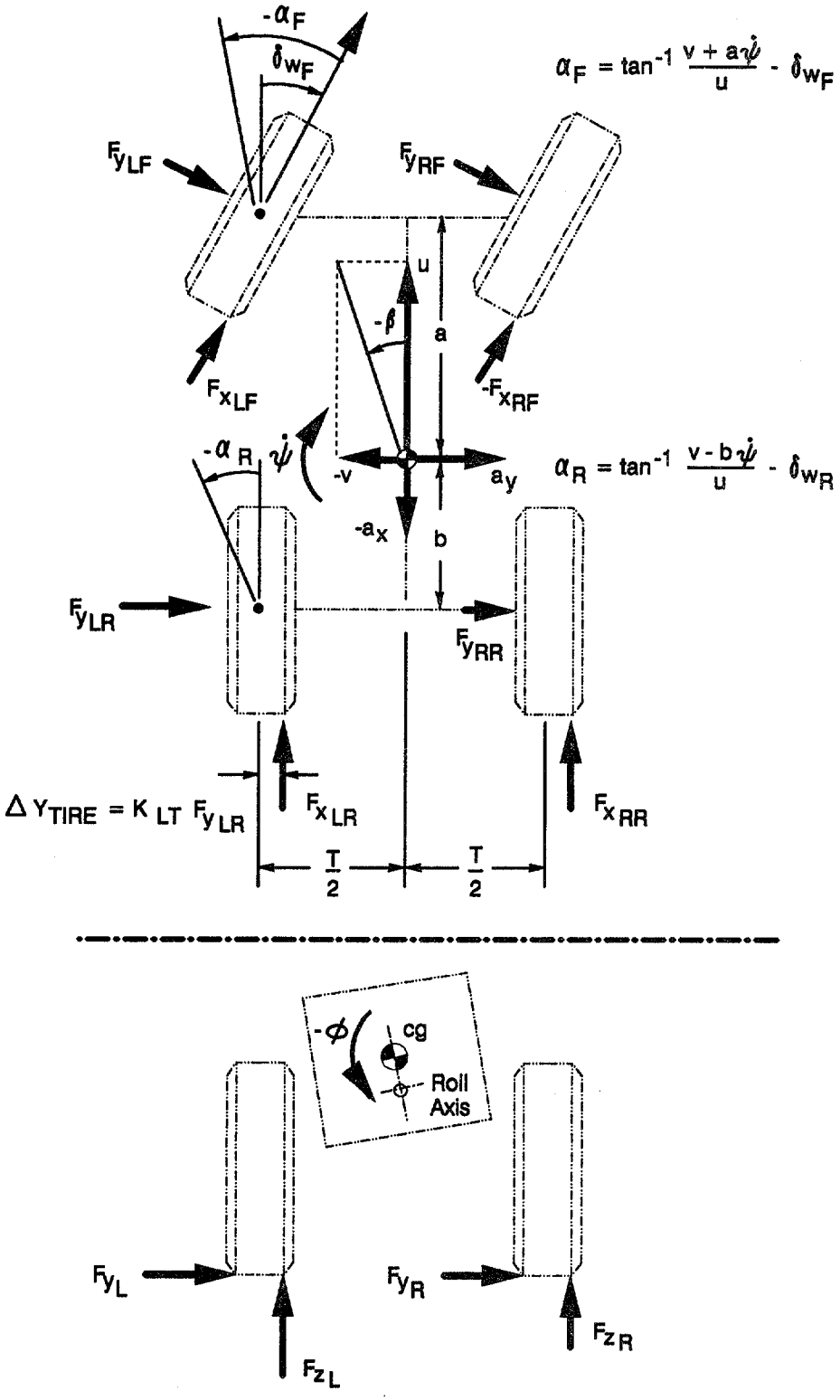

Figure A-3. Major Variables Included in the Transient Dynamic Model

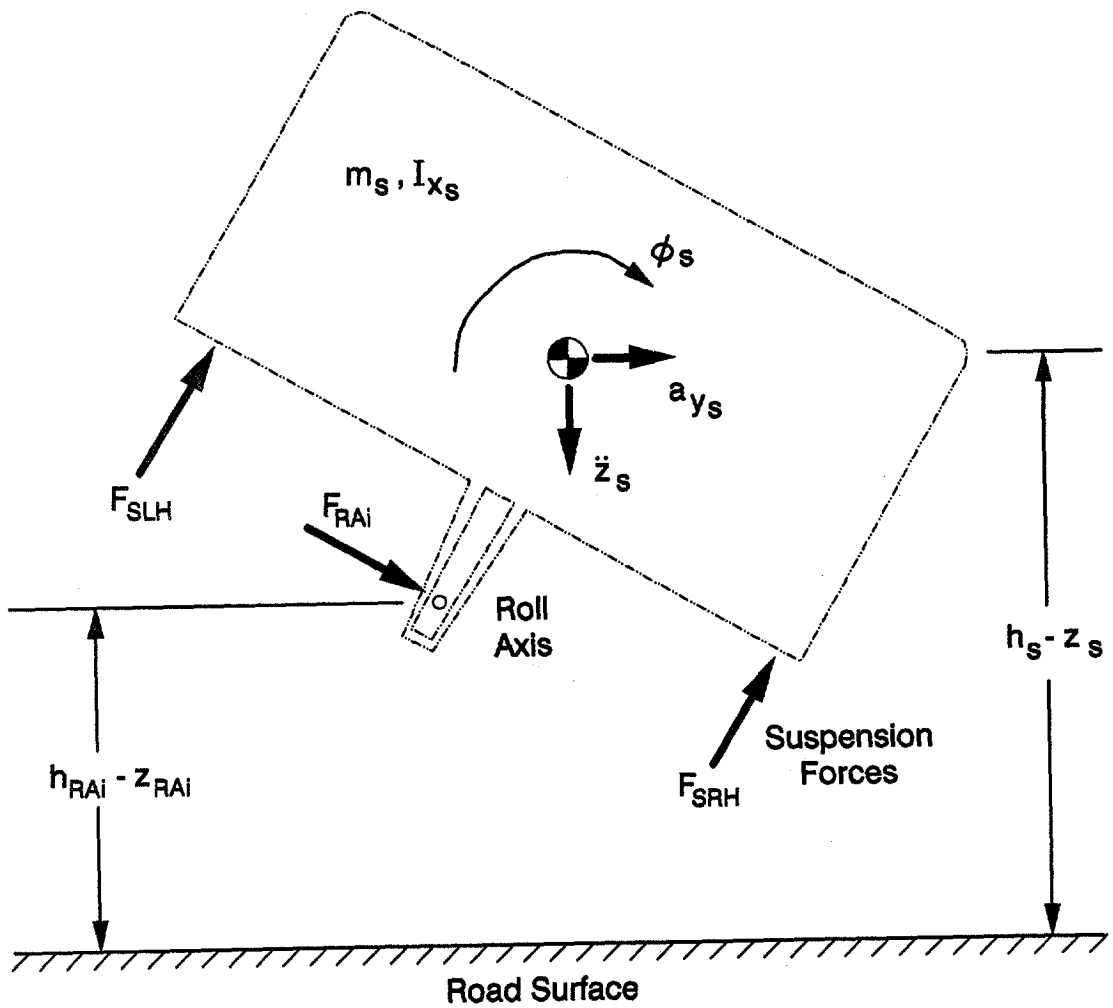

Figure A-4. Sprung Mass Free Body Diagram, End View

Sprung Mass Rolling Moment (roll rate) — Taking moments about the sprung mass c.g. in Fig. A-4, produces sprung mass roll motions.

$$I_{\phi_s} \ddot{\phi}_s - I_{xz_s} \ddot{\psi} = \Sigma L_s \tag{A-4}$$

Sprung Mass Vertical Force (vertical acceleration) – The sprung mass vertical motions result from vertical forces acting on it (see Fig. A-4).

$$m_s \ddot{z}_s = m_s g - \Sigma Z_s \tag{A-5}$$

Sprung Mass Pitch Moment (pitch rate) – Sprung mass pitch motions result from moments about the sprung mass c.g., in Fig. A-5.

$$I_{y_s} \ddot{\theta}_s = \Sigma M_s \tag{A-6}$$

D. FORCES AND MOMENTS ACTING ON INERTIAL DYNAMICS

These are the sums of forces and moments acting in each direction upon the sprung or total mass, as defined in section C (page A-6), as shown in the same Figs. A-3, A-4, A-5.

$$\begin{aligned}\Sigma X = {} & F_{x_{LR}} + F_{x_{RR}} + \left(F_{x_{LF}} + F_{x_{RF}}\right) \cos \delta_w \\ & - \left(F_{y_{LF}} + F_{y_{RF}}\right) \sin \delta_w\end{aligned} \tag{A-7}$$

$$\begin{aligned}\Sigma N = {} & \left(F_{y_{LF}} + F_{y_{RF}}\right) a \cos \delta_w + \left(F_{x_{LF}} + F_{x_{RF}}\right) a \sin \delta_w \\ & + \left(F_{y_{RF}} - F_{y_{LF}}\right) \frac{T_F}{2} \sin \delta_w + \left(F_{x_{LF}} - F_{x_{RF}}\right) \frac{T_F}{2} \cos \delta_w \\ & + \left(F_{x_{LR}} - F_{x_{RR}}\right) \frac{T_R}{2} - \left(F_{y_{LR}} + F_{y_{RR}}\right) b\end{aligned} \tag{A-8}$$

$$\begin{aligned}\Sigma Y = {} & \left(F_{RAF} + F_{RAR}\right) \cos \phi_s \\ & + \left(F_{SLF} + F_{SLR} + F_{SRF} + F_{SRR}\right) \sin \phi_s\end{aligned} \tag{A-9}$$

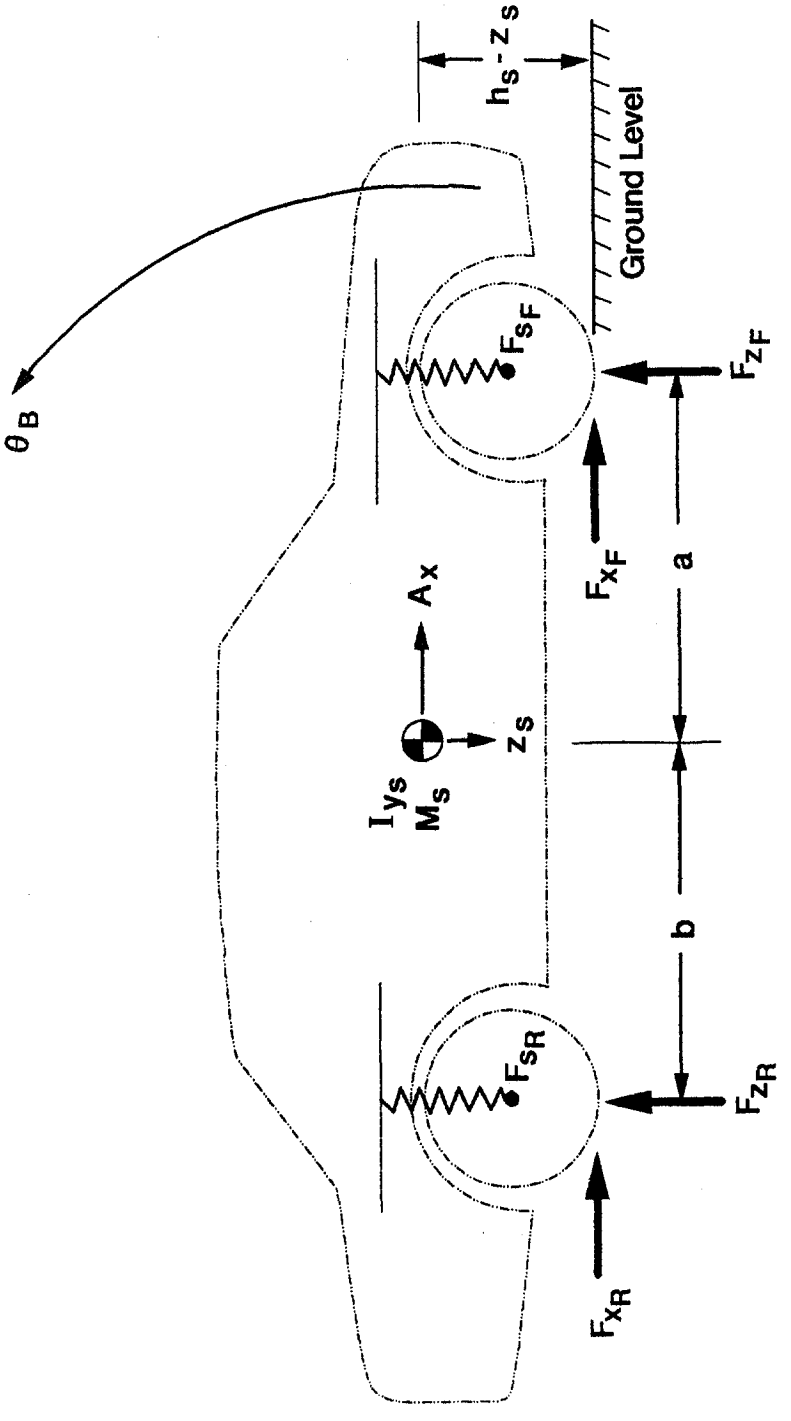

Figure A-5. Sprung Mass Free Body Diagram, Side View

$$\Sigma L = F_{SLF}\frac{T_F}{2} + F_{SLR}\frac{T_R}{2} - F_{SRF}\frac{T_F}{2} - F_{SRR}\frac{T_R}{2}$$
$$- \frac{F_{RAF}}{\cos \phi_s}\left(h_s - z_s - R_W + z_{UF} - \left[h_{RAF} - R_W\right] \cos \phi_{UF}\right)$$
$$- \frac{F_{RAR}}{\cos \phi_s}\left(h_s - z_s - R_W + z_{UR} - \left[h_{RAR} - R_W\right] \cos \phi_{UR}\right) \quad \text{(A-10)}$$

$$\Sigma Z = \left(F_{SLF} + F_{SLR} + F_{SRF} + F_{SRR}\right) \cos \phi_s$$
$$- \left(F_{RAF} + F_{RAR}\right) \sin \phi_s \quad \text{(A-11)}$$

$$\Sigma M = a\left(F_{SLF} + F_{SRF}\right) - b\left(F_{SLR} + F_{SRR}\right) + \left\{\left(F_{x_{LF}} + F_{x_{RF}}\right) \cos \delta_w\right.$$
$$\left. - \left(F_{y_{LF}} + F_{y_{RF}}\right) \sin \delta_w + F_{x_{LR}} + F_{x_{RR}}\right\}\left(h_s - z_s\right) \quad \text{(A-12)}$$

Aerodynamic forces and moments are also included in these equations.

$$Y_A = \frac{\partial Y_A}{\partial v}(v - v_g) \quad \text{(A-13)}$$

$$N_A = \frac{\partial N_A}{\partial v}(v - v_g) \quad \text{(A-14)}$$

$$L_A = \frac{\partial L_A}{\partial v}(v - v_g) \quad \text{(A-15)}$$

$$X_A = \frac{1}{2}\rho A\, C_D\, U^2 \quad \text{(A-16)}$$

E. UNSPRUNG MASS ROLLING MOMENT

The unsprung masses are acted upon by inertial and tire forces, and reaction forces at the roll axis pin and suspension as illustrated in Fig. A-6 for each axle. Following from the axle free body diagram in Fig. A-6 the rolling moment equation is the same at the front and rear:

$$I_{ui}\ddot{\phi}_{ui} = \Sigma L_{ui} \quad \text{(A-17)}$$

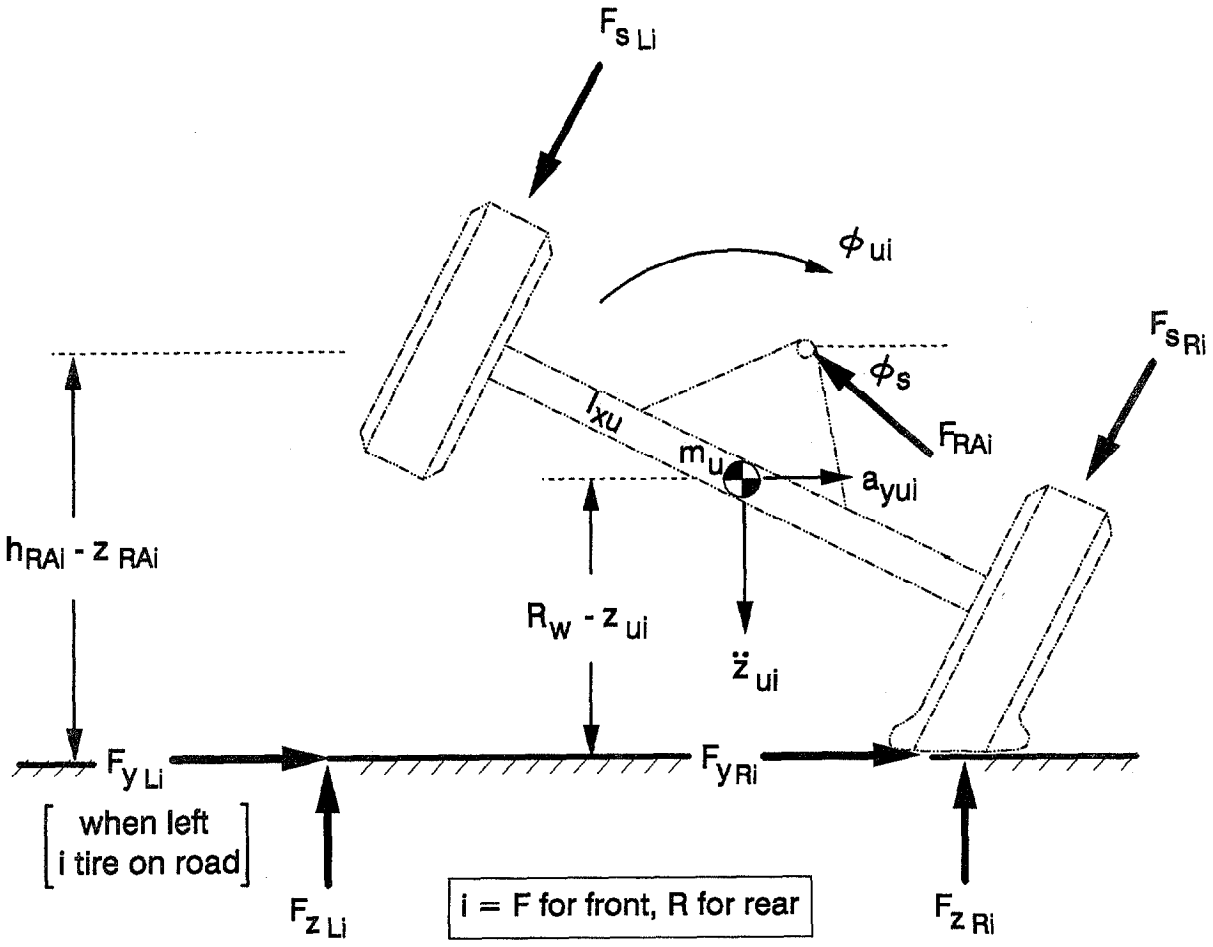

Figure A-6. Unsprung Mass Free Body Diagram

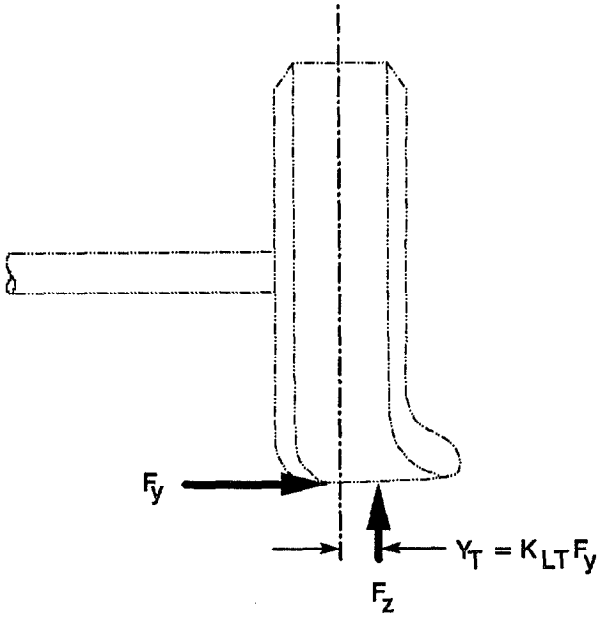

Figure A-7. Tire Lateral Deflection Characteristics

Unsprung Mass Vertical Acceleration – The tires are permitted vertical compliance, and large roll angles are a consequence of c.g. elevation, so vertical acceleration equations for each axle are required. Following from the Fig. A-6 axle free body diagram,

$$m_{ui}\,\ddot{z}_{ui} = m_{ui}g - \Sigma Z_{ui} \tag{A-18}$$

Unsprung Mass Lateral Acceleration – From Fig. A-6, the net sum of all lateral forces act on the unsprung mass to produce lateral acceleration.

$$m_{ui}\,a_{y_{ui}} = \Sigma Y_{ui} \tag{A-19}$$

where i = F for front, or R for rear

F. FORCES AND MOMENTS ACTING ON UNSPRUNG MASSES

Note that K_{LT} relates to lateral tire compliance as illustrated in Fig. A-7. This can be an important effect in rollover situations since it reduces the effective axle track width.

$$\begin{aligned}\Sigma L_{ui} = {} & F_{SRi}\frac{T_i}{2} - F_{SLi}\frac{T_i}{2} - F_{RAi}\left(h_{RAi} - R_w\right) \\ & + F_{Z_{Li}}\left[R_w \sin\phi_{ui} + \frac{T_i}{2}\cos\phi_{ui} - K_{LT}\,F_{y_{Li}}\right] \\ & - F_{Z_{Ri}}\left[-R_w \sin\phi_{ui} + \frac{T_i}{2}\cos\phi_{ui} + K_{LT}\,F_{y_{Ri}}\right] \\ & - \left[\left(F_{y_{Li}} + F_{y_{Ri}}\right)\cos\delta_{w_i} + \left(F_{x_{Li}} + F_{x_{Ri}}\right)\sin\delta_{w_i}\right]\left(R_W - z_{ui}\right)\end{aligned} \tag{A-20}$$

$$\Sigma Z_{ui} = F_{Z_{Li}} + F_{Z_{Ri}} + F_{R_{Ai}}\sin\phi_s - \left(F_{S_{Li}} + F_{S_{Ri}}\right)\cos\phi_s \tag{A-21}$$

$$\begin{aligned}\Sigma Y_{ui} = {} & \left(F_{y_{Li}} + F_{y_{Ri}}\right)\cos\delta_{w_i} + \left(F_{x_{Li}} + F_{x_{Ri}}\right)\sin\delta_{w_i} \\ & - F_{RAi}\cos\phi_s - \left[F_{SLi} + F_{SRi}\right]\sin\phi_s\end{aligned} \tag{A-22}$$

G. SUSPENSION FORCE DEVELOPMENT

The suspension forces acting on the sprung and unsprung masses depend on the suspension compression, relative roll angle, and squat lift reactions. In an effort to maintain generalized applicability to any type of suspension, all of the force reactions are modified to have their equivalent force acting at the track width, (i.e., at each wheel). This includes effects from suspension spring load, shock absorber damping, auxiliary roll stiffness, bump stop forces, and squat/lift forces from suspension geometry reactions (see Figs. A-8, A-9).

$$F_{SLF} = F_{SLF_o} - z_{SLF}\, K_{SF} - \dot{z}_{SLF}\, K_{SDF} + \frac{(\phi_s - \phi_{UF})\, K_{TSF}}{T_F} + F_{BSLF} + F_{SQLF} \tag{A-23}$$

where; if $|z_{SLF}| \leq h_{BS}$, then $F_{BSLF} = \text{zero}$

if $|z_{SLF}| > h_{BS}$, then $F_{BSLF} = \left(-z_{SLF} + [\text{sign } z_{SLF}] h_{BS}\right) K_{BS}$ (A-24)

$$F_{SRF} = F_{SRF_o} - z_{SRF}\, K_{SF} - \dot{z}_{SRF}\, K_{SDF} - \frac{(\phi_s - \phi_{UF})\, K_{TSF}}{T_F} + F_{BSRF} + F_{SQRF} \tag{A-25}$$

where; if $|z_{SRF}| \leq h_{BS}$, then $F_{BSRF} = \text{zero}$

if $|z_{SRF}| > h_{BS}$, then $F_{BSRF} = \left(-z_{SRF} + [\text{sign } z_{SRF}]\, h_{BS}\right) K_{BS}$ (A-26)

And, the same equations are used for F_{SLR}, F_{SRR}, with each F subscript replaced with R, for the rear axle.

In the preceding suspension force equations, the values for z_{Sij} and $\dot{z}_{Sij}$ need to be computed.

These equations define the change in spring length, starting from what the spring length is at curb load, F_{Sij_o} (use Fig. A-9).

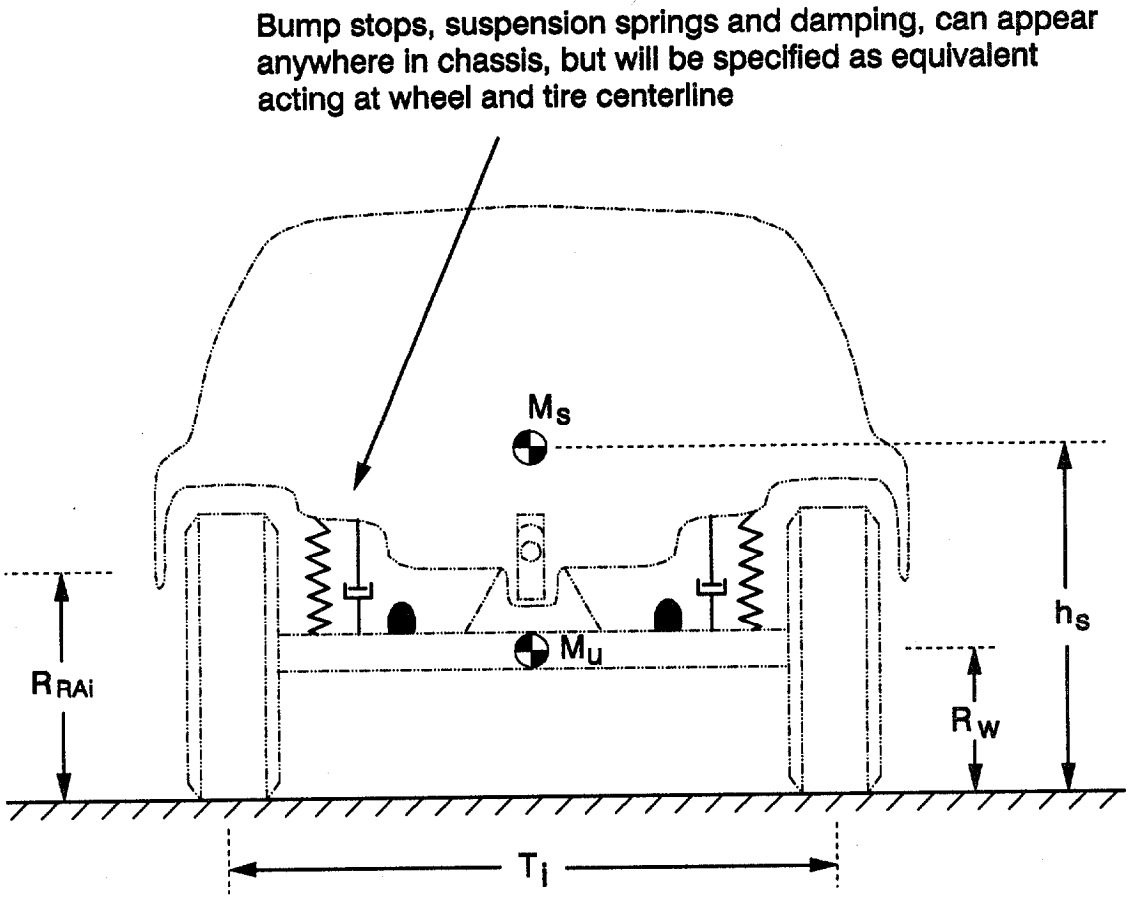

Figure A-8. Suspension Spring and Damping Components

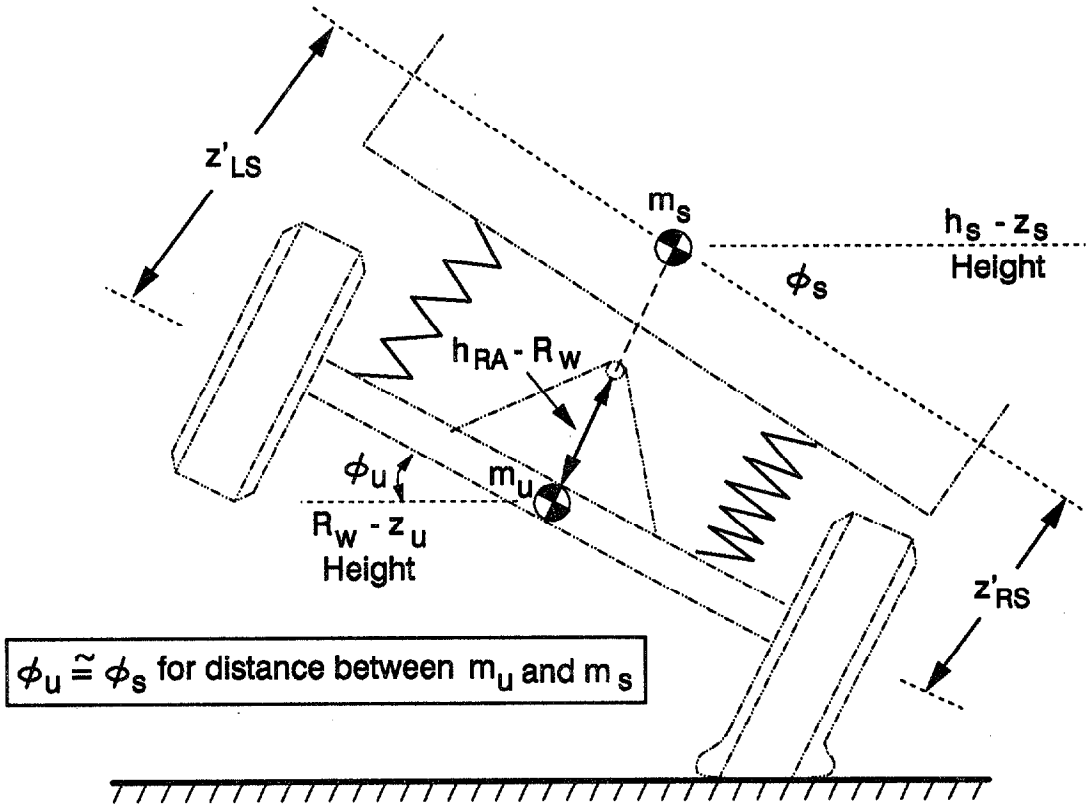

Initial condition distance from m_u to $m_s = h_s - R_w$

Current Distance = z'

Change from I.C. for suspension deflection at the wheel = $z' - h_s + R_w = z_{Sij}$

$$z'_{RS} = \frac{h_s - z_s - R_w + z_u}{\cos \phi_s} - (\phi_s - \phi_u)\frac{T_F}{2} + a\theta$$

$$z_{SRF} = \frac{h_s - z_s - R_w + z_u}{\cos \phi_s} - h_s + R_w + a\theta - (\phi_s - \phi_{UF})\frac{T_F}{2}$$

Figure A-9. Change in Suspension Spring Length

$$z_{SLF} = \frac{h_S - R_W + z_{UF} - z_S}{\cos \phi_S} - h_S + R_W + a\theta + \left(\phi_S - \phi_{UF}\right) \frac{T_F}{2} \quad \text{(A-23a)}$$

$$z_{SRF} = \frac{h_S - R_W + z_{UF} - z_S}{\cos \phi_S} - h_S + R_W + a\theta - \left(\phi_S - \phi_{UF}\right) \frac{T_F}{2} \quad \text{(A-24a)}$$

$$z_{SLR} = \frac{h_S - R_W + z_{UR} - z_S}{\cos \phi_S} - h_S + R_W - b\theta + \left(\phi_S - \phi_{UR}\right) \frac{T_R}{2} \quad \text{(A-25a)}$$

$$z_{SRR} = \frac{h_S - R_W + z_{UR} - z_S}{\cos \phi_S} - h_S + R_W - b\theta - \left(\phi_S - \phi_{UR}\right) \frac{T_R}{2} \quad \text{(A-26a)}$$

$$\dot{z}_{SLF} = \dot{z}_{UF} - \dot{z}_S + a\dot{\theta} + \left(\dot{\phi}_S - \dot{\phi}_{UF}\right) \frac{T_F}{2} \quad \text{(A-23b)}$$

$$\dot{z}_{SRF} = \dot{z}_{UF} - \dot{z}_S + a\dot{\theta} - \left(\dot{\phi}_S - \dot{\phi}_{UF}\right) \frac{T_F}{2} \quad \text{(A-24b)}$$

$$\dot{S}_{SLR} = \dot{z}_{UR} - \dot{z}_S - b\dot{\theta} + \left(\dot{\phi}_S - \dot{\phi}_{UR}\right) \frac{T_R}{2} \quad \text{(A-25b)}$$

$$\dot{S}_{SRR} = \dot{z}_{UR} - \dot{z}_S - b\dot{\theta} + \left(\dot{\phi}_S - \dot{\phi}_{UR}\right) \frac{T_R}{2} \quad \text{(A-26b)}$$

H. SUSPENSION AND STEERING GEOMETRY FUNCTIONS

The suspension and steering geometry defines the relative motions between the 4 wheels and the sprung mass body. Each vehicle's suspension could be defined by the length and orientation of each member in the suspension. But suspension geometry is so varied and sometimes very complex, that it would be very difficult to put all measurement data into one consistent organized scheme.

To avoid this problem, we have organized all suspension and steering effects in terms of effects at the tire contact point on the road surface. This makes the estimation of all parameters consistent and simple, which can be determined by a simple static test of wheel motions at the ground contact point. This composite approach is also consistent with keeping the equations of motion mathematics as simple and direct as possible, since all the F_x, F_y, F_z, M_z force inputs to the vehicle are defined at this same tire contact point on the road surface.

The composite parameter approach includes the following effects:

1. Wheel camber angle as a function of suspension deflection, which produces tire side force.

2. Suspension squat and lift forces, as a function of F_X, F_Y, F_Z forces at the tire contact point, which are affected by suspension deflection geometry.

3. Individual wheel steer angle as a function of;

   a) Suspension deflection

   b) Ackerman steer function.

   c) Aligning torque applied to steering system compliance.

   d) Lateral force applied to suspension compliance.

   e) Steering axis offset

   f) Steering system lag

4. Finally, the individual wheel steer angles along with V, U, $\dot{\psi}$, $\dot{\phi}_S$, are used to compute the tire side slip (α_{ij}) at each tire, which then produce tire side forces.

With all these above listed effects defined at the tire contact point on the road surface, then very straightforward static tests can be done to measure δ_W, γ, x, y, z motion relationships at each wheel (see Fig. A-10).

The following sections will describe in detail how these motion relationships are specified by math equations, and how the static test data relates to the equation parameters.

1. Wheel Camber Angle Versus Suspension Deflection

Typical wheel camber curves are shown in Fig. A-11, and can be represented by a second order equation in relation to the sprung mass body. Since the body also can have a roll angle, the wheel camber angle relative to the road surface is = ϕ_S + second order equation.

For independent suspensions

$$\gamma_{LF} = \phi_S + D_F z_{SLF} + E_F z_{SLF}^2 \qquad \text{(A-27)}$$

$$\gamma_{RF} = \phi_S - D_F z_{SRF} - E_F z_{SRF}^2 \qquad \text{(A-28)}$$

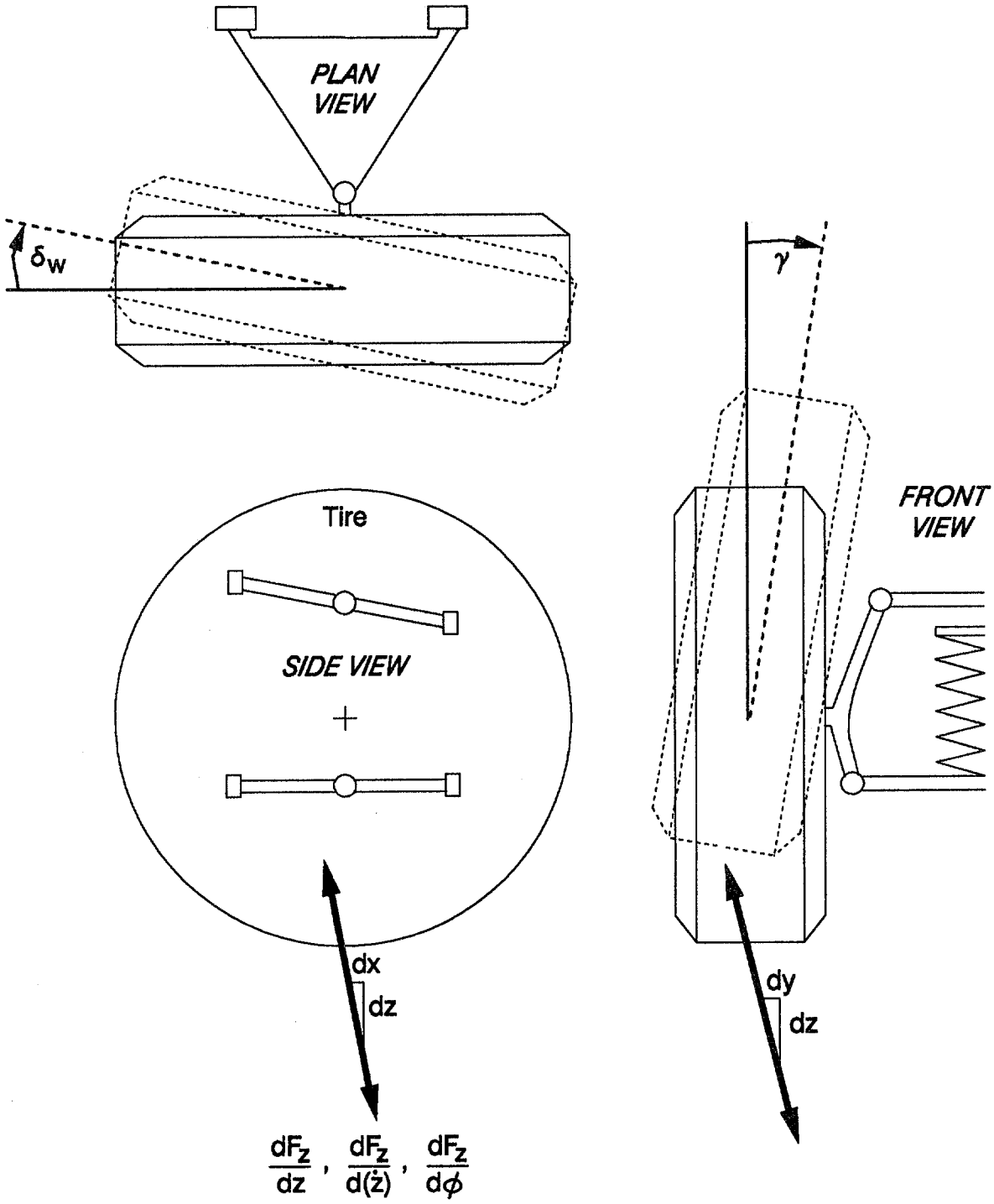

Figure A-10. Static Tests on Wheel Motions

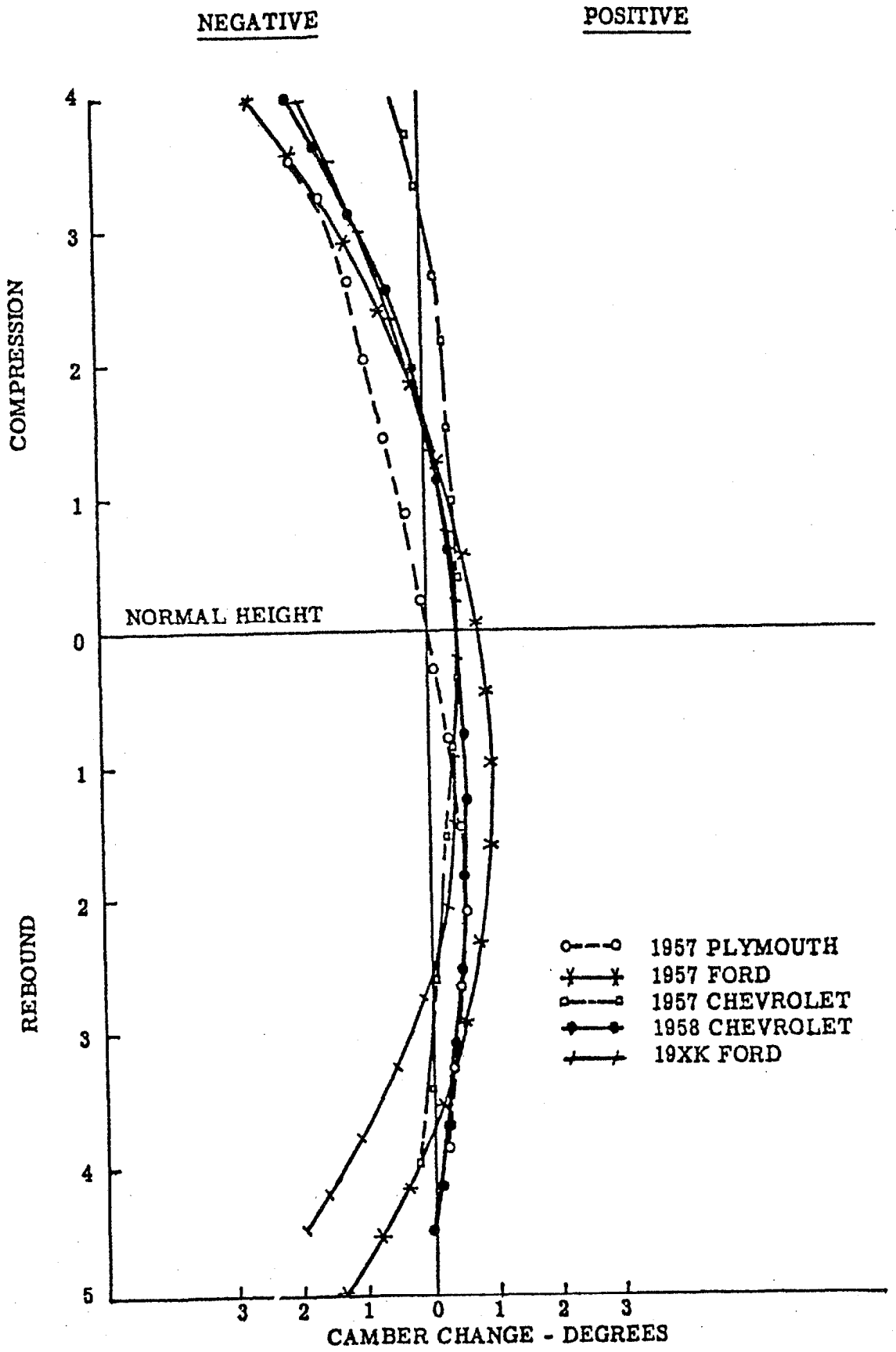

Figure A-11. Camber Change Versus Suspension Position

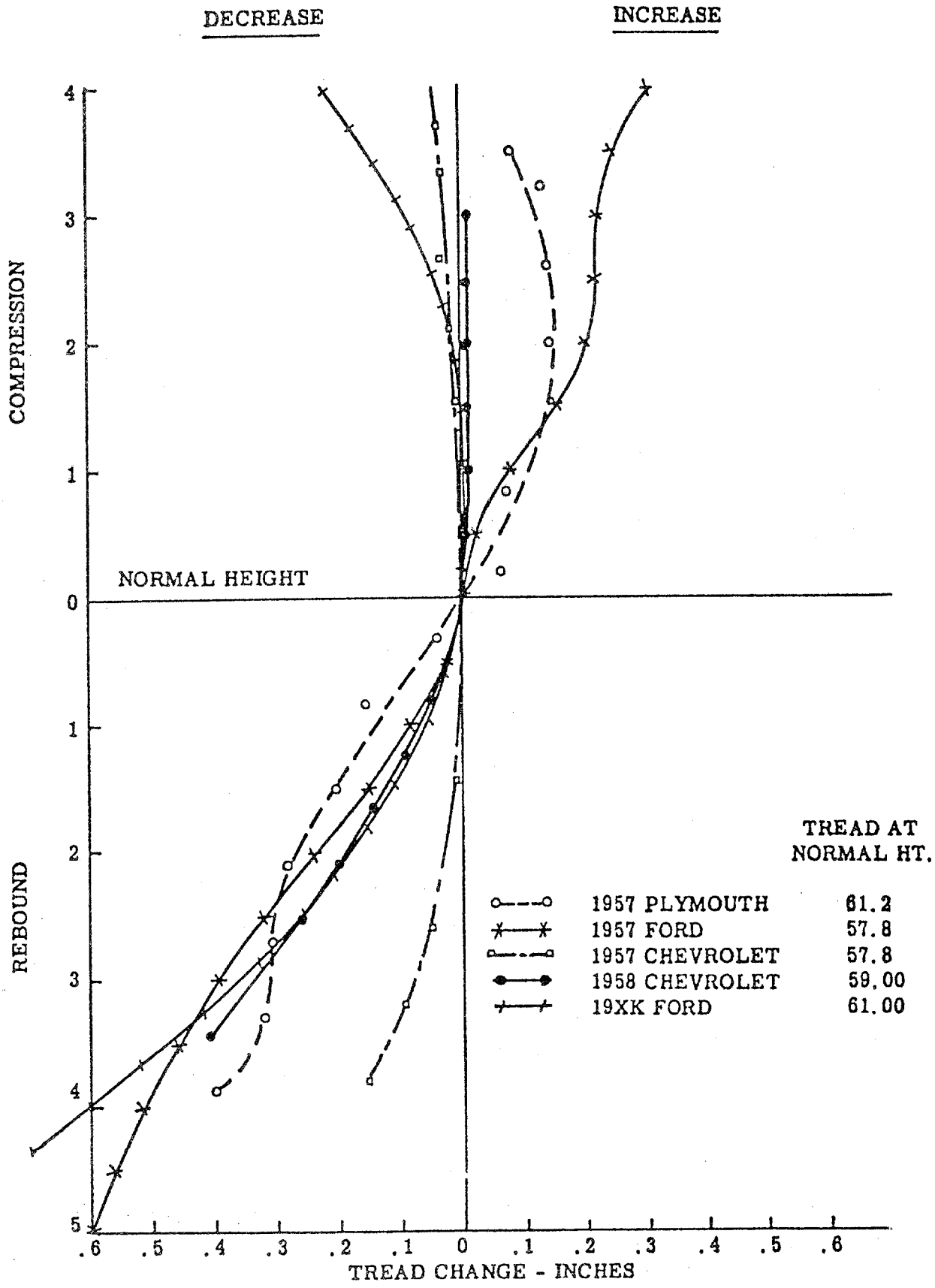

Figure A-12. Tread Change Versus Suspension Position

$$\gamma_{LR} = \phi_s + D_R\, z_{SLR} + E_R\, z_{SLR}^2 \qquad \text{(A-29)}$$

$$\gamma_{RR} = \phi_s - D_R\, z_{SRR} - E_R\, z_{SRR}^2 \qquad \text{(A-30)}$$

For solid or beam angle suspensions

The camber angle is same as axle angle,

$$\gamma_{ij} = \phi_{uj} \qquad i = L \text{ or } R,\quad j = F, \text{ or } R \qquad \text{(A-31)}$$

γ_{ij} is used in tire model to compute side force

2. Suspension Squat and Lift Forces

The mechanism of squat/lift forces is associated with the concept of the chassis roll axis. With solid axle suspensions there is a specific pivot point about which the sprung mass rolls, and which a single axle side force is transmitted to the sprung mass. For this case, the roll axis is specified at h_{RAF}, h_{RAR}, and there are no squat/lift reactions due to applied side forces.

However, with independent suspensions, there is no single roll axis pivot, in which the axle side forces are transmitted to the sprung mass. There is the tendency to represent this case as having an equivalent or imaginary roll axis location, where the side forces can be assumed to be acting at. But if analyzed this way, the squat/lift effects at each suspension are bypassed. A more direct analysis of the side force and moment application at each individual suspension, will not only carry them through more accurately, but will also show that vertical suspension forces are reduced or increased, which in turn cause the suspension to squat or lift.

The key geometry feature that causes squat/lift forces is the slope of the tire contact patch path in vertical motion, relative to pure vertical. In this regard, all multi-link suspensions can be reduced to a single swing arm suspension with the same tire patch path (slope and path arc radius). In the following analysis, it is shown that the effect of this geometric slope is to produce squat/lift forces in the suspension from applied side forces, while the side forces are effectively being applied at ground level for determination of roll moments to sprung mass.

SUSPENSION GEOMETRY FORCES AND MOMENTS, WITH

SWING ARM SUSPENSIONS

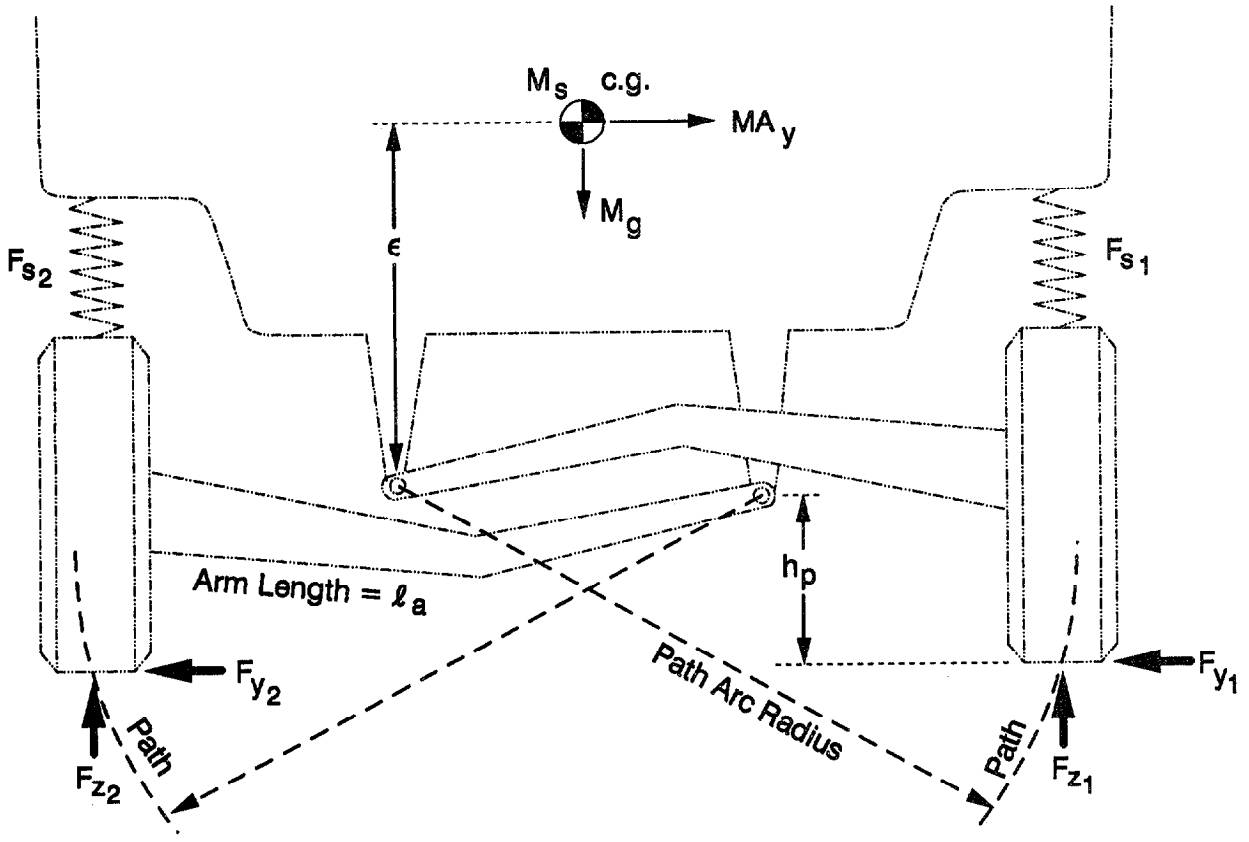

Moments about m_s c.g. come from springs and SUSP arm pivot points.

$$\Sigma m_{x_s} = F_{s_2}\left(\frac{T}{2}\right) - F_{s_1}\left(\frac{T}{2}\right) + F_{y_1}\,\epsilon + F_{y_2}\,\epsilon +$$

$$+ F_{y_1}\frac{h_p}{\ell_a}\left(\ell_a - \frac{T}{2}\right) + F_{y_2}\frac{h_p}{\ell_a}\left(\ell_a - \frac{T}{2}\right)$$

This equation converts to;

$$\Sigma m_{x_s} = \left(F_{s_2} - F_{s_1}\right)\frac{T}{2} + F_{y_1}\left(\epsilon + h_p\right) + F_{y_2}\left(\epsilon + h_p\right) +$$

$$- F_{y_1}\frac{h_p}{\ell_a}\left(\frac{T}{2}\right) - F_{y_2}\frac{h_p}{\ell_a}\left(\frac{T}{2}\right)$$

The $(\epsilon + h_p)$ distance means that F_{y_1} and F_{y_2} are effectively acting at ground level in producing the roll moment, $(\epsilon + h_p) = h_s$

The leftover terms acting at T/2 are effectively the squat/lift forces acting at the suspension.

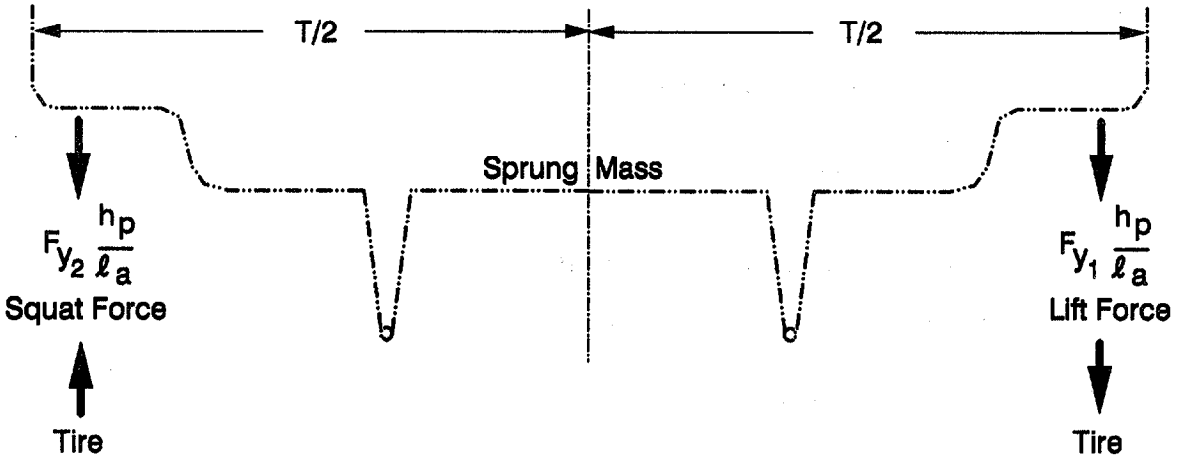

The lift forces bypass the springs and act up on the sprung mass and down on the tire. This reduces the load needed on the suspension spring, therefore it can extend, or lift up, until it reaches equilibrium.

Note that the h_p/ℓ_a ratio is merely the slope of the tire patch path relative to vertical, for any type of independent suspension.

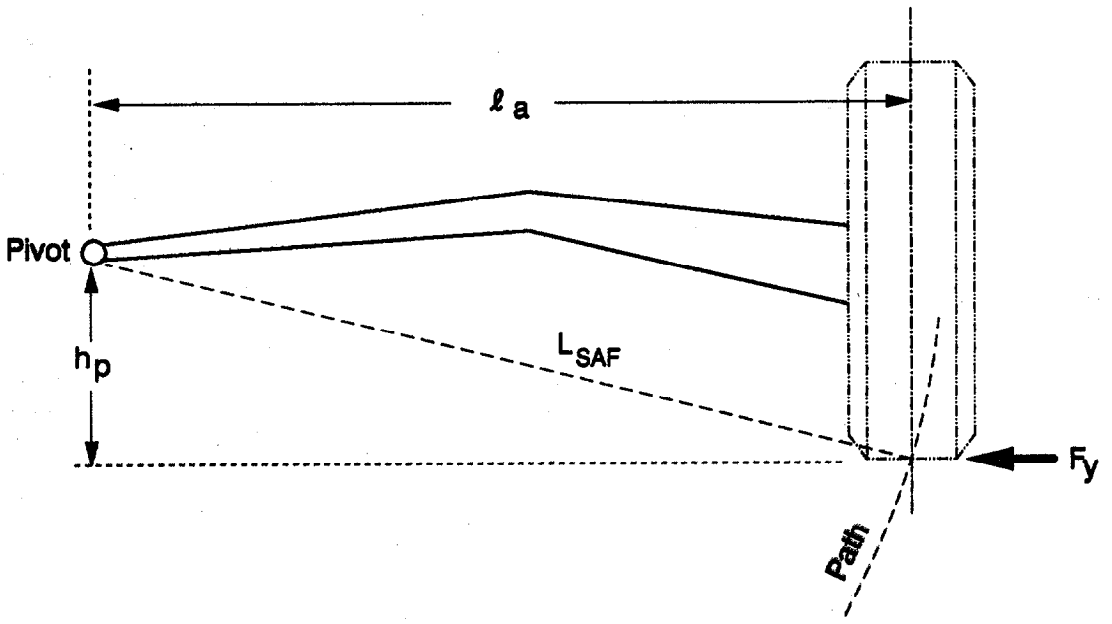

In the math model, this slope is;

$$\frac{h_p}{\ell_a} = K_{SLi}$$

and to provide for changes in slope as the suspension moves up or down, we add this change to the initial slope;

$$\text{Slope at any } z_s = K_{SLi} + \frac{Z_{sig}}{L_{SAF}}$$

The side force in the body axis system multiplied by this slope gives the squat/lift force at each suspension. For the left front suspension, this is;

$$F_{SQLF} = \left[K_{SLF} + \frac{Z_{SLF}}{L_{SAF}}\right]\left[F_{Y_{LF}} \cos \phi_s - F_{Z_{LF}} \sin \phi_s\right]$$

A final reason for applying the forces in this way, is that F_{SQLF} acts at the same place as the spring, damping, auziliary roll stiffness, and bump stop forces. In this way, there is no need to specify suspension pivot locations different for each vehicle, to pass these forces through. The composite suspension force approach allows all forces to act at one point.

Note that the net lift force per axle is; $= \left[F_{Y_1} - F_{y_2} \right] \frac{hp}{\ell_a}$ and this becomes significant only when $F_{y_1} >>> F_{y_2}$ in hard cornering.

The swing arm suspension was used in the analysis to show the effect of a given arc radius and path slope of tire patch motion. It will be shown below that MacPherson strut, double A arm, and any other multi-link suspensions will have an equivalent tire patch motion slope and arc radius, and produce the same squat/lift reactions.

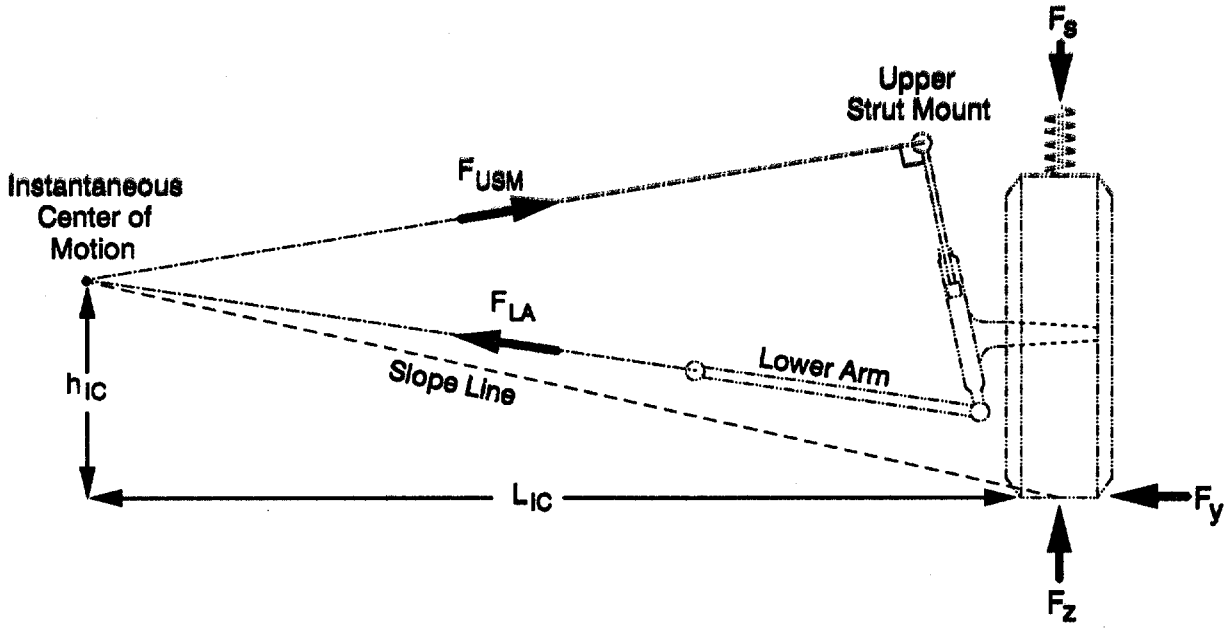

The only steady state force possible at the upper strut mount, F_{USM}, is at 90 deg to the strut axis. For the lower arm, this force, F_{LA}, must be in line with the arm pivots. These 2 forces also act through the instantaneous center of motion., Taking moments about this center,

$$F_y \, h_{ic} = (F_Z - F_s) \, L_{ic}$$

The additional lift force, is,

$$F_Z - F_s = F_y \frac{h_{i_c}}{L_{ic}}$$

Where $\frac{h_{ic}}{L_{ic}} L_{ic}$ is the line slope from center to tire patch, which is also the slope of tire patch motion relative to vertical.

The forces at the instant center, are therefore

$$F_y \text{ laterally}$$

$$F_Z - F_s \text{ vertically}$$

The moment on the sprung mass are now;

$$F_y\,(h_s - h_{ic}) - (F_Z - F_s)\left(\frac{T}{2} - L_{ic}\right) - F_s\,\frac{T}{2}$$

$$= F_y\left[h_s - h_{ic} - \frac{h_{ic}}{L_{ic}}\left(\frac{T}{2} - L_{ic}\right)\right] - F_s\,\frac{T}{2}$$

$$= F_y h_s - F_y\left(\frac{h_{ic}}{L_{ic}}\right)\frac{T}{2} - F_s\,\frac{T}{2}$$

This is identical to the right hand suspension terms for the single arm suspension, with the lift force, $F_y\left(\frac{h_{ic}}{L_{ic}}\right)$, applied at the composite suspension point.

A major difference with the MacPherson strut suspension occurs because the tire patch motion arc radius is usually very small. This means that the patch path slope changes very fast with small suspension deflection. This effect of the changing slope is covered by the Z_{sig}/L_{SAi} terms in equations A32 to 35. L_{SAi} is the path arc radius. Below is shown how this arc radius is determined.

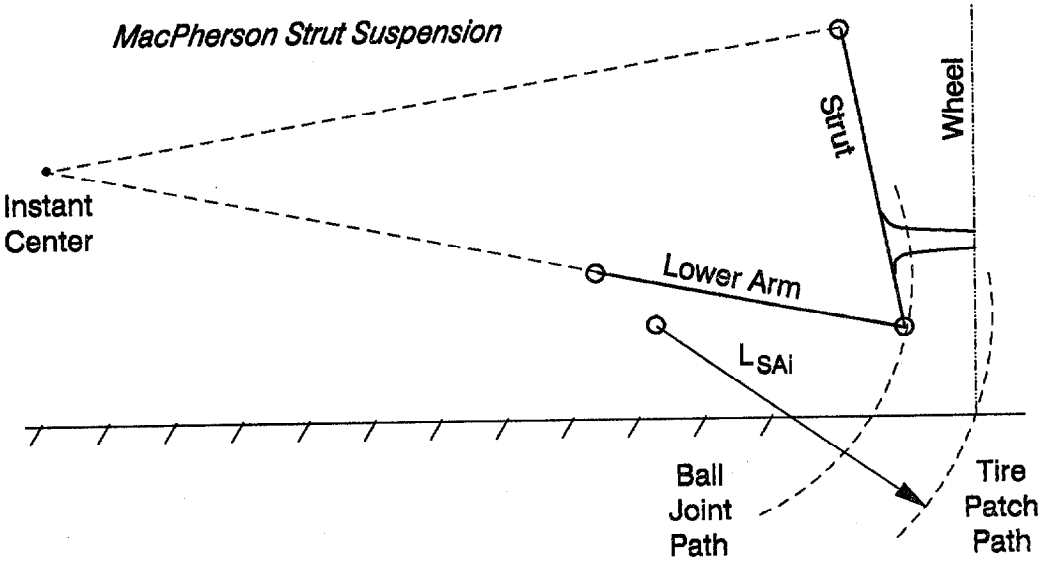

This is a graphical solution for the tire path arc radius, L_{SAi}. Note how short L_{SAi} is, and how fast the slope changes. Whereas, the distance to the instant center is fairly long.

Other suspension types, short and long arm, or multi link, would have the same layout, analysis, and result, as the MacPherson strut. All that is needed is to place the upper (short) arm, or the upper link, on the same line as F_{USM} is shown on the previous diagram. This upper arm force acts directly at the instantaneous center of motion, and produces the same analytical result.

Following from the above discussion, the simulation equations with the lift forces can be stated as follows.

In the front view, the slope at the operating point defines how much squat or lift force will be generated by the application of an F_y cornering force:

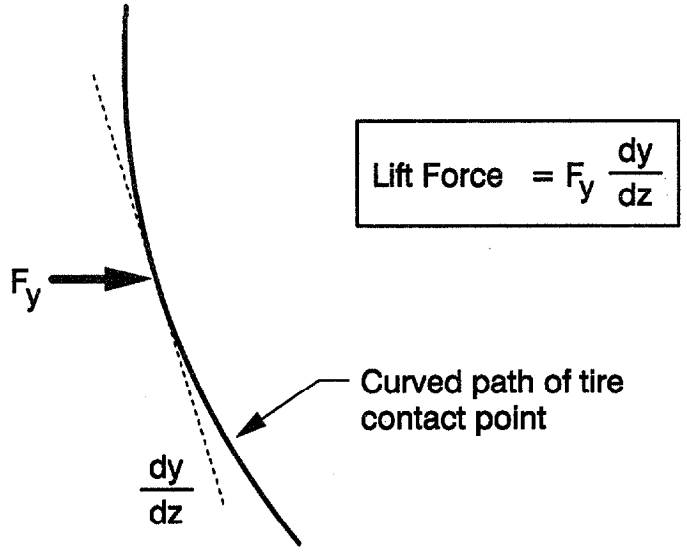

In the side view, a similar curved path can result in squat/or lift forces when F_x braking forces are applied at the tire contact point.

$$\text{lift force} = F_x \frac{dx}{dz}$$

These forces are then combined into one equation for each wheel and suspension (see Fig. A-13).

$$F_{SQLF} = \left(K_{SLF} + \frac{z_{SLF}}{L_{SAF}}\right)\left(F_{y_{LF}} \cos \phi_s - F_{Z_{LF}} \sin \phi_s\right) - F_{x_{LF}} K_{SADF} \quad \text{(A-32)}$$

$$F_{SQRF} = \left(K_{SLF} + \frac{z_{SRF}}{L_{SAF}}\right)\left(- F_{y_{RF}} \cos \phi_s + F_{Z_{RF}} \sin \phi_s\right) - F_{x_{RF}} K_{SADF} \quad \text{(A-33)}$$

$$F_{SQLR} = \left(K_{SLR} + \frac{z_{SLR}}{L_{SAR}}\right)\left(F_{y_{LR}} \cos \phi_s - F_{Z_{LR}} \sin \phi_s\right) + F_{x_{LR}} K_{SADR} \quad \text{(A-34)}$$

$$F_{SQRR} = \left(K_{SLR} + \frac{z_{SRR}}{L_{SAR}}\right)\left(- F_{y_{RR}} \cos \phi_s + F_{Z_{RR}} \sin \phi_s\right) + F_{x_{RR}} K_{SADR} \quad \text{(A-35)}$$

where K_{SLi} = Lateral Slope of quivalent single arm at curb load

L_{SAi} = Length of equivalent Single Arm at curb load

K_{SADi} = Anti Dive Slope

i = F, or R

These F_{SQij} forces are added to the suspension force equations, A-23, 24, 25, 26.

Scheme for setting suspension slope values for different conditions:

	CORNERING		BRAKING (NEG F_x)		FORWARD ACC (Pos F_x)	
SUSPENSION	IND.	SOLID AXLE	IND.	SOLID AXLE	IND.	SOLID AXLE
	As shown in Equations	$K_{SLi} = 0$ $L_{SAi} = \infty$	K_{SADi}	K_{SADi}	Switch to K_{SAD2i}	K_{SADi}

The above parameters can be preset for all cases, except that for FORWARD ACC. with an IND. suspension, the K_{SADi} parameter must be changed to the alternate value, K_{SAD2i}.

$K_{SADi} \longrightarrow K_1 S_{AD2i}$ for pos. F_x, ind. susp.

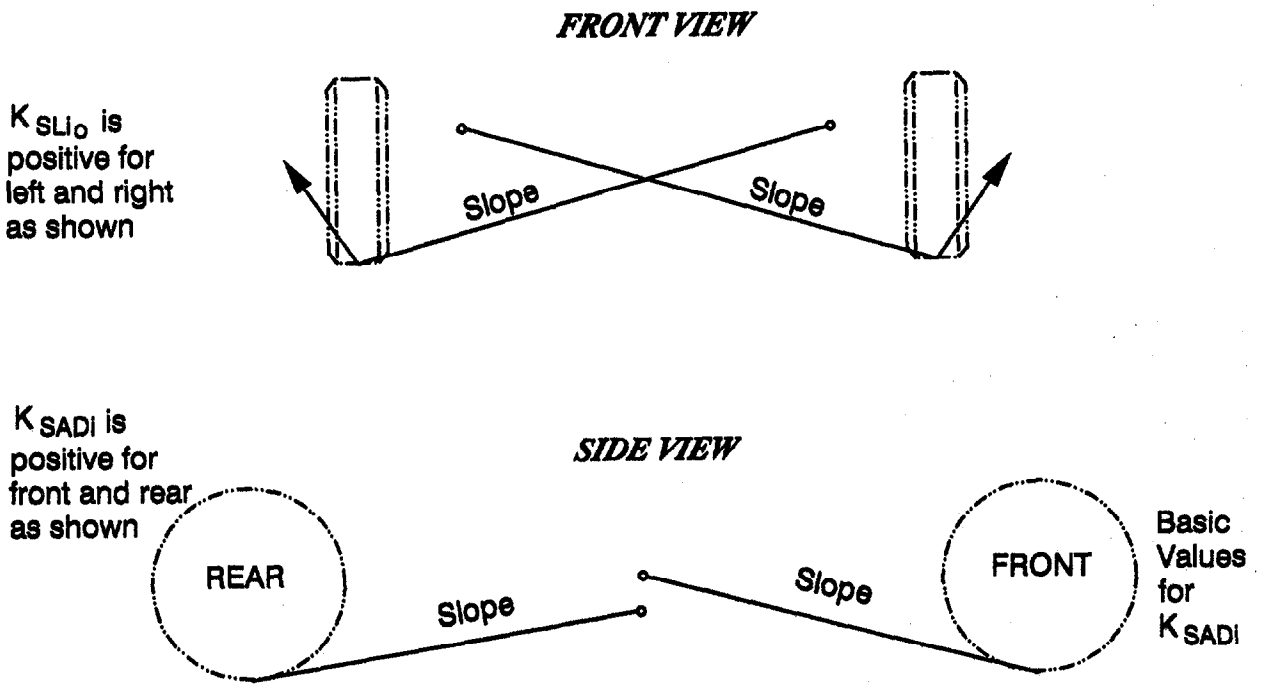

Figure A-13. Squat-Lift Function Slope Definitions

3. Individual Wheel Steer Angle

a. Due to suspension deflection

There are two classes of suspensions here; the solid or beam axle, and fully independent. Figure A-14 is an example of wheel steer vs. suspension deflection for a fully independent suspension.

For roll steer with solid axle or beam axle suspensions with trailing links controlling axle steer angle.

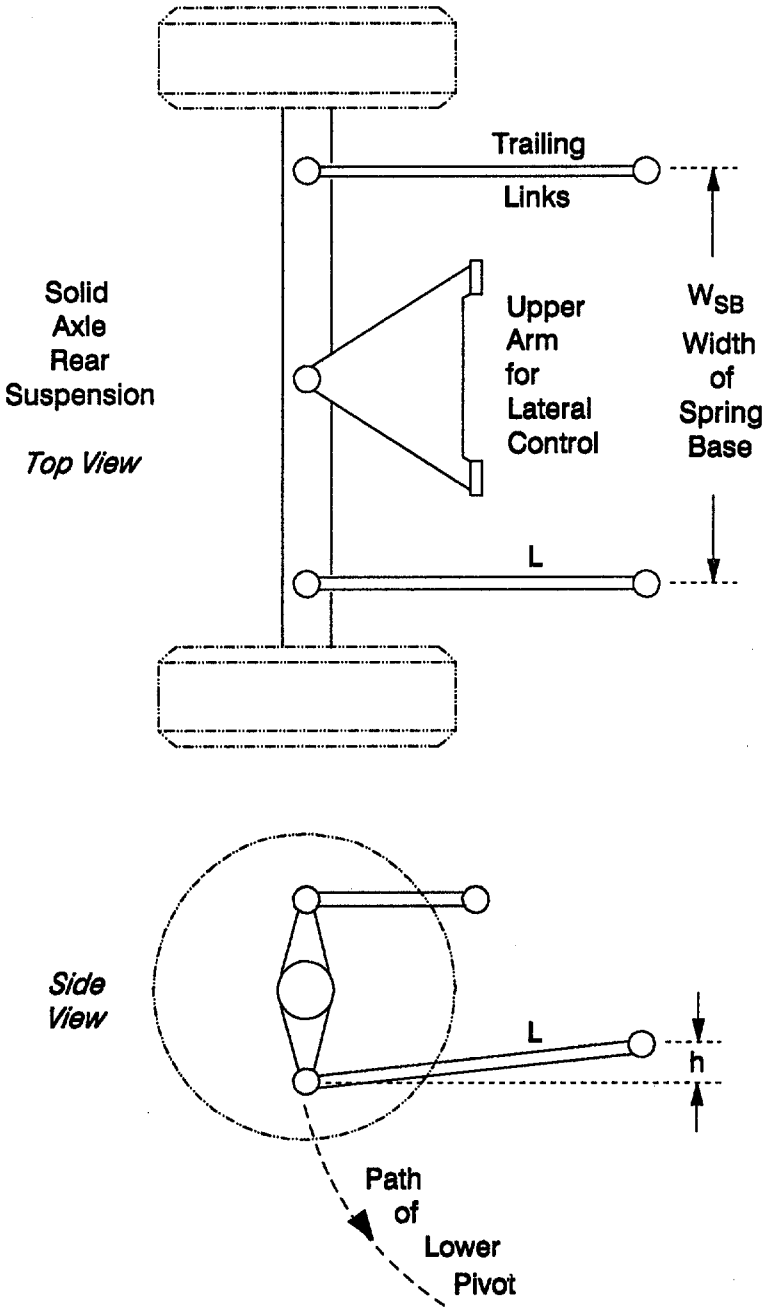

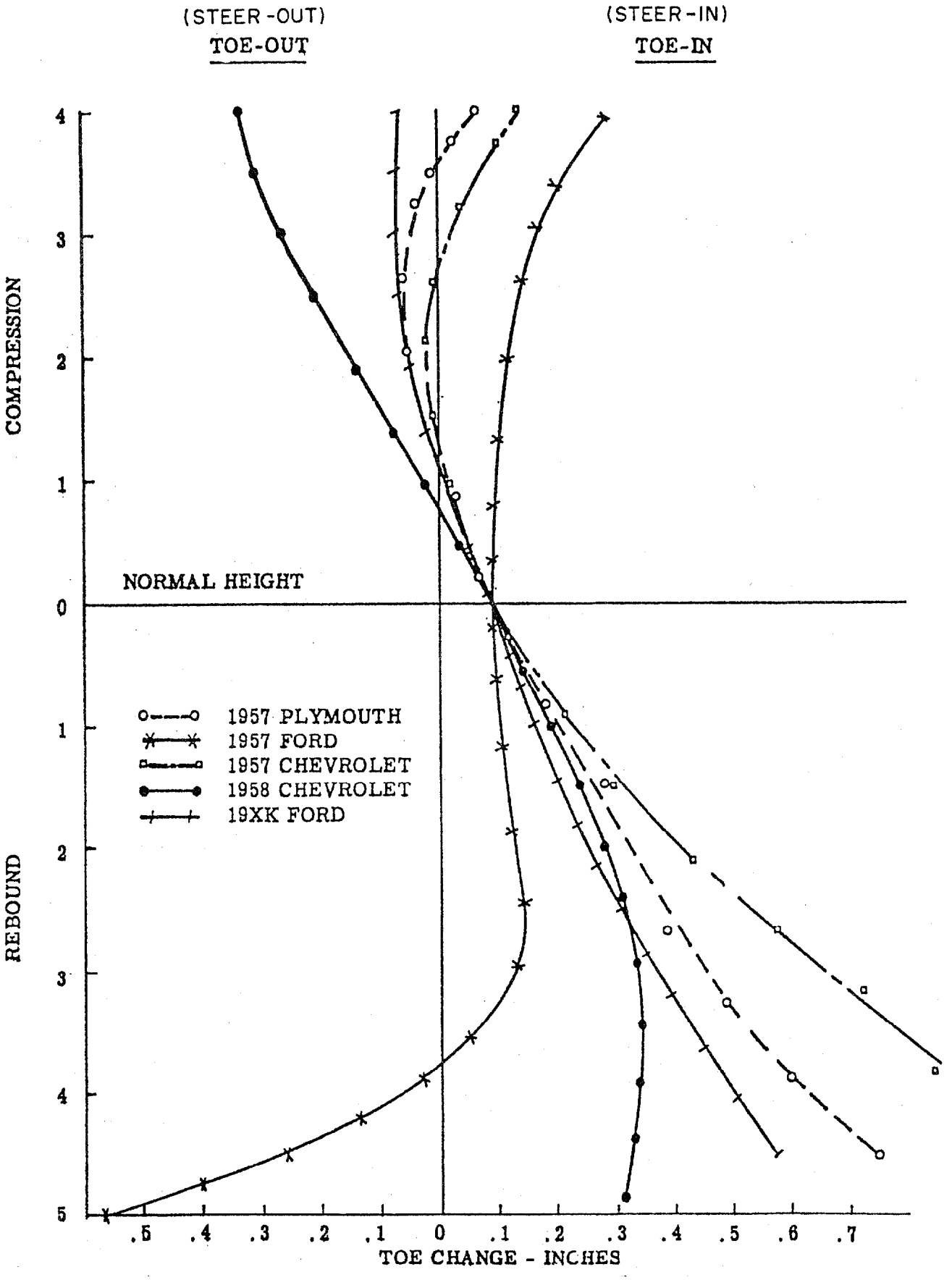

Figure A-14. Toe Change Versus Suspension Position

As the sprung mass rolls, the path of the lower pivot has a slope of $\frac{h}{L}$

Vertical deflection of this pivot is $= \phi \frac{W_{SB}}{2}$

Longitudinal movement of pivot is $= \phi \left(\frac{W_{SB}}{2}\right)\left(\frac{h}{L}\right)$

Axle steer angle with body roll $= \frac{\text{Long Movement}}{\frac{W_{SB}}{2}} = \phi\left(\frac{h}{L}\right)$

Thus, $\frac{h}{L}$ is the roll steer coefficient

However, this can be generalized for any situation of suspension squat/lift due to braking or acceleration forces. This means that true value for $h = h_o + z_s$.

Therefore, when average across left and right suspension deflection, the complete roll steer effect can be stated as follows:

$$\Delta \delta w_i = \left[\frac{h_i + .5\left(z_{SLi} + z_{SRi}\right)}{L_i}\right]\left(\phi_s - \phi_{ui}\right)$$

This accounts for changes in roll steer, when suspension squat/or lift is present via z_{sij}.

h, L are suspension arm parameters in side view.

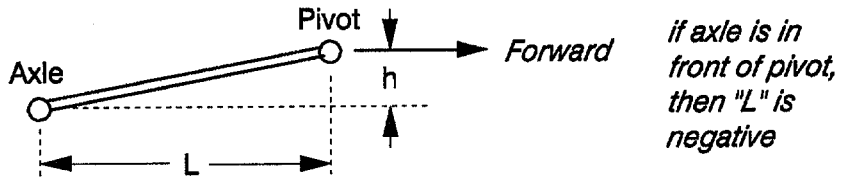

For independent suspensions, the steer effect is a nonlinear function of deflection, z_{sij}

$$\Delta\delta_{w_{ij}} = A_{ij} + B_{ij}\, z_{Sij} + C_{ij}\, z_{Sij}^2$$

The A_{ij} component is static toe in, which is supposed to be zero, in motion. Therefore we can ignore this.

The B_{ij} and C_{ij} are curve fitting parameters which are simply opposite sign identical values for left and right

$$\Delta\delta_{w_{LF}} = B_F\, z_{SLF} + C_F\, z_{SLF}^2$$

$$\Delta\delta_{w_{RF}} = -B_F\, z_{SRF} - C_F\, z_{SRF}^2$$

$$\Delta\delta_{w_{LR}} = B_R\, z_{SLR} + C_R\, z_{SLR}^2$$

$$\Delta\delta_{w_{RR}} = -B_R\, z_{SRR} - C_R\, z_{SRR}^2$$

Positive values of B_F steer the $\delta_{w_{LF}}$ to the left with negative z_{SLF}, and $\delta_{w_{RF}}$ to the left with positive z_{SRF}. Thus, in a RH turn, roll to the left will produce roll understeer.

b. Ackerman Steer Effects

Front wheel steer geometry is commonly designed for turning the inside wheel more than the outside wheel, for sharp small-radius turns

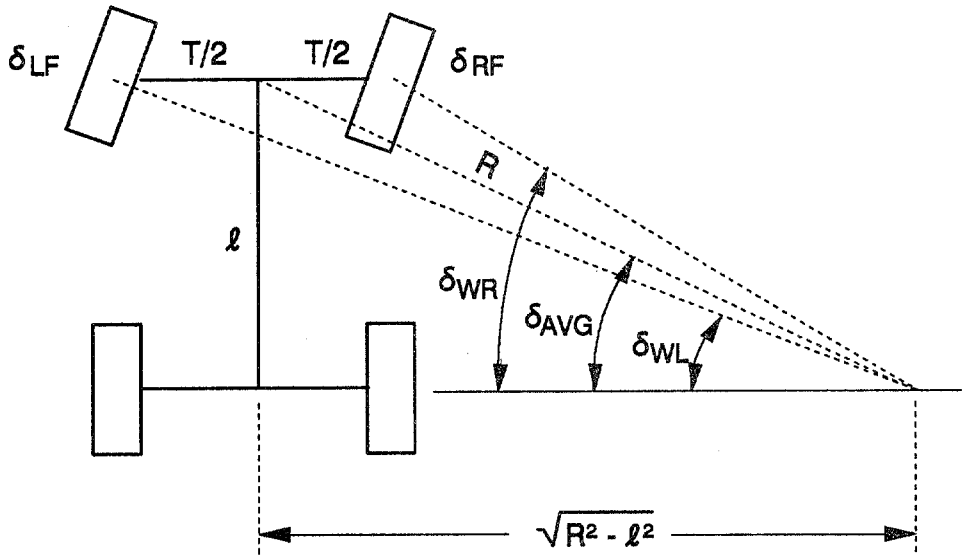

$$\tan\delta_{AVG} = \frac{\ell}{\sqrt{R^2 - \ell^2}}$$

$$\tan\delta_{w_L} = \frac{\ell}{\sqrt{R^2 - \ell^2} + \frac{T}{2}} = \frac{\tan\delta_{AVG}}{1 + \frac{T}{2\ell}\tan\delta_{AVG}}$$

$$\tan\delta_{w_R} = \frac{\ell}{\sqrt{R^2 - \ell^2} - \frac{T}{2}}$$

For small angle approximations (to avoid Tan^{-1} calculations), use $\tan \delta_w \simeq \delta_w$

$$\therefore \delta_{w_L} \simeq \frac{\delta_{AVG}}{1 + \frac{T}{2\ell} \delta_{AVG}} \simeq \delta_{AVG} \left(1 - \frac{T}{2\ell} \delta_{AVG}\right)$$

$$\text{and } \delta_{w_R} \simeq \delta_{AVG} \left(1 + \frac{T}{2\ell} \delta_{AVG}\right)$$

To make this into a general case, we can change $\frac{T_F}{2\ell} = K_{ACK}$, so that this can be changed to any value.

$$\delta_{w_{LF}} = \delta_{w_F} \left(1 - K_{ACK}\, \delta_{w_F}\right)$$

$$\delta_{w_{RF}} = \delta_{w_F} \left(1 + K_{ACK}\, \delta_{w_F}\right)$$

c. Aligning Torque Steer

This is the deflection in the steering gear due to tire aligning torque applied at the wheels.

$$\Delta\delta_{w_F} = \left(M_{Z_{LF}} + M_{Z_{RF}}\right) K_{SCF}$$

d. Lateral Force Compliance Steer

This is the deflection of the wheel steer angle due to lateral forces acting on compliant suspension components.

$$\Delta\delta_{w_{ij}} = F_{y_{ij}}\, K_{c_i}$$

e. Steer Moments due to F_x Acting on Steer

Note, for straight ahead driving, with FWD,

F_y = zero, Δy = zero, $F_{x_{LF}} = F_{x_{RF}}$

the steer moments = $F_x\, (\ell_{so} - \ell_{so})$ = zero

But in hard cornering , with large Δy, $F_{x_{LF}} = F_{x_{RF}}$,

the steer moments = F_x, $(-\Delta y_{LF} - \Delta y_{RF})$,

or produces very large understeer.

e. Steer Moments due to F_x Acting on Steer (concluded)

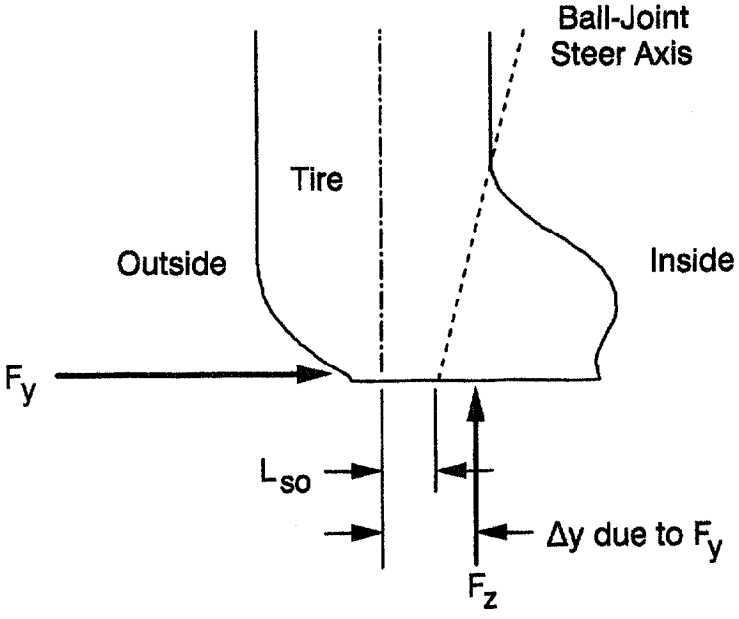

End View

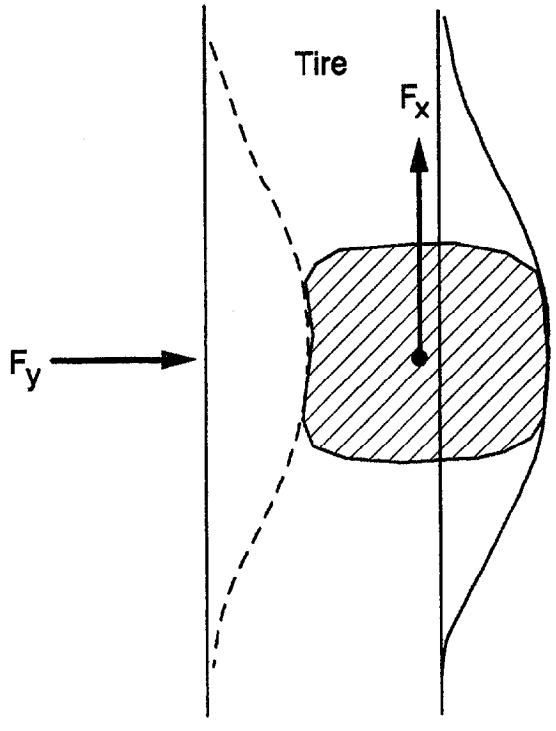

Top View
With F_x
Force Applied
at Laterally
Deflected Tire
Contract Patch

Steer Moment on LF
Wheel $= F_{x_{LF}} (L_{SO} - \Delta y_{LF})$

on RF Wheel

$= F_{x_{LF}} (L_{SO} - \Delta y_{LF})$

f. Steering system lag in response due to I_w, K_{SCF}

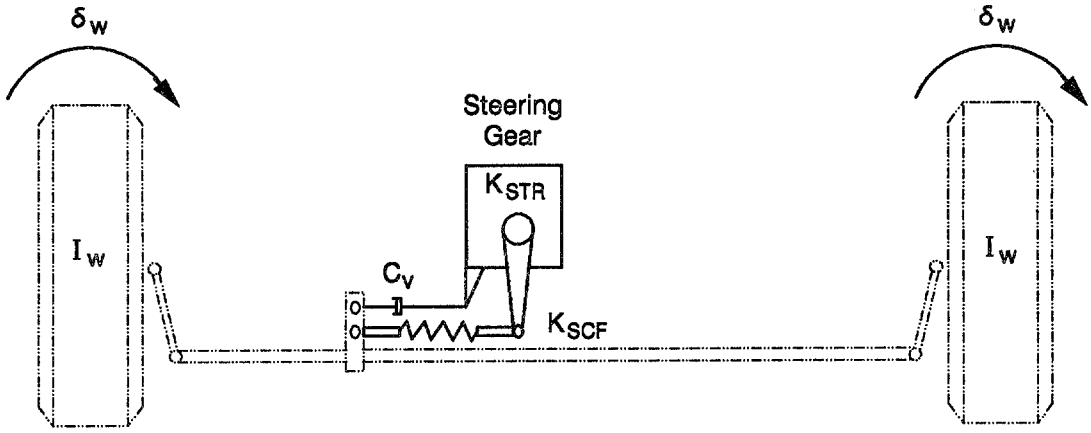

K_{SCF} = Steer Gear Compliance

K_{STR} = Steer Gear Ratio

C_v = Steering System Damping

$$2\ I_w\ \ddot{\delta}_w = \left(\frac{\delta_{SW}}{K_{STR}} + \begin{bmatrix}\text{ROLL}\\ \text{STEER}\end{bmatrix} - \delta_w\right)\frac{1}{K_{SCF}} - C_v\dot{\delta}_w + \begin{pmatrix}\text{STEER}\\ \text{MOMENTS}\\ \text{FROM TIRES}\end{pmatrix}$$

$$\delta_W = \frac{\frac{\delta_{sw}}{K_{STR}} + \begin{pmatrix}\text{ROLL}\\ \text{STEER}\end{pmatrix} + \begin{pmatrix}\text{STEER}\\ \text{MOMENTS}\end{pmatrix}\begin{pmatrix}K_{SCF}\end{pmatrix}}{2\ I_w\ K_{SCF}\ S^2 + C_v\ K_{SCF}\ S + 1}$$

thus, the steering system lag is a second order system,

where $\omega_m = \dfrac{1}{\sqrt{2\ I_w\ K_{SCF}}}$ $\zeta = C_v\sqrt{\dfrac{K_{SCF}}{8\ I_w}}$

Combining all these effects into the steering equations,

$$\delta_{w_F} = \frac{\delta_{SW}}{K_{STR}} + \frac{K_{SAF}}{L_F}\left[h_F + \left(\frac{Z_{SLF} + Z_{SRF}}{2}\right)\right]\left(\phi_s - \phi_{uF}\right) + \frac{\left[M_{Z_{LF}} + M_{Z_{RF}} + F_{x_{LF}}\left(L_{SO} - K_{LT}F_{y_{LF}}\right) - F_{x_{RF}}\left(L_{SO} + K_{LT}F_{y_{RF}}\right)\right]K_{SCF}}{\frac{S^2}{\omega_n^2} + \frac{2\zeta S}{\omega_n} + 1} \quad \text{(A-36)}$$

$$\delta_{w_R} = \delta_{SWB} + \frac{K_{SAR}}{L_R}\left[h_R + \frac{\left[z_{SLR} + z_{SRR}\right]}{2}\right]\left(\phi_s - \phi_{UR}\right) + \left(M_{Z_{LR}} + M_{Z_{RR}}\right)K_{SCR} \quad \text{(A-37)}$$

$$\delta_{w_{LF}} = \delta_{w_F}\left(1 - K_{ACK}\,\delta_{w_F}\right) + B_F\, z_{SLF} + C_F\, z_{SLF}^2 + F_{y_{LF}}\, K_{CF} \quad \text{(A-38)}$$

$$\delta_{w_{RF}} = \delta_{w_F}\left(1 + K_{ACK}\,\delta_{w_F}\right) - B_F\, z_{SRF} - C_F\, z_{SRF}^2 + F_{y_{RF}}\, K_{CF} \quad \text{(A-39)}$$

$$\delta_{w_{LR}} = \delta_{w_R} + B_R\, z_{SLR} + C_R\, z_{SLR}^2 + F_{y_{LR}}\, K_{CR} \quad \text{(A-40)}$$

$$\delta_{w_{RR}} = \delta_{w_R} - B_R\, z_{SRR} - C_R\, z_{SRR}^2 + F_{y_{RR}}\, K_{CR} \quad \text{(A-41)}$$

For independent suspensions, set B_i, C_i values, and set K_{SAi} = zero.

For solid axle suspensions, set K_{SAi}, h_i, L_i values and set B_i, C_i = zero.

4. Computing Tire Side Slip at Each Tire

Using $\delta_{w_{ij}}$, we can now compute tire side slip, using v, $\dot{\psi}$, ϕ_{ui}, U, to define correct wheel paths in relation to wheel angles. The purpose of the ϕ_{ui} terms is to compute the side velocity correctly for large roll angles during vehicle tip over.

$$\alpha_{LF} = + \tan^{-1}\left[\frac{V + a\dot{\psi} - \dot{\phi}_{UF}\left(R_W \cos \phi_{UF} - \frac{T_F}{2} \sin \phi_{UF}\right)}{U_o + \frac{T_F}{2}\dot{\psi}}\right] - \delta_{w_{LF}}$$

$$\alpha_{RF} = + \tan^{-1}\left[\frac{V + a\dot{\psi} - \dot{\phi}_{UF}\left(R_W \cos \phi_{UF} + \frac{T_F}{2} \sin \phi_{UF}\right)}{U_o - \frac{T_F}{2}\dot{\psi}}\right] - \delta_{w_{RF}}$$

$$\alpha_{LR} = + \tan^{-1}\left[\frac{V - b\dot{\psi} - \dot{\phi}_{UR}\left(R_W \cos \phi_{UR} - \frac{T_R}{2} \sin \phi_{UR}\right)}{U_o + \frac{T_R}{2}\dot{\psi}}\right] - \delta_{w_{LR}}$$

$$\alpha_{RR} = + \tan^{-1}\left[\frac{V - b\dot{\psi} - \dot{\phi}_{UR}\left(R_W \cos \phi_{UR} + \frac{T_R}{2} \sin \phi_{UR}\right)}{U_o - \frac{T_R}{2}\dot{\psi}}\right] - \delta_{w_{RR}}$$

Note that the side slip of the tire can be seen as occurring only on the ground. So that the $(R_W \cos \phi_{u_i} \pm \frac{T_i}{2} \sin \phi_{u_i})$ term, which is merely the height of the M_u c.g. above the point where side slip is defined, can be replaced by the height above ground, $= R_W - z_{ui}$.

Then; the α_{ij} equations would be:

$$\alpha_{LF} = + \tan^{-1}\left[\frac{V + a\dot{\psi} - \dot{\phi}_{UF}\left(R_W - z_{UF}\right)}{U_o + \frac{T_F}{2}\dot{\psi}}\right] - \delta_{w_{LF}} \qquad \text{(A-42)}$$

$$\alpha_{RF} = + \tan^{-1}\left[\frac{V + a\dot{\psi} - \dot{\phi}_{UF}\left(R_W - z_{UF}\right)}{U_o - \frac{T_F}{2}\dot{\psi}}\right] - \delta_{w_{RF}} \qquad \text{(A-43)}$$

$$\alpha_{LR} = + \tan^{-1}\left[\frac{V - b\dot{\psi} - \dot{\phi}_{UR}\left(R_W - z_{UR}\right)}{U_o + \frac{T_R}{2}\dot{\psi}}\right] - \delta_{w_{LR}} \qquad \text{(A-44)}$$

$$\alpha_{RR} = + \tan^{-1}\left[\frac{V - b\dot{\psi} - \dot{\phi}_{UR}\left(R_W - z_{UR}\right)}{U_o - \frac{T_R}{2}\dot{\psi}}\right] - \delta_{w_{RR}} \qquad \text{(A-45)}$$

One final relationship is needed in order to compute vehicle side slip which is used in the tire side slip equations.

Lateral acceleration at the longitudinal c.g., is defined at the unsprung mass so that the computed motions are directly usable in defining side slip at the tires, without having to correct for sprung mass roll motions.

$$A_{y_u} = \dot{v} + U\dot{\psi} \tag{A-46}$$

which is used to solve for v

where, at the longitudinal c.g.,

$$A_{y_u} = A_{y_s} - \epsilon \, (\cos \phi_s) \, \ddot{\phi}_s \tag{A-47}$$

ϵ = vertical distance between the M_s c.g., and the roll axis.

This ϵ normally = $h_s - \frac{b}{\ell} (h_{RAF}) - \frac{a}{\ell} (h_{RAR})$

However, the h_{RAi} parameter is not used, (set = 0), for independent suspensions, in order to model squat/lift effects.

For independent suspensions

$$h_{RAi} = K_{SLi} \left(\frac{T_i}{2}\right)$$

Therefore, compute ϵ using $h_{RAi} = K_{SLi} \left(\frac{T_i}{2}\right)$ for ind. susp.

$= h_{RAi}$ for solid axle susp.

I. TIRE FORCES

Vertical (normal) Tire Loads

Tire load, defined perpendicular to the road surface, depends on compression of the tire casing and its spring stiffness (see Fig. A-15).

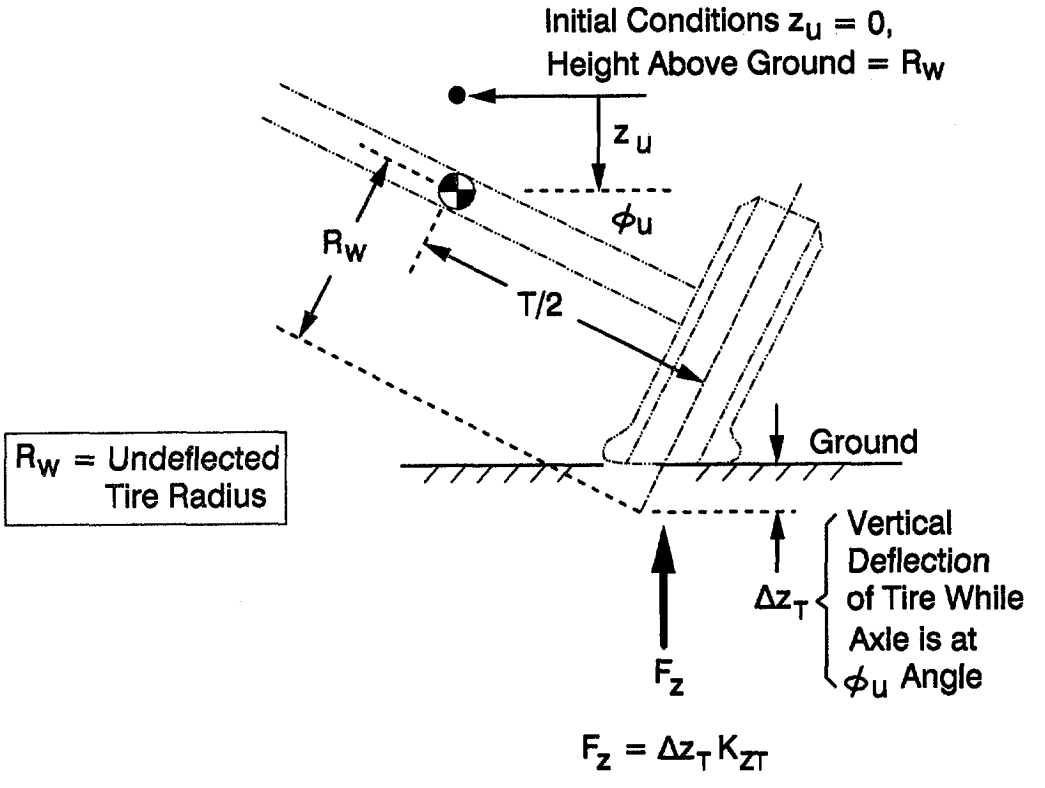

Therefore;

$$R_W = z_u + \frac{T}{2} \sin \phi_u + R_W \cos \phi_u - \Delta z_T$$

or,

$$\Delta z_T = z_u + R_W (\cos \phi_u - 1) + \frac{T}{2} \sin \phi_u$$

for right hand tire

Figure A-15. Tire Vertical Deflection Characteristics

$$F_{Z_{LF}} = \left(z_{UF} + R_W \left[\cos \phi_{UF} - 1\right] - \frac{T_F}{2} \sin \phi_{UF}\right) K_{ZT} \quad \text{(A-48)}$$

$$F_{Z_{RF}} = \left(z_{UF} + R_W \left[\cos \phi_{UF} - 1\right] + \frac{T_F}{2} \sin \phi_{UF}\right) K_{ZT} \quad \text{(A-49)}$$

$$F_{Z_{LR}} = \left(z_{UR} + R_W \left[\cos \phi_{UR} - 1\right] - \frac{T_R}{2} \sin \phi_{UR}\right) K_{ZT} \quad \text{(A-50)}$$

$$F_{Z_{RR}} = \left(z_{UR} + R_W \left[\cos \phi_{UR} - 1\right] + \frac{T_R}{2} \sin \phi_{UR}\right) K_{ZT} \quad \text{(A-51)}$$

Tire Side Force Lag — There is actually a dynamic delay involved in the tire's side force generation process. Second order lag models have been developed to account for the delay. Basically, the tire must roll through some distance in order for the tire patch to fully develop a commanded input side slip. This model assumes that the lag time constant is a function of a characteristic rolling distance, given by the product of a constant (K_{TL}) and the tire's rolling radius, R_R, and wheel speed, u:

$$TL = \frac{K_{TL} \cdot R_R}{u} \quad \text{(A-52)}$$

then the lagged tire force (F_{T_yL}) is given by the second order lag equation,

$$F_{T_yL} = \frac{F_{T_y}}{(T_L S + 1)^2} \quad \text{(A-53)}$$

However, this would imply $\omega_n = \frac{u}{\ell}$ = zero at u = zero, and this is not true.

At very low speeds, the vehicle mass reacts laterally to relieve all side force that might develop from a change in α.

At high speeds, the tire side force can develop before the vehicle can react laterally.

To cover these 2 operating areas, we have modified the tire lag to have a zero speed term

$$F_y = \frac{Y_{\alpha_o} \alpha}{\left(\frac{\ell_T}{u + K\ell_T} S + 1\right)^2} \quad \text{(A-54)}$$

For zero speeds, $F_y = \dfrac{Y_{\alpha_o}\,\alpha}{\left(\frac{1}{K}\,S + 1\right)^2}$

$\omega_n = K$

and this represents the vehicle mass lateral response on the tire casings, while parked. This tends to have a natural frequency of about $\omega_n = K = 15$ to 18 R/s.

At high speeds, the $\dfrac{\ell_T}{u + K\ell_T}$ terms tend to approach the original value for $\dfrac{\ell_T}{u}$.

Therefore, this K_{LAGV} parameter is usually set = 15 to 18 R/s, so that vehicle maneuvers can start out or end up at zero speed.

Wheel Spin Mode — Wheel spin dynamics are simulated in order to compute longitudinal slip ratio. The angular acceleration of the wheel (ω) is proportional to the sum of the applied braking, engine and road torques:

$$I_{y_w}\dot{\omega} = -R_W \cdot F_X(S) + T_B + T_E \qquad \text{(A-55)}$$

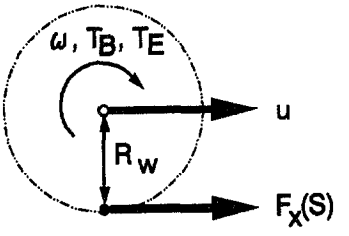

Solution of this equation then allows computation of longitudinal slip.

To obtain correct values for longitudinal slip for tires, we need the exact velocity of the wheel, in the wheel plane. This will vary from vehicle speed at each wheel due to sharp turns, and also spinouts. Since a vehicle can spin out while in a straight line (curvature = zero), using path curvature is not sufficient.

For any condition of vehicle velocity (U_o) in the body axis system, and yaw rate (r), the following equations will provide the wheel velocities (U_{w_i}) in each wheel plane.

Note that longitudinal tire/road force, $F_X(S)$, is a function of slip so that these equations must be solved interactively. An implicit integration technique is discussed in Refs. 11 and 13 for solving this problem in a computationally efficient manner.

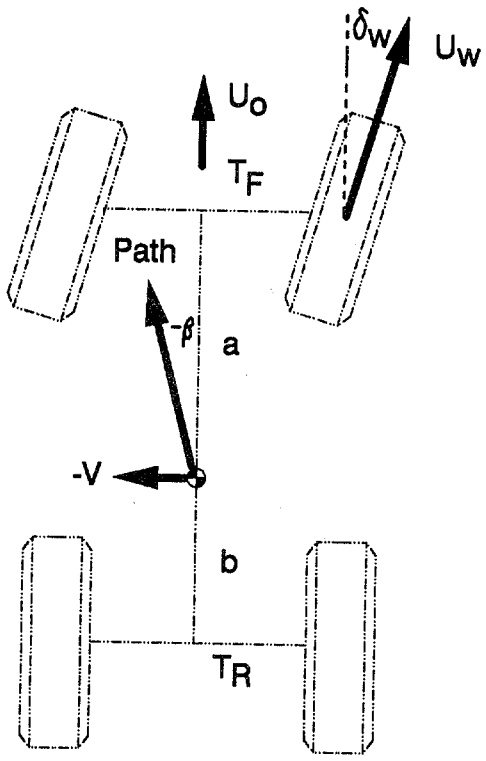

For vehicle side slip,

$$U_o \tan \beta = V$$

For wheel velocities in body axis direction,

L.F. Wheel $\quad V_1 = V + \dot{\psi}a$

$$U_1 = U_o + \frac{\dot{\psi}\, T_F}{2}$$

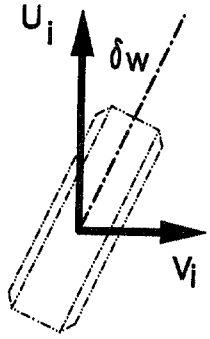

Converting to wheel plane velocities,

LF. Wheel $\quad U_{W_1} = U_i \cos \delta_{wF} + V_i \sin \delta_{w_F}$

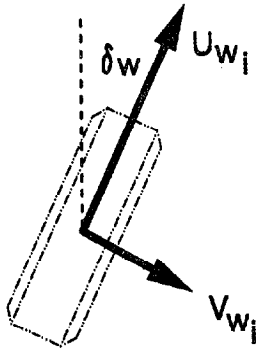

$$\therefore U_{W_1} = \left(U_o + \frac{\dot{\psi} T_F}{2}\right) \cos \delta_{W_F} + \left(U_o \tan \beta + \dot{\psi} a\right) \sin \delta_{W_F} \qquad \text{(A-56)}$$

$$U_{W_2} = \left(U_o - \frac{\dot{\psi} T_F}{2}\right) \cos \delta_{W_F} + \left(U_o \tan \beta + \dot{\psi} a\right) \sin \delta_{W_F} \qquad \text{(A-57)}$$

$$U_{W_3} = \left(U_o + \frac{\dot{\psi} T_R}{2}\right) \cos \delta_{W_R} + \left(U_o \tan \beta - \dot{\psi} b\right) \sin \delta_{W_R} \qquad \text{(A-58)}$$

$$U_{W_4} = \left(U_o - \frac{\dot{\psi} T_R}{2}\right) \cos \delta_{W_R} + \left(U_o \tan \beta - \dot{\psi} b\right) \sin \delta_{W_R} \qquad \text{(A-59)}$$

Then the longitudinal slip equations are,

$$S_i = \frac{U_{W_i} - R_{W_i} \omega_i}{U_{W_i}} = 1 - \frac{R_{W_i} \omega_i}{U_{W_i}} \qquad \text{(A-60)}$$

where

i	wheel
1	LF
2	RF
3	LR
4	RR

J. COMPLIANT PIN JOINTS BETWEEN M_s AND M_u

In order to avoid computational instabilities, the F_{RAF}, F_{RAR} forces acting at the roll axis between the M_s and M_{ui} will be passed through compliant pin joints. This is also true in real cars, as the lateral positioning members in the suspension have rubber cushioning pivot bushings.

This means that the F_{RAF}, F_{RAR} forces will be computed as follows, if ϕ_s = zero;

$$FRAR = (y_u - y_s)\, K_{RAS} + (\dot{y}_u - \dot{y}_s)\, K_{RAD}$$

where $y_u = \int \dot{y}_u$ $\quad y_s = \int \dot{y}_s$

$\dot{y}_u = \int A_{y_{UF}}$ from eq. 19

$\dot{y}_s = \int (A_{y_s} + a\,\ddot{\psi})$ from eq. 2,3

Similar for F_{RAR}

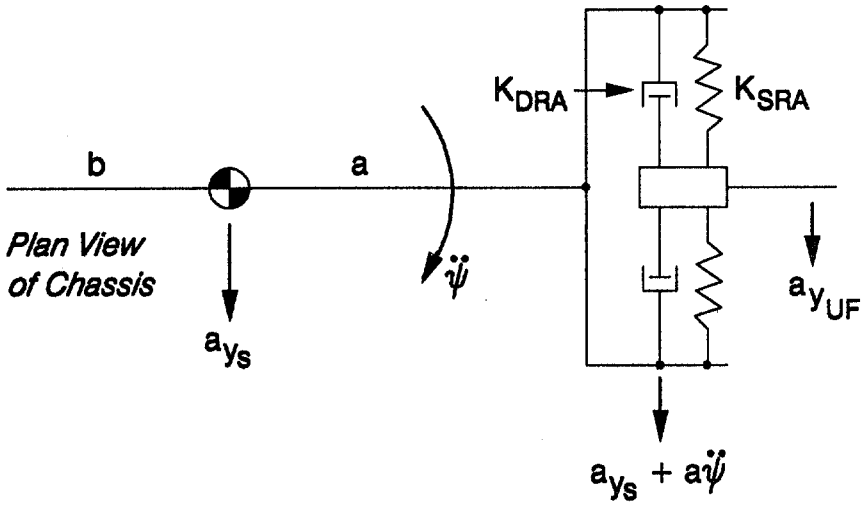

COMPLIANT JOINT AT ROLL AXIS, WITH BODY ROLL

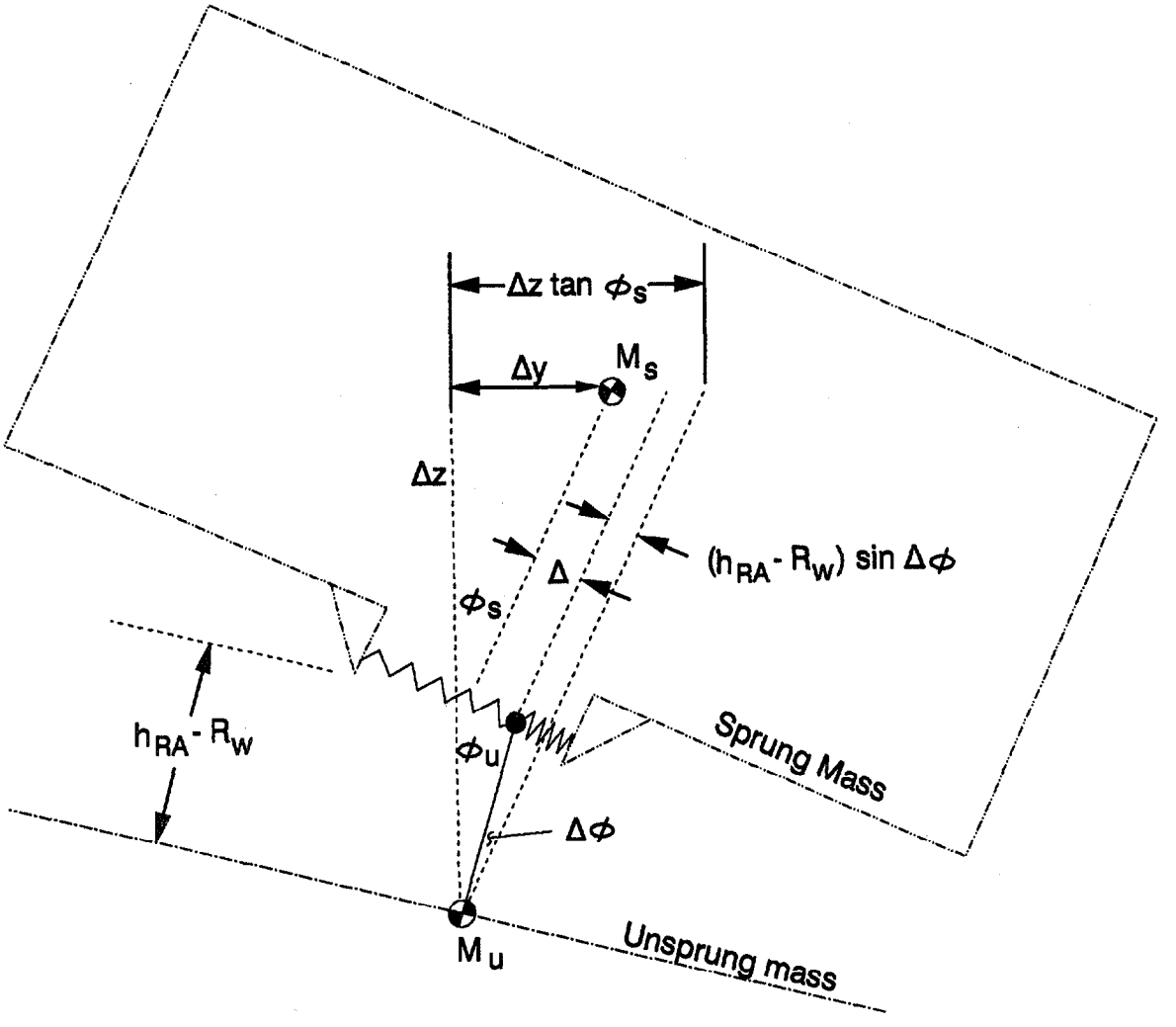

$$\Delta = (\Delta z \tan \phi_s - \Delta y) \cos \phi_s - (h_{RA} - R_w) \sin \Delta\phi$$

where $\Delta\phi = \phi_s - \phi_u$

$\Delta y = y_s - y_u$

$\Delta z = h_s - R_w + z_u - z_s$

$$F_{RA} = \Delta K_{RAS} + \dot{\Delta} K_{RAD}$$

$$\dot{\Delta} = \left[\Delta z \cos \phi_s + \Delta y \sin \phi_s\right] \dot{\phi}_s + \dot{\Delta} z \sin \phi_s +$$

$$- \dot{\Delta} y \cos \phi_s - (h_{RA} - R_w) \cos \Delta\phi \; (\dot{\Delta\phi})$$

Assuming that pitch and heave motions (accelerations) have no significant effect on deflection of the compliant joints, then;

$$z_s = z_{SF} = z_{SR}$$

Then;

$y_s - y_u$ at front would be $\iint(A_{y_{SF}} - A_{y_{UF}})$

where $A_{y_{SF}}$, at front axle $= A_{y_s} + a\ddot{\psi}$

$A_{y_{SR}}$, at rear axle $= A_{y_s} - b\ddot{\psi}$

A_{y_s} is obtained from eq. A-3

$A_{y_{UF}}$, $A_{y_{UR}}$ from eq. A-19

$\dot{\psi}$ from eq. A-2

$\therefore y_{SF} - y_{UF}$ for front axle $= \iint(A_{y_s} + a\ddot{\psi} - A_{y_{UF}})$

$y_{SR} - y_{UR}$ for rear axle $= \iint(A_{y_s} - b\ddot{\psi} - A_{y_{UR}})$

SUMMARY OF COMPLIANT JOINT EQUATIONS

$$F_{RAF} = \Delta_F K_{RAS} + \dot{\Delta}_F K_{RAD} \tag{A-61}$$

$$\Delta_F = \Delta z_F \sin \phi_s - \Delta y_F \cos \phi_s - (h_{RA} - R_w) \sin \Delta\phi_F \tag{A-62}$$

$$\dot{\Delta}_F = \left[\Delta z_F \cos \phi_s + \Delta y_F \sin \phi_s\right] \dot{\phi}_s + \Delta \dot{z}_F \sin \phi_s + - \Delta \dot{y}_F \cos \phi_s - (h_{RA} - R_w) \cos \Delta\phi_F \, (\Delta\dot{\phi}_F) \tag{A-63}$$

$$\Delta z_F = h_s - R_w + z_{UF} - z_s \tag{A-64}$$

$$\Delta y_F = y_{SF} - y_{UF} = \int (\Delta \dot{y}_F) \tag{A-65}$$

$$\Delta\phi_F = \phi_s - \phi_{UF} \tag{A-66}$$

$$\Delta \dot{z}_F = \dot{z}_{UF} - \dot{z}_s \tag{A-67}$$

$$\Delta \dot{y}_F = \int \left(A_{y_s} + a\ddot{\psi} - A_{y_{UF}}\right) \tag{A-68}$$

$$F_{RAR} = \Delta_R K_{RAS} + \dot{\Delta}_R K_{RAD}$$

Plus the above equations with the subscript F replaced by R, for rear axle

Where $\Delta \dot{y}_R = \int \left(A_{y_s} - b\ddot{\psi} - A_{y_{RU}}\right)$

Note; $\Delta\phi_F = \phi_s - \phi_{UF}$ $\quad \Delta\dot{\phi}_F = \dot{\phi}_s - \dot{\phi}_{UF}$

$\Delta\phi_R = \phi_s - \phi_{UR}$ $\quad \Delta\dot{\phi}_R = \dot{\phi}_s - \dot{\phi}_{UR}$

K. INITIAL CONDITIONS

In order to avoid startup transients in simulation, the initial loads on the tires and in the suspension have to be set in at the startup.

Initial Conditions For Suspension Loads F_{SLj_o}

$$F_{SLF_o} = F_{SRF_o} = \frac{M_s g\ b}{2\ell}$$

$$F_{SLR_o} = F_{SRR_o} = \frac{M_s g\ a}{2\ell}$$

} so that all z_{sij} start out = zero

For tire F_z forces

$$F_{zLF_o} = F_{zRF_o} = \frac{M_s g\ b}{2\ell} + \frac{M_{UF}\ g}{2}$$

$$F_{zLR_o} = F_{zRR_o} = \frac{M_s g\ a}{2\ell} + \frac{M_{UR}\ g}{2}$$

L. TABLES OF VARIABLES AND PARAMETERS, WHERE THEY ARE DEFINED, GIVEN A SIGN CONVENTION, AND AXIS SYSTEM

VARIABLES DEFINED

i = F, or R ij = LF, RF, LR, RR

VARIABLE	UNITS	DEFINITION	SIGN CONVENTION FOR POSITIVE VALUE	AXIS SYSTEM
δ_{SW}	radians	Steering wheel angle	clockwise	
δ_{SCR}	radians	Steering control input at rear	to the right	
δ_{Wij}	radians	Steer angle of road wheel	to the right	
ϕ_s	radians	Roll angle of m_s	to the right	body axis
ϕ_{ui}	radians	Roll angle of m_{ui}	to the right	body axis
α_{ij}	radians	Tire side slip angle	to the right	in road plane
θ	radians	Pitch angle of m_s	up at front	body axis
ψ	radians	Yaw angle of total mass, m	to the right	body longitudinal axis, but perpendicular to road
γ_{ij}	radians	Camber angle of each wheel	top of wheel to right	in road plane
S_{ij}	No Unit	Longitudinal wheel slip $= \frac{U - R_w \omega}{U}$		wheel plane
ω_{ij}	rad/sec	Wheel rotational velocity	rolling forward	wheel plane
U	ft/sec	Forward velocity of total mass	forward	body axis
a_x	ft/sec^2	Longitudinal acceleration of m	forward	body axis
V	ft/sec	Lateral velocity of m_u	to the right	horizontal with road plane, and perpendicular to centerline of body
a_{y_s}	ft/sec^2	Lateral acceleration m_s	to the right	

VARIABLES DEFINED (CONCLUDED)

i = F, or R ij = LF, RF, LR, RR

VARIABLE	UNITS	DEFINITION	SIGN CONVENTION FOR POSITIVE VALUE	AXIS SYSTEM
$a_{y_{ui}}$	ft/sec^2	Lateral acceleration of m_{ui}	to the right	horizontal with road plane, and perpendicular to centerline of body
z_s	ft	Vertical motion of m_s	down	road plane
z_{sij}	ft	Suspension deflection, change in length at wheel	increasing length	body axis
z_{ui}	ft	Vertical motion of m_{ui}	down	road plane
$F_{x_{ij}}$	lbs	Longitudinal force on tire	forward on tire, m	in road plane parallel to wheel
$F_{y_{ij}}$	lbs	Lateral force on tire	to the right on tire	in road plane perpendicular to wheel
$F_{z_{ij}}$	lbs	Vertical force on tire	up on tire and m_u	perpendicular to road plane
F_{RA_i}	lbs	Lateral force at roll axis, between m_s, m_u	to right on m_s, to left on m_u	body axis
$F_{s_{ij}}$	lbs	Suspension force equivalent at each wheel	up on m_s, down on m_u	body axis
$F_{BS_{ij}}$	lbs	Suspension force from bump stop	up on m_s, down on m_u	body axis
$F_{SQ_{ij}}$	lbs	Squat/lift force in suspension, due to F_x, F_y	up on m_s, down on m_u	body axis
$M_{z_{ij}}$	ft lbs	Tire aligning moment	clockwise to right	about an axis perpendicular to road

PARAMETERS

i = F, or R ij = LF, RF, LR, RR

PARAMETERS	SOURCE CODE MNEMONIC	UNITS	DEFINITION
a	LENA	ft	X distance from M_s c.g. to front axle
A	REFAREA	ft^2	Frontal area of vehicle, used for longitudinal drag
b	LENB	ft	X distance from M_s c.g. to rear axle
B_i	BF, BR	1/ft	First order coefficient for change in wheel steer angle with suspension deflection
C_i	CF, CR	$1/ft^2$	Second order coefficient for wheel steer with suspension deflection
Cd	CDX		Longitudinal drag coefficient
D_i	DF, DR	1/ft	First order coefficient for change in wheel camber angle, with suspension deflection
E_i	EF, ER	$1/ft^2$	Second order coefficient for wheel camber angle with suspension deflection
F_{sijo}		lbs	Static load on suspension spring at each wheel (computed in program)
F_{zio}		lbs	Static load on each tire (computed in program).
g		ft/sec^2	Gravity = 32.16 ft./sec.^{2}
h_{BS}	HBS	ft	Equivalent suspension clearance to bump stop at each wheel
h_i	HF, HR	ft	L_i times slope of trailing link in trailing arm suspension
h_{cg}	HCG	ft	c.g. height of total mass
h_{RAi}	HRAF, HRAR	ft	Height of roll axis above ground
h_s	HS	ft	M_s c.g. height above ground
I_{ϕ_s}	IXS	lb ft sec^2	Moment of inertia for sprung mass in roll
I_{xz_s}	IXZ	lb ft sec^2	Cross product of inertia for sprung mass about X-Z axis
I_{ui}	IXUF, IXUR	lb ft sec^2	M. of I. for unsprung mass about X axis

PARAMETERS (CONTINUED)

i = F, or R ij = LF, RF, LR, RR

PARAMETERS	SOURCE CODE MNEMONIC	UNITS	DEFINITION
I_{y_s}	IYS	lb ft sec^2	M. of I. for sprung mass about y axis
I_{y_w}	IYW	lb ft sec^2	Wheel inertia about spin axis
I_z	IZZ	lb ft sec^2	M. of I. for entire mass about Z axis
K_{ack}	KACK	ft/ft	Ackerman steer coefficient
K_{BS}	KBS	$\frac{lbs}{ft}$	Bump stop spring rate equivalent at each wheel
K_{ci}	KCF	$\frac{rad}{lb}$	Lateral force steering compliance for suspension and steer linkage
K_{LAGV}	KLAGV	rad/sec	Tire side force lag modifier for low speed operation
K_{LT}	KLT	ft/lb	Lateral compliance rate, of tire, wheel, and suspension, per tire
K_{RAD}	KRADP	$\frac{lb/sec}{ft}$	Damping rate at compliant pin joint between M_s and M_u
K_{RAS}	KRAS	lbs/ft	Lateral spring rate at compliant pin joint between M_s and M_u
K_{SAi}	KSAF, KSAR		= 1.0 for solid axle, = 0.0 for independent suspension
K_{SADi}	KSADF, KSADR	ft/ft	Anti dive coefficient, or slope in side view of an equivalent single suspension arm
K_{SAD2i}	KSAD2F, KSAD2R	ft/ft	Special case for K_{SADi} when there is positive F_x with independent suspension
K_{Si}	KSF, KSR	$\frac{lbs}{ft}$	suspension spring rate equivalent at each wheel
K_{SCi}	KSCF, KSCB	$\frac{rad}{ft\ lb}$	Steering compliance for steering gear
K_{SDi}	KSDF, KSDR	$\frac{lb\ sec}{ft}$	Suspension damping rate equivalent at each wheel

PARAMETERS (CONCLUDED)

i - F, or R ij - LF, RF, LR, RR

PARAMETERS	SOURCE CODE MNEMONIC	UNITS	DEFINITION
K_{SLi}	KSLF, KSLR	ft/ft	Lateral slope of an equivalent single suspension arm, at curb load
K_{STR}	KSTR	rad/rad	Overall steering ratio
K_{TL}	KTL	ft	Tire lag, expressed in rolling distance
K_{ZT}	TSPRINGR	$\frac{lbs}{ft}$	Vertical spring rate of tire
K_{TSi}	KTSF, KTSR	$\frac{ft\ lb}{radian}$	Auxiliary torsional roll stiffness per axle, (normally negative)
ℓ		ft	Wheelbase = a + b
L_i	LF, LR	ft	Length of trailing link, in a trailing arm suspension
L_{SAi}	LSAF, LSAR	ft	Length of the K_{SLi} arm
L_{so}	LSO	ft	Lateral steering axis offset from king pin to tire patch center
m	MASS	$\frac{lb\ sec^2}{ft}$	Total vehicle mass
m_s	SMASS	$\frac{lb\ sec^2}{ft}$	Sprung mass
m_{ui}	UMASSF, UMASSR	$\frac{lb\ sec^2}{ft}$	Front, or rear, unsprung mass
R_W		ft	Effective wheel/tire radius, and same as c.g. height of M_{ui}
T_i	TRWF, TRWB	ft	Track width
ω_{n_s}	SWW	rad/sec	Natural frequency for second order steering system lag
ζ_s	SWZ		Damping ratio for steering system lag
z_{sio}		ft	Initial static deflection of suspension spring at each wheel (computed in program)
z_{uio}		ft	Initial static deflection of each tire (and m_{ui}), (computed in program)

APPENDIX B

VEHICLE PARAMETER MEASUREMENT AND AND ESTIMATION PROCEDURES

APPENDIX B

VEHICLE PARAMETER MEASUREMENT AND ESTIMATION PROCEDURES

In the past, there has always been a problem in finding good parameters for vehicle dynamics simulation. Now, with the current state of development in VDANL, parameter specification has become a major chore, including suspension geometry functions, and a tire model which needs tire test data. This write-up is intended to make VDANL parameter selection more straightforward, more easy to understand, and make the parameter values more readily available by offering optional methods for measurement, calculation or estimation by rules of thumb.

To help make the parameter selection more rational and understandable, we have attempted to make the computer simulation mathematics as general as possible, using composite functions in place of endless mechanical details for every possible component found in different car designs, such as;

1. For vertical and anti-roll spring functions, all suspension springs, shocks, bump stops, and auxiliary roll stiffness, are specified to act at the tire contact patch for all cars. This is consistent with the way cars are tested for ride and roll force reactions at each tire, and makes it unnecessary to model complex suspension mechanisms in place above the tires.

2. Suspension geometry functions for deflection steer, camber angle change, squat-lift forces, and ackerman steer, are also specified as what occurs at the wheel. This is also consistent with the static test data for cars being at the wheel, and avoids complex models for many different suspension designs.

3. The tire model used is a rational and direct description of how tires respond undergoing composite slip, while being relatively simple and easy to understand. It only needs accurate "end point" coefficients to be specified from accurate tire test data.

Various methods to obtain vehicle parameters

1. Measure the vehicle directly (static tests)

   See STI Report WP-1119-4
   SAE Paper 720473
   DOT HS-801800

2. Simple "rule of thumb" calculated estimates

   See SAE Paper 840561
   SAE Paper 881767
   SAE Paper 870495

3. Sources for obtaining direct data on cars

   Miscellaneous NHTSA/VRTC reports

   Automotive Industries, magazine, the annual Engineering Specifications issue

   MVMA Passenger Car Specifications Forms

   Consumer Reports, magazine, the annual auto issue

   Car & Driver, magazine, Buyer's guide

   Motor Trend, magazine, Automotive year book

   Road & Track, magazine, Road test annual, and buyer's guide

4. Dimensional measurement, via tape measure, and conversion for suspension geometry functions.

5. Scale parameters up or down, from known car data.

   Various sources have published parameter input file data on many cars, which could be adjusted up or down for a larger or smaller car.

6. Tire Test Data

   Calspan tire test data, as published for NHTSA

   University of Maryland, tire test data

   Write directly to tire companies for tire test data, (such as Goodyear)

   Adjust data from available tire test data to a new size

These methods are now utilized in the following section, to provide for estimating parameters for the vehicle input files for VDANL.

An example of the vehicle parameter input file is shown below, for a Nissan Sentra.

THE CURRENT VEHICLE PARAMETERS ARE :

1) MASS = 73	20) AEROVEL = 44	39) IXUF = 24
2) SMASS = 64	21) KTL = 1	40) IXUR = 22
3) UMASSF = 4.5	22) KSF = 1600	41) KLT = .00015
4) UMASSR = 4.5	23) KSDF = 110	42) XACC = -2.3
5) LENA = 2.75	24) KSR = 1200	43) ZACC = 1.8
6) LENB = 5.09	25) KSDR = 70	44) DRAGC = -.015
7) IXS = 160	26) TRWF = 4.6	45) LENS = 5.3
8) IYS = 812	27) TRWB = 4.52	46) LM = 1.125
9) IZZ = 970	28) HCG = 1.71	47) KBTF = -.48
10) IXZ = 0	29) KBS = 3750	48) KVB = 22
11) KSTR = 16.9	30) HBS = .25	49) KMB = 3.5
12) KSCF = .00003	31) KTSF = 0	50) KBPVL = 55
13) KSCB = 0	32) KTSR = 0	51) SWZ = .5
14) DLADV = 0	33) KRAS = 12000	52) SWW = 100
15) DYADV = 0	34) KRADP = 700	53) KCF = 0
16) DNADV = 0	35) TSPRINGR = 9000	54) LSO = 0
17) DENSITY = .00237	36) HRAF = 0	55) KLAGV = 25
18) REFAREA = 20	37) HRAR = 0	R) RETURN
19) CDX = .5	38) HS = 1.83	

All parameters are defined in Appendix A.

Note the small distinction or difference between m and m_c. m should be the total mass as tested or to be run in the simulation. However, most static test data on I_x, I_y, I_z etc., is based on empty "curb load" states for the car. Therefore, all estimates for the inertias should use the "curb weight" state = m_c.

Then, if desired, these inertias can be corrected for the addition of a driver and test equipment, to provide the "as-tested" inertias.

For I_z, I_{y_s} this is not needed, because one driver and test equipment adds less than 1% to the I_{z_o}, $I_{y_{s_o}}$ for the empty car.

But for roll inertia, the I_{y_s} with the driver and equipment added could be 5% to 10% larger than $I_{x_{s_o}}$ empty, so that this difference may be large enough to add this correction into $I_{x_{s_o}}$. But one should also realize that the driver is not rigidly attached to the sprung mass, so that the effective I_{x_s} in dynamic roll response may be less than nominal calculations suggest.

LIST OF VEHICLE PARAMETERS AND ESTIMATION METHODS

The following table is set up with numbers and terms in the same order they appear in the VDANL computer simulation input files. All units and definitions are shown in Appendix A.

1. m, total mass.

   Weigh vehicle with driver and test equipment, or use published weight and add for driver and equipment.

2. m_s, sprung mass

   $$m_s = m - m_{UF} - m_{UR}$$

3. m_{UF}, front unsprung mass.

   $m_{UF} = 1 + .045\ m_c$ for suspensions with sprung differential

   $m_{UF} = .08\ m_c$ for solid axle suspensions with differential unsprung

   m_c = curb weight, to be used with formula

4. m_{UR}, rear unsprung mass

   use same formulas as for 3., m_{UF}

5. a, distance from front axle to c.g. of m_s

   $$a = \left(W_R - g\ m_{UR}\right) \frac{\ell}{g\ m_s}$$

   W_R = test vehicle weight at rear axle

   ℓ = wheelbase

6. b, distance from rear axle to c.g. of m_s

   $$b = \ell - a$$

7. I_{x_s}, sprung mass roll inertia

   This data is always difficult to obtain. If published data is available, it is usually for total inertia, I_x. To convert to I_{x_s},

$$I_{x_s} = I_x - I_{UF} - I_{UR} - m_s\left(h_s - h_{c_g}\right)^2 - \left(m_{U_F} + m_{UR}\right)\left(h_{c_G} - R_W\right)^2$$

$$\left.\begin{aligned} I_{U_F} &= m_{UF}\left(\frac{T_F}{2}\right)^2 \\ I_{U_R} &= m_{UF}\left(\frac{T_R}{2}\right)^2 \end{aligned}\right\} \text{For independent suspensions}$$

$$\left.\begin{aligned} I_{U_F} &= \frac{2}{3}\, m_{UF}\left(\frac{T_F}{2}\right)^2 \\ I_{U_R} &= \frac{2}{3}\, m_{UR}\left(\frac{T_R}{2}\right)^2 \end{aligned}\right\} \text{For solid axle with differential gear}$$

$$h_s = \frac{m_c h_{cg} - (m_{UF} + m_{UR})\, R_w}{m_s}$$

If no published data is available, then I_{x_s} can be estimated from data in Figure B-1, where,

$$I_{x_s} = .558(m_c)^{4/3}$$

m_c = curb load mass

For the special cases of unusual body shapes, the following shape corrected formulas can be used.

$$I_{x_s} = \frac{m_c}{18.5}\left(W^2 + \left[.69H\right]^2\right) \quad \text{For sedans}$$

$$I_{x_s} = \frac{m_c}{18.5}\left(W^2 + \left[.77H\right]^2\right) \quad \text{For station wagons and utility vehicles}$$

$$I_{x_s} = \frac{m_c}{18.5}\left(W^2 + \left[.85H\right]^2\right) \quad \text{For vans}$$

where W = vehicle body width

H = vehicle roof height

8. I_{y_s}, sprung mass pitch inertia

If published data available is only for total inertia, I_y, then convert to I_{y_s},

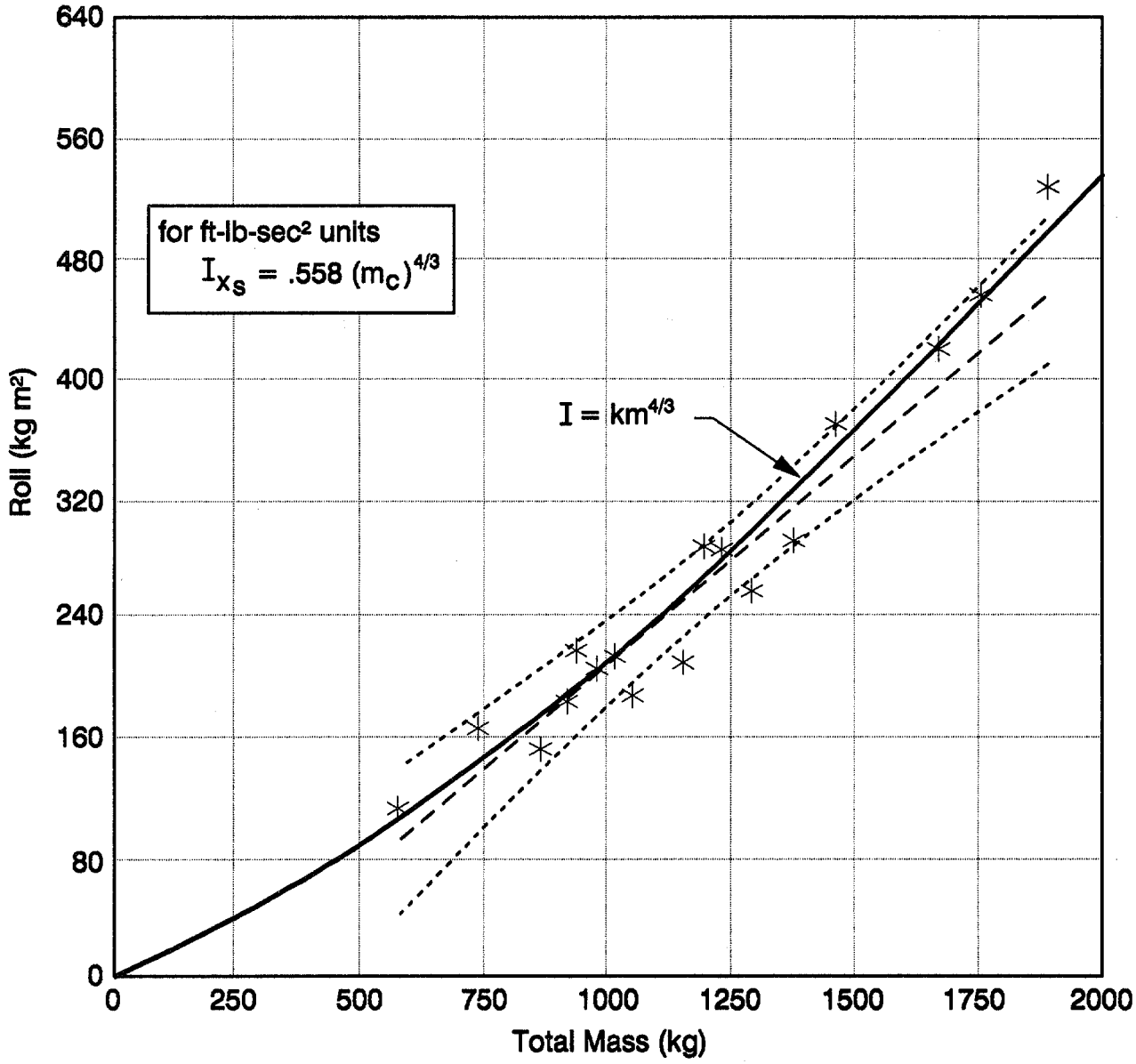

Figure B-1. Sprung Mass Roll Inertia about c.g. vs. Total Mass (from SAE 84056)

$$I_{y_s} = I_y - m_s\left[h_s - h_{cg}\right]^2$$

$$- m_{UR}\left[b^2 + \left[h_{cg} - R_w\right]^2\right] - M_{UF}\left[a^2 + \left[h_{cG} - R_w\right]^2\right]$$

If no published data is available, then I_{y_s} can be estimated from data in Figure B-2,

$$I_{y_s} = .733\ m_c^{5/3}$$

9. I_z, total yaw inertia

If no published data is available, then $I_z = m_c ab$ can be used, or can be estimated from data in Figure B-3,

$$I_{z'} = .99\ m_c^{5/3}$$

This 5/3 exponential is consistent with vehicle mass varying proportional to ℓ^3. So that ab varies as ℓ^2, or as $m^{2/3}$. Therefore I_z should vary as mab, or $m\ell^2$, or $m^{5/3}$.

However, there is a body shape correction needed for short vs. long body lengths for vehicles of the same mass. This is important when considering short bodied utility vehicles, as contrasted with sedans with long body overhangs. For these vehicles, I_z can be estimated by,

$$I_z = .0875\ m_c\ell^2 + .053\ m_c\ (\text{overall length})^2$$

10. I_{xz}, cross product of inertia

This data is almost always not available, and there is no rationale for estimating it. And since it is a very small number with no significant effect on vehicle handling, we will assume it can be set equal to zero, if the data is not available.

11. K_{STR}, overall steering ratio

This data is seldom available and must be tested directly. See Appendix E.

12. K_{SCF}, steering gear compliance at front

See Appendix D for test method.

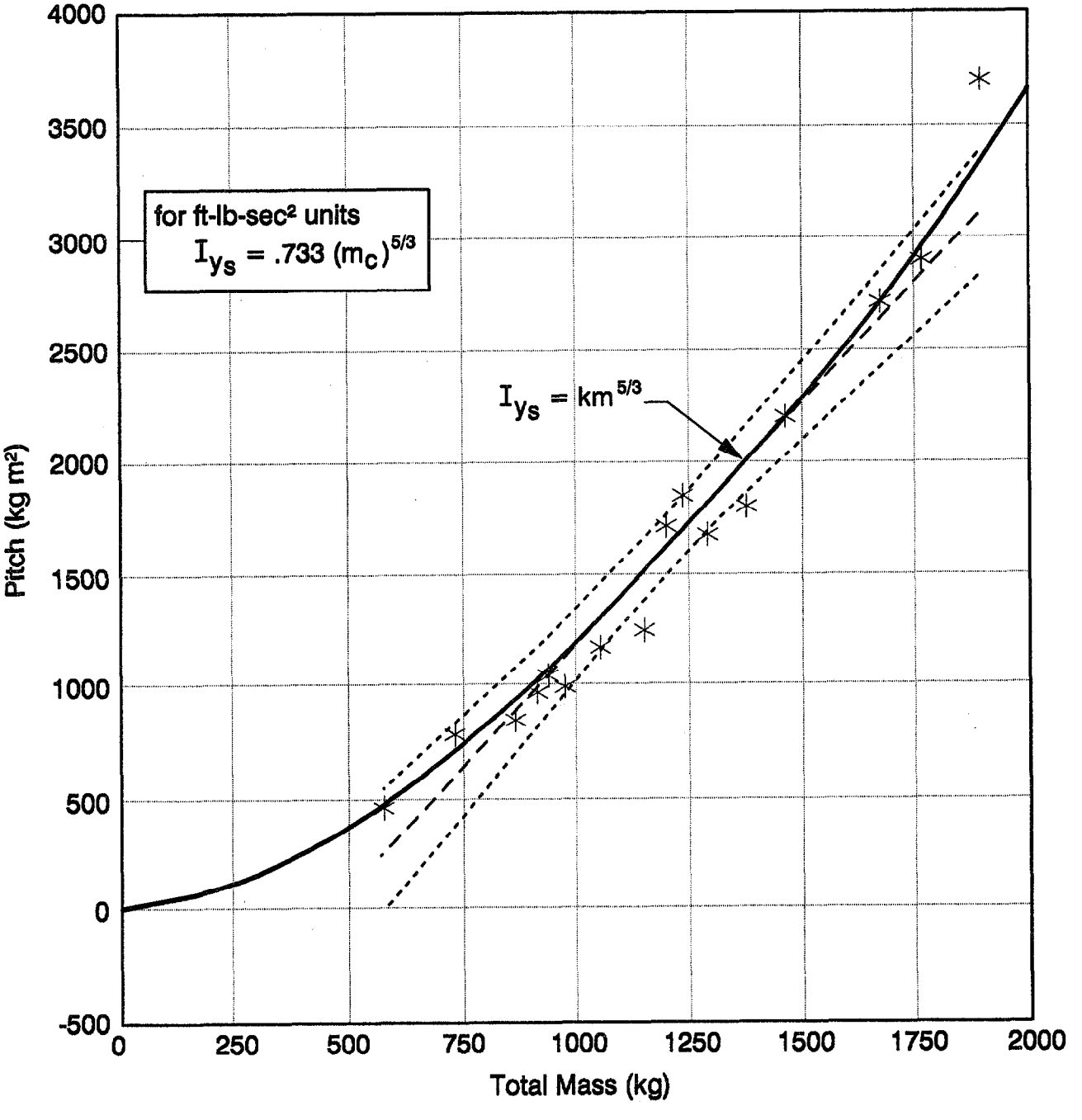

Figure B-2. Sprung Mass Pitch Inertia about c.g. vs. Total Mass (from SAE 84056)

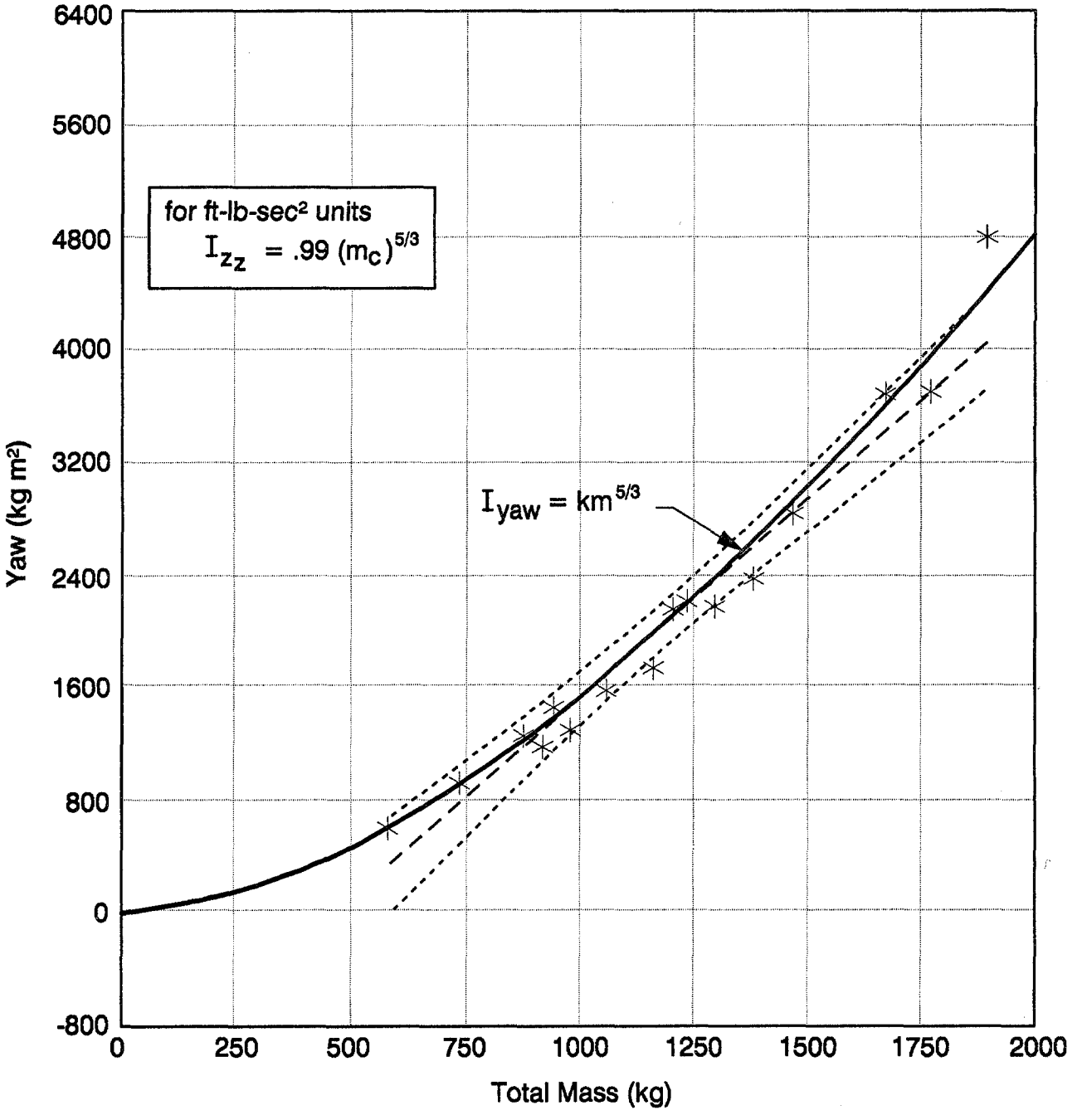

Figure B-3. Total Vehicle Yaw Inertia about c.g. vs. Total Mass (from SAE 84056)

13. K_{SCB}, steering gear compliance at rear

See Appendix E for test method.

14, 15,
16, 17. Y_A, N_A, L_A, X_A, aero terms

18. REFAREA, front view body cross-section area

If not available can be estimated from .75 h w

where h = body height
w = body width

19. C_{DX}, drag factor in X direction

This varies from .30 to .40 for most new cars and vans, and probably about .40 to .50 for most small trucks and older cars.

20. AEROVEL, aero input

21. K_{TL}, tire side force development lag

This is expressed in feet of rolling tire travel, in which the time constant = KTL/U for a second order system where ζ = 1.0. For this system, the tire will roll about 6 times the KTL distance to reach the final value for a step input.

$$\text{Therefore, KTL} = \frac{\text{Roll distance to S.S.}}{6}$$

Typical values for KTL range from 0.7 to 1.4 ft, which corresponds to a total roll distance of 4.2 to 8.4 feet.

22. K_{SF}, front suspension spring rate.

This is the suspension spring rate as measured at the wheel. See Appendix E for test method.

23. K_{SDF}, front suspension damping rate

No data is available for this, but most cars have ζ = .25 to .35 for good ride quality.

Choose ζ = .25 if ride is soft and floating
ζ = .35 if ride is firm
ζ = .45 if ride is very stiff and jerky

Then,

$$KSDF = 2\zeta\sqrt{(KSF)(m_{siF})}$$

where

$$m_{siF} = \frac{m_{sb}}{2\ell} = \text{sprung mass over one front wheel}$$

24. K_{SR}, rear suspension spring rate.

This is the spring rate as measured at the wheel. See Appendix D for test method.

25. K_{SR}, rear suspension damping rate

This is usually somewhat higher than the front.

Choose $\zeta = .30$ if ride is soft
$\zeta = .40$ if ride is firm
$\zeta = .50$ if ride is very stiff

Then,

$$KSDR = 2\zeta\sqrt{(KSR)(m_{siR}}$$

where

$$m_{SiR} = \frac{m_s a}{2\ell}$$

26. T_F, front track width

Measure this from tire center to tire center.

27. T_R, rear track width

Measure this from tire center to tire center.

28. h_{cg}, center of gravity of total vehicle

Use published data, or test method described in Appendix D. Or a simple rule of thumb can be used to estimate h_{cg}.

h_{cg} = .39 (roof height), for passenger cars
= .38 (roof height), for vans
= .37 (roof height), for pick up trucks
= .39 (roof height), for 4WD utility vehicles
= .41 (roof height), for 4WD vehicles designed extra high for clearance from unsprung front axle differential housing

29. K_{BS}, bump stop stiffness

This has to be approximated, but is generally about = 2 (KSF).

30. h_{BS}, suspension travel to bump stop.

This suspension travel to contact the bump stop can be directly measured on a test vehicle. Or, as a general rule, it is about .25' for larger vehicles, and ranges down to .20' for smaller vehicles.

31. K_{TSF}
32. K_{TSR}, } front and rear auxiliary roll stiffness.

This is seldom available, and must therefore be measured in a static test on the vehicle. See Appendix D for that method. However, this test provides the overall roll stiffness, (K_{ORSi}), at each axle. To compute the net auxiliary roll stiffness, the effects from the tire and suspension spring rates must be removed.

$$K_{TSi} = \frac{K_{ORSi}\, K_{TRSi}}{K_{TRSi} - K_{ORSi}} + \frac{K_{si}\, T_i^2}{2}$$

where K_{ORSi} = overall roll stiffness at i axle

T_i = track width

K_{si} = suspension spring rate

$K_{TRSi} = \frac{K_{ZT}\, T_i^2}{2}$

K_{ZT} = tire spring rate

Note that roll stiffness coefficients normally have negative values.

33. K_{RAS}, spring rate for pin joint between m_s, m_{ui}.

This provides for lateral compliance at the suspension pivot and sub-frame rubber bushing attachments. An additional purpose is to avoid digital computer computational instabilities. Thus, a value needs to be chosen to provide a natural frequency above the region of interest for vehicle handling, but below the region that would interact with the typical computer program sampling interval of .005 seconds.

$$\omega_n = \sqrt{\frac{(m_{UF}\ell + m_s b)\, K_{RAS}}{m_{UF}\, m_s b}}$$

K_{RAS} = 12,000 was chosen to be used for all vehicles.

34. K_{RAD}, damping rate for K_{RAS}

KRAD = 700, was chosen to provide nearly critical damping.

$$\zeta \approx \frac{K_{RAD}}{2\sqrt{m_{ui}\ K_{RAS}}}$$

35. K_{ZT}, tire spring rate

This is usually available from Calspan tire test data. If not, this can be estimated from formula;

$$K_{ZT} = 510 \left[\text{Wheel Rim Diam} + 2 \left(\text{tire sect. size}\right)\right]\frac{\text{Press}}{35}$$

Wheel rim diameter and tire section size need to be in inches, and tire pressure in lbs. per square inch.

Tire size is given on the side wall, such as P205/75 R15.

- R15 → wheel rim diameter, in inches
- P205/75 → section size, in mm., which then needs to be converted into inches by dividing by 25.4 mm/inch.

Correct tire pressure is given by a MFG. tag somewhere on the vehicle.

36. h_{RAF}
37. h_{RAR}

front and rear roll axis height.

For solid axle or beam axle suspensions, the roll axis height is the height of the lateral control link pivot above ground. This is the pivot about which the sprung mass will rotate in free geometric roll.

For all independent suspensions, where there is no physical roll axis pivot, all forces and moments are carried through each independent suspension. Therefore, for these cases, h_{RAF} and/or h_{RAR} are set = zero. And the force and moment effects are set by suspension geometry parameters, in the suspension input files.

38. H_s, center of gravity height of the sprung mass.

$$h_s = \frac{m_{hcg} - (m_{UF} + m_{UR})\ R_w}{m_s}$$

39. I_{XUF}
40. I_{XUR} } is the I_x for each axle

This data is not available, so that estimation by an approximate formula is necessary.

$$I_{xui} = \left(\frac{T_i}{2}\right)^2 m_{ui}$$

where $m_{ui} = 1 + .045\ m_c$

The extra mass of an unsprung differential gear is not included, because being at the axle c.g. center, it does not contribute any significant amount to I_{xu}

41. K_{LT}, lateral compliance rate of tire and suspension.

This is the total lateral compliance rate of everything that effectively reduces the half-track width, which plays a direct part in resisting vehicle roll over. This includes tire casing lateral compliance, wheel bending, suspension bending, suspension and sub-frame bushing deflection, and etc.

The tire lateral compliance rate is given in the Calspan tire test data as the C_1 parameter. If this is not available, it can be estimated from a known vertical spring rate of the tire.

$$\approx \frac{1}{.76\ K_{ZT}}$$

Data on the other sources of lateral compliance are difficult to obtain. But all other compliance is probably in the same order of magnitude of the tire compliance. So that if we combine this, we have a rough approximation for total compliance;

$$K_{LT} \approx \frac{2}{.76\ K_{ZT}} = \frac{2.6}{K_{ZT}}$$

or if C_1 is available,

$$K_{LT} = 2C_1$$

42. X_{ACC}, location of A_y accelerometer forward from total vehicle c.g., in a field test vehicle.

This is used to provide measured A_y values from simulation runs at the same location in the vehicle as used in field testing.

43. Z_{ACC}, location of Ay accelerometer in distance above roll axis.

This is for same purpose as #42, X_{ACC}, and can be calculated as follows;

$$Z_{ACC} = h_{Z_{ACC}} - h_{RAR} + \frac{X_{RA}}{\ell}\left(h_{RAR} - h_{RAF}\right)$$

where;

$h_{Z_{ACC}}$ = Ay accelerometer height above ground

X_{RA} = distance Ay accelerometer is forward from rear axle

hRAF, hRAR = front and rear roll axis heights which are items 36, 37 if it is for solid axle suspensions.

If it is an independent suspension,

$$hRAF = KSLF\left(\frac{T_F}{2}\right)$$

$$hRAR = KSLR\left(\frac{T_R}{2}\right)$$

where

KSLi = suspension motion slope as defined in suspension input file, items 17, 18

44. DRAGC, rolling drag coefficient.

For most vehicles with radial tires at 35 psi, on paved roads, this coefficient = −.015

45. LENS, is the distance from the vehicle rear axle back to the side slip sensor trolley wheels.

This is so the simulation β can be compared to a field test vehicle with a side slip sensing trolley.

46. LM, is the length of the trailing arm (lateral swing arm) of the side slip sensing trolley.

This is used to define the sensor response lag.

47. KBTF
48. KVB
49. KMB
50. KBPVL

} brake system function parameters.

A complete description of this system follows on the next 2 pages.

BRAKE SYSTEM FOR VEHICLE DYNAMICS SIMULATION, VDANL

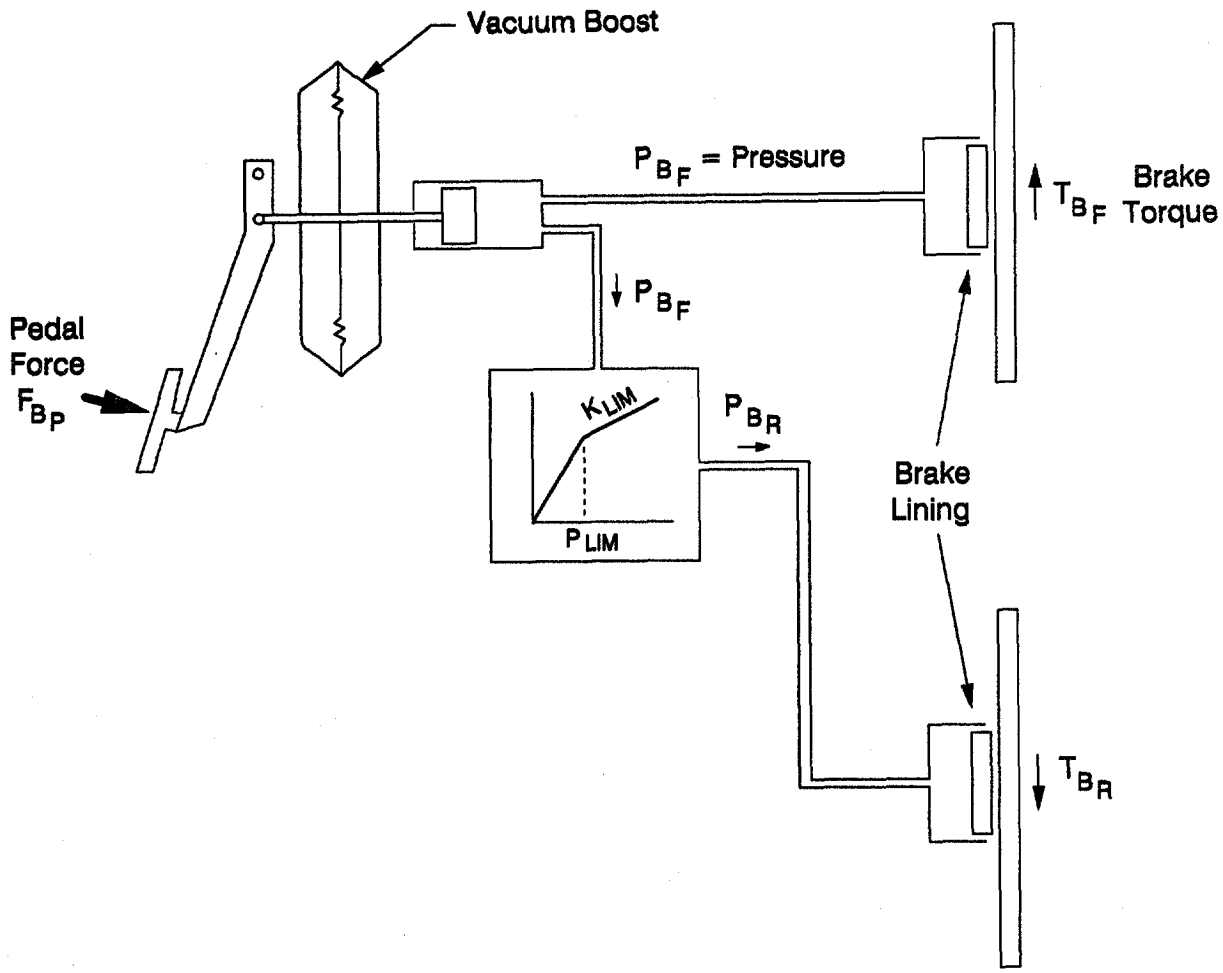

$$P_{B_F} = f(F_{B_P}, \text{Lever Ratio, Vac Boost, Mast. Cyl Pist Diam})$$

$$P_{B_F} = K_{VB} F_{BP}, \text{ for } F_{BP} \leq F_{BPVL}$$

$$= K_{VB} F_{BPVL} + K_{MB} \left(FBP - F_{BPVL}\right) \quad \text{for } F_{BP} > F_{BPVL}$$

$$P_{B_R} = P_{B_F} \text{ for } P_{B_F} \leq P_{LIM}$$

$$= P_{LIM} + K_{LIM} \left(P_{B_F} - P_{LIM}\right) \text{ for } P_{B_F} > P_{LIM}$$

$T_{B_F} = \left[K_{BT_F}\right] P_{BF}$ front brake effectiveness, per wheel

$T_{B_R} = \left[K_{BT_R}\right] P_{BR}$ rear brake effectiveness, per wheel

FOR OPTIMAL BRAKE PROPORTIONING

use K_1, k_2, F_x, as is from previous computation in program

then	$P_{LIM} = \frac{R_w F_{x_1}}{2 K_{BTF}}$	or	$F_{x_i} = \frac{2P_{LIM} K_{BTF}}{R_w}$
	$K_{BTR} = K_{BTF} K_1$		$K_1 = \frac{K_{BTR}}{K_{BTF}}$
	$K_{LIM} = \frac{K_2}{K_1}$		$K_2 = K_{LIM} K_1$

PARAMETERS SET FROM EXTERNAL INPUT FILE

K_{BTF}	= front brake effectiveness, per wheel (normally negative)	$\frac{FT\ LBS}{PSI}$
KVB	= brake gain in vacuum boost range,	$\frac{PSI}{LB}$
KMB	= brake gain in manual brake range,	$\frac{PSI}{LB}$
F_{BPVL}	= Pedal force at point where vacuum boost runs out (limits),	LBS

VARIABLES;	F_{BP}	Force on brake pedal	LBS
	P_{BF}	Hydraulic Pressure (front brakes)	PSI
	P_{BR}	Hydraulic Pressure (rear brakes)	PSI
	T_{BF}	Brake torque (for 1 front wheel)	FT-LBS
	T_{BR}	Brake torque (for 1 rear wheel)	FT-LBS

51. SWZ,
52. SWW, } are the damping ratio and natural frequency for the vehicle's steering system response lag.

These can be determined from an instrumented tire kick test while the front wheels of a stationary car are free and off the ground, and the steering wheel is clamped solid in a fixed position. This is the natural dynamic response of the 2 front wheel's inertial mass about the steering (ball joints) axis, while flexing against the steering system compliance.

or can be estimated as follows;

$$SWZ = \zeta \text{ is nominally set } = 0.5$$

$$SWW = \omega_m = \frac{1}{\sqrt{2\ I_W\ K_{SCF}}}$$

I_W will range from about 1.0 ft lb sec^2 for smaller wheels, up to 2.0 ft lb sec^2 for larger wheels

K_{SCF} is parameter #12

53. K_{CF}, is lateral force compliance steer

This is mainly centered in relative suspension deflections in the lateral direction. This can be measured directly, as shown in WP 1119-4. Or it can be assumed that for most vehicle designs, the manufacturer usually tries to minimize these effects, as they could cause handling problems in certain circumstances. Therefore set K_{CF} = zero.

The exception to this, is when the steering linkages are placed in front of the suspension arms. Then there will tend to be a significantly large compliance understeer effect due to soft suspension bushings. In this case, the static test should be done to measure this effect.

54. L_{SO}, is the offset of the steering axis (ball joints) inboard of the wheel centerline at the road surface. It is used to compute torque steer effects due to braking or traction from front wheel drive.

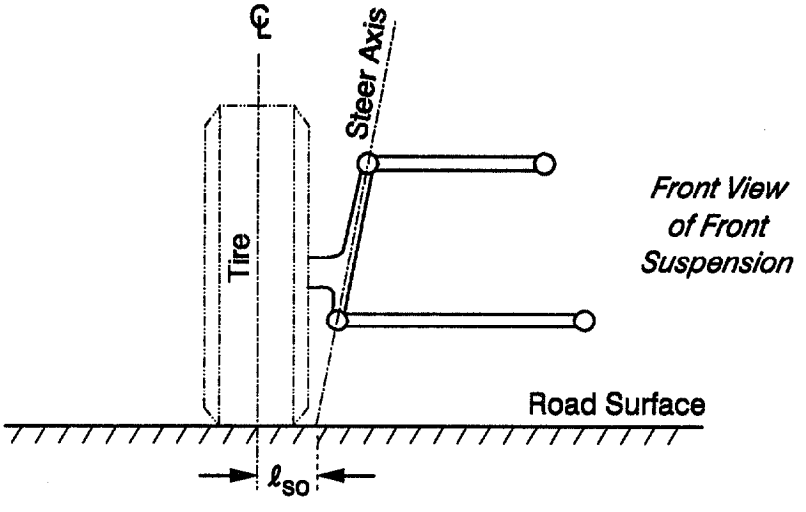

55. KLAGV, this is a modification to the tire side force lag function, to deal with low speed effects.

As discussed in Appendix A, the simple time constant term ℓ_{TL}/U needs to be modified at low speeds to account for the fact that the vehicle mass can respond laterally on the tire casing lateral spring rate, faster than the tire side slip force can develop. This means that the tire side force can reach its final value sooner than indicated by ℓ_{TL}/U, at low speeds.

$$F_y = \frac{Y_{\alpha_o}\ \alpha}{\left[\frac{1}{U/K_{LT} + (KLAGV)}\ S + 1\right]^2}$$

KLAGV is set typically = 15 to 18 rad/sec

APPENDIX C

SUSPENSION PARAMETER MEASUREMENT AND ESTIMATION PROCEDURES

APPENDIX C

SUSPENSION PARAMETER MEASUREMENT AND ESTIMATION PROCEDURES

Continuing from the appendix B discussion, this section deals with the suspension parameters. Again, we are dealing with a vehicle dynamics model which relies on composite functions rather than specific suspension design variations. Each parameter is the subject to simple external test procedures or definitions. The following is a sample of a suspension parameter input file for a Nissan Sentra, and the estimation procedures which follows this, will use the same numbering and parameter order.

THE CURRENT SUSPENSION PARAMETERS ARE :

```
 1) SUSPENSIONF = INDEPEN 20) LSAR = 1000
 2) SUSPENSIONR = INDEPEN 21) KSADF = 0
 3) HF = 0                22) KSADR = 0
 4) HR = 0                23) KSAD2F = .64
 5) LF = 1                24) KSAD2R = .64
 6) LR = 1                25) KACK = .29
 7) KSAF = 0
 8) KSAR = 0               R) RETURN
 9) BF = 0
10) BR = 0
11) CF = 0
12) CR = 0
13) DF = -.134
14) DR = 0
15) EF = 0
16) ER = 0
17) KSLF = .115
18) KSLR = .033
19) LSAF = .96
```

SUSPENSION PARAMETERS

1. SUSPENSIONF,] set = INDEPENDENT, for independent
2. SUSPENSIONR,] set = SOLID AXLE, for solid axle or beam axle suspension for front (F), and rear (R) suspension

3. H_F
4. H_R
5. L_F
6. L_R
7. K_{SAF}
8. K_{SAR}

these define the roll steer coefficient for solid axle or beam beam axle suspension at the front (F), or rear (R).

Typical axles have 2 trailing links or leaf springs with an equivalent link, which control the steer angle of the axle. The side view slope of this link gives the axle the roll steer coefficient.

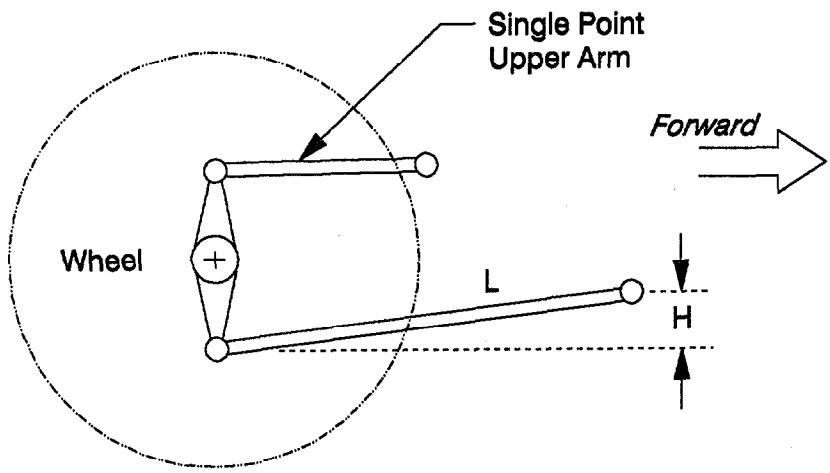

Roll Steer Function is;

$$\Delta\delta_w = \frac{K_{SAF}}{L_F}\left[h_F + \left(\frac{Z_{SLF} + Z_{SRF}}{2}\right)\right](\Phi_S - \Phi_{uF})$$

with H_i = height that forward pivot is above rear pivot

L_i = length of trailing link

K_{SAi} = 1.0, to activate function

If, for a front suspension, there are leading links (placed behind the front axle), the L_F should have a negative sign.

For independent suspensions, H_i = 0, and set L_i = 1.0 to avoid division by zero, and K_{SAi} = 0 to remove this function.

9. B_F
10. B_R
11. C_F
12. C_R

these are for the wheel steer functions for vertical suspension deflection.

For solid axle suspensions, these B_i and C_i parameters are set = zero, to remove the functions.

For independent suspensions, the B_i is the first order steer effect, and the C_i is the second order steer effect.

$$\Delta\delta_{w_{L_F}} = B_F Z_{SLF} + C_F Z_S^2 LF$$

$$\Delta\delta_{w_{L_R}} = B_R Z_{SLR} + C_R Z_S^2 LR$$

See Fig. C-1 which shows a suspension with a change in δ_w with vertical wheel motion, dz. See Fig. C-2 for examples of complex deflection steer.

Most modern suspension designs try to avoid what is sometimes called bump steer, because it tends to be detrimental to predictable handling on certain types of roadway disturbances. And since it is so difficult to obtain reliable test data on deflection steer, we would recommend that these parameters B_i and C_i be set = zero.

If the roll steer coefficient (ϵ) is known, then $B_i = \frac{2\,\epsilon_i}{T_i}$.

If it is suspected that a certain vehicle has a significant amount of deflection steer, then it may be necessary to test for these steer effects. The test is rather straight forward, which measures wheel steer angle change versus forced vertical movement of the sprung mass. Then values of B_i and C_i are chosen so as to fit the function to the test data curve.

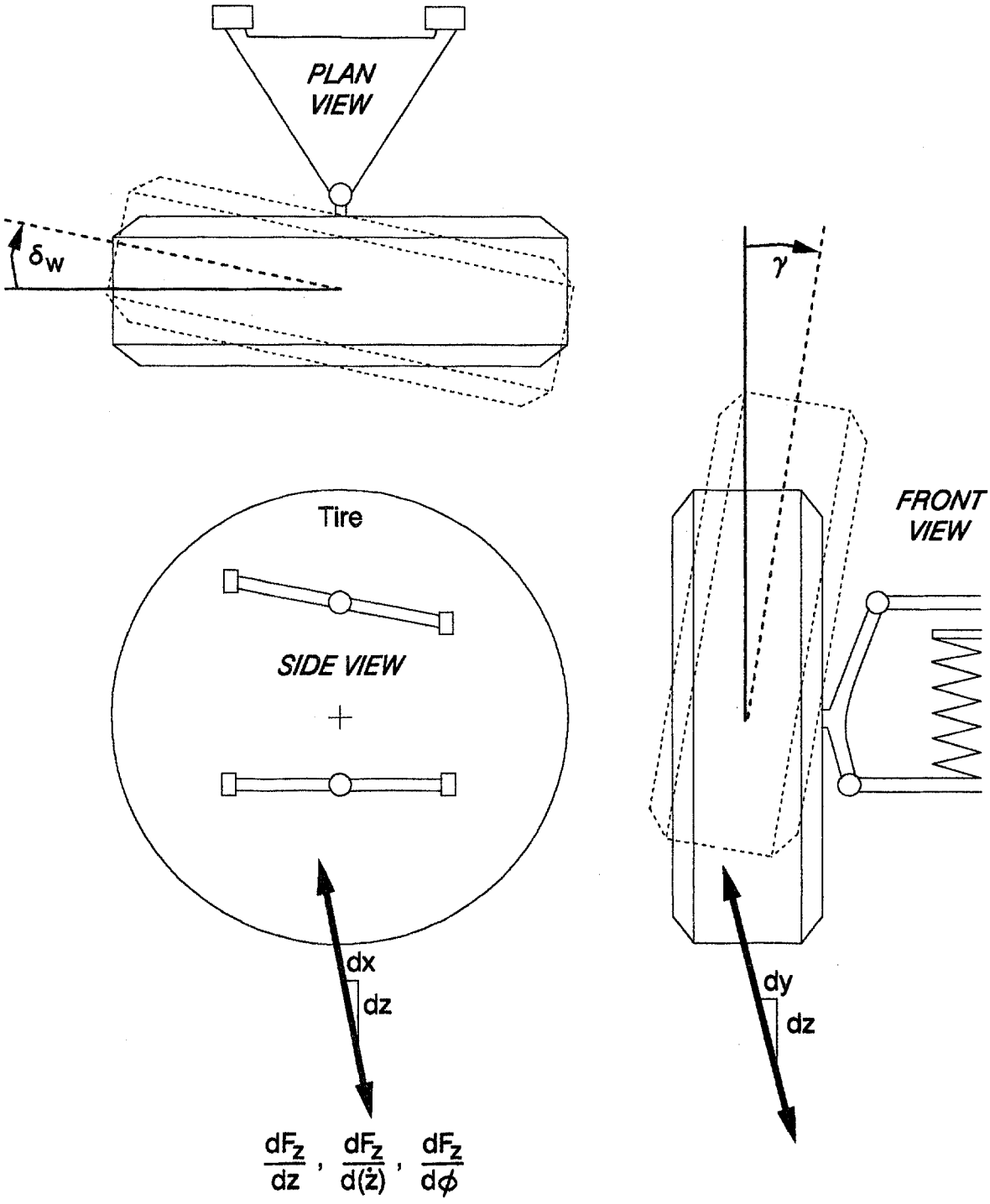

Figure C-1. Static Tests on Wheel Motions

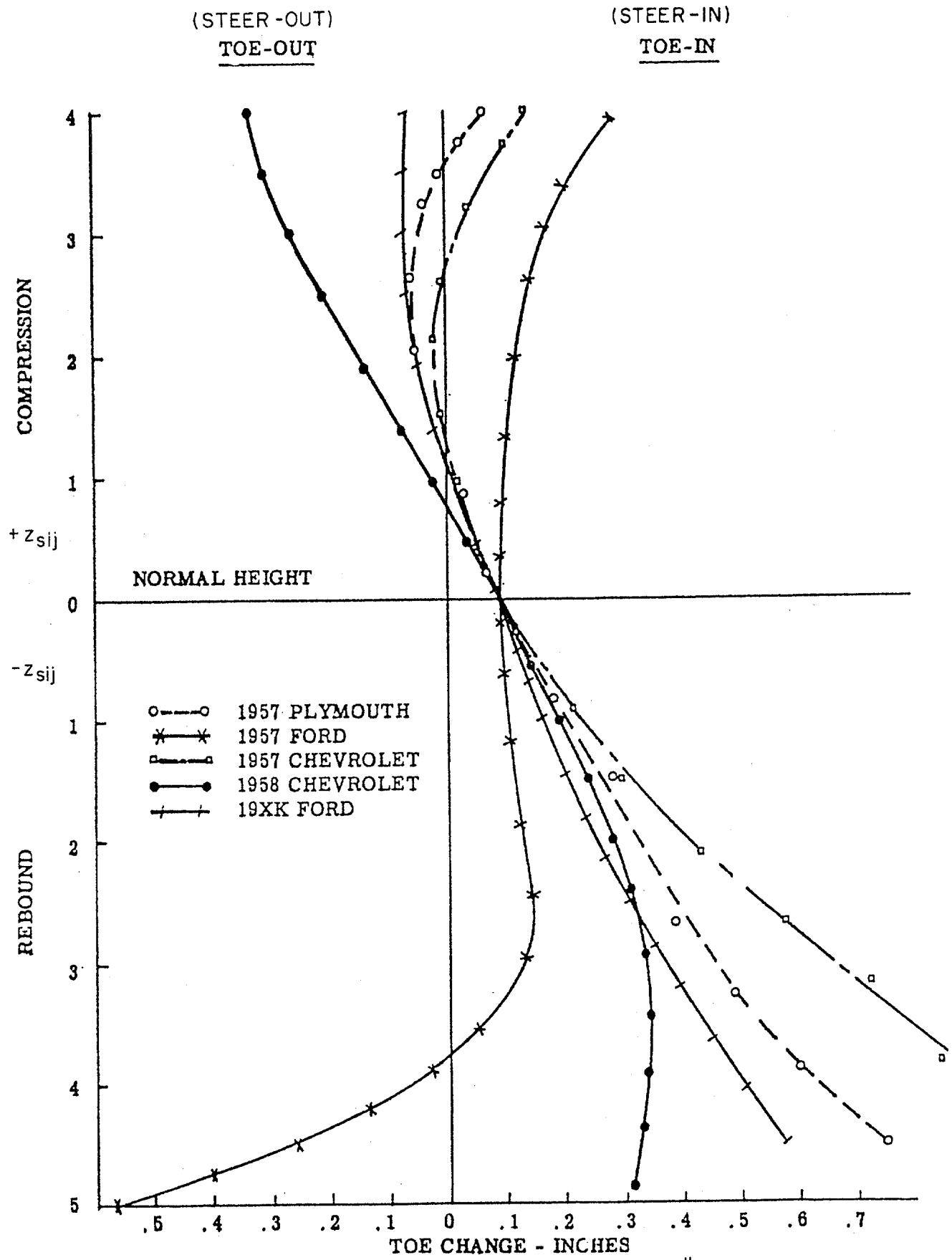

Figure C-2. Toe Change Versus Suspension Position

13. D_F
14. D_R
15. E_F
16. E_R

these are for the camber angle change vs vertical deflection functions.

See Fig. C-1, which shows camber angle (γ) change vs vertical wheel motion (dz). See Fig. C-3 for examples of typical camber angle change curves.

The functions for camber angle with independent suspension are:

$$\gamma_{LF} = \phi_s + D_F Z_{SLF} + E_F Z_S^2 LF$$

$$\gamma_{LR} = \phi_s + D_R Z_{SLR} + E_R Z_S^2 LR$$

These D_i and E_i coefficients can be estimated by matching the function to static test data, such as in Fig. C-3. The static test simply measures camber angle vs forced vertical motion of the sprung mass.

An alternative is to measure all suspension component pivot locations and link lengths. Then reconstruct the suspension on graph paper, and by plotting the linkage motions on paper, determine the camber angle change by graphical methods.

Also if the camber angle to roll angle coefficient is know, $K_{\gamma/\phi}$, then;

$$D_i = [K_{\gamma/\phi} - 1] \frac{2}{T_i}$$

For solid axle and beam axle suspensions, these functions are bypassed, such that the D_i and E_i parameters are set = zero.

17. K_{SLF}
18. K_{SLR}
19. L_{SAF}
20. L_{SAR}

these are for the suspension squat/lift functions with lateral forces.

The primary factor in squat/lift reactions is the path direction of the tire contact patch as the wheel moves up and down in suspension motions. These are shown in Fig. C-1 as dy/dz. And example of test data is shown in Fig. C-4.

The function for suspension squat/lift is simply;

$$F_{sQij} = K_{sLi} + \frac{z_{sij}}{L_{sAi}} [F_{y_{ij}}]$$

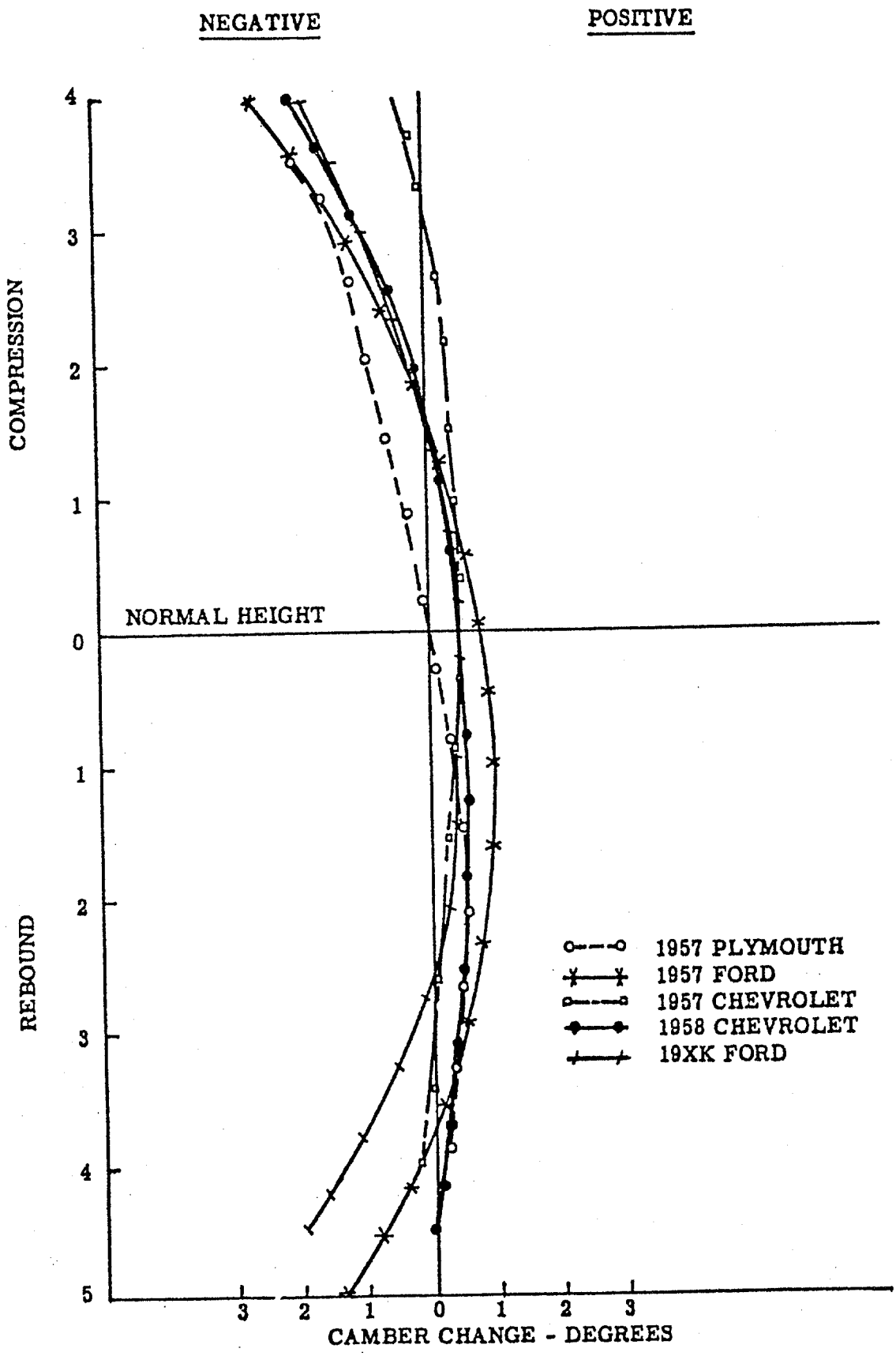

Figure C-3. Camber Change Versus Suspension Position

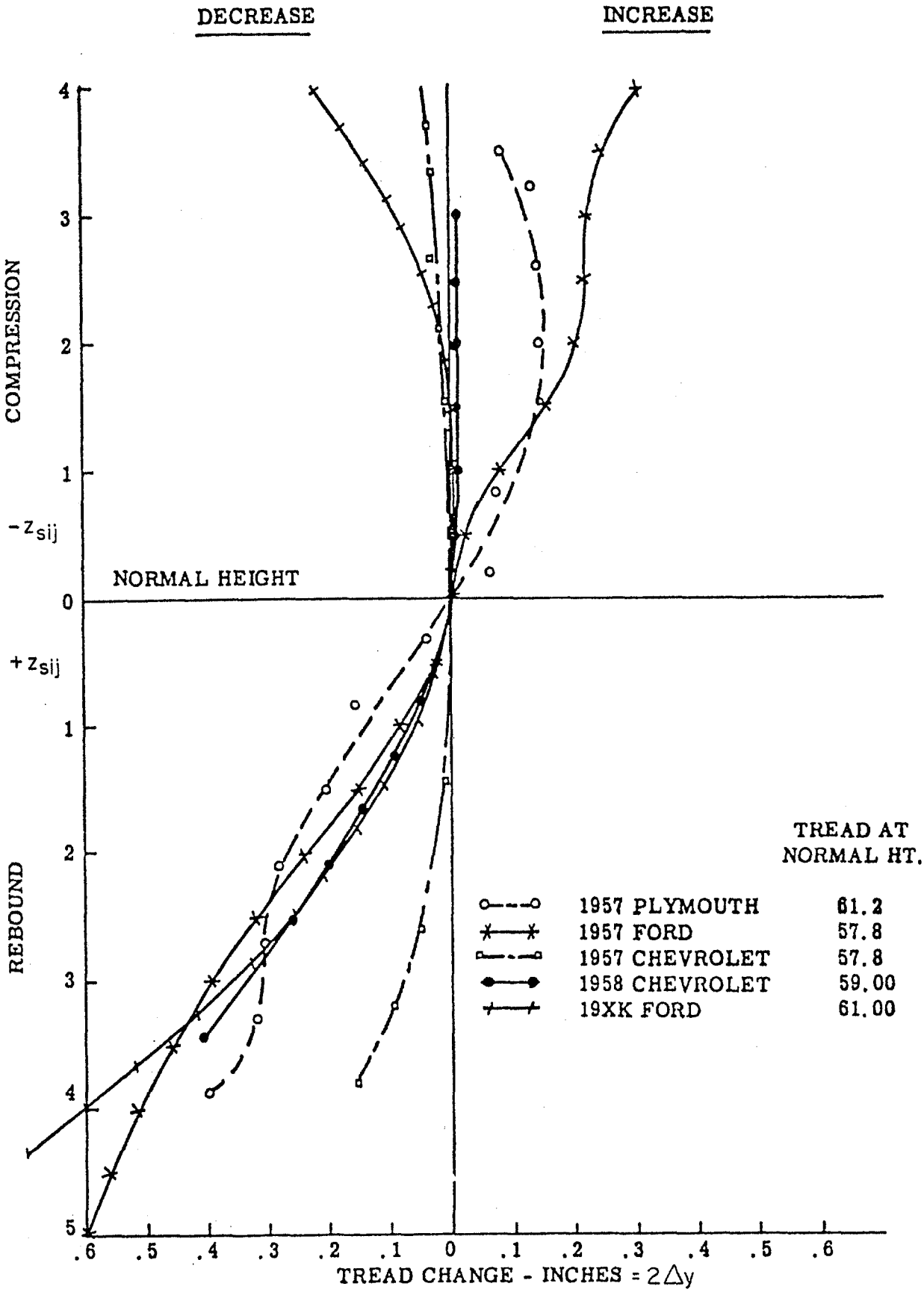

Figure C-4. Tread Change Versus Suspension Position

L_{SAi} = arc radius of the tire motion path shown in Fig. C-1.

These squat/lift effects apply only to independent suspensions. It should be explained here, that solid axles transmit lateral forces via a well defined roll axis pivot, such that the equations of motion rely on roll axis height parameters to define force application points. Whereas independent suspensions do not have a centrally located roll axis pivot for lateral force application. Rather, these independent suspensions have tires that apply side forces at ground level, so that the roll axis for the equations of motion is set = zero. When independent suspensions are given a specific geometry that produce the effect of an elevated roll axis, what really happens is that the force reactions are carried via suspension squat/lift forces, but not as a force at some imaginary roll axis height and K_{SLi}, is;

$$\text{roll axis height} = K_{SLi}\left(\frac{T_i}{2}\right)$$

These parameters can be obtained from static test data by measuring lateral movement of tire contact patch vs forced vertical motion of the sprung mass.

An alternative is to measure all suspension component pivot locations and link lengths. Then reconstruct the suspension on graph paper, and by plotting the linkage motions on paper, determining the path of the tire contact patch. An example of this is shown in Fig. C-5, where K_{SLi} and L_{SAi} are identified.

Thus, for independent suspensions, K_{SLi} and L_{SAi} must be estimated, while H_{RAi} is set = zero.

And for solid axle and beam axle suspensions, K_{SLI} = 0, and L_{SAi} is set to a very large number (1,000) to remove this effect, and H_{RAi} set = to actual roll axis height.

21. K_{SADF}
22. K_{SADR}
23. K_{SAD2F}
24. K_{SAD2R}

these are for the suspension squat/lift functions with longitudinal forces.

These are effects in suspension squat/lift, similar to reactions to lateral forces (in preceding pages), but here are in reaction to longitudinal forces. In this case, we will only use the primary effects of the tire contact patch motion slope, and ignore the insignificant effects due to path curvature.

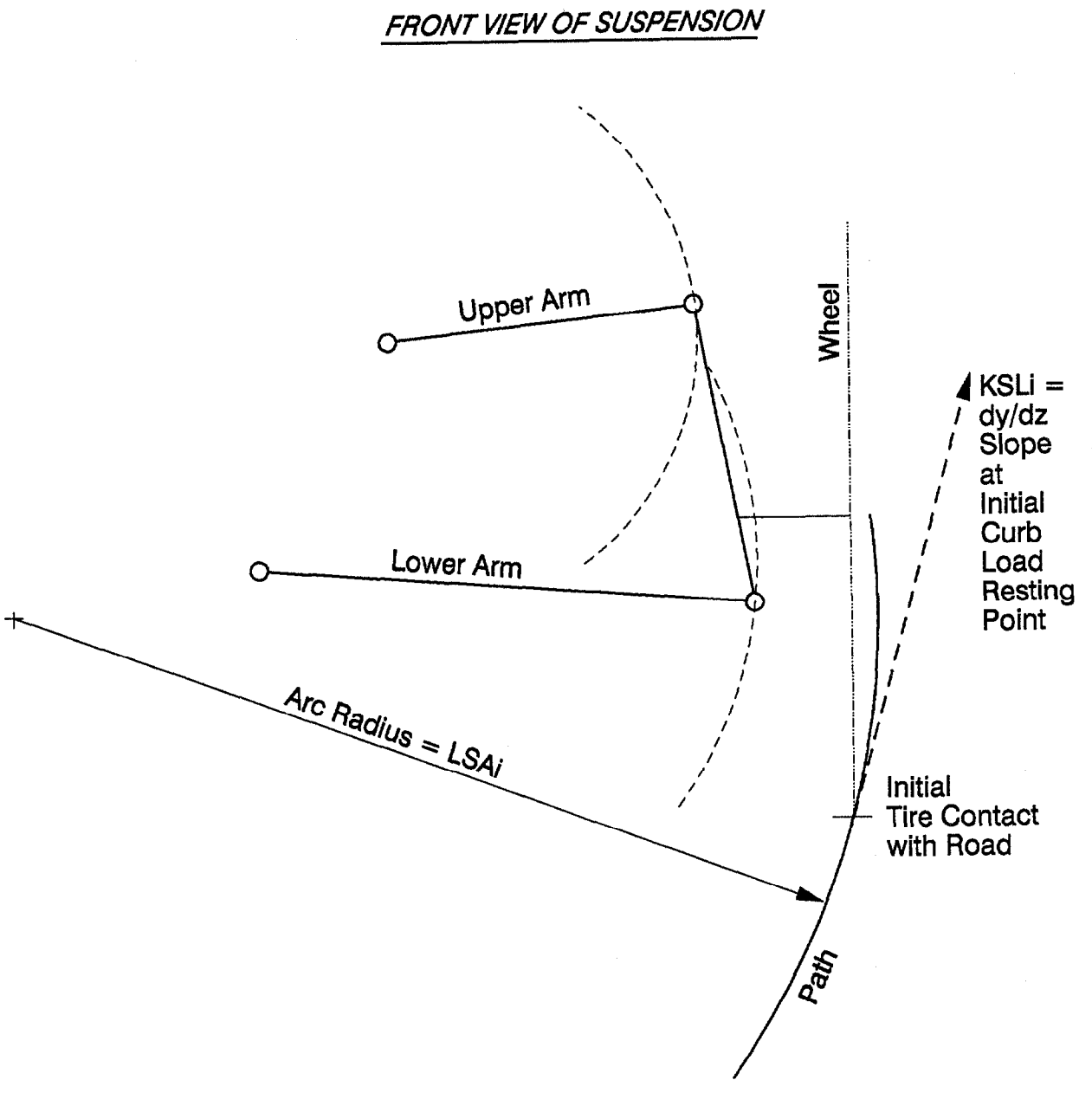

Layout of each suspension member is drawn in to scale from measurements taken according to page C-9. Then move 3 bar linkage to generate curved path at tire contact point.

Figure C-5. Suspension Geometry Plot of Motion

Static testing for this data would be very difficult. Therefore, it is recommended that graphical representations of the suspensions in the side view be used. By showing the direction of motion of the suspension components in the side view, the motion of the tire contact patch can be projected. The K_{SADi} parameter is the slope of this tire patch path away from pure vertical. Fig. C-6 shows some examples of graphically determining K_{SADi} for solid axle and independent suspensions.

Finally it needs to be pointed out that the K_{SADi} parameters apply to cases where brake torque is applied and reacted to by the suspension members. Also for engine power applied to a solid axle, where the reaction torque is taken by the suspension.

A special case arises when applying engine power via an independent suspension, where the reaction torque is taken by the sprung mass mounted differential gears. In this case, the only force on the suspension is the drive thrust applied at the wheel axle center. Therefore, the applicable slope for this case is the motion path of the wheel center, and is utilized in the VDANL input file as the K_{SAD2i} parameters. These come into play whenever engine power application is called for with an independent suspension.

25. K_{ACK}, this controls the difference in δ_{WLF} vs δ_{WRF} due to ackerman steer geometry.

This is explained and developed in appendix A. For most straight away high speed hangling test runs, the steering angle levels are too small to result in any significant ackerman steer effect. So that for these cases, parallel steering can be assumed and K_{ACK} set = zero. For low speed maneuvering, ackerman steering might have some effect, and K_{ACK} can be set by the following method.

From the steering ratio test described in appendix E, the steer angles of the front wheels when the steering wheel is turned 360° to the right, can be used in the following formula to estimate K_{ACK}. With ackerman steering, the right hand wheel normally turns to a larger angle than the left hand wheel, for a right hand turn.

$$K_{ACK} = \frac{2(\delta_{WRF} - \delta_{WLF})}{(\delta_{WLF} + \delta_{WRF})^2}$$

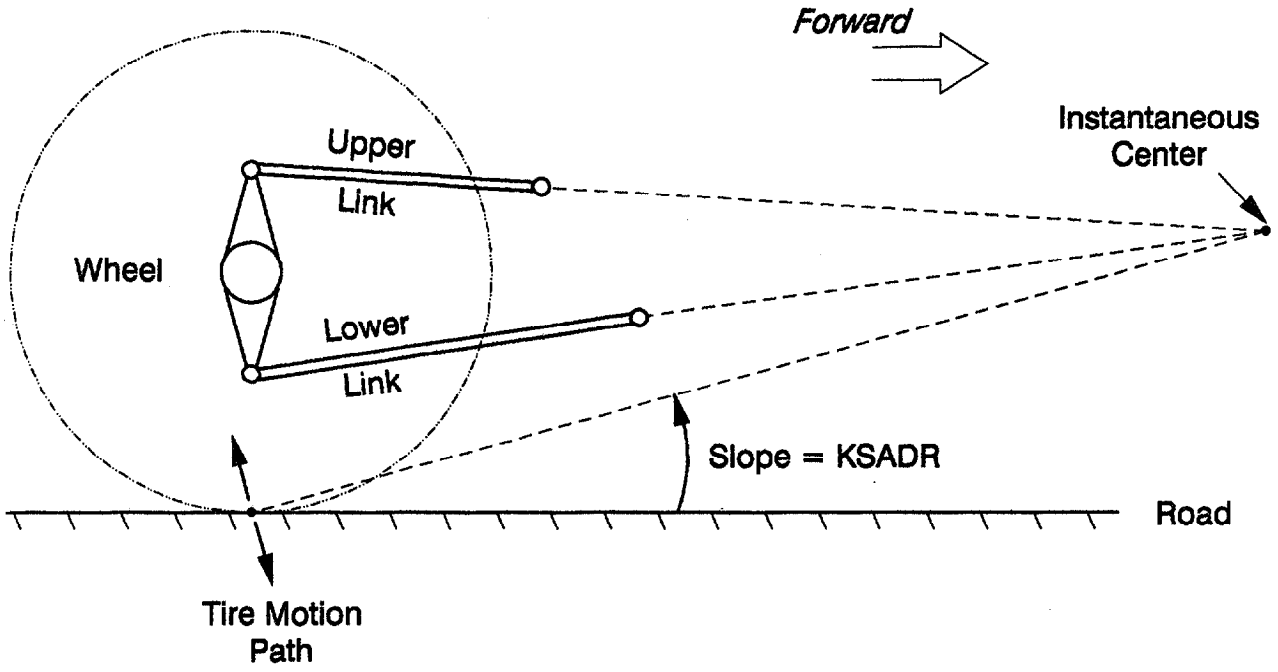

Side View of Solid Axle Rear Suspension

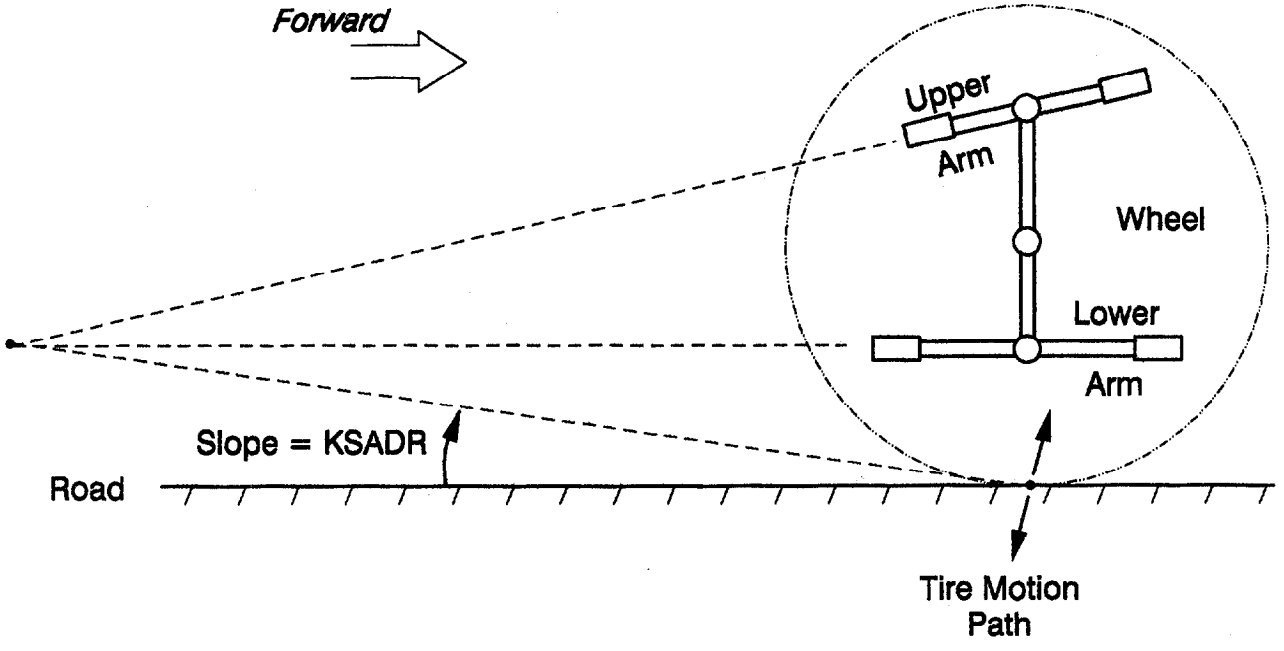

Side View of Independent Front Suspension

Figure C-6. Suspension Geometry Plot of Motion

APPENDIX D

VEHICLE PARAMETER MEASUREMENT TEST METHODS

APPENDIX D

VEHICLE PARAMETER MEASUREMENT TEST METHODS

A. OVERVIEW

The following methods were used to measure vehicle parameters which are used in vehicle dynamics simulation.

1. Center of Gravity Height Test

The vehicle wheels are placed on individual platform scales, with one axle on a vehicle hoist so that it can be raised up to a significant height above ground. Measure heights and weights while level, and raised up. Because suspension deflection changes while lifting up will affect apparent c.g. height, it is necessary to measure changes in suspension height and correct for this. Figure D-1 shows the basic layout in the lifted state, with the simple formula for h_{cg}. Figure D-2 shows the effects of suspension deflection change on apparent c.g. height.

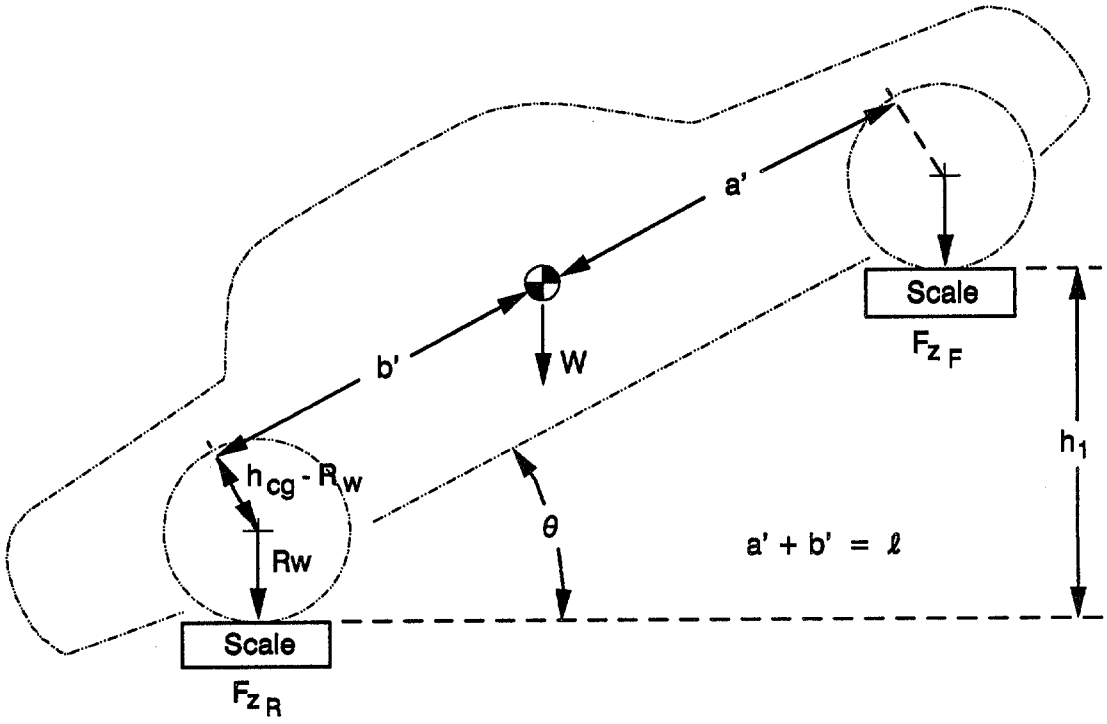

Figure D-1. Center of Gravity Height Test

Start with car level

$$F_{z_{F_o}} = \frac{W'b}{\ell} \qquad F_{z_{R_o}} = \frac{W'a}{\ell}$$

With one end of car up h_1

$$F_{z_F} = \frac{W'b\ (\cos\theta - [h_{cg} - R_w] \sin\theta)}{\ell \cos\theta}$$

$$\Delta F_z = F_{z_{F_o}} - F_{z_F} = \frac{W}{\ell}\,[h_{cg} - R_w] \tan\theta = \frac{W}{\ell}\,[h_{cg} - R_w]\,\frac{h_1}{\sqrt{\ell^2 - h_1^2}}$$

or $$h_{cg} = \frac{(\Delta F_z)\ \ell\sqrt{\ell^2 - h_1^2}}{Wh_1} + R_w$$

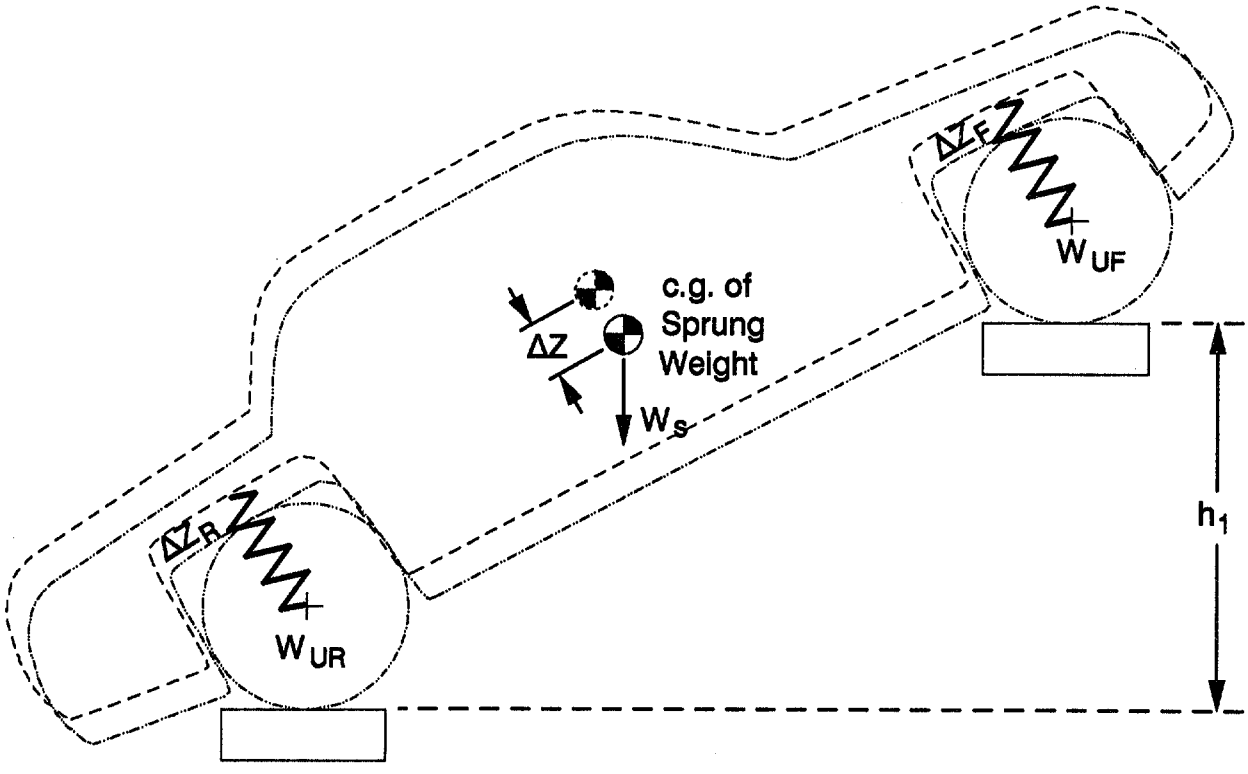

Figure D-2. Correction for Effects of Suspension Extension when One Axle is Raised off the Ground

ΔZ_F = change in front suspension riding height

ΔZ_R = change in rear suspension riding height

ΔZ = resultant change in height of sprung mass c.g.

ΔZ_i = $Z_{i_2} - Z_{i_1}$; where Z_i; where Z_i is measured from fender opening down to bottom of wheel rim

a = horizontal distance of W_s c.g. to front axle

b = horizontal distance of W_s c.g. to rear axle

ℓ = wheelbase length

W_s = sprung weight = $S - W_{UR} - W_{UF}$

W = total weight

Therefore, the following equations can be used to compute the center of gravity height.

$$\Delta Z = \Delta Z_F \left(\frac{b}{\ell}\right) + \Delta Z_R \left(\frac{a}{\ell}\right) \qquad \text{(D-1)}$$

Thus, the actual test data is for a c.g. height that is higher than normal because the W_s center of mass was higher by ΔZ.

$$\text{Test } h'_{cg} = \frac{W_s(h_s + \Delta Z) + (W_{UF} + W_{UR})\, R_W}{W}$$

$$\text{True } h_{cg} = \frac{W_s\, h_s + (W_{UF} + W_{UR})R_W}{W}$$

$$\therefore \text{ True } h_{cg} = \text{Test } h'_{cg} - \frac{W_s\, \Delta Z}{W}$$

$$\text{True } h_{cg} = \frac{(\Delta F_Z)\, \ell \sqrt{\ell^2{}_2 - h_1^2}}{W h_1} + R_W - \frac{W_s\, \Delta Z}{W} \qquad \text{(D-2)}$$

where ΔF_Z is the change in F_Z at either axle, which can be an average of the change at the front axle and at the rear axle.

h_1 = change in height of lifted axle

R_W = wheel/tire radius under curb load

a, b, W_s are values for the sprung weight, which differ slightly from total weight values. These can be estimated using the following equations:

$$\frac{a\ W_s}{\ell} = W_R - W_{UR}$$

$$W_s = W - W_{UF} - W_{UR}$$

$$a = \frac{(W_R - W_{UR})\ \ell}{W - W_{UF} - W_{UR}} \qquad \text{(D-3)}$$

$$b = \ell - a \qquad \text{(D-4)}$$

and the unsprung weights can be estimated from equations based on typical data

$$W_{Ui} = 32.2 + .045W \qquad \text{(D-5)}$$

if the drive train differential is carried in the sprung weight

$$W_{Ui} = .08W \qquad \text{(D-6)}$$

if the axle differential is carried in the unsprung weight.

2. Roll Stiffness Test

For this test, a moment is applied to the sprung mass, and the reaction moment at each axle is measured by the changing load at the individual scales each wheel is resting on. The sprung mass roll angle is measured independently. The slope of the plotted data is the overall roll stiffness at each axle (K_{orsi}), with the tire spring rate included. Figure D-3 shows the experimental set-up and computations to obtain data for plotting. Figures D-4 and D-5 show a sample of plotted test data.

3. Steering Compliance Test

With steering wheel clamped in straight ahead position, with the engine running for power steering, apply pure moments to one front wheel about its steer axis, in 10 lb pull increments, as shown in Figure D-6. Then reverse the procedure back to zero pull.

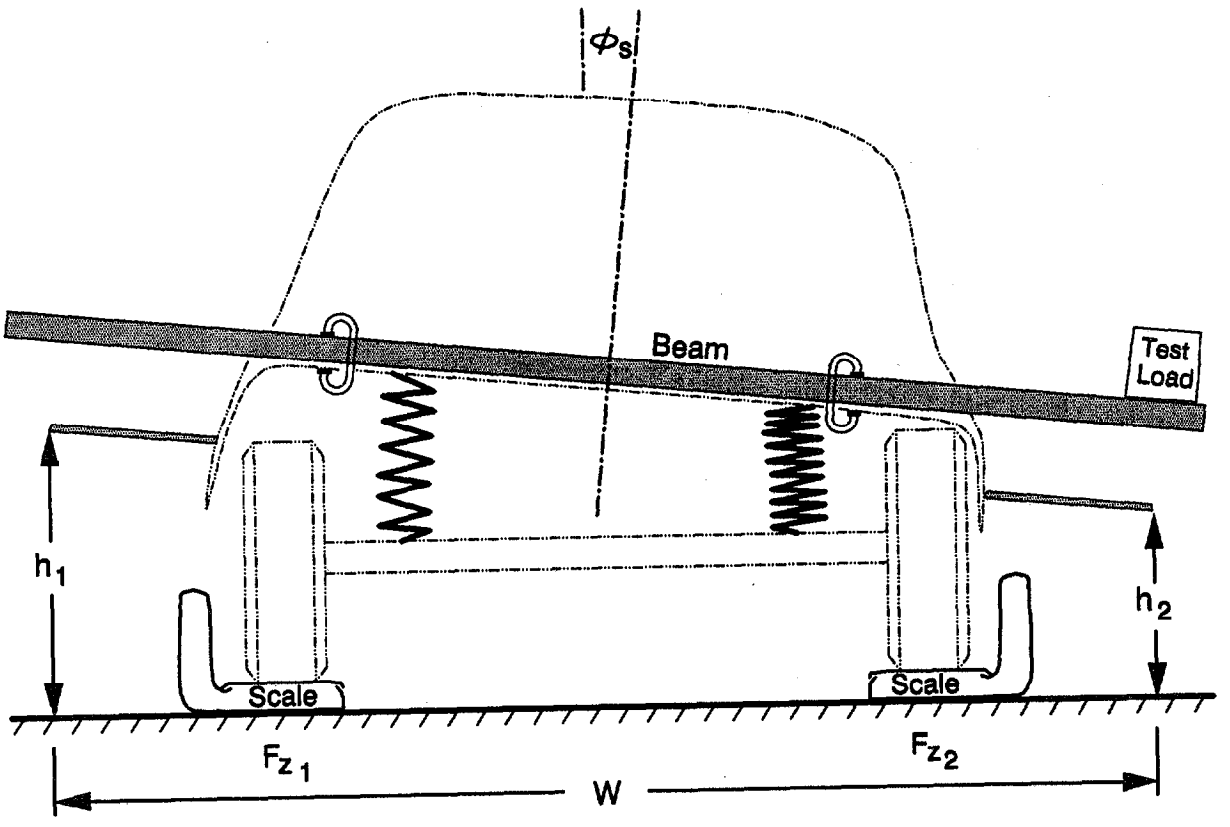

Beam is clamped solid to body, to support test load

Since the beam bends under load, a separate rod is attached to body to measure h_1, h_2 above ground

Test load is constant, but is shifted from right to left and back again, in small increments

h_1 , h_2 is measured at each load position, and wheel loads on scales also recorded

$$\text{Roll Angle} = \frac{h_1 - h_2}{W} = \phi$$

$$\text{Roll Moment (per axle)} = (F_{z_1} - F_{z_2}) \frac{\text{Track}}{2} = M_x$$

Plot M_x vs ϕ

Slope of $dM_x/d\phi$ = overall roll stiffness including tires, per axle

Figure D-3. Roll Stiffness Test

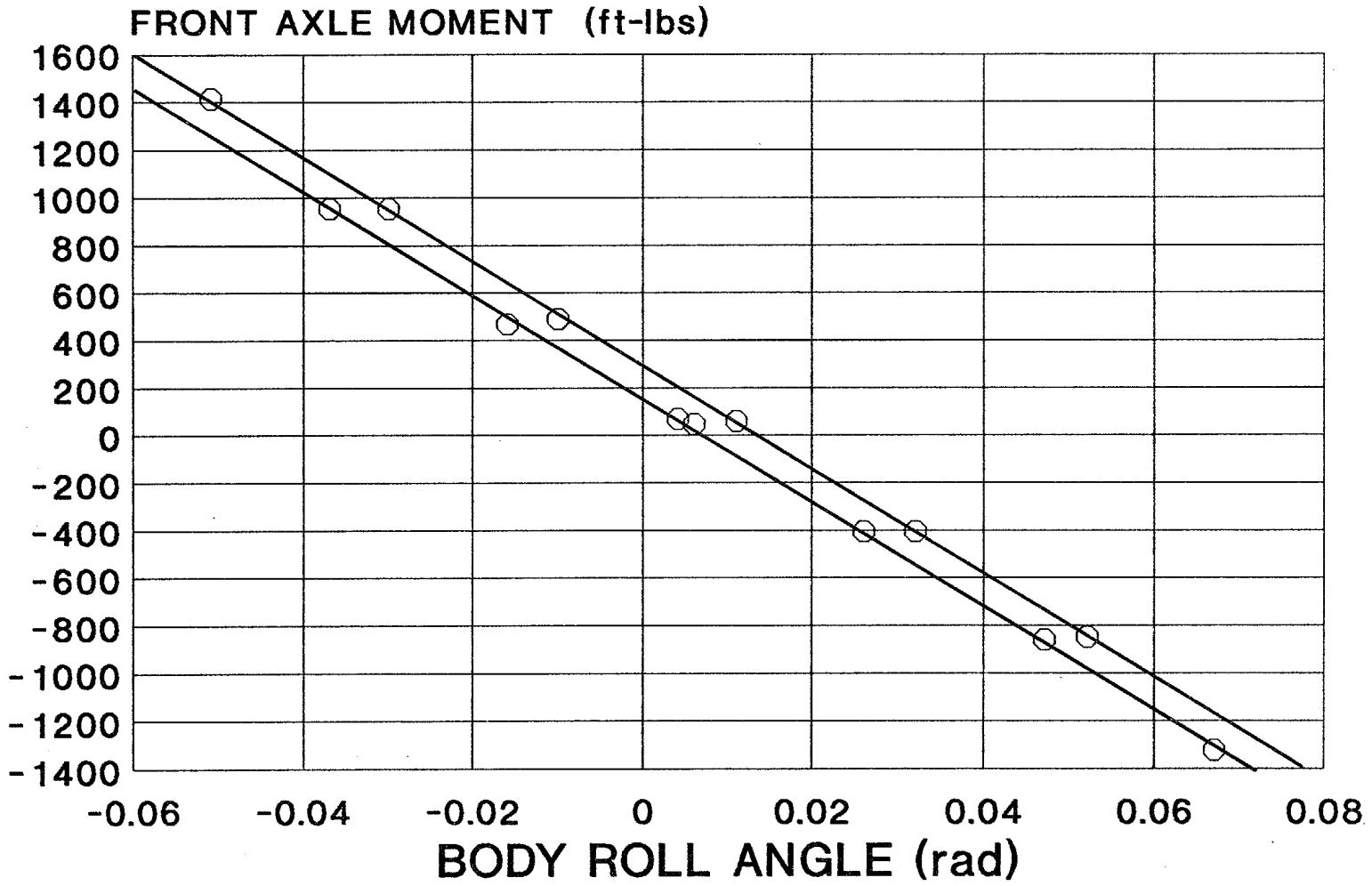

Figure D-4. Front Axle Roll Stiffness Datsun 200SX
(3060/.14 = -21,850)

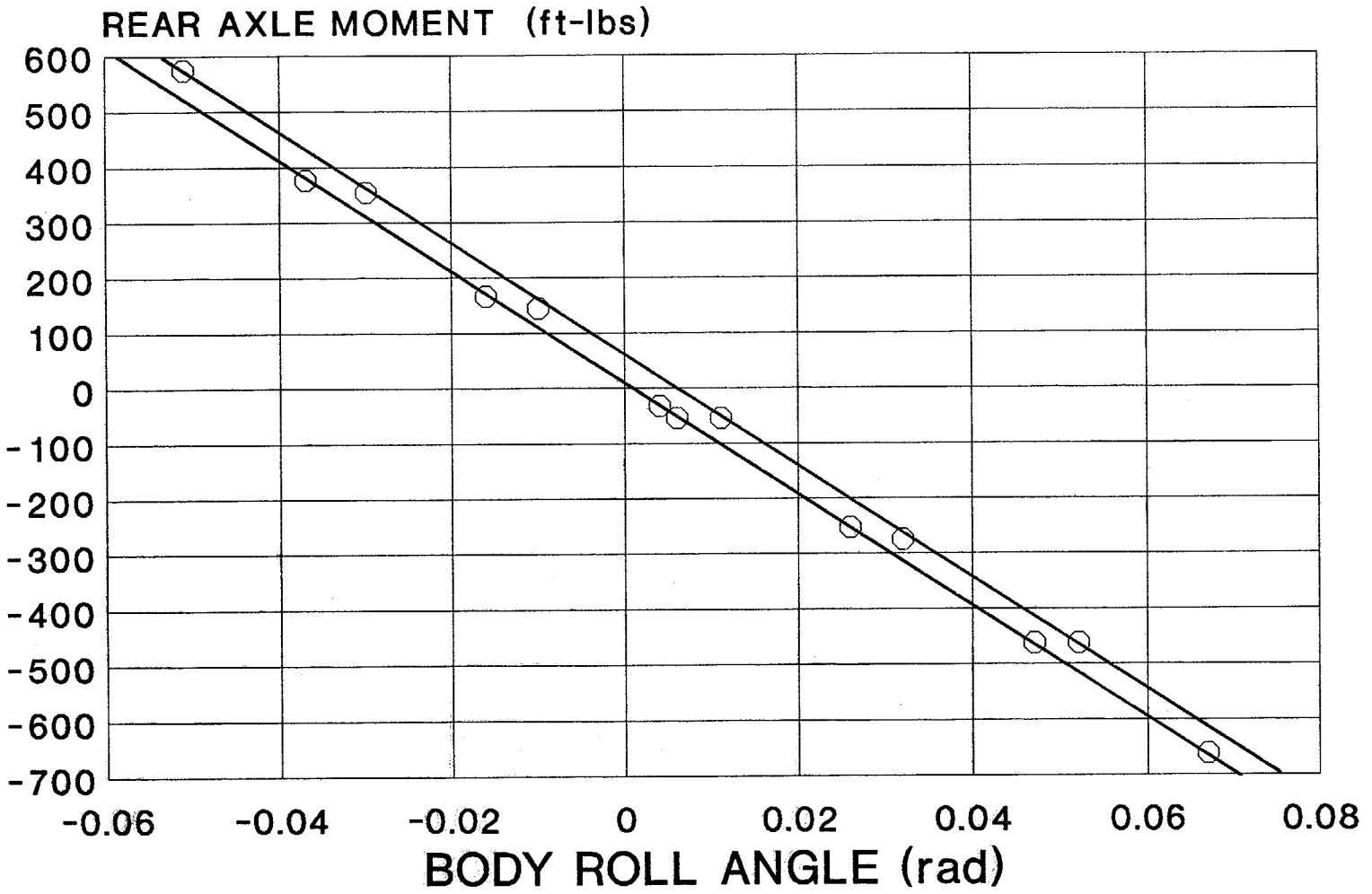

Figure D-5. Rear Axle Roll Stiffness Datsun 200SX
(1400/.14 = 10,000)

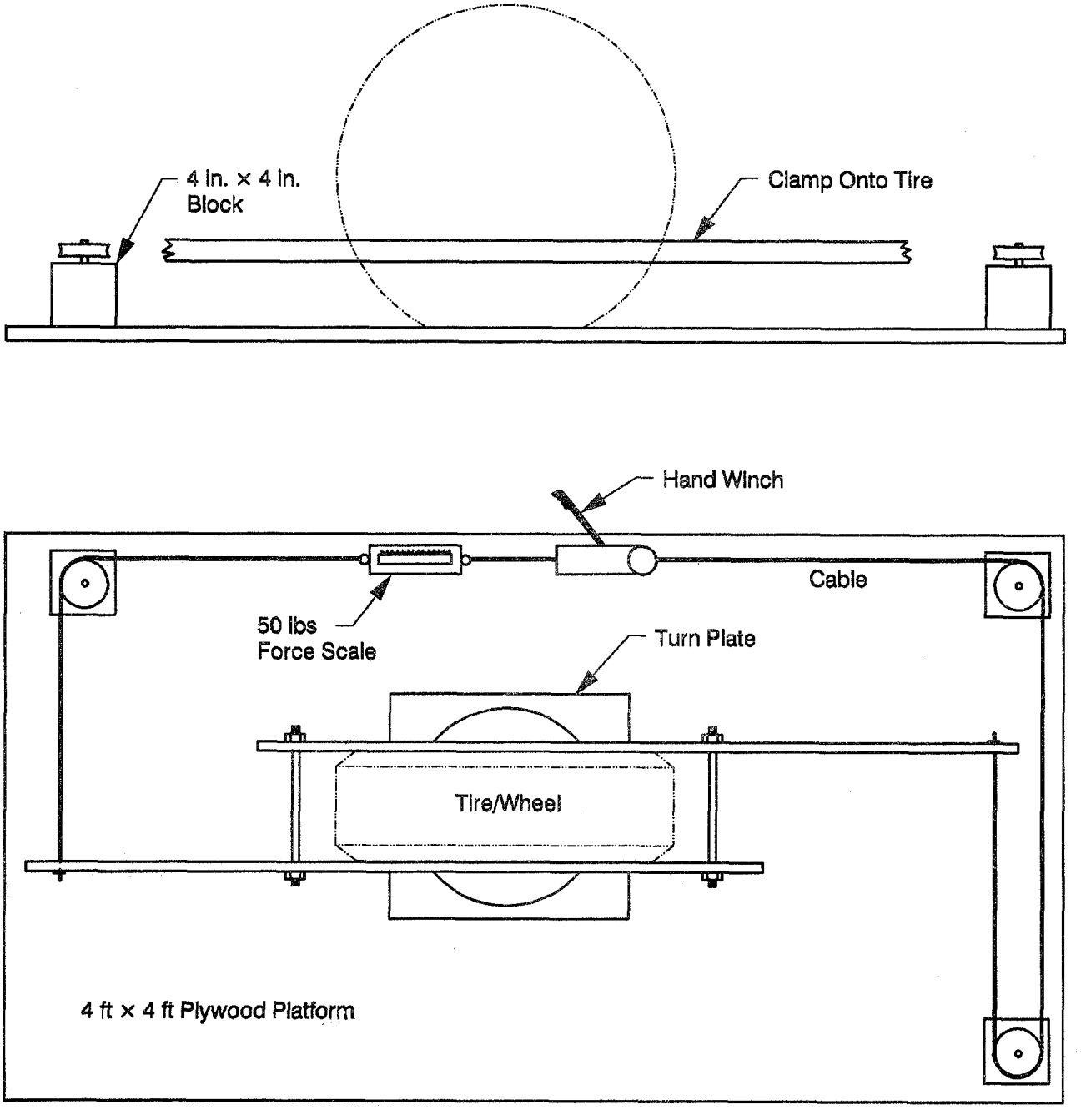

Figure D-6. Steering Compliance Test Device

Read the pull scale force, and steer angle of the opposite tire, and the length of moment arm from cable end to cable end. The steer angle deflection must be read at the wheel without the clamped load on it because the wheel with the clamped load on it will have tire casing deflection which can add up to 5 deg more angle at the turn plate that is true for the wheel angle only.

The resulting data plot of Moment vs. Angle will have a hysteresis loop because of steering free play and friction in the system. The hysteresis is to be ignored, and only the consistent slope used for estimate of steering compliance.

$$K_{sc} = \frac{d\ \delta_W}{d\ m_W}$$

An example of plotted data is shown in Figure D-7.

4. Suspension Geometry Measurements

The X, Y, Z locations of the suspension pivots are measured as shown in Figures D-8, D-9, D-10, D-11. These dimensions are then used in the suspension geometry parameter estimation procedures described in Appendix C. This converts raw dimensions into parameters for composite suspension geometry functions which are used in the vehicle dynamics simulation model described in Appendix A.

There are many types of suspensions, of which the most common are shown in Figures D-12, D-13. On some of these, the pivot locations have different implications for the composite function parameters, and this is explained in Appendix C.

5. Steering Ratio Test

The steering ratio is moved in increments of 90 deg to ±360 deg, and both front wheel angles are measured on ball bearing free turn plates. The engine is running for power steering. The slope of the averaged data gives the overall steering ratio. An example of plotted data is shown in Figure D-14.

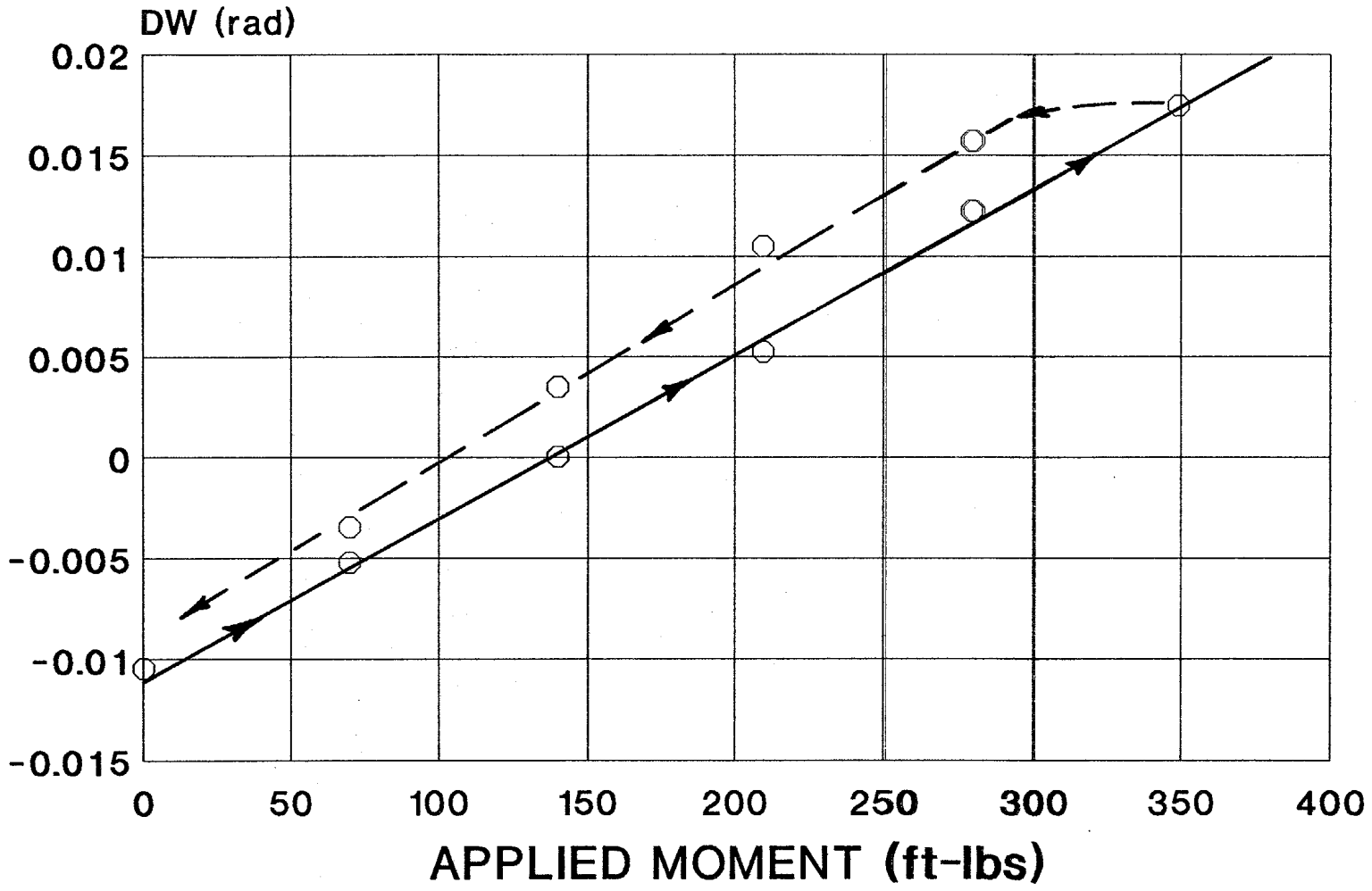

Figure D-7. Steering Compliance Test Datsom 200SX
(.02/250 = .00008

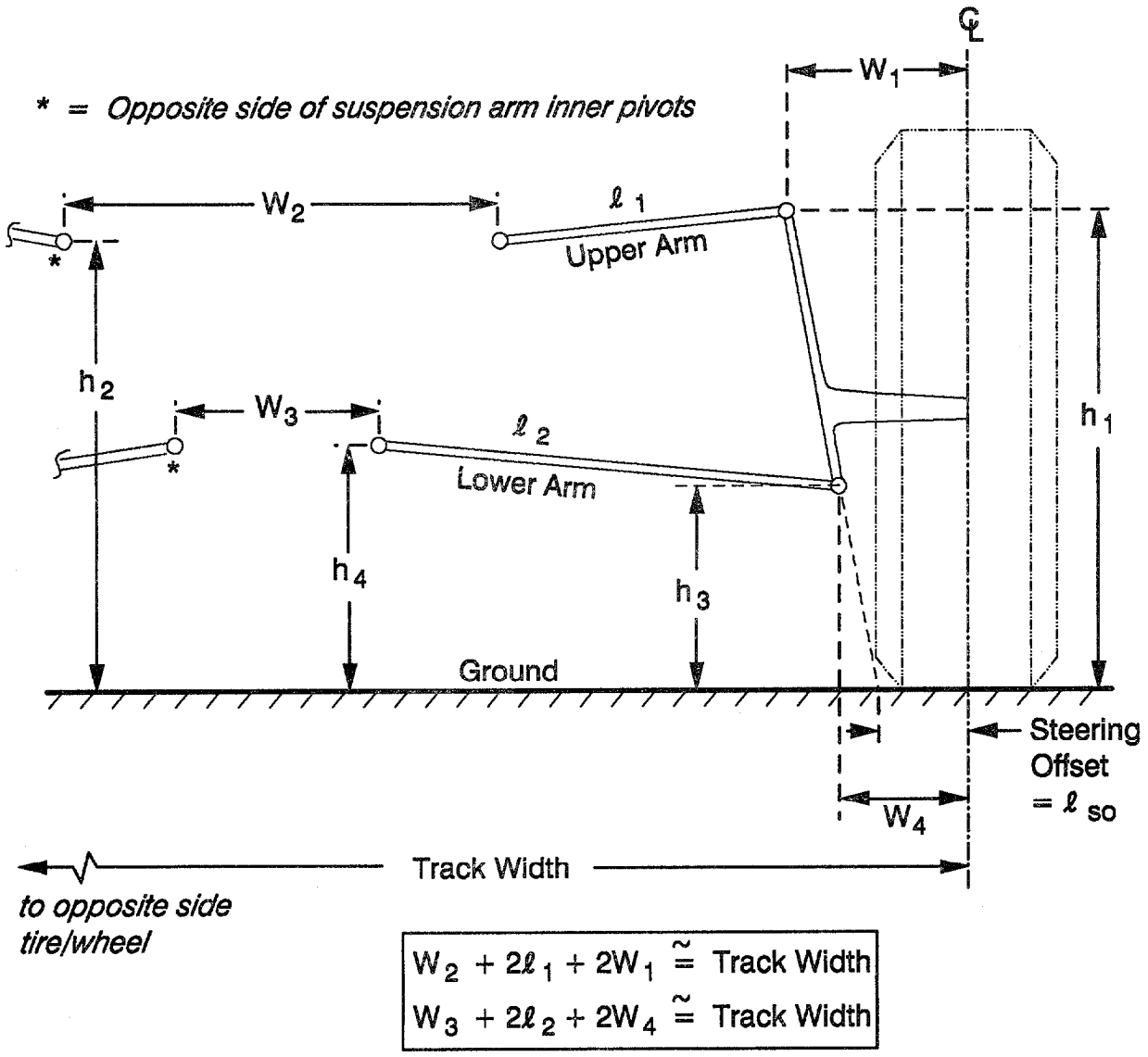

Mcphearson strut suspension are indentical, with the upper arm ball joint pivot at W_1, h_1 now becoming the location for the upper mounting point of the strut, and $\ell_1 = \infty$ in length and at 90° to the spindle/strut line

Figure D-8. Measurements to be taken on the Vehicle's Suspension Components, from Front View

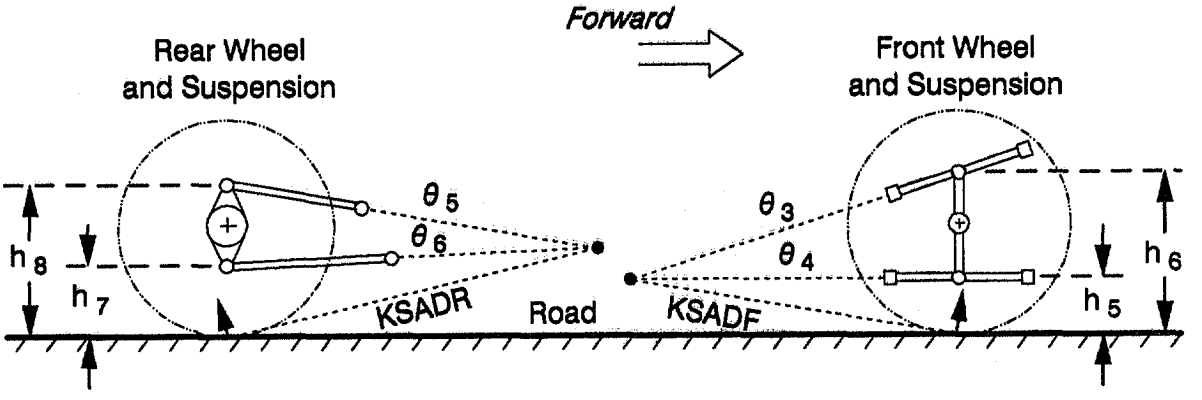

The vertical dimensions of all suspension arms and linkages need to be measured in order to identify the dx/dz path (slope) of wheel spindle ball joints or axle pivot points, (θ_i). From these, the slope or dx/dz of the tire contact point path can be calculated (assuming a brake-locked wheel). KSADF is the slope of the line shown from the instantaneous center to the tire contact point, for the front wheel, (positive value as shown). KSADR is slope for rear. The θ_3, θ_4, θ_5, θ_6 are all positive, if the line shown is going upwards toward the wheel.

$$\text{then} \quad \text{KSADF (slope)} = \frac{h_5\,\theta_3 - h_6\,\theta_4}{h_6 - h_5}$$

$$\text{KSADF (slope)} = \frac{h_7\,\theta_5 - h_8\,\theta_6}{h_8 - h_7}$$

Figure D-9. Measurements to be Taken on Vehicle's Suspension from Side View

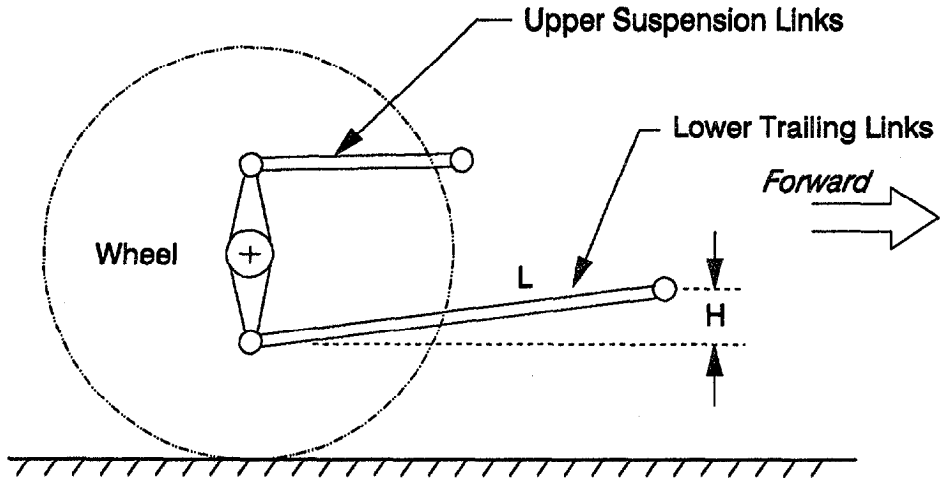

Typical axles have 2 trailing links which control the axle steer angle during body roll, and the side view slope (H/L) gives the rolls steer coefficient for this axle:

L = lenght of trailing link
H = height of front pivot above rear pivot

Figure D-10. Measurements to be Taken for Solid or Beam Axle Roll Steer Functions

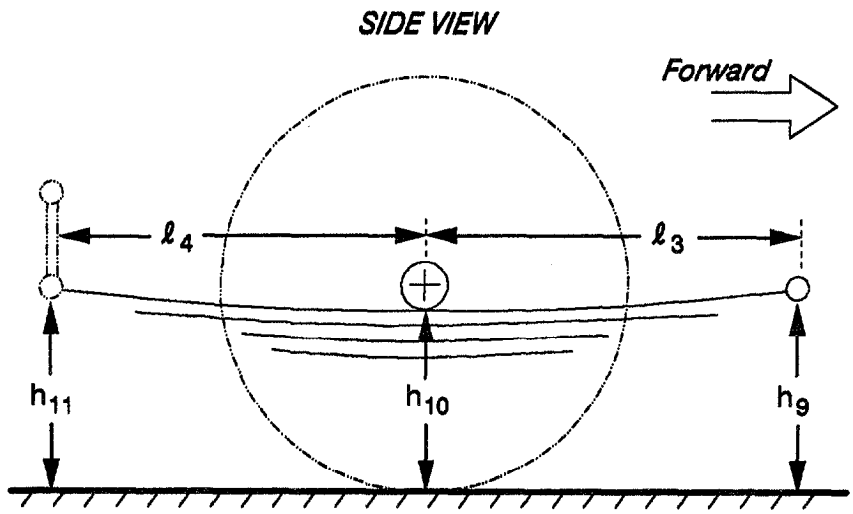

Figure D-11. Special Case for Leaf Springs on Solid Axle Suspension

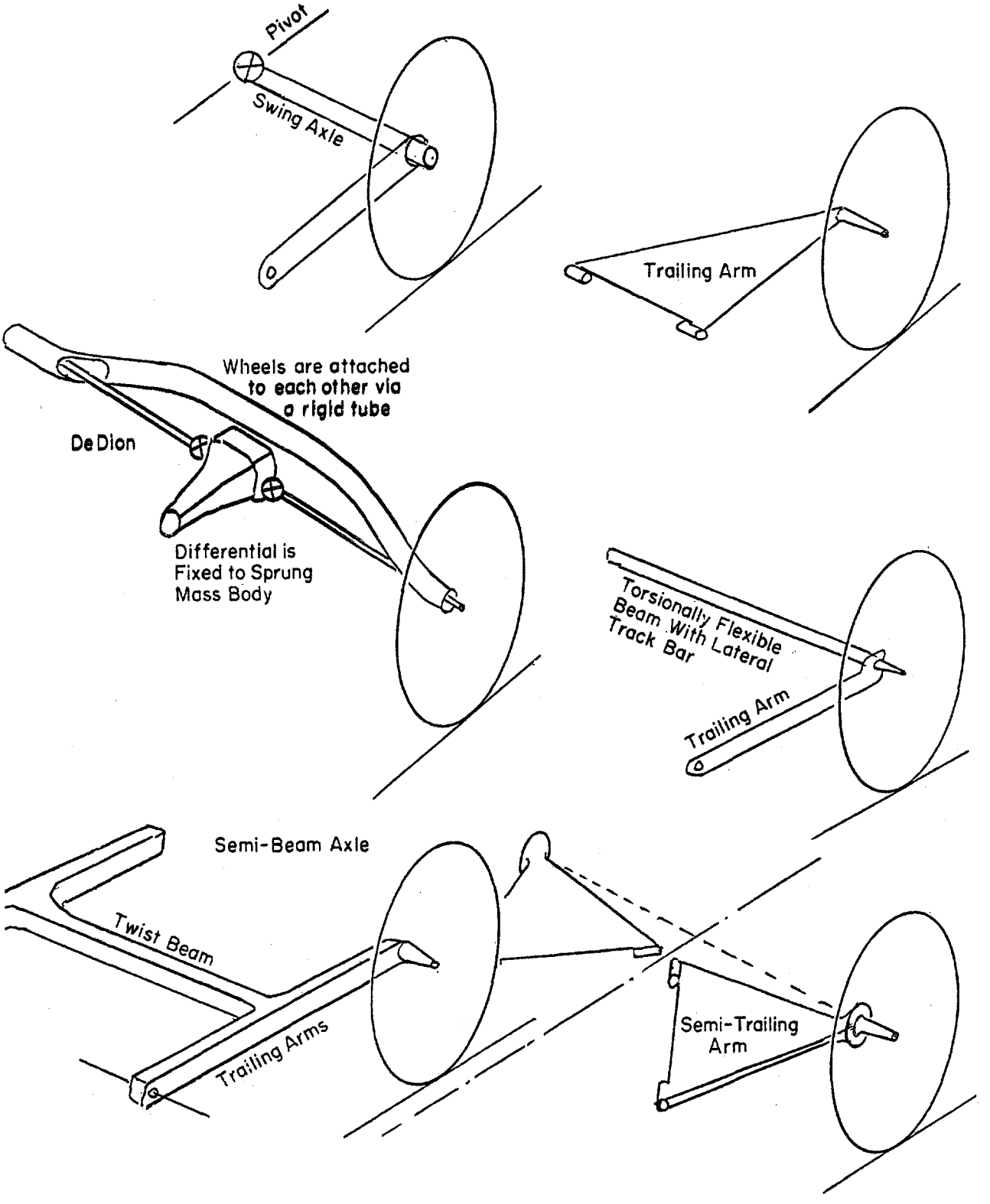

Figure D-12. Typical Examples of Suspension Geometry Layouts

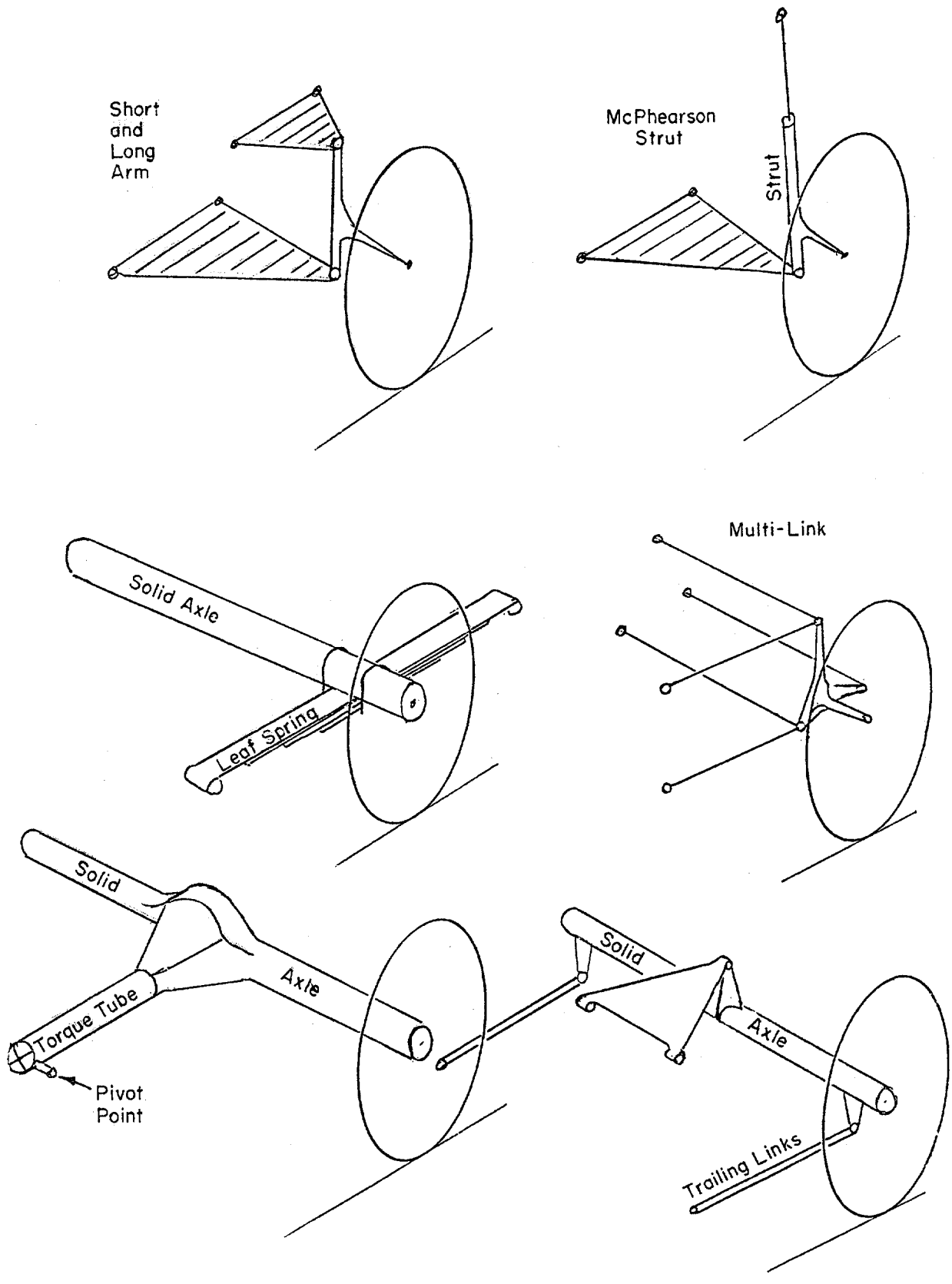

Figure D-13. Typical Examples of Suspension Geometry Layouts

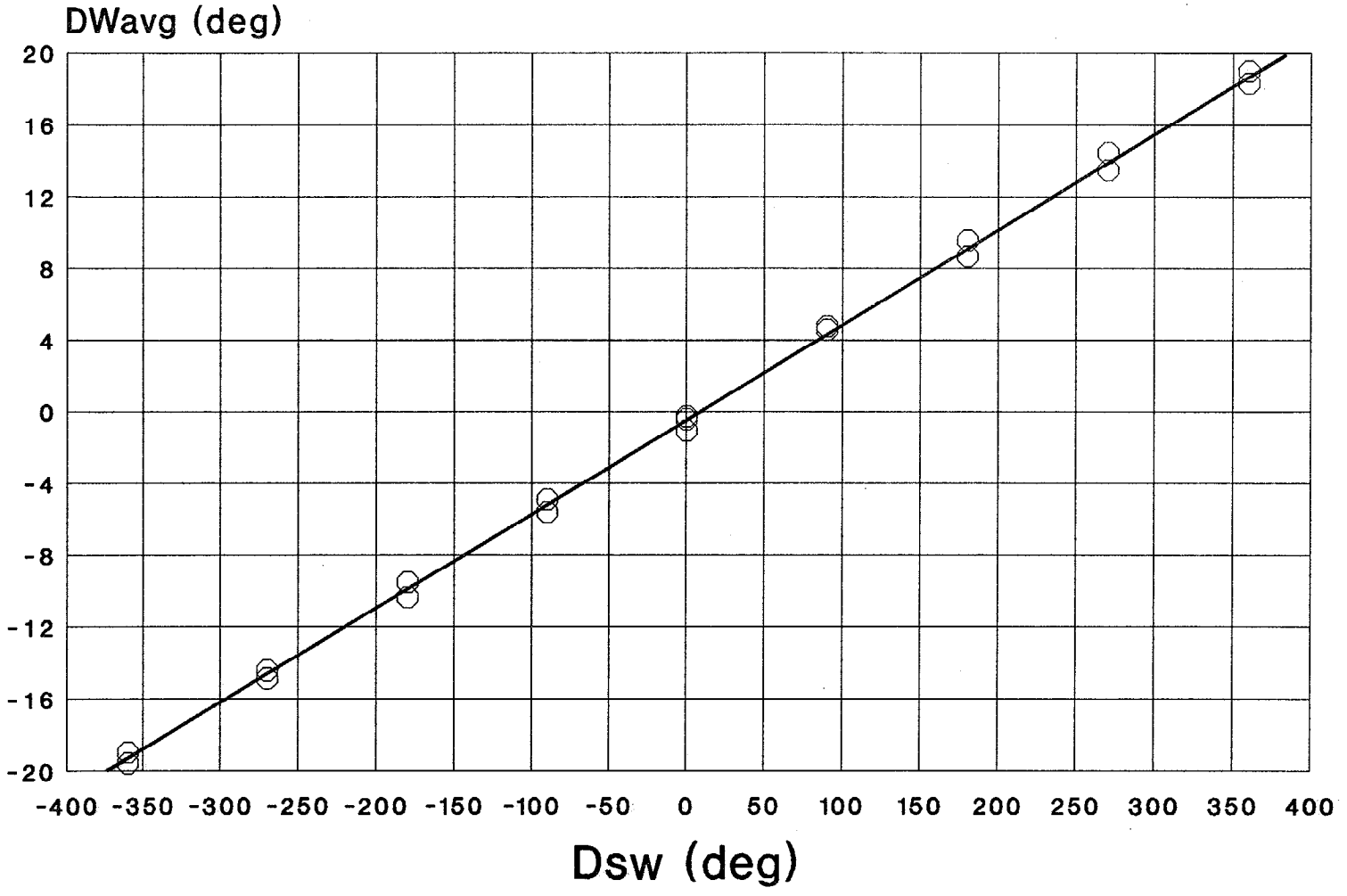

Figure D-14. Steering Ratio Test Datsun 200SX
(800/43.3 = 18.5)

6. **Suspension Spring Rate Test**

The suspension is moved up and then down about ±1.5 by loading and unloading the vehicle sprung mass. Changes in wheel loads are recorded from individual wheel platform scales, and changes in suspension deflection are measured between each wheel and fender. The averaged data slope gives the equivalent suspension spring rate at the wheel. The tire spring rate is not involved here. An example of plotted data is shown in Figures D-15, D-16.

7. **Vehicle weight and Longitudinal c.g. Location**

Individual wheel loads are measured by individual platform scales, with empty vehicle (curb load), but with a full gas tank.

$$a = \frac{(\text{weight on rear axle})\ \ell}{\text{total weight}}$$

$$b = \frac{(\text{weight on front axle})\ \ell}{\text{total weight}}$$

8. **Track width** is measured from tire center to tire center, for each axle.

9. **Wheelbase** is measured from front wheel center to rear wheel center, and averaged for both sides.

10. **Tire loaded radius**, at curb load, is measured from wheel center to ground, and averaged for the 4 wheels.

11. **Spring base width** is measured whenever there is a solid or beam axle suspension.

12. **Roof height** is measured from the highest point on the roof to the ground.

13. **Copies** of the data collection sheet forms are shown here in following pages:

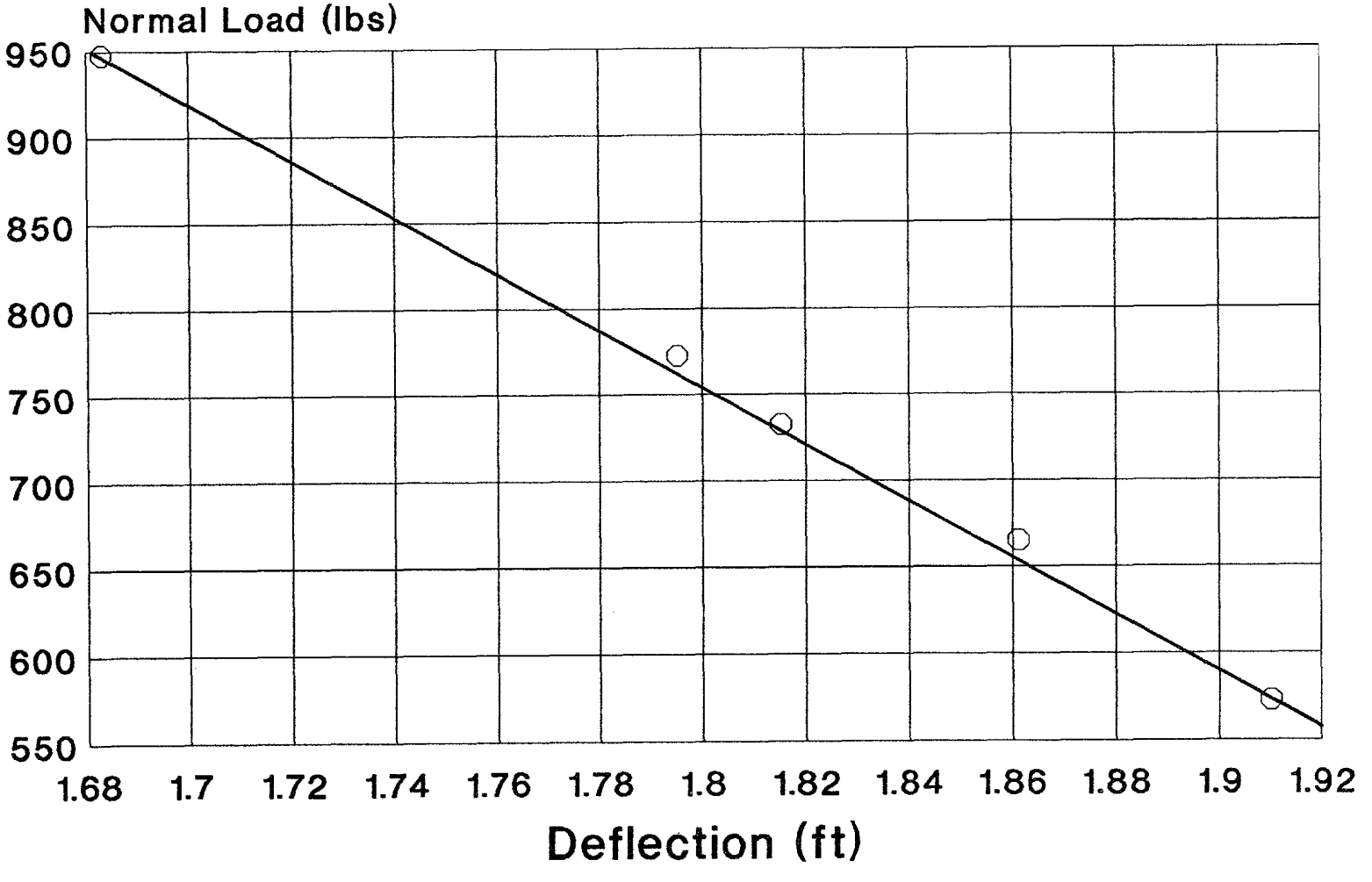

Figure D-15. Front Suspension Spring Rate Datsun 200SX
(395/.24 = 1650)

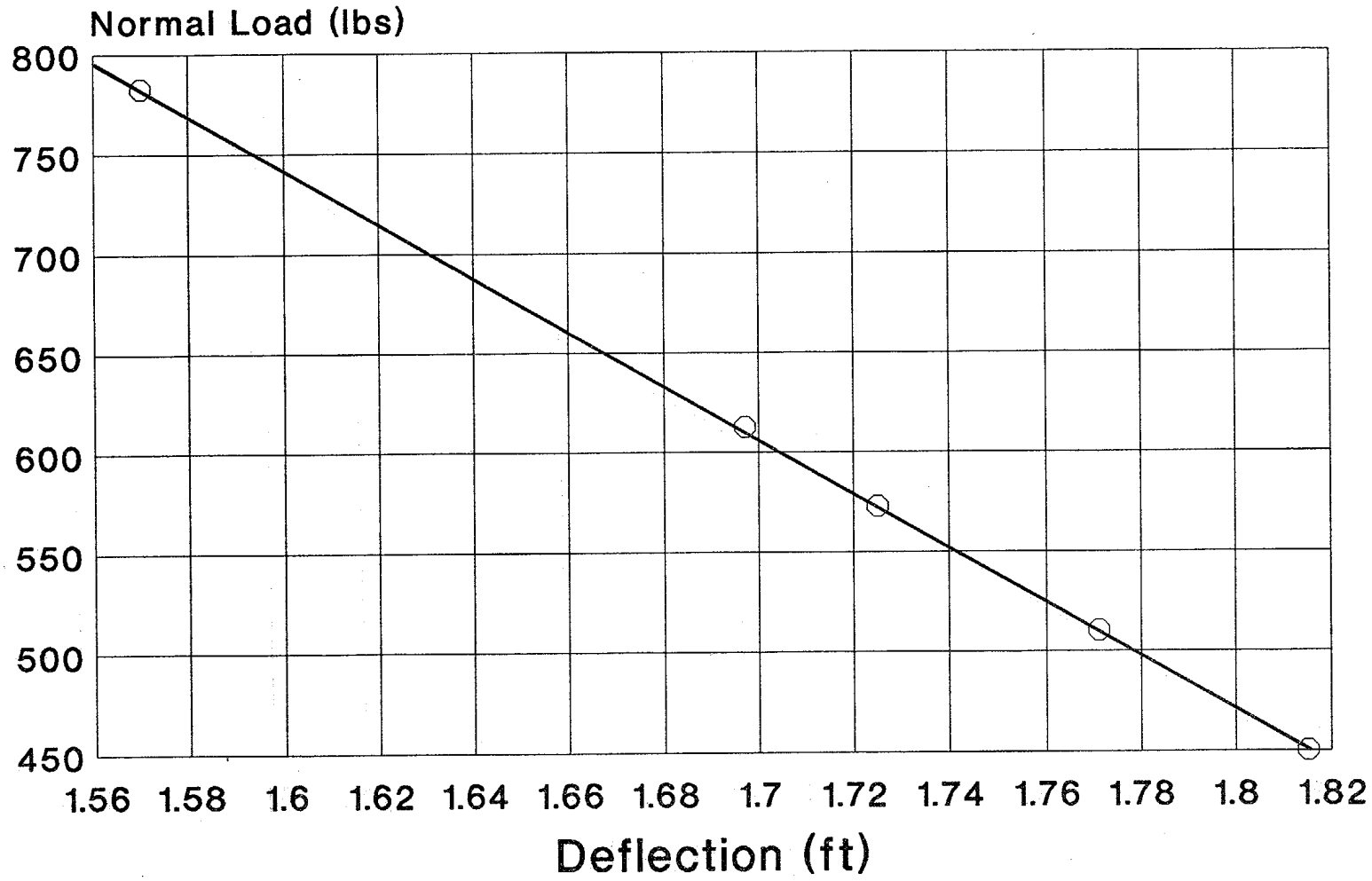

Figure D-16. Rear Suspension Spring Rate Datsun 200SX
(351/.26 = 1350)

APPENDIX E

TEST VEHICLE DATA AND SIMULATION PARAMETERS

APPENDIX E

TEST VEHICLE DATA AND SIMULATION PARAMETERS

This appendix contains basic information on the test vehicles employed in this project as measured at STI. Some of this basic information is slightly different from similar measurements conducted at VRTC on similar vehicles. A study was conducted at VRTC to determine possible explanations for these differences. The study was titled, "An Evaluation of Static Rollover Propensity Measures", and is available from the National Technical Information Service, Springfield, VA 22161 and has a document number DOT-HS-807-747. The results of the above cited study are also summarized in section 4.4.1 of the Technical Assessment Paper: "Relationship Between Rollover and Vehicle Factors" published by NHTSA in July, 1991 and is available in the NHTSA Docket No. 91-68.

In Table E-1 the vehicles are identified by model and single vehicle accident rates obtained from the NHTSA/NCSA. Table E-2 contains basic test vehicle data on their configuration as tested. Stability metrics used in the statistical analysis of Section VIII are listed in Table E-3. Tire parameters are summarized in Table E-4 according to definitions found in the main text, Table 8 and Reference 5. Finally, in Table E-5, the computer simulation parameters for all test vehicles are listed as described in Appendices B and C for all 41 test vehicles.

TABLE E-1. TEST VEHICLES AND ROLLOVER RATES (% OF SINGLE VEHICLE ACCIDENTS) DETERMINED FROM NHTSA ACCIDENT DATA BASE ANALYSIS

Vehicle	Ref #	Type	Year	Drive Train	Tire Size	GVWR (lbs)	Rollovr Rate (%SVA)
Escort (2 dr)	1	Small *	89	FWD	P165/80R13	3420	19.0
Le Car (2 dr)	2	Small	77	FWD	145/SR13	2480	34.9
Toyota Starlet (2 dr)	3	Small	82	RWD	145/SR13	2535	16.8
Datsun 510 (4 dr)	4	Small	77	RWD	165/SR13	3130	15.6
Datsun 200SX (2 dr)	5	Small	80	RWD	P185/75R14	3280	12.8
Sentra (4 dr)	6	Small *	83	FWD	155/SR13	2875	11.2
Honda CRX (2 dr)	7	Small	84	FWD	175/70R13	2370	12.6
Civic (4 door)	8	Small *	82	FWD	P175/70R13	2910	20.3
Civic Htch Bk (2 dr)	9	Small	84	FWD	175/70R13	2850	8.0
Chevette (2dr)	10	Small *	80	RWD	P155/80R13	2763	15.1
Fiero (2 dr)	11	Small	84	RWD	P185/80R13	3042	7.2
Jetta (4? dr)	12	Small	83	FWD	P175/70R13	3042	17.0
Stanza (4 dr)	13	Small	85	FWD	185/70R13	3303	12.5
BMW 320i (2 dr)	14	Medium	81	RWD	185/70R13	3440	12.8
Chev Cavalier (4? dr)	15	Medium	85	FWD	P175/80R13	3360	12.3
Thunderbird (2 dr)	16	Medium *	87	RWD	P215/70R14	4470	7.2
Buick Le Sabre (2 dr)	17	Large *	80	RWD	205/75R15	5064	1.9
Plym Voyager (3 dr)	18	Van *	89	FWD	P195/75R14	4940	11.6
Ford Aerostar (3 dr)	19	Van *	88	RWD	215/70R14	5000	24.9
Toyota (3 dr)	20	Van	86	RWD	P195/75R14	4950	18.9
VW Vanagon (3 dr)	21	Van	84	RWD	P185/70R14	5269	19.5
Chv G10 Sptsvn (3 dr)	22	Van	88	RWD	P255/75R15	6600	16.1
Toy 4x4 Lng Bd (2 dr)	23	Pick Up *	80	4WD	31x10.5R15	4550	36.3
Chevrolet S10 (2 dr)	24	Pick Up	83	RWD	P195/75R14	4011	19.1
GMC T15 4x4 (2 dr)	25	Pick Up	86	4WD	P215/75R15	4604	19.2
Ford Rngr (2 dr)	26	Pick Up	88	RWD	P215/70R14	3940	31.2
Frd Rngr 4x4 (2 dr)	27	Pick Up	86	4WD	LT235/75R15	4100	40.9
Nissan Pick Up (2 dr)	28	Pick Up	85	RWD	195/70R14	4420	17.0
Nissan 4x4	29	Pick Up	88	4WD	31x10.50R15	5200	33.3
Chevrolet C10 (2 dr)	30	Pick Up	76	RWD	P235/75R15	6050	15.4
Chevrolet C20 (2 dr)	31	Pick Up	84	RWD	LT235/85R16	8600	18.6
Ford F150 4x4 (2 dr)	32	Pick Up	87	4WD	31x10.5R15	6250	18.2
Ford F250 (2 dr)	33	Pick Up	81	RWD	9.50-16.5LT	8700	19.4
Suz Samurai (2 dr)	34	Utility *	88	4WD	P205/70R15	2935	29.3
Jeep CJ-7 (2 dr)	35	Utility	86	4WD	31x10.50R15	4220	39.2
Toyota 4Rnr (2 dr)	36	Utility	86	4WD	P255/75R15	5080	38.1
Chev Blzer S10 (2 dr)	37	Utility *	83	RWD	P255/70HR15	4773	29.4
GMC Jimmy (2 dr)	38	Utility	85	4WD	32x11.50R15	6100	26.1
Frd Bronco FS (2 dr)	39	Utility	85	4WD	P235/75R15	6000	20.7
Frd Bronco II (2 dr)	40	Utility *	83	4WD	P235/75R15	4280	43.6
Wrangler (2 dr)	41	Utility	89	4WD	P215/75R15	4300	21.2

* Dynamic Field Test Vehicle

TABLE E-2. BASIC TEST VEHICLE CHARACTERISTICS

Ref No.	Type	Field Test (Phase I)	Year	Drive Train†	Weight (lbs)	Roof Height (ft)	c.g. Location a (ft)	c.g. Location b (ft)	c.g. Location h_{cg} (ft)	Track Width T_w (ft)	Track Width TWR $T_w/2h_{cg}$	Wheel Base ℓ (ft)	Wheel Base WBR ℓ/h_{cg}
1	Small	*	89	FWD	2550	4.48	2.96	4.89	1.83	4.62	1.261	7.85	4.290
2	Small		77	FWD	1795	4.59	3.16	4.77	1.79	4.16	1.162	7.93	4.432
3	Small		82	RWD	1800	4.46	3.39	4.18	1.72	4.23	1.228	7.57	4.396
4	Small		77	RWD	2395	4.48	3.41	4.48	1.79	4.39	1.226	7.89	4.405
5	Small		80	RWD	2620	4.28	3.44	4.43	1.74	4.42	1.267	7.87	4.515
6	Small	*	83	FWD	2035	4.50	2.68	5.16	1.71	4.56	1.333	7.84	4.585
7	Small		84	FWD	1860	4.17	2.60	4.63	1.61	4.62	1.432	7.23	4.482
8	Small	*	82	FWD	2015	4.37	2.90	4.68	1.68	4.47	1.329	7.58	4.512
9	Small		84	FWD	1980	4.32	3.00	4.82	1.64	4.64	1.414	7.82	4.768
10	Small	*	80	RWD	2110	4.44	3.63	4.23	1.73	4.27	1.234	7.86	4.543
11	Small		84	RWD	2627	3.91	4.44	3.35	1.67	4.87	1.459	7.79	4.665
12	Small		83	FWD	2130	4.60	2.86	5.01	1.88	4.56	1.215	7.87	4.197
13	Small		85	FWD	2500	4.52	2.82	5.28	1.81	4.68	1.290	8.11	4.468
14	Medium		81	RWD	2410	4.56	3.84	4.62	1.88	4.51	1.200	8.46	4.501
15	Medium		85	FWD	2520	4.51	2.92	5.53	1.74	4.64	1.337	8.45	4.867
16	Medium	*	87	RWD	3355	4.61	3.43	5.26	1.84	4.89	1.327	8.70	4.726
17	Large	*	80	RWD	3830	4.56	4.28	5.39	1.83	5.11	1.395	9.67	5.284
18	Van	*	89	FWD	3572	5.40	4.01	5.89	2.13	5.08	1.194	9.90	4.659
19	Van	*	88	RWD	3622	6.08	4.29	5.63	2.28	5.07	1.111	9.92	4.351
20	Van		86	RWD	3205	5.98	3.03	4.29	2.03	4.63	1.138	7.32	3.599
21	Van		84	RWD	3260	6.37	3.81	4.30	2.45	5.12	1.044	8.11	3.310
22	Van		88	RWD	4740	6.52	4.77	5.65	2.60	5.71	1.098	10.41	4.005
23	Pick Up	*	80	4WD	3240	5.67	4.02	5.21	2.12	4.62	1.088	9.23	4.354
24	Pick Up		83	RWD	2945	5.04	4.06	5.75	1.79	4.53	1.263	9.81	5.471
25	Pick Up		86	4WD	3600	5.27	4.05	6.21	1.93	4.70	1.218	10.26	5.318
26	Pick Up		88	RWD	2970	5.25	4.00	5.50	2.06	4.54	1.104	9.51	4.625
27	Pick Up		86	4WD	3545	5.65	3.81	5.71	2.29	4.76	1.040	9.52	4.163
28	Pick Up		85	RWD	2605	5.04	3.61	4.86	1.72	4.37	1.271	8.46	4.920
29	Pick Up		88	4WD	3875	5.67	4.05	5.64	2.21	4.97	1.127	9.69	4.393
30	Pick Up		76	RWD	4360	5.85	4.54	6.45	2.31	5.36	1.160	10.99	4.758
31	Pick Up		84	RWD	4550	6.04	4.78	6.18	2.38	5.49	1.152	10.96	4.605
32	Pick Up		87	4WD	4590	6.11	4.52	6.60	2.49	5.46	1.096	11.12	4.466
33	Pick Up		81	RWD	4400	6.06	4.96	6.14	2.40	5.42	1.130	11.10	4.628
34	Utility	*	88	4WD	2135	5.47	3.33	3.34	1.92	4.30	1.122	6.67	3.479
35	Utility		86	4WD	3110	6.03	3.78	4.00	2.13	4.80	1.126	7.78	3.653
36	Utility		86	4WD	3570	5.63	4.06	4.57	2.30	4.68	1.018	8.64	3.758
37	Utility	*	83	RWD	3650	5.41	3.88	4.49	2.08	4.65	1.118	8.37	4.024
38	Utility		85	4WD	5215	6.25	4.25	4.59	2.54	5.59	1.099	8.84	3.478
39	Utility		85	4WD	4670	6.14	4.35	4.40	2.46	5.60	1.140	8.75	3.560
40	Utility	*	83	4WD	3520	5.77	3.72	4.13	2.42	4.86	1.004	7.85	3.244
41	Utility		89	4WD	3170	5.75	3.63	4.17	1.97	4.83	1.227	7.81	3.963

† FWD = front wheel drive
RWD = rear wheel drive
4WD = 4 wheel drive

TABLE E-3. STABILITY METRICS

Ref No.	Type	Field Test (Phase I)	Year	Drive Train	Weight (lbs)	Rollover				Directional		
						Roll Grad. K_ϕ (deg/g)	Vert. Defl. Δh_{cg} (ft)	Lat. Defl. Δy (in.)	$a_{y_{RO}}$ (g's)	Weight (%front)	Roll Stf. (%front)	LTD (%front)
1	Small	*	89	FWD	2550	5.71	0.130	5.2	0.96	62.35	59.71	62.70
2	Small		77	FWD	1795	9.12	0.092	6.3	0.88	60.17	55.80	56.31
3	Small		82	RWD	1800	5.65	0.058	2.8	1.07	55.28	78.21	59.12
4	Small		77	RWD	2395	5.99	0.130	4.6	0.98	56.78	81.37	60.48
5	Small		80	RWD	2620	5.52	0.117	6.3	0.94	56.30	71.37	52.33
6	Small	*	83	FWD	2035	7.48	0.040	5.5	1.00	65.85	58.10	59.74
7	Small		84	FWD	1860	4.87	0.097	4.8	1.20	63.98	63.03	55.82
8	Small	*	82	FWD	2015	4.80	0.080	5.0	1.07	61.79	53.91	54.19
9	Small		84	FWD	1980	4.24	0.070	3.3	1.20	61.62	60.15	56.13
10	Small	*	80	RWD	2110	6.15	0.040	4.5	0.96	53.79	68.05	55.57
11	Small		84	RWD	2627	3.52	0.120	5.0	1.16	43.01	56.81	57.72
12	Small		83	FWD	2130	6.34	0.085	7.3	1.02	63.62	40.34	42.64
13	Small		85	FWD	2500	8.20	0.046	5.5	0.99	65.20	50.61	50.31
14	Medium		81	RWD	2410	7.14	0.100	6.5	0.92	54.56	59.27	54.84
15	Medium		85	FWD	2520	5.47	0.065	6.3	1.06	65.48	62.71	63.64
16	Medium	*	87	RWD	3355	5.29	0.040	6.0	1.03	60.51	79.35	59.31
17	Large	*	80	RWD	3830	4.46	0.170	6.0	1.09	55.74	84.36	56.09
18	Van	*	89	FWD	3572	7.50	0.075	4.0	0.93	59.49	67.54	60.04
19	Van	*	88	RWD	3622	7.83	0.050	4.8	0.88	56.79	75.17	60.80
20	Van		86	RWD	3205	5.39	0.056	5.3	0.91	58.66	64.39	52.49
21	Van		84	RWD	3260	5.43	-0.080	5.2	0.92	53.07	58.16	58.97
22	Van		88	RWD	4740	6.93	0.060	5.9	0.86	54.22	58.38	47.23
23	Pick Up	*	80	4WD	3240	4.34	0.140	5.0	0.93	56.48	55.13	55.40
24	Pick Up		83	RWD	2945	7.13	0.037	4.7	1.00	58.57	56.48	48.29
25	Pick Up		86	4WD	3600	5.32	0.040	3.8	1.00	60.56	71.74	57.00
26	Pick Up		88	RWD	2970	7.25	0.175	3.5	0.80	57.91	67.04	55.15
27	Pick Up		86	4WD	3545	4.30	0.063	3.2	0.88	59.94	72.34	58.67
28	Pick Up		85	RWD	2605	4.34	0.030	4.2	1.07	57.39	66.78	56.45
29	Pick Up		88	4WD	3875	7.48	0.047	3.9	0.94	58.19	68.95	51.42
30	Pick Up		76	RWD	4360	7.06	0.021	2.8	0.93	58.72	67.93	49.15
31	Pick Up		84	RWD	4550	6.28	0.050	3.0	0.97	56.37	64.04	46.43
32	Pick Up		87	4WD	4590	5.11	0.120	3.0	0.89	59.37	67.43	55.50
33	Pick Up		81	RWD	4400	4.98	0.102	3.5	0.93	55.34	53.63	46.59
34	Utility	*	88	4WD	2135	5.07	0.083	4.4	0.92	50.12	56.13	52.25
35	Utility		86	4WD	3110	2.95	0.070	4.0	0.98	51.45	62.22	53.92
36	Utility		86	4WD	3570	5.98	0.042	5.5	0.85	52.94	53.19	43.38
37	Utility	*	83	RWD	3650	5.90	0.120	5.6	0.92	53.70	75.98	61.25
38	Utility		85	4WD	5215	5.92	0.048	5.3	0.88	51.87	62.84	52.96
39	Utility		85	4WD	4670	4.97	0.092	4.3	0.93	50.32	46.95	42.69
40	Utility	*	83	4WD	3520	4.79	0.130	3.2	0.81	52.56	68.40	55.62
41	Utility		89	4WD	3170	2.61	0.050	5.1	1.04	53.47	58.82	51.81

TABLE E-4. COMPUTER SIMULATION (VDANL)
TIRE MODEL PARAMETER DEFINITIONS

MATHEMATICAL SYMBOLS	PROGRAM VARIABLE INPUT NAME	TIRE MODEL PARAMETER DEFINITION
T_W	TWIDTH	Width of the tire tread; inches
K_{AO} K_{A1} K_{A2}	KAO KA1 KA2	Calspan coefficients for defining $= \left.\frac{dFy}{d\alpha}\right\|_{\alpha = 0}$ vs F_z
K_{A3} K_{A4}	KA3 KA4	Calspan coefficients for defining $= \left.\frac{dFy}{d\gamma}\right\|_{\gamma = 0}$ vs F_z
K_a	KA	Coefficient of elongation of the tire patch length due to braking or acceleration
$K\mu$	KMU	Coefficient of decay in μ with increasing tire slip
T_p	TPRES	Cold pressure in the tire; lbs/in^2
K_{B1} K_{B3} K_{B4}	KB1 KB3 KB4	Calspan coefficients for defining the peak lateral force coefficient
K_γ	KGAMMA	Camber side force saturation coefficient
$\frac{CS}{F_z}$	CSFZ	Calspan Coefficient for defining $\left.\frac{\delta F_x}{\delta_s}\right\|_{s = 0}$ (Normalized for F_z
μ_{nom}	MUNOM	Surface coefficient of friction
F_{ZT}	FZTRL	100% design load for tire at given TPRES
K_1	KK1	Calspan coefficient for aligning torque
RR	-RAD	Tire rolling radius, ft
TIRE$	TIRE	Tire type (i.e., radial, bias ply); used for output plot legends in tire model program
C_1 C_2 C_3 C_4	C1 C2 C3 C4	Coefficients for the polynominal saturation function
G_1 G_2	G1 G2	Shaping coefficients for aligning torque

TABLE E-5. COMPUTER SIMULATION PARAMETERS FOR ALL TEST VEHICLES

VDANL Simulation Parameter Files: Vehicle #1

a) Vehicle Parameters

```
MASS = 84
SMASS = 75
UMASSF = 4.5
UMASSR = 4.5
LENA = 2.9
LENB = 4.95
IXS = 180
IYS = 990
IZZ = 1135
IXZ = 0
KSTR = 18.2
KSCF = .00005
KSCB = 0
DLADV = 0
DYADV = 0
DNADV = 0
DENSITY = .00237
REFAREA = 20
CDX = .4
AEROVEL = 44
KTL = 1
KSF = 1500
KSDF = 100
KSR = 1500
KSDR = 100
TRWF = 4.56
TRWB = 4.67
HCG = 1.83
KBS = 1800
HBS = .25
KTSF = -9500
KTSR = 0
KRAS = 12000
KRADP = 700
TSPRINGR = 13000
HRAF = 0
HRAR = 0
HS = 1.95
IXUF = 24
IXUR = 24
KLT = .00015
XACC = -2.34
ZACC = 1.32
DRAGC = -.015
LENS = 5.4
LM = 1.125
KBTF = -.85
KVB = 18
KMB = 18
KBPVL = 100
SWZ = .5
SWW = 100
KCF = 0
LSO = 0
KLAGV = 25
```

b) Suspension Parameters

```
SUSPENSIONF = INDEPENDENT
SUSPENSIONR = INDEPENDENT
HF = 0
HR = 0
LF = 1
LR = 1
KSAF = 0
KSAR = 0
BF = 0
BR = .043
CF = 0
CR = .174
DF = -.19
DR = -.064
EF = 0
ER = 0
KSLF = .24
KSLR = .16
LSAF = .95
LSAR = 1.16
KSADF = 0
KSADR = .086
KSAD2F = 0
KSAD2R = 0
KACK = .29
```

c) Tire Parameters

```
TWIDTH = 6.5
KA0 = 0
KA1 = 15.66
KA2 = 2350
KA3 = .53
KA4 = -24450
KA = .05
KMU = .234
TPRESS = 30
KB1 = -.000058
KB3 = 1.014
KB4 = -3.86E-08
KGAMMA = .9
CSFZ = 17
MUNOM = .92
FZTRL = 1070
KK1 = -.000206
RR = .9
TIRE = RADIAL
C1 = 1
C2 = .34
C3 = .57
C4 = .32
G1 = 1
G2 = 1
```

TABLE E-5. (Continued)

VDANL Simulation Parameter Files: Vehicle #2

a) Vehicle Parameters

```
MASS = 55.79733
SMASS = 48.77557
UMASSF = 3.51088
UMASSR = 3.51088
LENA = 3.040759
LENB = 4.884241
IXS = 108.6193
IYS = 588.2825
IZZ = 727.5253
IXZ = 0
KSTR = 20.8
KSCF = .000016
KSCB = 0
DLADV = 0
DYADV = 0
DNADV = 0
DENSITY = .002377
REFAREA = 17.52233
CDX = .5
AEROVEL = 80
KTL = 1
KSF = 804
KSDF = 76.95045
KSR = 890
KSDR = 73.00667
TRWF = 4.23
TRWB = 4.08
HCG = 1.775157
KBS = 1608
HBS = .25
KTSF = -6162.679
KTSR = -3169.831
KRAS = 12000
KRADP = 700
TSPRINGR = 9251.691
HRAF = 0
HRAR = 0
HS = 1.90604
IXUF = 15.70496
IXUR = 14.61088
KLT = 2.810297E-04
XACC = 0
ZACC = 0
DRAGC = -.015
LENS = 0
LM = 0
KBTF = 0
KVB = 0
KMB = 0
FBPVL = 0
SWZ = .5
SWW = 70
KCF = 0
LSO = 0
KLAGV = 16.5
```

b) Suspension Parameters

```
SUSPENSIONF$ = INDEPENDENT
SUSPENSIONR$ = INDEPENDENT
HF = 0
HR = 0
LF = 1
LR = 1
KSAF = 0
KSAR = 0
BF = 0
BR = 0
CF = 0
CR = 0
DF = 0
DR = 0
EF = 0
ER = 0
KSLF = .07
KSLR = 0
LSAF = 1000
LSAR = 1000
KSADF = 0
KSADR = .78
KSAD2F = 0
KSAD2R = 0
KACK = .16
```

c) Tire Parameters

```
TWIDTH = 3.5
KA0 = 1260
KA1 = 13.2
KA2 = 1830
KA3 = .533
KA4 = -31200
KA = .05
KMU = .234
TPRESS = 26
KB1 = -.000619
KB3 = 1.184
KB4 = 2.38E-07
KGAMMA = 0.9
CSFZ = 19.3
MUNOM = .85
FZTRL = 735
KK1 = -.00026
RR = .866
TIRE = RADIAL
C1 = 1
C2 = .34
C3 = .57
C4 = .32
G1 = 1
G2 = 1
```

TABLE E-5. (Continued)

VDANL Simulation Parameter Files: Vehicle #3

a) Vehicle Parameters

```
MASS = 55.95275
SMASS = 47.95866
UMASSF = 3.517874
UMASSR = 4.47622
LENA = 3.243241
LENB = 4.326759
IXS = 104.7754
IYS = 649.4427
IZZ = 777.1104
IXZ = 0
KSTR = 16.6
KSCF = .000025
KSCB = 0
DLADV = 0
DYADV = 0
DNADV = 0
DENSITY = .002377
REFAREA = 16.75845
CDX = .5
AEROVEL = 80
KTL = 1
KSF = 1460
KSDF = 99.02079
KSR = 1050
KSDR = 83.08926
TRWF = 4.28
TRWB = 4.18
HCG = 1.731953
KBS = 2920
HBS = .25
KTSF = -5527.002
KTSR = 3908.393
KRAS = 12000
KRADP = 700
TSPRINGR = 11386.7
HRAF = 0
HRAR = 0
HS = 1.87763
IXUF = 16.11046
IXUR = 15.36642
KLT = 2.283366E-04
XACC = 0
ZACC = 0
DRAGC = -.015
LENS = 0
LM = 0
KBTF = 0
KVB = 0
KMB = 0
FBPVL = 0
SWZ = .5
SWW = 70
KCF = 0
LSO = 0
KLAGV = 16.5
```

b) Suspension Parameters

```
SUSPENSIONF$ = INDEPENDENT
SUSPENSIONR$ = SOLID AXLE
HF = 0
HR = .06
LF = 1
LR = 1.47
KSAF = 0
KSAR = 1
BF = 0
BR = 0
CF = 0
CR = 0
DF = -.14
DR = 0
EF = 0
ER = 0
KSLF = .155
KSLR = 0
LSAF = .75
LSAR = 1000
KSADF = 0
KSADR = 0
KSAD2F = 0
KSAD2R = 0
KACK = .034
```

c) Tire Parameters

```
TWIDTH = 3.5
KA0 = 1260
KA1 = 13.2
KA2 = 1830
KA3 = .533
KA4 = -31200
KA = .05
KMU = .234
TPRESS = 32
KB1 = -.000619
KB3 = 1.184
KB4 = 2.38E-07
KGAMMA = 0.9
CSFZ = 19.3
MUNOM = .85
FZTRL = 735
KK1 = -.00026
RR = .858
TIRE = RADIAL
C1 = 1
C2 = .34
C3 = .57
C4 = .32
G1 = 1
G2 = 1
```

TABLE E-5. (Continued)

VDANL Simulation Parameter Files: Vehicle #4

a) Vehicle Parameters

```
MASS = 74.44825
SMASS = 64.14222
UMASSF = 4.350172
UMASSR = 5.95586
LENA = 3.222852
LENB = 4.662148
IXS = 147.9954
IYS = 1008.563
IZZ = 1191.693
IXZ = 0
KSTR = 18.75
KSCF = .00015
KSCB = 0
DLADV = 0
DYADV = 0
DNADV = 0
DENSITY = .002377
REFAREA = 17.5056
CDX = .5
AEROVEL = 80
KTL = 1
KSF = 1490
KSDF = 117.6631
KSR = 1200
KSDR = 100.336
TRWF = 4.41
TRWB = 4.368
HCG = 1.792419
KBS = 2980
HBS = .25
KTSF = -14748.56
KTSR = 4752.34
KRAS = 12000
KRADP = 700
TSPRINGR = 9850.286
HRAF = 0
HRAR =  0
HS = 1.935808
IXUF = 21.15064
IXUR = 20.74969
KLT = 2.639517E-04
XACC = 0
ZACC = 0
DRAGC = -.015
LENS = 0
LM = 0
KBTF = 0
KVB = 0
KMB = 0
FBPVL = 0
SWZ = .5
SWW = 70
KCF = 0
LSO = 0
KLAGV = 16.5
```

b) Suspension Parameters

```
SUSPENSIONF$ = INDEPENDENT
SUSPENSIONR$ = SOLID AXLE
HF = 0
HR = .04
LF = 1
LR = 1.6
KSAF = 0
KSAR = 1
BF = 0
BR = 0
CF = 0
CR = 0
DF = -.096
DR = 0
EF = 0
ER = 0
KSLF = .094
KSLR = 0
LSAF =  .93
LSAR =  1000
KSADF =  0
KSADR =  .17
KSAD2F = 0
KSAD2R = 0
KACK = 0
```

c) Tire Parameters

```
TWIDTH = 6.5
KA0 = 0
KA1 = 15.66
KA2 = 2350
KA3 = .53
KA4 = -24450
KA = .05
KMU = .234
TPRESS = 26
KB1 = -.000058
KB3 = 1.014
KB4 = -3.86E-08
KGAMMA = 0.9
CSFZ = 17
MUNOM = .92
FZTRL = 1070
KK1 = -.000206
RR = .9
TIRE = RADIAL
C1 = 1
C2 = .34
C3 = .57
C4 = .32
G1 = 1
G2 = 1
```

TABLE E-5. (Continued)

VDANL Simulation Parameter Files: Vehicle #5

a) Vehicle Parameters

```
MASS = 81.44234
SMASS = 72.11253
UMASSF = 4.664906
UMASSR = 4.664906
LENA = 3.375246
LENB = 4.494754
IXS = 170.4689
IYS = 1198.512
IZZ = 1350.16
IXZ = 0
KSTR = 18.5
KSCF = .00008
KSCB = 0
DLADV = 0
DYADV = 0
DNADV = 0
DENSITY = .002377
REFAREA = 17.5587
CDX = .5
AEROVEL = 80
KTL = 1
KSF = 1650
KSDF = 129.0316
KSR = 1350
KSDR = 115.588
TRWF = 4.42
TRWB = 4.415
HCG = 1.742563
KBS = 3300
HBS = .25
KTSF = -11426.68
KTSR = 2109.632
KRAS = 12000
KRADP = 700
TSPRINGR = 10820.16
HRAF = 0
HRAR = 0
HS = 1.842775
IXUF = 22.78387
IXUR = 22.73235
KLT = 2.402922E-04
XACC = 0
ZACC = 0
DRAGC = -.015
LENS = 0
LM = 0
KBTF = 0
KVB = 0
KMB = 0
FBPVL = 0
SWZ = .5
SWW = 70
KCF = 0
LSO = 0
KLAGV = 16.5
```

b) Suspension Parameters

```
SUSPENSIONF$ = INDEPENDENT
SUSPENSIONR$ = SOLID AXLE
HF = 0
HR = .05
LF = 1
LR = 1.58
KSAF = 0
KSAR = 1
BF = 0
BR = 0
CF = 0
CR = 0
DF = -.088
DR = 0
EF = 0
ER = 0
KSLF = .113
KSLR = 0
LSAF = .98
LSAR = 1000
KSADF = 0
KSADR = .20
KSAD2F = 0
KSAD2R = 0
KACK = 0
```

c) Tire Parameters

```
TWIDTH = 4.75
KA0 = 1580
KA1 = 11.9
KA2 = 3030
KA3 = .264
KA4 = -1770
KA = .05
KMU = .234
TPRESS = 26
KB1 = -.000114
KB3 = 1.01
KB4 = 1.06E-09
KGAMMA = 0.9
CSFZ = 18.4
MUNOM = .85
FZTRL = 1160
KK1 = -.00026
RR = .968
TIRE = RADIAL
C1 = 1
C2 = .34
C3 = .57
C4 = .32
G1 = 1
G2 = 1
```

TABLE E-5. (Continued)

VDANL Simulation Parameter Files: Vehicle #6

a) Vehicle Parameters

```
MASS =  73
SMASS =  64
UMASSF =  4.5
UMASSR =  4.5
LENA =  2.75
LENB =  5.09
IXS =  160
IYS =  812
IZZ =  970
IXZ =  0
KSTR =  16.9
KSCF =  .00003
KSCB = 0
DLADV = 0
DYADV = 0
DNADV = 0
DENSITY = .00237
REFAREA =  20
CDX = .5
AEROVEL =  44
KTL =  1
KSF =  1600
KSDF =  110
KSR =  1200
KSDR =  70
TRWF =  4.6
TRWB =  4.52
HCG =  1.71
KBS =  3750
HBS =  .25
KTSF =  0
KTSR =  0
KRAS =  12000
KRADP = 700
TSPRINGR =  9000
HRAF =  0
HRAR =  0
HS =  1.83
IXUF =  24
IXUR =  22
KLT =  .00015
XACC =  -2.3
ZACC =  1.8
DRAGC =  -.015
LENS =  5.3
LM =  1.125
KBTF =  -.48
KVB =  22
KMB =  3.5
KBPVL =  55
SWZ =  .5
SWW =  100
KCF = 0
LSO = 0
KLAGV = 25
```

b) Suspension Parameters

```
SUSPENSIONF =  INDEPENDENT
SUSPENSIONR =  INDEPENDENT
HF = 0
HR = 0
LF =  1
LR =  1
KSAF =  0
KSAR =  0
BF = 0
BR = 0
CF = 0
CR = 0
DF =  -.134
DR = 0
EF = 0
ER = 0
KSLF =  .115
KSLR =  .033
LSAF =  .96
LSAR = 1000
KSADF = 0
KSADR = 0
KSAD2F =  .64
KSAD2R =  .64
KACK =  .29
```

c) Tire Parameters

```
TWIDTH = 5
KA0 = 2380
KA1 = 9.21
KA2 = 2280
KA3 = .523
KA4 = -7225
KA = .05
KMU = .234
TPRESS = 26
KB1 = -.000087
KB3 = .89
KB4 = -2.1E-08
KGAMMA = .9
CSFZ = 24
MUNOM = .92
FZTRL = 1010
KK1 = -.0003
RR = .88
TIRE = BIAS
C1 = .535
C2 = 1.05
C3 = 1.15
C4 = .8
G1 = 1
G2 = 1
```

TABLE E-5. (Continued)

VDANL Simulation Parameter Files: Vehicle #7

a) Vehicle Parameters

```
MASS = 57.81784
SMASS = 50.61424
UMASSF = 3.601803
UMASSR = 3.601803
LENA = 2.460516
LENB = 4.769484
IXS = 115.2329
IYS = 582.576
IZZ = 699.1234
IXZ = 0
KSTR = 21.6
KSCF = .000025
KSCB = 0
DLADV = 0
DYADV = 0
DNADV = 0
DENSITY = .002377
REFAREA = 16.70085
CDX = .5
AEROVEL = 80
KTL = 1
KSF = 1520
KSDF = 111.5084
KSR = 925
KSDR = 71.4046
TRWF = 4.61
TRWB = 4.63
HCG = 1.603799
KBS = 3040
HBS = .25
KTSF = -5229.807
KTSR = -2628.683
KRAS = 12000
KRADP = 700
TSPRINGR = 9365.349
HRAF = 0
HRAR = 0
HS = 1.704677
IXUF = 19.13647
IXUR = 19.30287
KLT = 2.776191E-04
XACC = 0
ZACC = 0
DRAGC = -.015
LENS = 0
LM = 0
KBTF = 0
KVB = 0
KMB = 0
FBPVL = 0
SWZ = .5
SWW = 70
KCF = 0
LSO = 0
KLAGV = 16.5
```

b) Suspension Parameters

```
SUSPENSIONF$ = INDEPENDENT
SUSPENSIONR$ = SOLID AXLE
HF = 0
HR = -.06
LF = 1
LR = 1.63
KSAF = 0
KSAR = 1
BF = 0
BR = 0
CF = 0
CR = 0
DF = -.133
DR = 0
EF = 0
ER = 0
KSLF = .072
KSLR = 0
LSAF = .92
LSAR = 1000
KSADF = 0
KSADR = .51
KSAD2F = 0
KSAD2R = 0
KACK = .11
```

c) Tire Parameters

```
TWIDTH = 4.5
KA0 = 570
KA1 = 12
KA2 = 2880
KA3 = .618
KA4 = 15900
KA = .05
KMU = .234
TPRESS = 24
KB1 = -.000162
KB3 = 1.035
KB4 = 3.5E-09
KGAMMA = 0.9
CSFZ = 18.7
MUNOM = .85
FZTRL = 980
KK1 = -.000296
RR = .895
TIRE = RADIAL
C1 = 1
C2 = .34
C3 = .57
C4 = .32
G1 = 1
G2 = 1
```

TABLE E-5. (Continued)

VDANL Simulation Parameter Files: Vehicle #8

a) Vehicle Parameters

```
MASS =  69
SMASS =  61
UMASSF =  4
UMASSR =  4
LENA =  2.87
LENB =  4.71
IXS =  145
IYS =  710
IZZ =  870
IXZ = 0
KSTR =  21.2
KSCF =  .000045
KSCB = 0
DLADV = 0
DYADV = 0
DNADV = 0
DENSITY = .00237
REFAREA = 20
CDX = .5
AEROVEL = 44
KTL = 1
KSF =  1400
KSDF =  115
KSR =  1750
KSDR =  115
TRWF =  4.43
TRWB =  4.5
HCG =  1.68
KBS =  2800
HBS =  .25
KTSF =  -6400
KTSR = 0
KRAS = 12000
KRADP = 700
TSPRINGR =  9600
HRAF = 0
HRAR = 0
HS =  1.78
IXUF =  20
IXUR =  20
KLT =  .0002
XACC =  -2.1
ZACC =  1.2
DRAGC = -.015
LENS =  5.4
LM = 1.125
KBTF = -.48
KVB = 22
KMB = 3.5
KBPVL = 55
SWZ = .5
SWW = 100
KCF = 0
LSO = 0
KLAGV = 25
```

b) Suspension Parameters

```
SUSPENSIONF = INDEPENDENT
SUSPENSIONR = INDEPENDENT
HF = 0
HR = 0
LF = 1
LR = 1
KSAF = 0
KSAR = 0
BF = 0
BR =  -.06
CF = 0
CR = 0
DF =  -.15
DR =  -.175
EF = 0
ER = 0
KSLF =  .18
KSLR =  .25
LSAF =  1.0
LSAR =  .95
KSADF = 0
KSADR = 0
KSAD2F =  0
KSAD2R =  0
KACK = .29
```

c) Tire Parameters

```
TWIDTH = 5
KA0 = 289
KA1 = 13.9
KA2 = 2950
KA3 = -.05
KA4 = 175
KA = .05
KMU = .234
TPRESS = 26
KB1 = -.00006
KB3 = 1
KB4 = -2E-08
KGAMMA = .9
CSFZ = 16
MUNOM = .92
FZTRL = 1000
KK1 = -.0002
RR = .88
TIRE = BIAS
C1 = .535
C2 = 1.05
C3 = 1.15
C4 = .8
G1 = 1
G2 = 1
```

TABLE E-5. (Continued)

VDANL Simulation Parameter Files: Vehicle #9

a) Vehicle Parameters

```
MASS = 61.54803
SMASS = 54.00871
UMASSF = 3.769661
UMASSR = 3.769661
LENA = 2.874811
LENB = 4.945189
IXS = 126.1182
IYS = 702.105
IZZ = 830.9055
IXZ = 0
KSTR = 21.1
KSCF = .0000275
KSCB = 0
DLADV = 0
DYADV = 0
DNADV = 0
DENSITY = .002377
REFAREA = 17.4312
CDX = .5
AEROVEL = 80
KTL = 1
KSF = 1670
KSDF = 118.2119
KSR = 1350
KSDR = 92.61366
TRWF = 4.65
TRWB = 4.625
HCG = 1.617211
KBS = 3340
HBS = .25
KTSF = -5219.091
KTSR = -979.4981
KRAS = 12000
KRADP = 700
TSPRINGR = 10145.79
HRAF = 0
HRAR = 0
HS = 1.718168
IXUF = 20.37738
IXUR = 20.15885
KLT = 2.562638E-04
XACC = 0
ZACC = 0
DRAGC = -.015
LENS = 0
LM = 0
KBTF = 0
KVB = 0
KMB = 0
FBPVL = 0
SWZ = .5
SWW = 70
KCF = 0
LSO = 0
KLAGV = 16.5
```

b) Suspension Parameters

```
SUSPENSIONF$ = INDEPENDENT
SUSPENSIONR$ = SOLID AXLE
HF = 0
HR = -.06
LF = 1
LR = 1.48
KSAF = 0
KSAR = 1
BF = 0
BR = 0
CF = 0
CR = 0
DF = -.15
DR = 0
EF = 0
ER = 0
KSLF = .17
KSLR = 0
LSAF = 1.1
LSAR = 1000
KSADF = 0
KSADR = .56
KSAD2F = 0
KSAD2R = 0
KACK = .11
```

c) Tire Parameters

```
TWIDTH = 4.5
KA0 = 570
KA1 = 12
KA2 = 2880
KA3 = .618
KA4 = 15900
KA = .05
KMU = .234
TPRESS = 26
KB1 = -.000162
KB3 = 1.035
KB4 = 3.5E-09
KGAMMA = 0.9
CSFZ = 18.7
MUNOM = .85
FZTRL = 980
KK1 = -.000296
RR = .894
TIRE = RADIAL
C1 = 1
C2 = .34
C3 = .57
C4 = .32
G1 = 1
G2 = 1
```

TABLE E-5. (Continued)

VDANL Simulation Parameter Files: Vehicle #10

a) Vehicle Parameters

```
MASS = 71.3
SMASS = 61.3
UMASSF = 4
UMASSR = 6
LENA = 3.49
LENB = 4.37
IXS = 137
IYS = 713
IZZ = 962
IXZ = 0
KSTR = 19
KSCF = .00005
KSCB = 0
DLADV = 0
DYADV = 0
DNADV = 0
DENSITY = .00237
REFAREA = 18
CDX = .5
AEROVEL = 44
KTL = 1
KSF = 920
KSDF = 88
KSR = 1220
KSDR = 103
TRWF = 4.27
TRWB = 4.27
HCG = 1.73
KBS = 2000
HBS = .2
KTSF = -15600
KTSR = 0
KRAS = 12000
KRADP = 700
TSPRINGR = 9750
HRAF = 0
HRAR = .75
HS = 1.87
IXUF = 18
IXUR = 18
KLT = .0002
XACC = -2.36
ZACC = 1.83
DRAGC = -.015
LENS = 5.12
LM = 1.125
KBTF = -.39
KVB = 10.8
KMB = 4.55
KBPVL = 147
SWZ = .5
SWW = 100
KCF = 0
LSO = .125
KLAGV = 25
```

b) Suspension Parameters

```
SUSPENSIONF = INDEPENDENT
SUSPENSIONR =  SOLID A
HF = 0
HR =  -.083
LF = 1
LR =  1.33
KSAF = 0
KSAR =  1
BF = 0
BR =  0
CF = 0
CR = 0
DF =  0
DR =  0
EF = 0
ER = 0
KSLF =  0
KSLR =  0
LSAF =  1000
LSAR =  1000
KSADF =  .1
KSADR =  .366
KSAD2F = 0
KSAD2R = 0
KACK =  .0014
```

c) Tire Parameters

```
TWIDTH = 5
KA0 = 2613
KA1 = 9.2
KA2 = 2500
KA3 = .52
KA4 = -7225
KA = .05
KMU = .12
TPRESS = 26
KB1 = -.00041
KB3 = 1.19
KB4 = 1.5E-07
KGAMMA = .9
CSFZ = 24
MUNOM = .8
FZTRL = 900
KK1 = -.0003
RR = .875
TIRE = BIAS
C1 = .535
C2 = 1.05
C3 = 1.15
C4 = .8
G1 = 1
G2 = 1
```

TABLE E-5. (Continued)

VDANL Simulation Parameter Files: Vehicle #11

a) Vehicle Parameters

```
MASS = 80.66522
SMASS = 71.40535
UMASSF = 4.629935
UMASSR = 4.629935
LENA = 4.479985
LENB = 3.310015
IXS = 182.8714
IYS = 1043.092
IZZ = 1195.986
IXZ = 0
KSTR = 19
KSCF = .000046
KSCB = 0
DLADV = 0
DYADV = 0
DNADV = 0
DENSITY = .002377
REFAREA = 17.2431
CDX = .5
AEROVEL = 80
KTL = 1
KSF = 1900
KSDF = 152.7974
KSR = 2750
KSDR = 237.6218
TRWF = 4.815
TRWB = 4.93
HCG = 1.726659
KBS = 3800
HBS = .25
KTSF = -22721.38
KTSR = -595.0891
KRAS = 12000
KRADP = 700
TSPRINGR = 13861.8
HRAF = 0
HRAR = 0
HS = 1.828673
IXUF = 26.83537
IXUR = 28.13253
KLT = 1.875658E-04
XACC = 0
ZACC = 0
DRAGC = -.015
LENS = 0
LM =  1
KBTF =  1
KVB =  1
KMB =  1
FBPVL =  1
SWZ = .5
SWW = 70
KCF = 0
LSO = .1
KLAGV = 16.5
```

b) Suspension Parameters

```
SUSPF=INDEPENDENT
SUSPR=INDEPENDENT
HF=0
HR=0
LF=1
LR=1
KSAF=0
KSAR=0
BF=0
BR=0
CF=0
CR=0
DF=0
DR=-.11
EF=0
ER=0
KSLF=.14
KSLR=.06
LSAF=1000
LSAR=1.0
KSADF=0
KSADR=0
KSAD2F=0
KSAD2R=0
KACK=.03
```

c) Tire Parameters

```
TWIDTH = 4.5
KA0 = 570
KA1 = 12
KA2 = 2880
KA3 = .618
KA4 = 15900
KA = .05
KMU = .234
TPRESS = 35
KB1 = -.000162
KB3 = 1.035
KB4 = 3.5E-09
KGAMMA = 0.9
CSFZ = 18.7
MUNOM = .85
FZTRL = 980
KK1 = -.000296
RR = .94
TIRE = RADIAL
C1 = 1
C2 = .34
C3 = .57
C4 = .32
G1 = 1
G2 = 1
```

TABLE E-5. (Continued)

VDANL Simulation Parameter Files: Vehicle #12

a) Vehicle Parameters

```
MASS = 66.21076
SMASS = 58.25179
UMASSF = 3.979484
UMASSR = 3.979484
LENA = 2.717098
LENB = 5.152902
IXS = 126.8701
IYS = 950.4432
IZZ = 1094.597
IXZ = 0
KSTR = 20.9
KSCF = .00007
KSCB = 0
DLADV = 0
DYADV = 0
DNADV = 0
DENSITY = .002377
REFAREA = 17.3535
CDX = .5
AEROVEL = 80
KTL = 1
KSF = 1500
KSDF = 118.3919
KSR = 1125
KSDR = 85.08856
TRWF = 4.63
TRWB = 4.48
HCG = 1.816265
KBS = 3000
HBS = .25
KTSF = -1219.889
KTSR = -14295.19
KRAS = 12000
KRADP = 700
TSPRINGR = 10536.02
HRAF = 0
HRAR = 0
HS = 1.942001
IXUF = 21.32695
IXUR = 19.96746
KLT = 2.467726E-04
XACC = 0
ZACC = 0
DRAGC = -.015
LENS = 0
LM =  1
KBTF =  1
KVB =  1
KMB =  1
FBPVL =  1
SWZ = .5
SWW = 70
KCF = 0
LSO = 0
KLAGV = 16.5
```

b) Suspension Parameters

```
SUSPF=INDEPENDENT
SUSPR=INDEPENDENT
HF=0
HR=0
LF=1
LR=1
KSAF=0
KSAR=0
BF=0
BR=0
CF=0
CR=0
DF=-.11
DR=0
EF=0
ER=0
KSLF=.07
KSLR=0
LSAF=.90
LSAR=1000
KSADF=0
KSADR=.57
KSAD2F=0
KSAD2R=0
KACK=.08
```

c) Tire Parameters

```
TWIDTH = 4.5
KA0 = 570
KA1 = 12
KA2 = 2880
KA3 = .618
KA4 = 15900
KA = .05
KMU = .234
TPRESS = 27
KB1 = -.000162
KB3 = 1.035
KB4 = 3.5E-09
KGAMMA = 0.9
CSFZ = 18.7
MUNOM = .85
FZTRL = 980
KK1 = -.000296
RR = .896
TIRE = RADIAL
C1 = 1
C2 = .34
C3 = .57
C4 = .32
G1 = 1
G2 = 1
```

TABLE E-5. (Continued)

VDANL Simulation Parameter Files: Vehicle #13

a) Vehicle Parameters

```
MASS = 77.71216
SMASS = 68.71806
UMASSF = 4.497047
UMASSR = 4.497047
LENA = 2.659296
LENB = 5.445704
IXS = 162.2403
IYS = 1130.337
IZZ = 1303.124
IXZ = 0
KSTR = 16.6
KSCF = .000025
KSCB = 0
DLADV = 0
DYADV = 0
DNADV = 0
DENSITY = .002377
REFAREA = 18.18416
CDX = .5
AEROVEL = 80
KTL = 1
KSF = 1460
KSDF = 128.5125
KSR = 1600
KSDR = 107.4428
TRWF = 4.73
TRWB = 4.63
HCG = 1.789597
KBS = 2920
HBS = .25
KTSF = -1009.744
KTSR = 226.7064
KRAS = 12000
KRADP = 700
TSPRINGR = 10441.3
HRAF = 0
HRAR = 0
HS = 1.905507
IXUF = 25.153
IXUR = 24.10069
KLT = 2.490111E-04
XACC = 0
ZACC = 0
DRAGC = -.015
LENS = 0
LM =  1
KBTF =  1
KVB =  1
KMB =  1
FBPVL =  1
SWZ = .5
SWW = 70
KCF = 0
LSO = .15
KLAGV = 16.5
```

b) Suspension Parameters

```
SUSPF=INDEPENDENT
SUSPR=INDEPENDENT
HF=0
HR=0
LF=1
LR=1
KSAF=0
KSAR=0
BF=0
BR=0
CF=0
CR=0
DF=-1.3
DR=0
EF=-.09
ER=0
KSLF=.09
KSLR=.15
LSAF=.90
LSAR=.80
KSADF=0
KSADR=0
KSAD2F=0
KSAD2R=0
KACK=.10
```

c) Tire Parameters

```
TWIDTH = 4.5
KA0 = 570
KA1 = 12
KA2 = 2880
KA3 = .618
KA4 = 15900
KA = .05
KMU = .234
TPRESS = 26
KB1 = -.000162
KB3 = 1.04
KB4 = 3.5E-09
KGAMMA = 0.9
CSFZ = 18.7
MUNOM = .85
FZTRL = 980
KK1 = -.000296
RR = .904
TIRE = RADIAL
C1 = 1
C2 = .34
C3 = .57
C4 = .32
G1 = 1
G2 = 1
```

TABLE E-5. (Continued)

VDANL Simulation Parameter Files: Vehicle #14

a) Vehicle Parameters

```
MASS = 74.91452
SMASS = 66.17221
UMASSF = 4.371153
UMASSR = 4.371153
LENA = 3.793293
LENB = 4.667707
IXS = 152.871
IYS = 1154.888
IZZ = 1321.416
IXZ = 0
KSTR = 20.8
KSCF = .00005
KSCB = 0
DLADV = 0
DYADV = 0
DNADV = 0
DENSITY = .002377
REFAREA = 18.0234
CDX = .5
AEROVEL = 80
KTL = 1
KSF = 1675
KSDF = 122.3966
KSR = 1345
KSDR = 112.9981
TRWF = 4.55
TRWB = 4.475
HCG = 1.886053
KBS = 3350
HBS = .25
KTSF = -5100.155
KTSR = -1949.82
KRAS = 12000
KRADP = 700
TSPRINGR = 10842.89
HRAF = 0
HRAR =  0
HS = 2.01355
IXUF = 22.62345
IXUR = 21.88377
KLT = 2.397884E-04
XACC = 0
ZACC = 0
DRAGC = -.015
LENS = 0
LM = 0
KBTF = 0
KVB = 0
KMB = 0
FBPVL = 0
SWZ = .5
SWW = 70
KCF = 0
LSO = 0
KLAGV = 16.5
```

b) Suspension Parameters

```
SUSPENSIONF$ = INDEPENDENT
SUSPENSIONR$ = INDEPENDENT
HF = 0
HR = 0
LF = 1
LR = 1
KSAF = 0
KSAR = 0
BF = 0
BR = 0
CF = 0
CR = 0
DF = -.12
DR = -.276
EF = 0
ER = 0
KSLF = .105
KSLR = .22
LSAF =  .95
LSAR =  3.44
KSADF =  0
KSADR =  .50
KSAD2F = 0
KSAD2R = 0
KACK = 0
```

c) Tire Parameters

```
TWIDTH = 4.75
KA0 = 1580
KA1 = 11.9
KA2 = 3030
KA3 = .264
KA4 = -1770
KA = .05
KMU = .234
TPRESS = 27
KB1 = -.000114
KB3 = 1.01
KB4 = 1.06E-09
KGAMMA = 0.9
CSFZ = 18.4
MUNOM = .85
FZTRL = 1160
KK1 = -.00026
RR = .921
TIRE = RADIAL
C1 = 1
C2 = .34
C3 = .57
C4 = .32
G1 = 1
G2 = 1
```

TABLE E-5. (Continued)

VDANL Simulation Parameter Files: Vehicle #15

a) Vehicle Parameters

```
MASS = 78.33385
SMASS = 69.28381
UMASSF = 4.525023
UMASSR = 4.525023
LENA = 2.744816
LENB = 5.700183
IXS = 167.1199
IYS = 1180.278
IZZ = 1367.753
IXZ = 0
KSTR = 14
KSCF = .00005
KSCB = 0
DLADV = 0
DYADV = 0
DNADV = 0
DENSITY = .002377
REFAREA = 18.43463
CDX = .5
AEROVEL = 80
KTL = 1
KSF = 1150
KSDF = 81.99066
KSR = 1180
KSDR = 69.1592
TRWF = 4.66
TRWB = 4.62
HCG = 1.691125
KBS = 2300
HBS = .25
KTSF = -20523.74
KTSR = -7036.658
KRAS = 12000
KRADP = 700
TSPRINGR = 13657.8
HRAF = 0
HRAR = 0
HS = 1.794072
IXUF = 24.5659
IXUR = 24.14598
KLT = 1.903674E-04
XACC = 0
ZACC = 0
DRAGC = -.015
LENS = 0
LM =  1
KBTF =  1
KVB =  1
KMB =  1
FBPVL =  1
SWZ = .5
SWW = 70
KCF = 0
LSO = -.1
KLAGV = 16.5
```

b) Suspension Parameters

```
SUSPF = INDEPENDENT
SUSPR = SOLID AXLE
HF = 0
HR = 0
LF = 1
LR = 1
KSAF = 0
KSAR = 0
BF = 0
BR = 0
CF = 0
CR = 0
DF = -.13
DR = 0
EF = 0
ER = 0
KSLF = .068
KSLR = 0
LSAF = 1.1
LSAR = 1000
KSADF = 0
KSADR = .62
KSAD2F = 0
KSAD2R = 0
KACK = .07
```

c) Tire Parameters

```
TWIDTH = 4.5
KA0 = 570
KA1 = 12
KA2 = 2880
KA3 = .618
KA4 = 15900
KA = .05
KMU = .234
TPRESS = 35
KB1 = -.000162
KB3 = 1.035
KB4 = 3.5E-09
KGAMMMA = 0.9
CSFZ = 18.7
MUNOM = .85
FZTRL = 980
KK1 = -.000296
RR = .903
TIRE = RADIAL
C1 = 1
C2 = .34
C3 = .57
C4 = .32
G1 = 1
G2 = 1
```

TABLE E-5. (Continued)

VDANL Simulation Parameter Files: Vehicle #16

a) Vehicle Parameters

```
MASS = 113
SMASS = 99
UMASSF = 5.693038
UMASSR = 8.343177
LENA = 3.49
LENB = 5.20
IXS = 257.2464
IYS = 1871.271
IZZ = 2194.726
IXZ = 0
KSTR = 14.3
KSCF = .00001
KSCB = 0
DLADV = 0
DYADV = 0
DNADV = 0
DENSITY = .002377
REFAREA = 20.58997
CDX = .40
AEROVEL = 44
KTL =  1.2
KSF = 1080
KSDF = 123.2497
KSR = 1260
KSDR = 115.0774
TRWF = 4.9
TRWB = 4.87
HCG = 1.8375
KBS = 2160
HBS = .25
KTSF = -30207.35
KTSR = 3705.587
KRAS = 12000
KRADP = 700
TSPRINGR = 13516.46
HRAF = 0
HRAR = 1.35
HS = 1.96697
IXUF = 34.17246
IXUR = 33.7553
KLT = 1.923581E-04
XACC = -2.33
ZACC = 1.05
DRAGC = -.015
LENS = 6.2
LM = 1.125
KBTF = 1
KVB = 1
KMB = 1
FBPVL = 1
SWZ = .99
SWW = 40
KCF = -.00003
LSO = .15
KLAGV = 16.5
```

b) Suspension Parameters

```
SUSPENSIONF$ = INDEPENDENT
SUSPENSIONR$ = SOLID AXLE
HF = 0
HR =  .1
LF = 1
LR = 1.5
KSAF = 0
KSAR = 1
BF = 0
BR = 0
CF = 0
CR = 0
DF =  -.125
DR = 0
EF = 0
ER = 0
KSLF =  .12
KSLR = 0
LSAF =  1.15
LSAR =  1000
KSADF =  0
KSADR =  .1035
KSAD2F = 0
KSAD2R = 0
KACK = 0
```

c) Tire Parameters

```
TWIDTH = 6.5
KA0 = 733
KA1 = 19.5
KA2 = 2900
KA3 = 1.37
KA4 = 4420
KA = .05
KMU = .234
TPRESS = 30
KB1 = -.00025
KB3 = 1.2
KB4 = 3.2E-08
KGAMMA = .9
CSFZ = 12
MUNOM = .85
FZTRL = 1444
KK1 = -.0002
RR = 1
TIRE = BIAS
C1 = .535
C2 = 1.05
C3 = 1.15
C4 = .8
G1 = 1
G2 = 1
```

TABLE E-5. (Continued)

VDANL Simulation Parameter Files: Vehicle #17

a) Vehicle Parameters

```
MASS = 125
SMASS = 110
UMASSF = 6
UMASSR = 9
LENA = 4.1
LENB = 5.57
IXS = 320
IYS = 2600
IZZ = 3000
IXZ = 0
KSTR = 15.25
KSCF = .000123
KSCB = 0
DLADV = 0
DYADV = 0
DNADV = 0
DENSITY = .00237
REFAREA = 24
CDX = .44
AEROVEL = 44
KTL =  .66
KSF = 1500
KSDF = 120
KSR = 1500
KSDR = 120
TRWF = 5.15
TRWB = 5.06
HCG = 1.83
KBS = 3000
HBS = .25
KTSF = -28300
KTSR = 6900
KRAS = 12000
KRADP = 700
TSPRINGR = 15000
HRAF = 0
HRAR = 1.48
HS = 1.94
IXUF = 39
IXUR = 39
KLT = .00015
XACC = -1.43
ZACC = .6
DRAGC = -.015
LENS = 7.02
LM = 1.125
KBTF = -1.525
KVB = 23.5
KMB = 9.4
KBPVL = 55
SWZ = .5
SWW = 70
KCF = 0
LSO = 0
KLAGV = 25
```

b) Suspension Parameters

```
SUSPENSIONF =  INDEPENDENT
SUSPENSIONR =  SOLID AXLE
HF =  0
HR =  .07
LF =  1
LR =  1.79
KSAF =  0
KSAR =  1
BF = 0
BR = 0
CF = 0
CR = 0
DF = 0
DR = 0
EF = 0
ER = 0
KSLF =  .034
KSLR = 0
LSAF =  100
LSAR =  1000
KSADF =  .175
KSADR =  .175
KSAD2F = 0
KSAD2R = 0
KACK =  -.266
```

c) Tire Parameters

```
TWIDTH = 8
KA0 = 5000
KA1 = 6.4
KA2 = 3700
KA3 = .353
KA4 = -2630
KA = .05
KMU = .234
TPRESS = 30
KB1 = -.000135
KB3 = 1.09
KB4 = 1E-08
KGAMMA = .9
CSFZ = 13
MUNOM = .92
FZTRL = 1600
KK1 = -.000215
RR = 1.05
TIRE = RADIAL
C1 = 1
C2 = .34
C3 = .57
C4 = .32
G1 = 1
G2 = 1
```

TABLE E-5. (Continued)

VDANL Simulation Parameter Files: Vehicle #18

a) Vehicle Parameters

```
MASS = 121
SMASS = 109
UMASSF = 6
UMASSR = 6
LENA = 4.05
LENB = 5.85
IXS =  370
IYS = 2540
IZZ = 3000
IXZ = 0
KSTR = 17.5
KSCF = .00005
KSCB = 0
DLADV = 0
DYADV = 0
DNADV = 0
DENSITY = .00237
REFAREA = 25
CDX = 0
AEROVEL = 44
KTL = 1
KSF = 1850
KSDF = 148
KSR = 1700
KSDR = 115
TRWF = 5
TRWB = 5.15
HCG = 2.21
KBS = 3500
HBS = .25
KTSF = -17900
KTSR = 2850
KRAS = 12000
KRADP = 700
TSPRINGR = 14000
HRAF = 0
HRAR = .92
HS = 2.37
IXUF = 37.5
IXUR = 37.5
KLT = .00015
XACC = -.85
ZACC = 1.04
DRAGC = 0
LENS = 5.5
LM = 1.125
KBTF = -.935
KVB = 30
KMB = 0
KBPVL = 100
SWZ = 0.5
SWW = 100
KCF = 0
LSO = 0
KLAGV = 25
```

b) Suspension Parameters

```
SUSPENSIONF =  INDEPENDENT
SUSPENSIONR = SOLID AXLE
HF =  0
HR =  .05
LF =  1
LR =  1.5
KSAF =  0
KSAR = 1
BF = 0
BR = 0
CF = 0
CR = 0
DF =  -.11
DR = 0
EF = 0
ER = 0
KSLF =  .1
KSLR = 0
LSAF =  1.08
LSAR = 1000
KSADF = 0
KSADR = 0
KSAD2F = 0
KSAD2R = 0
KACK =  .256
```

c) Tire Parameters

```
TWIDTH = 8
KA0 = 516
KA1 = 16.7
KA2 = 3600
KA3 = .368
KA4 = -11300
KA = .05
KMU = .234
TPRESS = 35
KB1 = -.00013
KB3 = 1.1
KB4 = -4E-09
KGAMMA = .9
CSFZ = 18
MUNOM = .92
FZTRL = 1400
KK1 = -.00019
RR = .98
TIRE = BIAS
C1 = .535
C2 = 1.05
C3 = 1.15
C4 = .8
G1 = 1
G2 = 1
```

TABLE E-5. (Continued)

VDANL Simulation Parameter Files: Vehicle #19

a) Vehicle Parameters

```
MASS = 120
SMASS = 105
UMASSF = 6
UMASSR = 9
LENA = 3.93
LENB = 5.99
IXS = 355
IYS = 1900
IZZ = 2300
IXZ = 0
KSTR = 18.46
KSCF = .00005
KSCB = 0
DLADV = 0
DYADV = 0
DNADV = 0
DENSITY = .00237
REFAREA = 30
CDX = .39
AEROVEL = 44
KTL =  1.4
KSF = 2000
KSDF = 150
KSR = 2000
KSDR = 120
TRWF = 5.11
TRWB = 5.02
HCG = 2.28
KBS = 4000
HBS = .25
KTSF = -11300
KTSR = 12600
KRAS = 12000
KRADP = 700
TSPRINGR = 16000
HRAF = 0
HRAR = 1.27
HS = 2.46
IXUF = 37.5
IXUR = 37.5
KLT = .00015
XACC = -.75
ZACC = 1.38
DRAGC = -.015
LENS = 4.54
LM = 1.125
KBTF =  -.835
KVB =  19
KMB =  3.75
KBPVL =  60
SWZ = 0.5
SWW = 100
KCF = -.00004
LSO = 0
KLAGV = 25
```

b) Suspension Parameters

```
SUSPENSIONF = INDEPENDENT
SUSPENSIONR = SOLID AXLE
HF = 0
HR =  .2
LF = 1
LR = 1.5
KSAF = 0
KSAR = 1
BF = 0
BR = 0
CF = 0
CR = 0
DF =  -.13
DR = 0
EF = 0
ER = 0
KSLF =  .2
KSLR = 0
LSAF =  4
LSAR = 1000
KSADF =  .09
KSADR =  .13
KSAD2F = 0
KSAD2R =  .13
KACK =  0
```

c) Tire Parameters

```
TWIDTH = 7
KA0 = 0
KA1 = 17.92
KA2 = 2886
KA3 = .45
KA4 = -11464
KA = .05
KMU = .234
TPRESS = 33
KB1 = -.000068
KB3 = .965
KB4 = -7E-09
KGAMMA = .9
CSFZ = 18
MUNOM = .92
FZTRL = 1554
KK1 = -.00016
RR = .99
TIRE = BIAS
C1 = .535
C2 = 1.05
C3 = 1.15
C4 = .8
G1 = 1
G2 = 1
```

TABLE E-5. (Continued)

VDANL Simulation Parameter Files: Vehicle #20

a) Vehicle Parameters

```
MASS = 99.62698
SMASS = 86.17361
UMASSF = 5.483214
UMASSR = 7.970159
LENA = 2.821635
LENB = 4.498364
IXS = 298.5419
IYS = 1389.698
IZZ = 1603.45
IXZ = 0
KSTR = 21.3
KSCF = .00002
KSCB = 0
DLADV = 0
DYADV = 0
DNADV = 0
DENSITY = .002377
REFAREA = 24.35355
CDX = .5
AEROVEL = 80
KTL = 1
KSF = 3125
KSDF = 201.3571
KSR = 3458
KSDR = 191.7209
TRWF = 4.72
TRWB = 4.54
HCG = 2.023631
KBS = 6250
HBS = .25
KTSF = -13566.39
KTSR = 8884.749
KRAS = 12000
KRADP = 700
TSPRINGR = 14973.6
HRAF = 0
HRAR = .9
HS = 2.186718
IXUF = 30.53931
IXUR = 28.25446
KLT = 1.736389E-04
XACC = 0
ZACC = 0
DRAGC = -.015
LENS = 0
LM =  1
KBTF =  1
KVB =  1
KMB =  1
FBPVL =  1
SWZ = .5
SWW = 70
KCF = 0
LSO = .12
KLAGV = 16.5
```

b) Suspension Parameters

```
SUSPF=INDEPENDENT
SUSPR=SOLID AXLE
HF=0
HR=0
LF=1
LR=1.35
KSAF=0
KSAR=1
BF=0
BR=0
CF=0
CR=0
DF=0
DR=0
EF=0
ER=0
KSLF=0
KSLR=0
LSAF=1000
LSAR=1000
KSADF=0
KSADR=.09
KSAD2F=0
KSAD2R=0
KACK=.09
```

c) Tire Parameters

```
TWIDTH = 5
KA0 = 2380
KA1 = 8.03
KA2 = 3730
KA3 = .525
KA4 = -6920
KA = .05
KMU = .234
TPRESS = 35
KB1 = -.000158
KB3 = 1.04
KB4 = 2.85E-08
KGAMMA = 0.9
CSFZ = 14.15
MUNOM = .85
FZTRL = 1400
KK1 = -.000219
RR = .979
TIRE = RADIAL
C1 = 1
C2 = .34
C3 = .57
C4 = .32
G1 = 1
G2 = 1
```

TABLE E-5. (Continued)

VDANL Simulation Parameter Files: Vehicle #21

a) Vehicle Parameters

```
MASS = 101.3367
SMASS = 90.21635
UMASSF = 5.56015
UMASSR = 5.56015
LENA = 3.775563
LENB = 4.334437
IXS = 353.9445
IYS = 1625.825
IZZ = 1824.078
IXZ = 0
KSTR = 20
KSCF = .000043
KSCB = 0
DLADV = 0
DYADV = 0
DNADV = 0
DENSITY = .002377
REFAREA = 28.33057
CDX = .5
AEROVEL = 80
KTL = 1
KSF = 2300
KSDF = 164.8335
KSR = 2680
KSDR = 189.7866
TRWF = 5.165
TRWB = 5.065
HCG = 2.453467
KBS = 4600
HBS = .25
KTSF = -25038.92
KTSR = -5702.369
KRAS = 12000
KRADP = 700
TSPRINGR = 14565.6
HRAF = 0
HRAR = 0
HS = 2.639405
IXUF = 37.08234
IXUR = 35.66033
KLT = 1.785028E-04
XACC = 0
ZACC = 0
DRAGC = -.015
LENS = 0
LM = 0
KBTF = 0
KVB = 0
KMB = 0
FBPVL = 0
SWZ = .5
SWW = 70
KCF = 0
LSO = 0
KLAGV = 16.5
```

b) Suspension Parameters

```
SUSPENSIONF$ = INDEPENDENT
SUSPENSIONR$ = INDEPENDENT
HF = 0
HR = 0
LF = 1
LR = 1
KSAF = 0
KSAR = 0
BF = 0
BR = 0
CF = 0
CR = 0
DF = 0
DR = 0
EF = 0
ER = 0
KSLF = .21
KSLR = 0
LSAF = 1000
LSAR = 1000
KSADF = 0
KSADR = .58
KSAD2F = 0
KSAD2R = 0
KACK = 0
```

c) Tire Parameters

```
TWIDTH = 4.75
KA0 = 1580
KA1 = 11.9
KA2 = 3030
KA3 = .264
KA4 = -1770
KA = .05
KMU = .234
TPRESS = 44
KB1 = -.000114
KB3 = 1.01
KB4 = 1.06E-09
KGAMMA = 0.9
CSFZ = 18.4
MUNOM = .85
FZTRL = 1160
KK1 = -.00026
RR = .945
TIRE = RADIAL
C1 = 1
C2 = .34
C3 = .57
C4 = .32
G1 = 1
G2 = 1
```

TABLE E-5. (Continued)

VDANL Simulation Parameter Files: Vehicle #22

a) Vehicle Parameters

```
MASS = 147.3423
SMASS = 127.9245
UMASSF = 7.630402
UMASSR = 11.78738
LENA = 4.531688
LENB = 5.882312
IXS = 601.2608
IYS = 3093.382
IZZ = 3667.009
IXZ = 0
KSTR = 18.75
KSCF = .000075
KSCB = 0
DLADV = 0
DYADV = 0
DNADV = 0
DENSITY = .002377
REFAREA = 32.6652
CDX = .5
AEROVEL = 80
KTL = 1
KSF = 3375
KSDF = 244.4342
KSR = 3500
KSDR = 249.6934
TRWF = 5.775
TRWB = 5.64
HCG = 2.613196
KBS = 6750
HBS = .25
KTSF = -272.6622
KTSR = 15350.11
KRAS = 12000
KRADP = 700
TSPRINGR = 16687.2
HRAF = 0
HRAR = 0
HS = 2.844403
IXUF = 63.61967
IXUR = 60.68
KLT = 1.55808E-04
XACC = 0
ZACC = 0
DRAGC = -.015
LENS = 0
LM = 0
KBTF = 0
KVB = 0
KMB = 0
FBPVL = 0
SWZ = .5
SWW = 70
KCF = 0
LSO = 0
KLAGV = 16.5
```

b) Suspension Parameters

```
SUSPENSIONF$ = INDEPENDENT
SUSPENSIONR$ = SOLID AXLE
HF = 0
HR = 0
LF = 1
LR = 1.4
KSAF = 0
KSAR = 1
BF = 0
BR = 0
CF = 0
CR = 0
DF = 0
DR = 0
EF = 0
ER = 0
KSLF = .086
KSLR = 0
LSAF = 1000
LSAR = 1000
KSADF = 0
KSADR = 0
KSAD2F = 0
KSAD2R = 0
KACK = 0
```

c) Tire Parameters

```
TWIDTH = 8
KA0 = 0
KA1 = 18.96
KA2 = 3438
KA3 = .449
KA4 = -11464
KA = .05
KMU = .234
TPRESS = 35
KB1 = -.00008
KB3 = 1.03
KB4 = 0
KGAMMA = 0.9
CSFZ = 16
MUNOM = .92
FZTRL = 2017
KK1 = -.00016
RR = 1.09
TIRE = RADIAL
C1 = 1
C2 = .34
C3 = .57
C4 = .32
G1 = 1
G2 = 1
```

TABLE E-5. (Continued)

VDANL Simulation Parameter Files: Vehicle #23

a) Vehicle Parameters

```
MASS =  113
SMASS =  95
UMASSF =  9
UMASSR =  9
LENA =  4.05
LENB =  5.18
IXS =  250
IYS =  1700
IZZ = 2100
IXZ = 0
KSTR =  22.3
KSCF =  .00024
KSCB = 0
DLADV = 0
DYADV = 0
DNADV = 0
DENSITY = .00237
REFAREA = 22
CDX = .5
AEROVEL = 44
KTL = 1.4
KSF =  3300
KSDF =  180
KSR =  3300
KSDR =  160
TRWF =  4.67
TRWB =  4.56
HCG =  2.12
KBS =  6600
HBS =  .2
KTSF =  14000
KTSR =  16400
KRAS = 12000
KRADP = 700
TSPRINGR =  20000
HRAF =  1.5
HRAR =  1.5
HS =  2.29
IXUF =  38
IXUR =  36
KLT =  .00016
XACC =  -2.1
ZACC =  1.83
DRAGC = -.015
LENS =  6.4
LM = 1.125
KBTF = -1.2
KVB = 26.3
KMB = 0
KBPVL = 100
SWZ = 0.5
SWW =  44
KCF =  0
LSO = 0
KLAGV = 25
```

b) Suspension Parameters

```
SUSPENSIONF =  SOLID AXLE
SUSPENSIONR = SOLID AXLE
HF = 0
HR = 0
LF =  -1.4
LR =  1.3
KSAF =  1
KSAR = 1
BF = 0
BR = 0
CF = 0
CR = 0
DF = 0
DR = 0
EF = 0
ER = 0
KSLF =  0
KSLR = 0
LSAF = 1000
LSAR = 1000
KSADF =  0
KSADR = 0
KSAD2F = 0
KSAD2R = 0
KACK =  .25
```

c) Tire Parameters

```
TWIDTH = 8
KA0 = 0
KA1 = 15.52
KA2 = 6787
KA3 = 1.11
KA4 = 1000000
KA = .05
KMU = .234
TPRESS = 30
KB1 = -.000061
KB3 = 1.01
KB4 = 0
KGAMMA = .9
CSFZ = 16
MUNOM = .92
FZTRL = 2180
KK1 = -.00016
RR = 1.2
TIRE = BIAS
C1 = .535
C2 = 1.05
C3 = 1.15
C4 = .8
G1 = 1
G2 = 1
```

TABLE E-5. (Continued)

VDANL Simulation Parameter Files: Vehicle #24

a) Vehicle Parameters

```
MASS = 91.54492
SMASS = 79.10181
UMASSF = 5.119522
UMASSR = 7.323594
LENA = 3.794925
LENB = 6.015076
IXS = 216.6107
IYS = 1761.502
IZZ = 2124.01
IXZ = 0
KSTR = 20.25
KSCF = .000033
KSCB = 0
DLADV = 0
DYADV = 0
DNADV = 0
DENSITY = .002377
REFAREA = 20.223
CDX = .5
AEROVEL = 80
KTL = 1
KSF = 2150
KSDF = 159.8385
KSR = 2125
KSDR = 144.2496
TRWF = 4.535
TRWB = 4.52
HCG = 1.769614
KBS = 4300
HBS = .25
KTSF = 2109.739
KTSR = 6296.805
KRAS = 12000
KRADP = 700
TSPRINGR = 14973.6
HRAF = 0
HRAR =  0
HS = 1.892251
IXUF = 26.32231
IXUR = 26.14847
KLT = 1.736389E-04
XACC = 0
ZACC = 0
DRAGC = -.015
LENS = 0
LM = 0
KBTF = 0
KVB = 0
KMB = 0
FBPVL = 0
SWZ = .5
SWW = 70
KCF = 0
LSO = 0
KLAGV = 16.5
```

b) Suspension Parameters

```
SUSPENSIONF$ = INDEPENDENT
SUSPENSIONR$ = SOLID AXLE
HF = 0
HR = 0
LF = 1
LR = 1.5
KSAF = 0
KSAR = 1
BF = 0
BR = 0
CF = 0
CR = 0
DF = 0
DR = 0
EF = 0
ER = 0
KSLF = .13
KSLR = 0
LSAF =  1000
LSAR =  1000
KSADF =  0
KSADR =  0
KSAD2F = 0
KSAD2R = 0
KACK = .094
```

c) Tire Parameters

```
TWIDTH = 8
KA0 = 516
KA1 = 16.7
KA2 = 3600
KA3 = .368
KA4 = -11300
KA = .05
KMU = .234
TPRESS = 35
KB1 = -.00013
KB3 = 1.053
KB4 = -4E-09
KRAD = 0
CSFZ = 6
MUNOM = .92
FZTRL = 1400
KK1 = -.00019
RR = .99
TIRE = RADIAL
C1 = 1
C2 = .34
C3 = .57
C4 = .32
G1 = 1
G2 = 1
```

TABLE E-5. (Continued)

VDANL Simulation Parameter Files: Vehicle #25

a) Vehicle Parameters

```
MASS = 111.9055
SMASS = 96.91732
UMASSF = 6.035748
UMASSR = 8.95244
LENA = 3.726218
LENB = 6.536781
IXS = 270.0817
IYS = 2170.25
IZZ = 2677.535
IXZ = 0
KSTR = 15.6
KSCF = .000025
KSCB = 0
DLADV = 0
DYADV = 0
DNADV = 0
DENSITY = .002377
REFAREA = 20.94825
CDX = .5
AEROVEL = 80
KTL = 1
KSF = 3125
KSDF = 217.397
KSR = 2200
KSDR = 157.3925
TRWF = 4.78
TRWB = 4.625
HCG = 1.899501
KBS = 6250
HBS = .25
KTSF = -15260.01
KTSR = 3454.243
KRAS = 12000
KRADP = 700
TSPRINGR = 16279.2
HRAF = 0
HRAR = 0
HS = 2.027009
IXUF = 34.4768
IXUR = 32.27711
KLT = 1.59713E-04
XACC = 0
ZACC = 0
DRAGC = -.015
LENS = 0
LM = 0
KBTF = 0
KVB = 0
KMB = 0
FBPVL = 0
SWZ = .5
SWW = 70
KCF = 0
LSO = 0
KLAGV = 16.5
```

b) Suspension Parameters

```
SUSPENSIONF$ = INDEPENDENT
SUSPENSIONR$ = SOLID AXLE
HF = 0
HR = 0
LF = 1
LR = 1.7
KSAF = 0
KSAR = 1
BF = 0
BR = 0
CF = 0
CR = 0
DF = 0
DR = 0
EF = 0
ER = 0
KSLF = .07
KSLR = 0
LSAF = 1000
LSAR = 1000
KSADF = 0
KSADR = 0
KSAD2F = 0
KSAD2R = 0
KACK = -.123
```

c) Tire Parameters

```
TWIDTH = 6
KA0 = 2430
KA1 = 9.51
KA2 = 4040
KA3 = .449
KA4 = -11500
KA = .05
KMU = .234
TPRESS = 35
KB1 = -.0000677
KB3 = .965
KB4 = -7.15E-09
KGAMMA = 0.9
CSFZ = 3.79
MUNOM = .85
FZTRL = 1550
KK1 = -.000161
RR = 1.075
TIRE = RADIAL
C1 = 1
C2 = .34
C3 = .57
C4 = .32
G1 = 1
G2 = 1
```

TABLE E-5. (Continued)

VDANL Simulation Parameter Files: Vehicle #26

a) Vehicle Parameters

```
MASS = 92.32204
SMASS = 79.78179
UMASSF = 5.154492
UMASSR = 7.385763
LENA = 3.749294
LENB = 5.755707
IXS = 254.4183
IYS = 1670.093
IZZ = 1995.006
IXZ = 0
KSTR = 19.3
KSCF = .000065
KSCB = 0
DLADV = 0
DYADV = 0
DNADV = 0
DENSITY = .002377
REFAREA = 24.14745
CDX = .5
AEROVEL = 80
KTL = 1
KSF = 1800
KSDF = 145.9636
KSR = 1800
KSDR = 134.6362
TRWF = 4.57
TRWB = 4.505
HCG = 2.009783
KBS = 3600
HBS = .25
KTSF = -2554.108
KTSR = 7769.431
KRAS = 12000
KRADP = 700
TSPRINGR = 15769.2
HRAF = 0
HRAR = 1.4
HS = 2.167717
IXUF = 26.91277
IXUR = 26.15264
KLT = 1.648784E-04
XACC = 0
ZACC = 0
DRAGC = -.015
LENS = 0
LM =  1
KBTF =  1
KVB =  1
KMB =  1
FBPVL =  1
SWZ = .5
SWW = 70
KCF = 0
LSO = .25
KLAGV = 16.5
```

b) Suspension Parameters

```
SUSPF=INDEPENDENT
SUSPR=SOLID AXLE
HF=0
HR=0
LF=1
LR=1.65
KSAF=0
KSAR=1
BF=0
BR=0
CF=0
CR=0
DF=-.323
DR=0
EF=0
ER=0
KSLF=.329
KSLR=0
LSAF=2.81
LSAR=1000
KSADF=.525
KSADR=.09
KSAD2F=0
KSAD2R=0
KACK=.05
```

c) Tire Parameters

```
TWIDTH = 6
KA0 = 2430
KA1 = 9.51
KA2 = 4040
KA3 = .449
KA4 = -11500
KA = .05
KMU = .234
TPRESS = 30
KB1 = -.0000677
KB3 = .965
KB4 = -7.15E-09
KGAMMA = 0.9
CSFZ = 3.79
MUNOM = .85
FZTRL = 1550
KK1 = -.000161
RR = 1.005
TIRE = RADIAL
C1 = 1
C2 = .34
C3 = .57
C4 = .32
G1 = 1
G2 = 1
```

TABLE E-5. (Continued)

VDANL Simulation Parameter Files: Vehicle #27

a) Vehicle Parameters

```
MASS = 110.1958
SMASS = 95.42136
UMASSF = 5.958813
UMASSR = 8.815667
LENA = 3.52429
LENB = 5.995711
IXS = 284.9391
IYS = 2012.561
IZZ = 2416.096
IXZ = 0
KSTR = 19.2
KSCF = .00008
KSCB = 0
DLADV = 0
DYADV = 0
DNADV = 0
DENSITY = .002377
REFAREA = 22.73926
CDX = .5
AEROVEL = 80
KTL = 1
KSF = 3250
KSDF = 218.7507
KSR = 2220
KSDR = 158.4133
TRWF = 4.8
TRWB = 4.71
HCG = 2.277919
KBS = 6500
HBS = .25
KTSF = -20060.65
KTSR = 2638.884
KRAS = 12000
KRADP = 700
TSPRINGR = 17085
HRAF = 0
HRAR = 0
HS = 2.452559
IXUF = 34.32277
IXUR = 33.04773
KLT = 1.521803E-04
XACC = 0
ZACC = 0
DRAGC = -.015
LENS = 0
LM = 0
KBTF = 0
KVB = 0
KMB = 0
FBPVL = 0
SWZ = .5
SWW = 70
KCF = 0
LSO = 0
KLAGV = 16.5
```

b) Suspension Parameters

```
SUSPENSIONF$ = INDEPENDENT
SUSPENSIONR$ = SOLID AXLE
HF = 0
HR = 0
LF = 1
LR = 1.3
KSAF = 0
KSAR = 1
BF = 0
BR = 0
CF = 0
CR = 0
DF = -.33
DR = 0
EF = 0
ER = 0
KSLF = .371
KSLR = 0
LSAF = 2.11
LSAR = 1000
KSADF = .64
KSADR = 0
KSAD2F = 0
KSAD2R = 0
KACK = 0
```

c) Tire Parameters

```
TWIDTH = 5
KA0 = 4910
KA1 = 7.28
KA2 = 4360
KA3 = .439
KA4 = -6400
KA = .05
KMU = .234
TPRESS = 35
KB1 = -.0000191
KB3 = .953
KB4 = -1.72E-08
KGAMMA = 0.9
CSFZ = 14.5
MUNOM = .92
FZTRL = 2000
KK1 = -.000193
RR = 1.15
TIRE = RADIAL
C1 = 1
C2 = .34
C3 = .57
C4 = .32
G1 = 1
G2 = 1
```

TABLE E-5. (Continued)

VDANL Simulation Parameter Files: Vehicle #28

a) Vehicle Parameters

```
MASS = 80.97607
SMASS = 69.85406
UMASSF = 4.643923
UMASSR = 6.478085
LENA = 3.395236
LENB = 5.067264
IXS = 185.6283
IYS = 1155.531
IZZ = 1383.803
IXZ = 0
KSTR = 21.8
KSCF = .000087
KSCB = 0
DLADV = 0
DYADV = 0
DNADV = 0
DENSITY = .002377
REFAREA = 19.73943
CDX = .5
AEROVEL = 80
KTL = 1
KSF = 2560
KSDF = 161.9706
KSR = 1900
KSDR = 130.5369
TRWF = 4.335
TRWB = 4.41
HCG = 1.737139
KBS = 5120
HBS = .25
KTSF = -9163.24
KTSR = 1950.974
KRAS = 12000
KRADP = 700
TSPRINGR = 13690.15
HRAF = 0
HRAR = 0
HS = 1.8596
IXUF = 21.81741
IXUR = 22.57887
KLT = 1.899176E-04
XACC = 0
ZACC = 0
DRAGC = -.015
LENS = 0
LM = 0
KBTF = 0
KVB = 0
KMB = 0
FBPVL = 0
SWZ = .5
SWW = 70
KCF = 0
LSO = 0
KLAGV = 16.5
```

b) Suspension Parameters

```
SUSPENSIONF$ = INDEPENDENT
SUSPENSIONR$ = SOLID AXLE
HF = 0
HR = 0
LF = 1
LR = 1.4
KSAF = 0
KSAR = 1
BF = 0
BR = 0
CF = 0
CR = 0
DF = 0
DR = 0
EF = 0
ER = 0
KSLF = .19
KSLR = 0
LSAF = 1000
LSAR = 1000
KSADF = 0
KSADR = 0
KSAD2F = 0
KSAD2R = 0
KACK = .12
```

c) Tire Parameters

```
TWIDTH = 5
KA0 = 2380
KA1 = 8.03
KA2 = 3730
KA3 = .525
KA4 = -6920
KA = .05
KMU = .234
TPRESS = 28
KB1 = -.000158
KB3 = 1.04
KB4 = 2.85E-08
KGAMMA = 0.9
CSFZ = 14.15
MUNOM = .85
FZTRL = 1400
KK1 = -.000219
RR = .968
TIRE = RADIAL
C1 = 1
C2 = .34
C3 = .57
C4 = .32
G1 = 1
G2 = 1
```

VDANL Simulation Parameter Files: Vehicle #29

a) Vehicle Parameters

```
MASS = 120.4538
SMASS = 104.3971
UMASSF = 6.420423
UMASSR = 9.636307
LENA = 3.778709
LENB = 5.908791
IXS = 311.9449
IYS = 2252.422
IZZ = 2699.906
IXZ = 0
KSTR = 19
KSCF = .00006
KSCB = 0
DLADV = 0
DYADV = 0
DNADV = 0
DENSITY = .002377
REFAREA = 22.79454
CDX = .5
AEROVEL = 80
KTL = 1
KSF = 2080
KSDF = 180.1368
KSR = 2375
KSDR = 175.9207
TRWF = 5.015
TRWB = 4.927
HCG = 2.205
KBS = 4160
HBS = .25
KTSF = -13183.74
KTSR = 11115.08
KRAS = 12000
KRADP = 700
TSPRINGR = 13638.86
HRAF = 0
HRAR = 1.58
HS = 2.362265
IXUF = 40.36877
IXUR = 38.96447
KLT = 1.906318E-04
XACC = 0
ZACC = 0
DRAGC = -.015
LENS = 0
LM = 1
KBTF = 1
KVB = 1
KMB = 1
FBPVL = 1
SWZ = .5
SWW = 70
KCF = 0
LSO = .18
KLAGV = 16.5
```

b) Suspension Parameters

```
SUSPENSIONF$ = INDEPENDENT
SUSPENSIONR$ = SOLID AXLE
HF = 0
HR = 0
LF = 1
LR = 1.3
KSAF = 0
KSAR = 1
BF = 0
BR = 0
CF = 0
CR = 0
DF = 0
DR = 0
EF = 0
ER = 0
KSLF = .083
KSLR = 0
LSAF =  1000
LSAR =  1000
KSADF =  0
KSADR =  0
KSAD2F = 0
KSAD2R = 0
KACK = .09
```

c) Tire Parameters

```
TWIDTH = 8
KA0 = 0
KA1 = 15.52
KA2 = 6787
KA3 = 1.11
KA4 = 1000000
KA = .05
KMU = .234
TPRESS = 26
KB1 = -.000061
KB3 = 1.01
KB4 = 0
KGAMMA = 0.9
CSFZ = 16
MUNOM = .92
FZTRL = 2180
KK1 = -.00016
RR = 1.1825
TIRE = RADIAL
C1 = 1
C2 = .34
C3 = .57
C4 = .32
G1 = 1
G2 = 1
```

TABLE E-5. (Continued)

VDANL Simulation Parameter Files: Vehicle #30

a) Vehicle Parameters

```
MASS = 135.53
SMASS = 117.5887
UMASSF = 7.09885
UMASSR = 10.8424
LENA = 4.214923
LENB = 6.772078
IXS = 470.6809
IYS = 3124.208
IZZ = 3779.589
IXZ = 0
KSTR = 19.8
KSCF = .00002
KSCB = 0
DLADV = 0
DYADV = 0
DNADV = 0
DENSITY = .002377
REFAREA = 29.04525
CDX = .5
AEROVEL = 80
KTL = 1
KSF = 2300
KSDF = 202.093
KSR = 3300
KSDR = 218.258
TRWF = 5.41
TRWB = 5.3
HCG = 2.278697
KBS = 4600
HBS = .25
KTSF = -18240.35
KTSR = 21845.75
KRAS = 12000
KRADP = 700
TSPRINGR = 14679.26
HRAF = 0
HRAR = 1.7
HS = 2.453579
IXUF = 51.94246
IXUR = 49.85168
KLT = 1.771207E-04
XACC = 0
ZACC = 0
DRAGC = -.015
LENS = 0
LM =  1
KBTF =  1
KVB =  1
KMB =  1
FBPVL =  1
SWZ = .5
SWW = 70
KCF = 0
LSO = .2
KLAGV = 16.5
```

b) Suspension Parameters

```
SUSPF=INDEPENDENT
SUSPR=SOLID AXLE
HF=0
HR=0
LF=1
LR=1.6
KSAF=0
KSAR=1
BF=0
BR=0
CF=0
CR=0
DF=0
DR=0
EF=0
ER=0
KSLF=0
KSLR=0
LSAF=1000
LSAR=1000
KSADF=.158
KSADR=.05
KSAD2F=0
KSAD2R=0
KACK=.06
```

c) Tire Parameters

```
TWIDTH = 5.5
KA0 = 7780
KA1 = 4.56
KA2 = 3680
KA3 = .48
KA4 = -6720
KA = .05
KMU = .234
TPRESS = 30
KB1 = -.0000464
KB3 = .996
KB4 = -1.01E-08
KGAMMA = 0.9
CSFZ = 15.45
MUNOM = .85
FZTRL = 1870
KK1 = -.000218
RR = 1.13
TIRE = RADIAL
C1 = 1
C2 = .34
C3 = .57
C4 = .32
G1 = 1
G2 = 1
```

VDANL Simulation Parameter Files: Vehicle #31

a) Vehicle Parameters

```
MASS = 141.4361
SMASS = 122.7566
UMASSF = 7.364626
UMASSR = 11.31489
LENA = 4.49881
LENB = 6.46119
IXS = 506.5446
IYS = 3326.325
IZZ = 3970.962
IXZ = 0
KSTR = 19.75
KSCF = .000034
KSCB = 0
DLADV = 0
DYADV = 0
DNADV = 0
DENSITY = .002377
REFAREA = 30.2151
CDX = .5
AEROVEL = 80
KTL = 1
KSF = 2730
KSDF = 220.0076
KSR = 4500
KSDR = 269.3688
TRWF = 5.51
TRWB = 5.46
HCG = 2.346788
KBS = 5460
HBS = .25
KTSF = -6446.788
KTSR = 40187.51
KRAS = 12000
KRADP = 700
TSPRINGR = 23878.93
HRAF = 0
HRAR = 0
HS = 2.515205
IXUF = 55.8977
IXUR = 54.88782
KLT = 1.088826E-04
XACC = 0
ZACC = 0
DRAGC = -.015
LENS = 0
LM = 0
KBTF = 0
KVB = 0
KMB = 0
FBPVL = 0
SWZ = .5
SWW = 70
KCF = 0
LSO = 0
KLAGV = 16.5
```

b) Suspension Parameters

```
SUSPENSIONF$ = INDEPENDENT
SUSPENSIONR$ = SOLID AXLE
HF = 0
HR = 0
LF = 1
LR = 1.6
KSAF = 0
KSAR = 1
BF = 0
BR = 0
CF = 0
CR = 0
DF = 0
DR = 0
EF = 0
ER = 0
KSLF = .12
KSLR = 0
LSAF = 1000
LSAR = 1000
KSADF = 0
KSADR = 0
KSAD2F = 0
KSAD2R = 0
KACK = .16
```

c) Tire Parameters

```
TWIDTH = 8
KA0 = 0
KA1 = 15.5
KA2 = 6790
KA3 = 1.11
KA4 = 1000000
KA = .05
KMU = .234
TPRESS = 48
KB1 = -.000061
KB3 = 1.01
KB4 = 0
KGAMMA = 0.9
CSFZ = 16
MUNOM = .85
FZTRL = 2180
KK1 = -.00016
RR = 1.24
TIRE = RADIAL
C1 = 1
C2 = .34
C3 = .57
C4 = .32
G1 = 1
G2 = 1
```

TABLE E-5. (Continued)

VDANL Simulation Parameter Files: Vehicle #32

a) Vehicle Parameters

```
MASS = 142.6795
SMASS = 123.8446
UMASSF = 7.420578
UMASSR = 11.41436
LENA = 4.180522
LENB = 6.939477
IXS = 491.5912
IYS = 3293.281
IZZ = 3980.258
IXZ = 0
KSTR = 18.6
KSCF = .00007
KSCB = 0
DLADV = 0
DYADV = 0
DNADV = 0
DENSITY = .002377
REFAREA = 29.5113
CDX = .5
AEROVEL = 80
KTL = 1
KSF = 4060
KSDF = 277.2653
KSR = 2680
KSDR = 199.8222
TRWF = 5.5
TRWB = 5.42
HCG = 2.474967
KBS = 8120
HBS = .25
KTSF = 5306.113
KTSR = 12269.37
KRAS = 12000
KRADP = 700
TSPRINGR = 19933.71
HRAF = 0
HRAR =  0
HS = 2.668871
IXUF = 56.11813
IXUR = 54.49747
KLT = 1.304323E-04
XACC = 0
ZACC = 0
DRAGC = -.015
LENS = 0
LM = 0
KBTF = 0
KVB = 0
KMB = 0
FBPVL = 0
SWZ = .5
SWW = 70
KCF = 0
LSO = 0
KLAGV = 16.5
```

b) Suspension Parameters

```
SUSPENSIONF$ = INDEPENDENT
SUSPENSIONR$ = SOLID AXLE
HF = 0
HR = -.20
LF = 1
LR = 1.3
KSAF = 0
KSAR = 1
BF = 0
BR = 0
CF = 0
CR = 0
DF = -.30
DR = 0
EF = 0
ER = 0
KSLF = .374
KSLR = 0
LSAF =  2.42
LSAR =  1000
KSADF =  .64
KSADR =  0
KSAD2F = 0
KSAD2R = 0
KACK = 0
```

c) Tire Parameters

```
TWIDTH = 8
KA0 = 0
KA1 = 15.52
KA2 = 6787
KA3 = 1.11
KA4 = 1000000
KA = .05
KMU = .234
TPRESS = 38
KB1 = -.000061
KB3 = 1.01
KB4 = 0
KGAMMA = 0.9
CSFZ = 16
MUNOM = .92
FZTRL = 2180
KK1 = -.00016
RR = 1.2
TIRE = RADIAL
C1 = 1
C2 = .34
C3 = .57
C4 = .32
G1 = 1
G2 = 1
```

TABLE E-5. (Continued)

VDANL Simulation Parameter Files: Vehicle #33

a) Vehicle Parameters

```
MASS = 136.7734
SMASS = 118.6767
UMASSF = 7.154803
UMASSR = 10.94187
LENA = 4.689231
LENB = 6.409769
IXS = 450.7065
IYS = 3159.794
IZZ = 3799.516
IXZ = 0
KSTR = 19.3
KSCF = .00005
KSCB = 0
DLADV = 0
DYADV = 0
DNADV = 0
DENSITY = .002377
REFAREA = 28.40625
CDX = .5
AEROVEL = 80
KTL = 1
KSF = 3700
KSDF = 249.2562
KSR = 6600
KSDR = 325.4158
TRWF = 5.47
TRWB = 5.37
HCG = 2.405748
KBS = 7400
HBS = .25
KTSF = 13169
KTSR = 58691.05
KRAS = 12000
KRADP = 700
TSPRINGR = 18105
HRAF = 0
HRAR =  0
HS = 2.58656
IXUF = 53.51953
IXUR = 51.58058
KLT = 1.436067E-04
XACC = 0
ZACC = 0
DRAGC = -.015
LENS = 0
LM = 0
KBTF = 0
KVB = 0
KMB = 0
FBPVL = 0
SWZ = .5
SWW = 70
KCF = 0
LSO = 0
KLAGV = 16.5
```

b) Suspension Parameters

```
SUSPENSIONF$ = INDEPENDENT
SUSPENSIONR$ = SOLID AXLE
HF = 0
HR = -.1
LF = 1
LR = 1.5
KSAF = 0
KSAR = 1
BF = 0
BR = 0
CF = 0
CR = 0
DF = -.3
DR = 0
EF = 0
ER = 0
KSLF = .355
KSLR = 0
LSAF =  2.43
LSAR =  1000
KSADF =  .64
KSADR =  0
KSAD2F = 0
KSAD2R = 0
KACK = .10
```

c) Tire Parameters

```
TWIDTH = 8
KA0 = 0
KA1 = 15.5
KA2 = 6790
KA3 = 1.11
KA4 = 1000000
KA = .05
KMU = .234
TPRESS = 35
KB1 = -.000061
KB3 = 1.01
KB4 = 0
KGAMMA = 0.9
CSFZ = 16
MUNOM = .85
FZTRL = 2180
KK1 = -.00016
RR = 1.22
TIRE = RADIAL
C1 = 1
C2 = .34
C3 = .57
C4 = .32
G1 = 1
G2 = 1
```

TABLE E-5. (Continued)

VDANL Simulation Parameter Files: Vehicle #34

a) Vehicle Parameters

```
MASS = 72
SMASS = 59
UMASSF = 6.5
UMASSR = 6.5
LENA = 3.33
LENB = 3.33
IXS = 200
IYS = 790
IZZ = 720
IXZ = 0
KSTR = 18.75
KSCF = .001
KSCB = 0
DLADV = 0
DYADV = 0
DNADV = 0
DENSITY = .00237
REFAREA = 20
CDX = .65
AEROVEL = 44
KTL =  2.8
KSF = 3000
KSDF = 180
KSR = 2400
KSDR = 180
TRWF = 4.3
TRWB = 4.3
HCG = 2.05
KBS = 5000
HBS = .2
KTSF = 8400
KTSR = 6400
KRAS = 12000
KRADP = 700
TSPRINGR = 10000
HRAF = .88
HRAR = 1.02
HS = 2.26
IXUF = 20
IXUR = 20
KLT = .00020
XACC = -1.75
ZACC = 1.0
DRAGC = -.015
LENS = 4.3
LM = 1.17
KBTF = -.77
KVB = 21
KMB = 8.6
KBPVL = 48
SWZ = .5
SWW =  44
KCF = 0
SSL = .01
```

b) Suspension Parameters

```
SUSPENSIONF=SOLID AXLE
SUSPENSIONR=SOLID AXLE
HF = -.03
HR = .025
LF = -1.1
LR = 1.1
KSAF = 1
KSAR = 1
BF = 0
BR= 0
CF=0
CR= 0
DF= 0
DR= 0
EF= 0
ER= 0
KSLF= 0
KSLR= 0
LSAF= 1000
LSAR= 1000
KSADF= 0
KSADR= 0
KSAD2F=0
KSAD2R=0
KACK=.32
```

c) Tire Parameters

```
TWIDTH = 8
KA0 = -668
KA1 = 26.5
KA2 = 2147
KA3 = 1.27
KA4 = 2225
KA = .05
KMU = .234
TPRESS = 25
KB1 = -.000675
KB3 = 1.31
KB4 = 2.95E-07
KGAMMA = .9
CSFZ = 11
MUNOM = .85
FZTRL = 1000
KK1 = -.0002
RR = 1
TIRE = RADIAL
C1 = 1
C2 = .34
C3 = .57
C4 = .32
G1 = 1
G2 = 1
```

TABLE E-5. (Continued)

VDANL Simulation Parameter Files: Vehicle #35

a) Vehicle Parameters

```
MASS = 96.67393
SMASS = 81.2061
UMASSF = 7.733914
UMASSR = 7.733914
LENA = 3.755985
LENB = 4.024015
IXS = 241.198
IYS = 1150.512
IZZ = 1387.266
IXZ = 0
KSTR = 22.2
KSCF = .00009
KSCB = 0
DLADV = 0
DYADV = 0
DNADV = 0
DENSITY = .002377
REFAREA = 22.38638
CDX = .5
AEROVEL = 80
KTL = 1
KSF = 3050
KSDF = 177.1606
KSR = 2800
KSDR = 187.422
TRWF = 4.81
TRWB = 4.78
HCG = 2.142581
KBS = 6100
HBS = .25
KTSF = 5395.768
KTSR = 13843.1
KRAS = 12000
KRADP = 700
TSPRINGR = 18360
HRAF = 0
HRAR = 0
HS = 2.311644
IXUF = 30.94642
IXUR = 30.56161
KLT = 1.416122E-04
XACC = 0
ZACC = 0
DRAGC = -.015
LENS = 0
LM = 0
KBTF = 0
KVB = 0
KMB = 0
FBPVL = 0
SWZ = .5
SWW = 70
KCF = 0
LSO = 0
KLAGV = 16.5
```

b) Suspension Parameters

```
SUSPENSIONF$ = SOLID AXLE
SUSPENSIONR$ = SOLID AXLE
HF = 0
HR = 0
LF = 1.3
LR = 1.4
KSAF = 1
KSAR = 1
BF = 0
BR = 0
CF = 0
CR = 0
DF = 0
DR = 0
EF = 0
ER = 0
KSLF = 0
KSLR = 0
LSAF = 1000
LSAR = 1000
KSADF = 0
KSADR = 0
KSAD2F = 0
KSAD2R = 0
KACK = 0
```

c) Tire Parameters

```
TWIDTH = 8
KA0 = 0
KA1 = 15.52
KA2 = 6787
KA3 = 1.11
KA4 = 1000000
KA = .05
KMU = .234
TPRESS = 35
KB1 = -.000061
KB3 = 1.01
KB4 = 0
KGAMMA = 0.9
CSFZ = 16
MUNOM = .92
FZTRL = 2180
KK1 = -.00016
RR = 1.255
TIRE = RADIAL
C1 = 1
C2 = .34
C3 = .57
C4 = .32
G1 = 1
G2 = 1
```

TABLE E-5. (Continued)

VDANL Simulation Parameter Files: Vehicle #36

a) Vehicle Parameters

```
MASS = 110.973
SMASS = 96.10134
UMASSF = 5.993783
UMASSR = 8.877837
LENA = 3.894657
LENB = 4.740343
IXS = 279.0763
IYS = 1684.192
IZZ = 1998.427
IXZ = 0
KSTR = 24
KSCF = .00005
KSCB = 0
DLADV = 0
DYADV = 0
DNADV = 0
DENSITY = .002377
REFAREA = 22.19063
CDX = .5
AEROVEL = 80
KTL = 1
KSF = 3200
KSDF = 203.3745
KSR = 2940
KSDR = 201.9374
TRWF = 4.73
TRWB = 4.63
HCG = 2.275658
KBS = 6400
HBS = .25
KTSF = -1627.7
KTSR = -1419.592
KRAS = 12000
KRADP = 700
TSPRINGR = 15555
HRAF = 0
HRAR = 0
HS = 2.45759
IXUF = 33.52458
IXUR = 32.12204
KLT = 1.671488E-04
XACC = 0
ZACC = 0
DRAGC = -.015
LENS = 0
LM = 0
KBTF = 0
KVB = 0
KMB = 0
FBPVL = 0
SWZ = .5
SWW = 70
KCF = 0
LSO = 0
KLAGV = 16.5
```

b) Suspension Parameters

```
SUSPENSIONF$ = INDEPENDENT
SUSPENSIONR$ = SOLID AXLE
HF = 0
HR = 0
LF = 1
LR = 1.25
KSAF = 0
KSAR = 1
BF = 0
BR = 0
CF = 0
CR = 0
DF = 0
DR = 0
EF = 0
ER = 0
KSLF = .16
KSLR = 0
LSAF = 1000
LSAR = 1000
KSADF = 0
KSADR = 0
KSAD2F = 0
KSAD2R = 0
KACK = 0
```

c) Tire Parameters

```
TWIDTH = 5.5
KA0 = 7780
KA1 = 4.56
KA2 = 3680
KA3 = .48
KA4 = -6720
KA = .05
KMU = .234
TPRESS = 31
KB1 = -.0000464
KB3 = .996
KB4 = -1.01E-08
KGAMMA = 0.9
CSFZ = 15.45
MUNOM = .85
FZTRL = 1870
KK1 = -.000218
RR = 1.1
TIRE = RADIAL
C1 = 1
C2 = .34
C3 = .57
C4 = .32
G1 = 1
G2 = 1
```

TABLE E-5. (Continued)

VDANL Simulation Parameter Files: Vehicle #37

a) Vehicle Parameters

```
MASS = 122.5
SMASS = 107.5
UMASSF = 6
UMASSR = 9
LENA = 3.85
LENB = 4.52
IXS = 310
IYS = 1740
IZZ = 2100
IXZ = 0
KSTR = 17.1
KSCF = .00014
KSCB = 0
DLADV = 0
DYADV = 0
DNADV = 0
DENSITY = .00237
REFAREA = 22
CDX = .5
AEROVEL = 44
KTL =  1.4
KSF = 3600
KSDF = 190
KSR = 3600
KSDR = 175
TRWF = 4.72
TRWB = 4.58
HCG = 2.08
KBS = 7200
HBS = .25
KTSF = -15000
KTSR = 20000
KRAS = 12000
KRADP = 700
TSPRINGR = 18000
HRAF = 0
HRAR = 1
HS = 2.24
IXUF = 35
IXUR = 32
KLT = .00015
XACC = -1.67
ZACC = 2.15
DRAGC = -.015
LENS = 5.5
LM = 1.125
KBTF = -.835
KVB = 19
KMB = 3.75
KBPVL = 60
SWZ = 0.5
SWW = 60
KCF = -.00002
LSO = 0
KLAGV = 25
```

b) Suspension Parameters

```
SUSPENSIONF = INDEPENDENT
SUSPENSIONR = SOLID AXLE
HF = 0
HR =  0
LF = 1
LR =  1.67
KSAF = 0
KSAR = 1
BF = 0
BR = 0
CF = 0
CR = 0
DF =  0
DR = 0
EF = 0
ER = 0
KSLF =  .04
KSLR = 0
LSAF =  1000
LSAR = 1000
KSADF =  .2
KSADR =  0
KSAD2F = 0
KSAD2R =  0
KACK = 0
```

c) Tire Parameters

```
TWIDTH = 8
KA0 = 0
KA1 = 18.96
KA2 = 3438
KA3 = .449
KA4 = -11464
KA = .05
KMU = .234
TPRESS = 30
KB1 = -.000204
KB3 = 1.12
KB4 = 0
KGAMMA = .9
CSFZ = 4
MUNOM = .92
FZTRL = 2017
KK1 = -.00016
RR = 1.12
TIRE = BIAS
C1 = .535
C2 = 1.05
C3 = 1.15
C4 = .8
G1 = 1
G2 = 1
```

TABLE E-5. (Continued)

VDANL Simulation Parameter Files: Vehicle #38

a) Vehicle Parameters

```
MASS = 162.1076
SMASS = 136.1703
UMASSF = 12.9686
UMASSR = 12.9686
LENA = 4.223247
LENB = 4.616754
IXS = 595.1868
IYS = 2716.162
IZZ = 3234.319
IXZ = 0
KSTR = 18.2
KSCF = .0001
KSCB = 0
DLADV = 0
DYADV = 0
DNADV = 0
DENSITY = .002377
REFAREA = 31.3125
CDX = .5
AEROVEL = 80
KTL = 1
KSF = 7200
KSDF = 354.1871
KSR = 3500
KSDR = 269.9276
TRWF = 5.74
TRWB = 5.435
HCG = 2.559078
KBS = 14400
HBS = .25
KTSF = 70249.14
KTSR = 23095.99
KRAS = 12000
KRADP = 700
TSPRINGR = 19380
HRAF = 1.35
HRAR = 1.65
HS = 2.811283
IXUF = 68.32377
IXUR = 61.25579
KLT = 1.341589E-04
XACC = 0
ZACC = 0
DRAGC = -.015
LENS = 0
LM =  1
KBTF =  1
KVB =  1
KMB =  1
FBPVL =  1
SWZ = .5
SWW = 70
KCF = 0
LSO = .2
KLAGV = 16.5
```

b) Suspension Parameters

```
SUSPF=SOLID AXLE
SUSPR=SOLID AXLE
HF=0
HR=0
LF=1.5
LR=1.65
KSAF=1
KSAR=1
BF=0
BR=0
CF=0
CR=0
DF=0
DR=0
EF=0
ER=0
KSLF=0
KSLR=0
LSAF=1000
LSAR=1000
KSADF=0
KSADR=0
KSAD2F=0
KSAD2R=0
KACK=.075
```

c) Tire Parameters

```
TWIDTH = 8
KA0 = 0
KA1 = 15.5
KA2 = 6790
KA3 = 1.11
KA4 = 1000000
KA = .05
KMU = .234
TPRESS = 35
KB1 = -.000061
KB3 = 1.01
KB4 = 0
KGAMMA = 0.9
CSFZ = 16
MUNOM = .85
FZTRL = 2180
KK1 = -.00016
RR = 1.24
TIRE = BIAS PLY
C1 = .535
C2 = 1.05
C3 = 1.15
C4 = .8
G1 = 1
G2 = 1
```

TABLE E-5. (Continued)

VDANL Simulation Parameter Files: Vehicle #39

a) Vehicle Parameters

```
MASS = 145.1663
SMASS = 126.0205
UMASSF = 7.532484
UMASSR = 11.6133
LENA = 4.200953
LENB = 4.549047
IXS = 503.9013
IYS = 2288.365
IZZ = 2673.733
IXZ = 0
KSTR = 18.9
KSCF = .00006
KSCB = 0
DLADV = 0
DYADV = 0
DNADV = 0
DENSITY = .002377
REFAREA = 29.7483
CDX = .5
AEROVEL = 80
KTL = 1
KSF = 2400
KSDF = 196.2752
KSR = 3600
KSDR = 264.0078
TRWF = 5.64
TRWB = 5.565
HCG = 2.376915
KBS = 4800
HBS = .25
KTSF = -6006.458
KTSR = 5818.462
KRAS = 12000
KRADP = 700
TSPRINGR = 17085
HRAF = 0
HRAR = 1.55
HS = 2.564075
IXUF = 59.90133
IXUR = 58.3188
KLT = 1.521803E-04
XACC = 0
ZACC = 0
DRAGC = -.015
LENS = 0
LM =  1
KBTF =  1
KVB =  1
KMB =  1
FBPVL =  1
SWZ = .5
SWW = 70
KCF = 0
LSO = .25
KLAGV = 16.5
```

b) Suspension Parameters

```
SUSPF = INDEPENDENT
SUSPR = SOLID AXLE
HF = 0
HR = -.26
LF = 1
LR = 1.65
KSAF = 0
KSAR = 1
BF = 0
BR = 0
CF = 0
CR = 0
DF = -.29
DR = 0
EF = 0
ER = 0
KSLF = .34
KSLR = 0
LSAF = 3.1
LSAR = 1000
KSADF = .59
KSADR = .11
KSAD2F = 0
KSAD2R = 0
KACK = .04
```

c) Tire Parameters

```
TWIDTH = 5
KA0 = 4910
KA1 = 7.28
KA2 = 4360
KA3 = .439
KA4 = -6400
KA = .05
KMU = .234
TPRESS = 38
KB1 = -.0000191
KB3 = .953
KB4 = -1.72E-08
KGAMMA = 0.9
CSFZ = 14.5
MUNOM = .92
FZTRL = 2000
KK1 = -.000193
RR = 1.145
TIRE = RADIAL
C1 = 1
C2 = .34
C3 = .57
C4 = .32
G1 = 1
G2 = 1
```

TABLE E-5. (Continued)

VDANL Simulation Parameter Files: Vehicle #40

a) Vehicle Parameters

```
MASS = 114.3923
SMASS = 99.09326
UMASSF = 6.147654
UMASSR = 9.151383
LENA = 3.586227
LENB = 4.267773
IXS = 289.8169
IYS = 1916.642
IZZ = 1746
IXZ = 0
KSTR = 21
KSCF = .00005
KSCB = 0
DLADV = 0
DYADV = 0
DNADV = 0
DENSITY = .002377
REFAREA = 23.26434
CDX = .5
AEROVEL = 44
KTL = 1.4
KSF = 2090
KSDF = 150
KSR = 2090
KSDR = 150
TRWF = 4.864
TRWB = 4.864
HCG = 2.3
KBS = 9122.136
HBS = .25
KTSF =  -21400
KTSR =  3400
KRAS = 12000
KRADP = 700
TSPRINGR = 17085
HRAF = 0
HRAR =  1.5
HS =  2.48
IXUF = 36.36106
IXUR = 36.36106
KLT = 1.521803E-04
XACC = -2.12
ZACC = 1.43
DRAGC = -.015
LENS = 4.06
LM = 1.125
KBTF = -1.2
KVB = 26.3
KMB = 0
FBPVL = 100
SWZ = .5
SWW = 100
KCF = 0
LSO = .25
KLAGV = 16.5
```

b) Suspension Parameters

```
SUSPENSIONF$ = INDEPENDENT
SUSPENSIONR$ = SOLID AXLE
HF = 0
HR = 0
LF = 1
LR = 1.5
KSAF = 0
KSAR = 1
BF = 0
BR = 0
CF = 0
CR = 0
DF = -.3289474
DR = 0
EF = 0
ER = 0
KSLF = .3766447
KSLR = 0
LSAF =  2.5
LSAR = 0
KSADF = .63997
KSADR = .1698434
KSAD2F = 0
KSAD2R = 0
KACK = 0
```

c) Tire Parameters

```
TWIDTH = 5
KA0 = 4907.84
KA1 = 7.28
KA2 = 4362.67
KA3 = .439
KA4 = -6397.61
KA = .05
KMU = .234
TPRESS = 35
KB1 = -1.907E-05
KB3 = .953
KB4 = -1.72E-08
KGAMMA = .9
CSFZ = 14.5
MUNOM = .92
FZTRL = 2000
KK1 = -.0001926
RR = 1.125
TIRE = RADIAL
C1 = 1
C2 = .34
C3 = .57
C4 = .32
G1 = 1
G2 = 1
```

TABLE E-5. (Concluded)

VDANL Simulation Parameter Files: Vehicle #41

a) Vehicle Parameters

```
MASS = 98.53902
SMASS = 82.77277
UMASSF = 7.883121
UMASSR = 7.883121
LENA = 3.581452
LENB = 4.226548
IXS = 237.0032
IYS = 1104.612
IZZ = 1381.315
IXZ = 0
KSTR = 16
KSCF = .00007
KSCB = 0
DLADV = 0
DYADV = 0
DNADV = 0
DENSITY = .002377
REFAREA = 21.47625
CDX = .5
AEROVEL = 80
KTL = 1
KSF = 2500
KSDF = 165.6608
KSR = 2620
KSDR = 178.4141
TRWF = 4.83
TRWB = 4.835
HCG = 1.961474
KBS = 5000
HBS = .25
KTSF = -17062.84
KTSR = -1732.261
KRAS = 12000
KRADP = 700
TSPRINGR = 13953.6
HRAF = 1.25
HRAR = 1.55
HS = 2.126993
IXUF = 31.6938
IXUR = 31.75946
KLT = 1.863318E-04
XACC = 0
ZACC = 0
DRAGC = -.015
LENS = 0
LM =  1
KBTF =  1
KVB =  1
KMB =  1
FBPVL =  1
SWZ = .5
SWW = 70
KCF = 0
LSO = .2
KLAGV = 16.5
```

b) Suspension Parameters

```
SUSPF=SOLID AXLE
SUSPR=SOLID AXLE
HF=.10
HR=0
LF=1.45
LR=1.40
KSAF=1
KSAR=1
BF=0
BR=0
CF=0
CR=0
DF=0
DR=0
EF=0
ER=0
KSLF=0
KSLR=0
LSAF=1000
LSAR=1000
KSADF=0
KSADR=0
KSAD2F=0
KSAD2R=0
KACK=.04
```

c) Tire Parameters

```
TWIDTH = 5.5
KA0 = 7780
KA1 = 4.56
KA2 = 3680
KA3 = .48
KA4 = -6720
KA = .05
KMU = .234
TPRESS = 30
KB1 = -.0000464
KB3 = .996
KB4 = 1.01E-08
KGAMMA = 0.9
CSFZ = 15.45
MUNOM = .85
FZTRL = 1870
KK1 = -.000218
RR = 1.093
TIRE = RADIAL
C1 = 1
C2 = .34
C3 = .57
C4 = .32
G1 = 1
G2 = 1
```

APPENDIX F

LATERAL LOAD TRANSFER DISTRIBUTION

APPENDIX F

LATERAL LOAD TRANSFER DISTRIBUTION

Under steady state cornering conditions lateral acceleration causes load to shift from the inside to the outside tires as illustrated in Fig. F-1. Total load transfer is clearly a function of the c.g. (center of gravity) height and the track width, and is proportional to the track width ratio as discussed in the main text. Load transfer distribution between the front and rear axles is further dependent on the relative roll stiffness between the two axles.

Lateral load transfer at each wheel derives from three components:

(1) the moment due to suspension roll stiffness (front or rear) times the roll angle deflection.

(2) the lateral force from the sprung mass acceleration ($m_s\ a_y$) applied at the roll axis points h_{RAF} and h_{RAR}.

(3) the lateral force from the unsprung mass acceleration ($m_u\ a_y$) applied at the axle height R_w.

These components can be computed as follows at the longitudinal c.g. of the sprung mass, m_s,

From Fig. F-1,

$$h_{RA} = h_{RAF}\left(\frac{b}{\ell}\right) + h_{RAR}\left(\frac{a}{\ell}\right) \tag{F-1}$$

$$\epsilon = hs - h_{RA} \tag{F-2}$$

Now, given roll stiffness due to springs and anti roll bars at the front and rear axles respectively, (K_{FSRS} and K_{RSRS}) the front and rear load transfer to the outside tires is given by,

$$\frac{F_{LF} - F_{RF}}{2} = \Delta F_F = \frac{K_{FSRS}\,\phi_{SUSP} + m_s\,a_y\,\frac{b}{\ell}\,h_{RAF} + m_{UF}\,a_y\,R_w}{T_F} \tag{F-3}$$

$$\frac{F_{LR} - F_{RR}}{2} = \Delta F_R = \frac{K_{RSRS}\,\phi_{SUSP} + m_s\,a_y\,\frac{a}{\ell}\,h_{RAR} + m_{UR}\,a_y\,R_w}{T_R} \tag{F-4}$$

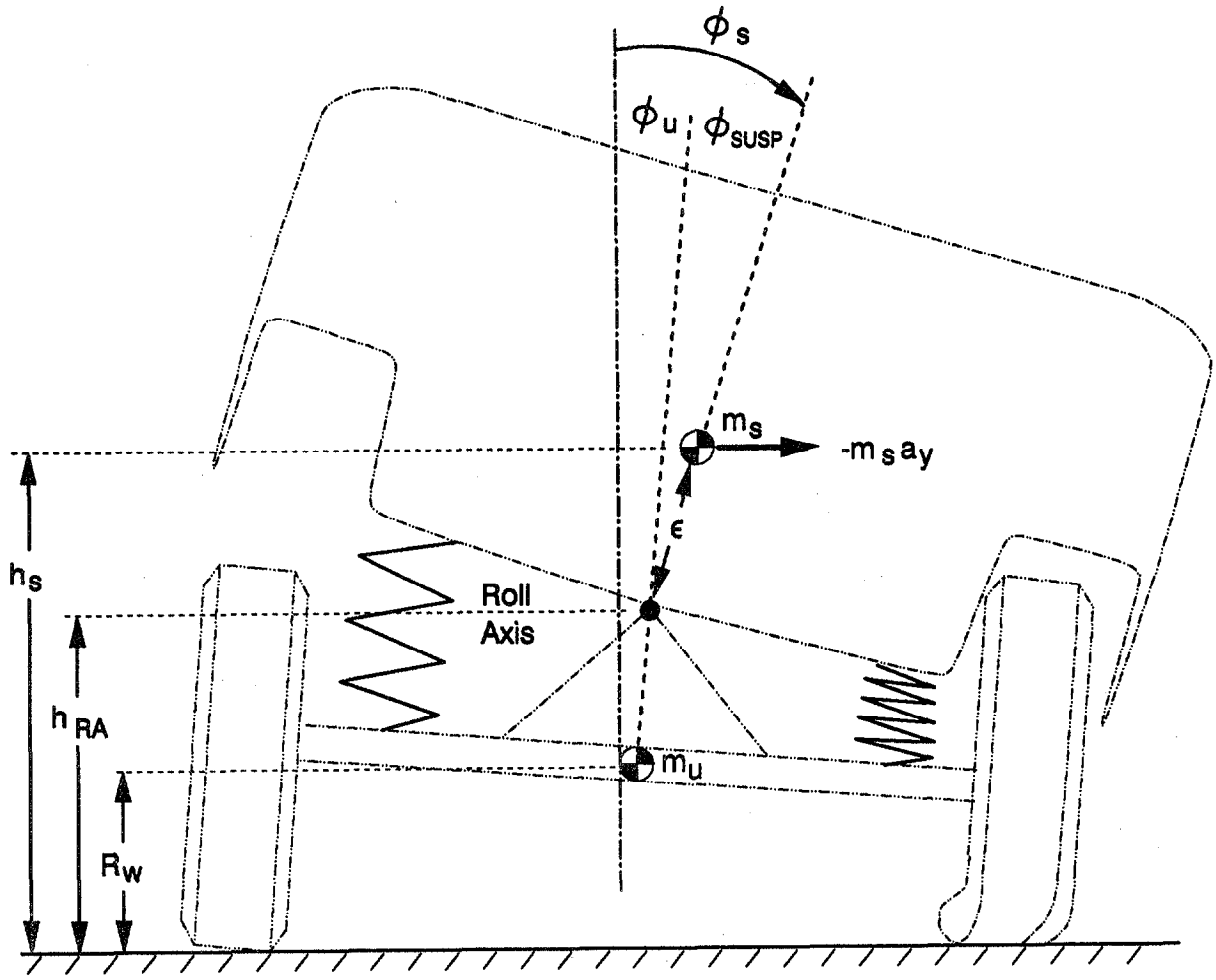

a) End View

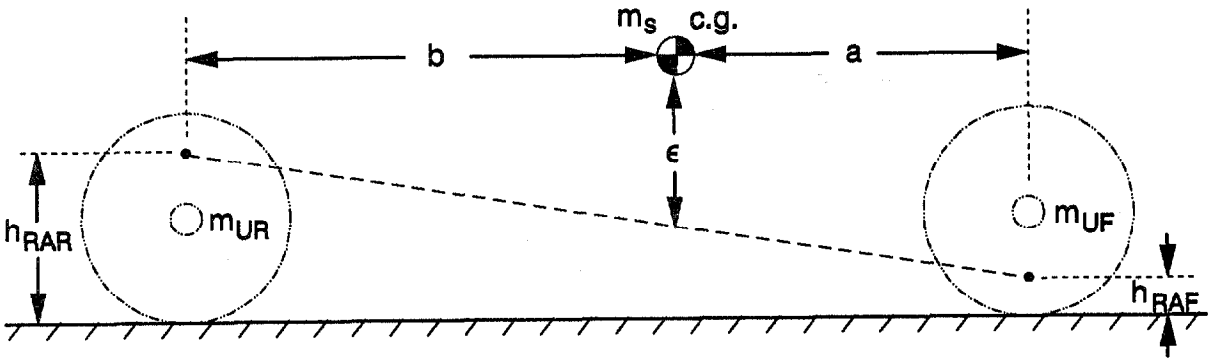

b) Side View

Figure F-1. Variables Affecting Load Transfer Under Steady State Cornering Conditions

Assuming that $\sin \phi_s \simeq \phi_s$ for $\phi_s < .2$, then

$$\phi_{SUSP} = \frac{m_s\ a_y\ \epsilon - m_s\ g\ \epsilon\phi_s}{K_{FSRS} + K_{RSRS}} \qquad (F\text{-}5)^*$$

$$\phi_{SUSP} = \phi_s - \phi_u$$

We can estimate ϕ_u due to the $m\ a_y\ h_{cg}$ moment acting on the tire roll stiffness at the 2 axles ($m = m_s + m_u$):

$$2\left(-\frac{K_{TSR}\ T^2}{2}\right)\phi_u \simeq m\ a_y\ h_{cg} \qquad (F\text{-}6)$$

From this we can compute ϕ_s

$$\phi s = \frac{m_s\ a_y\ \epsilon - \left(K_{FSRS} + K_{RSRS}\right)\dfrac{m\ a_y\ h_{CG}}{K_{TSR}\ T^2}}{K_{FSRS} + K_{RSRS} + m_s\ g\ \epsilon} \qquad (F\text{-}7)^*$$

Equation F-7 can also be used to estimate the roll gradient, $= \dfrac{\phi_s}{a_y}$

Finally, the percentage of lateral load transfer, or load transfer distribution (LTD) at the front axle is given by,

$$\%\ LTD = \frac{100\ \Delta F_F}{\Delta F_F + \Delta F_R} \qquad (F\text{-}8)$$

*Note that roll stiffness coefficients normally have negative values.

APPENDIX G

SIDE PULL TEST PROCEDURES

APPENDIX G

A METHOD FOR STATIC TIP OVERTESTING

A. GENERAL BACKGROUND

Simple calculated a_y needed for tip over, uses the steady state moments at the point of initial lift-off of the inside tires, for a rigid body with no suspension or tires.

$$M\, a_{y_{T.O.}}\, h_{cg} = g\, M\, \frac{T}{2}$$

or

$$a_{y_{T.O.}} = \frac{T}{2h_{cg}} \text{ in g units}$$

The problem with this computation, is that with suspension and tires, the effective track width and cg height are altered just before initiating a tip over.

1. There is a lateral shift of the center of gravity as the sprung mass rolls to one side.
2. There is an additional shortening of T/2 because of lateral deflection of the tire casing and suspension components and wheels.
3. There is usually a lifting up of the body cg due to side forces on the suspension.

The result is, that in cornering, a vehicle can tip over at a lower a_y level than indicated by the simple T/2h ratio. Current tests on a variety of vehicles, shows that the actual a_y needed for tip over (the dynamic tip over ratio) ranges between .75 to .80 of T/2h ratio.

B. STI TEST METHOD

The tip over test devised by Systems Technology, Inc. (STI), applies a pure horizontal side pull force acting through the vehicle cg at whatever height the body cg ends up at, just at initiating a tip over. This simulates the same forces present in steady state cornering, and produces the same body roll angle, same lateral deflection of tire, wheel, and suspension, and same lifting up of the body due to suspension forces, as is present in actual cornering.

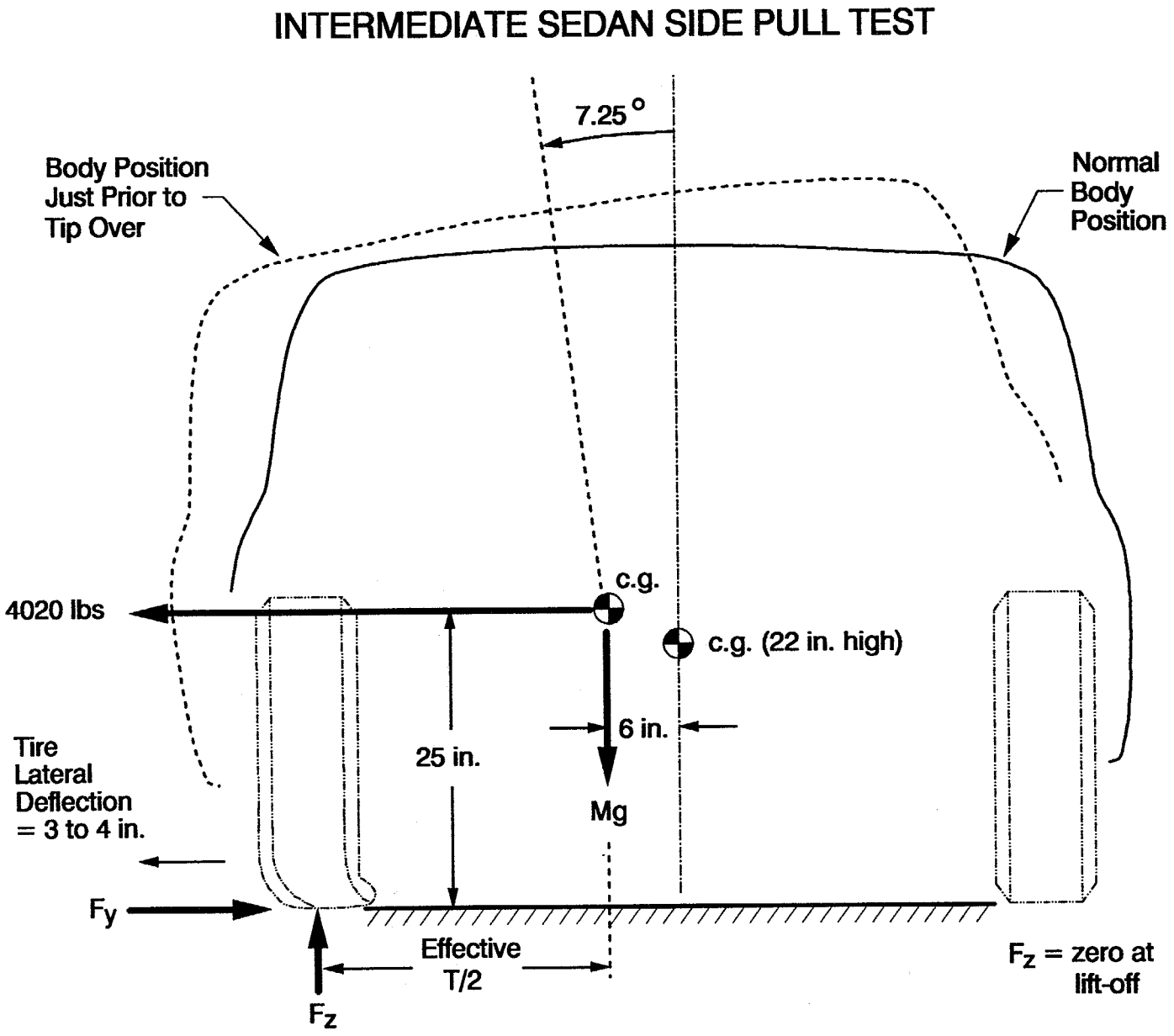

Typical Shift in C.G., and T/2, at Tip-Over

$$\text{Thus, the dynamic tip over ratio, or actual } a_y \text{ needed for tip over} = \frac{\frac{T}{2} - \left\{\begin{array}{l}\text{cg shift due to roll angle,}\\ \text{reduction in T/2 due to tire}\\ \text{and suspension deflection}\end{array}\right\}}{h_{cg} \pm \quad \text{(Suspension lift/squat)}}$$

And this test method provides the final value for $a_{y_{T.O.}}$ without having to compute the detailed effects.

C. PROCEDURE

The side pull cable is attached through a free pivot, to a canvas strap which is looped over the roof and back through the windows for the single point upper attachment, and two sections of steel chain, one hooked to the body frame at the front and one hooked to the body frame at the rear.

The chain sections are shortened or lengthened until the horizontal pull cable force acts directly through the vehicle cg height at the point of initiating tip over.

The front, or rear chain section is shortened or lengthened until the pull force acts directly perpendicular (in plan view) and through the longitudinal location of the vehicle cg.

Measurements

Pull cable height

Pull force (Dillon Dyno Force Scale)

Body roll angle (Inclinometer)

Lateral shift of body cg, from initial starting point

Vertical rise of body cg, from initial starting point

Lateral deflection of tire, from initial starting point

Vehicle weight (as tested) and X,Z location of vehicle cg, are needed before testing

The pull force and roll angle data can be crossplotted to show the peak pull force at some given angle. However, this peak pull force also coincides with the initial lift-off of both other side tires. So that when a sheet of paper can be slid under these two tires, the pull force should be recorded as the force needed for initiating tip over.

MEASUREMENT DEVICES

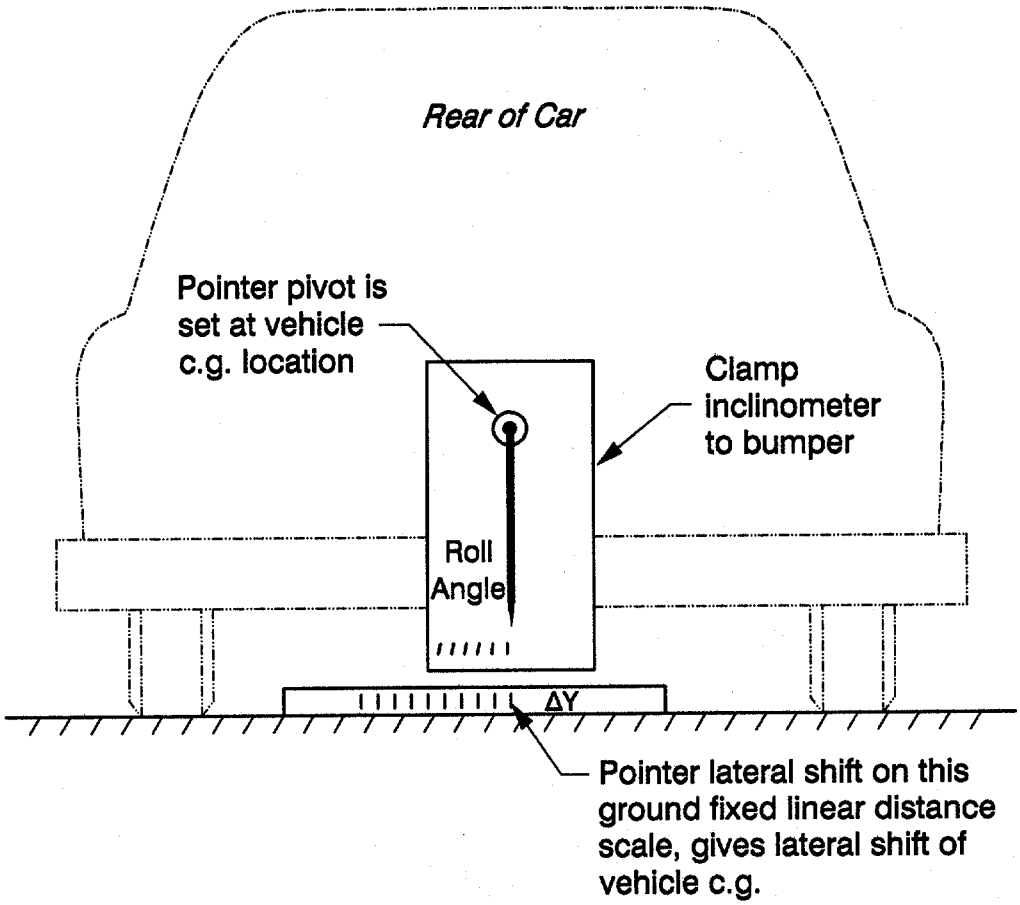

Rise of vehicle c.g. can be measured by a tape measure from ground up to pointer pivot.

At the same time, pull cable height can be measured, to make sure it is the same as vehicle c.g. height at the point of tip-over.

Also, lateral deflection of the tire can be measured by tape measure, from the side of the wheel rim to some fixed ground point.

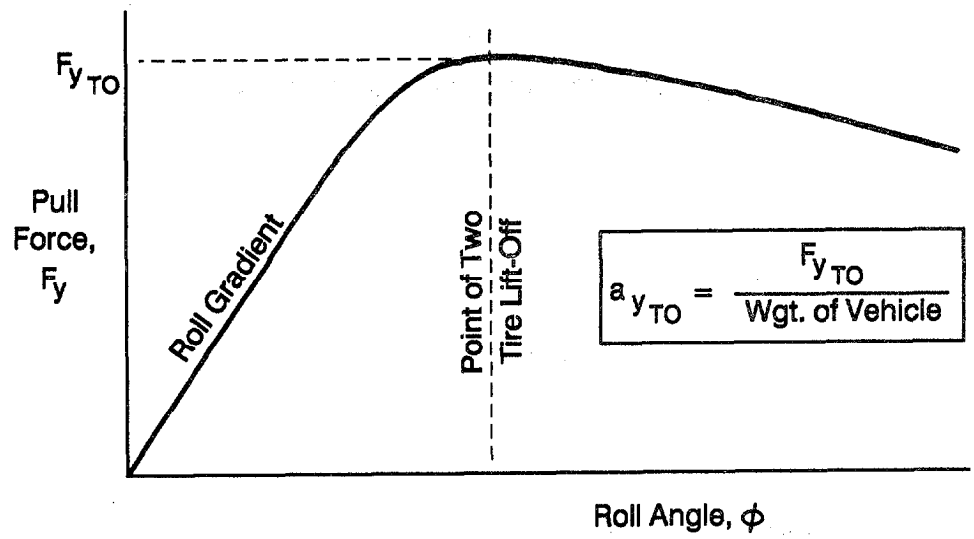

D. CORRECTION FACTORS FOR PULL CABLE POSITION WHICH IS NOT LEVEL, AND/OR NOT DIRECTED THROUGH VEHICLE C.G.

The side pull force should be directed through the vehicle c.g., so that the rollover moment is reached with the correct side force acting at the tires, in order to produce the correct lateral tire deflection. However, small errors in cable position can be corrected for, as long as the pull force is not significantly different from the correct value.

The tipover moment should be = $[F_{yTO}][h_{cg}]$, where h_{cg} is the height of the c.g. at the position of tipover.

The actual applied moment in the tipover test is

$$= F_p(\text{Cos } \theta_c)h_o - F_p(\sin \theta_c)Y_T$$

These two moments should be equal at tipover, so that the true F_yTO is

$$FyTO = \frac{F_p(h_o - Y_T \sin \theta_c)}{h_{cg}} \qquad \text{(G-1)}$$

assuming $\cos \theta_c \approx 1.00$

Note, that if θ_c = zero, and $h_o = h_{cg}$

then $F_{yTO} = F_p$

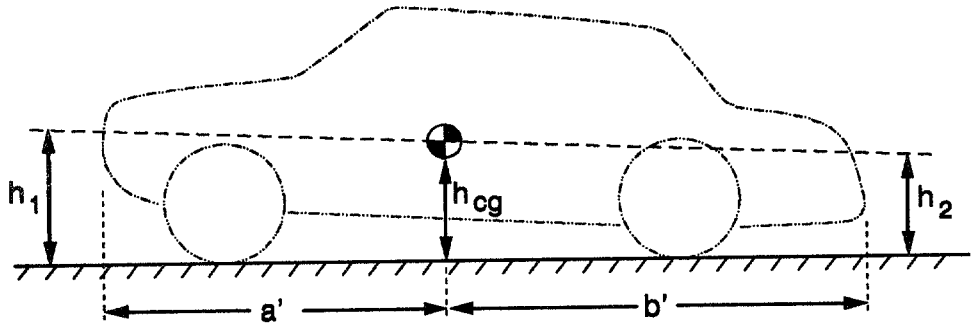

h_{cg} is obtained from c.g. marks on the car body at the front and rear, and at tipover, measure the height at each end. Then from these, compute the c.g. height at the longitudinal c.g. location.

$$h_{cg} = h_2 + \left(\frac{b'}{a' + b'}\right)\left(h_1 - h_2\right) \qquad \text{(G-2)}$$

This may be different from h_{cg} before the side pull application, because most vehicles tend to lift upwards prior to reaching the tip over point.

Also, $$\sin \theta_c = \frac{h_H - h_W}{\ell_1} \qquad \text{(G-3)}$$

$$h_o = h_H + \ell_2 \sin \theta_c \qquad \text{(G-4)}$$

Example tip over test, Nissan Sentra, with 3 different cable heights.

F_P	h_H	h_1 h_{cgF}	h_2 h_{cgR}	CALC. hcg	CALC. $\sin\theta_c$	CALC. h_o	CALC. F_{yTO}
1904 lb	23.5"	19.75"	23.75"	21.35"	$-\frac{1}{130}$	22.5"	2040 lb
2620 lb	20.0"	19.5"	24.5"	21.5"	$-\frac{4.5}{130}$	15.5"	2010 lb
2160 lb	22"	19.75"	23.4"	21.2"	$-\frac{2.5}{130}$	19.5"	2045 lb
						avg =	2032

$h_W = 24.5$ $\quad y_T1 = 30$

$\ell_1 = 130$ $\quad a' = 66$

$\ell_2 = 130$ $\quad b' = 99$

error range = 1%

PULL FORCE CABLE, STRAP; CHAIN LAYOUT

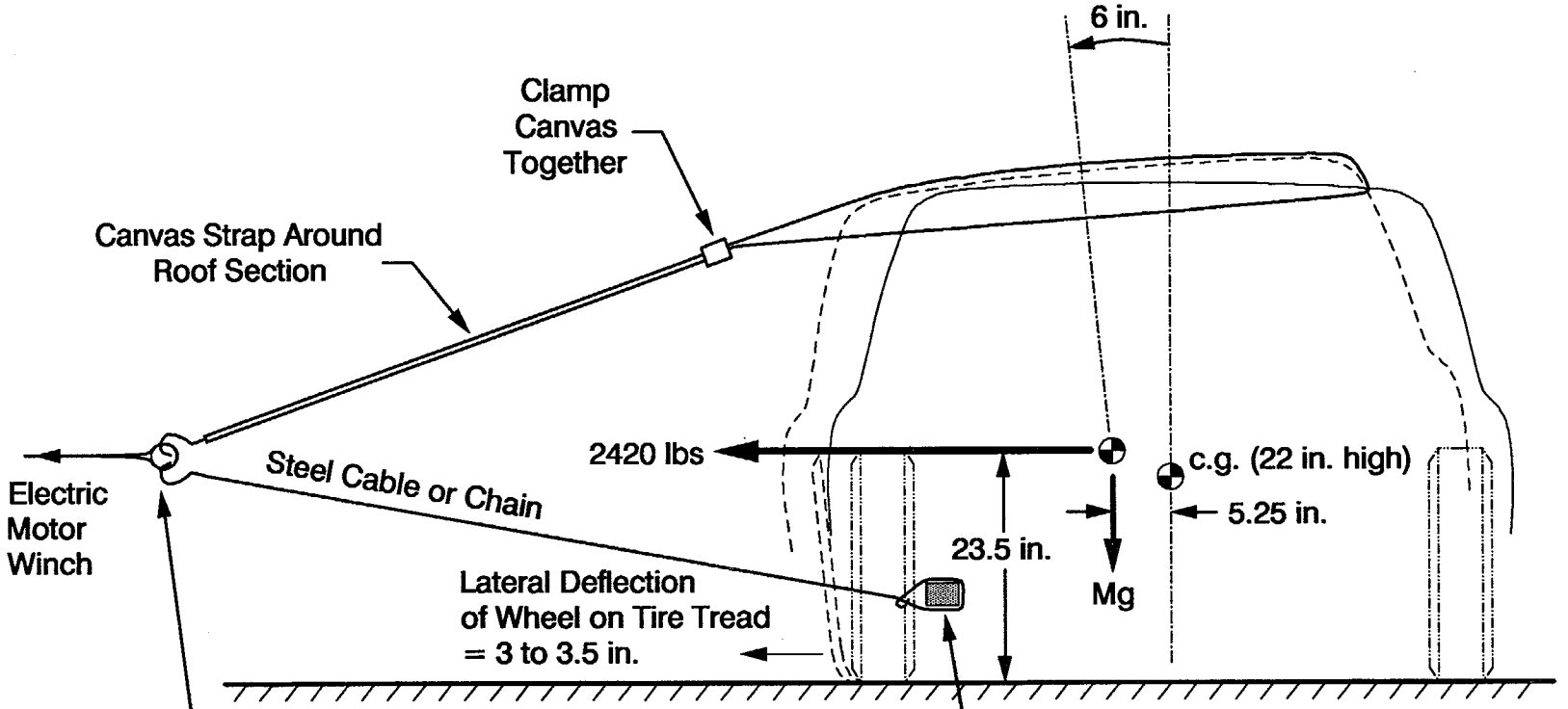

This is a free pivot such that force resolutions show up at this pivot height and at the direction (slope) of the winch pull line. Therefore, it is that strap lenght be adjusted untill winch pull line ends up level and at c.g. height at the moment of tip-over

Cable hooked to door, wrapped around frame rail, or hard structural member. (on the escort, it was the front and rear jacking points)

E. ADVANTAGES OF THIS METHOD

1. Does not require any costly sophisticated instruments.

2. Exactly replicates the forces acting in steady state cornering.

3. Includes all the effects due to lateral shift of cg due to ϕ, reduction in T/2 due to tire, wheel, suspension deflection, rise in cg height due to suspension squat/lift effects.

4. The tip over point is an exact steady state test condition, easily identified by sliding a sheet of paper under the two other-side tires, and easily held at this point while taking measurements (there are no teeter-totter unstable balancing acts).

5. This is a safe method, because the vehicle is still essentially on its 4 wheels, and cannot go any further on its own. Any increase in the usually small body roll angles, just makes the pull force cable go slack.

6. Provides additional data on vehicle roll angle, tire wheel and suspension deflection, suspension lift effect on h_{cg}, at point of tip over.

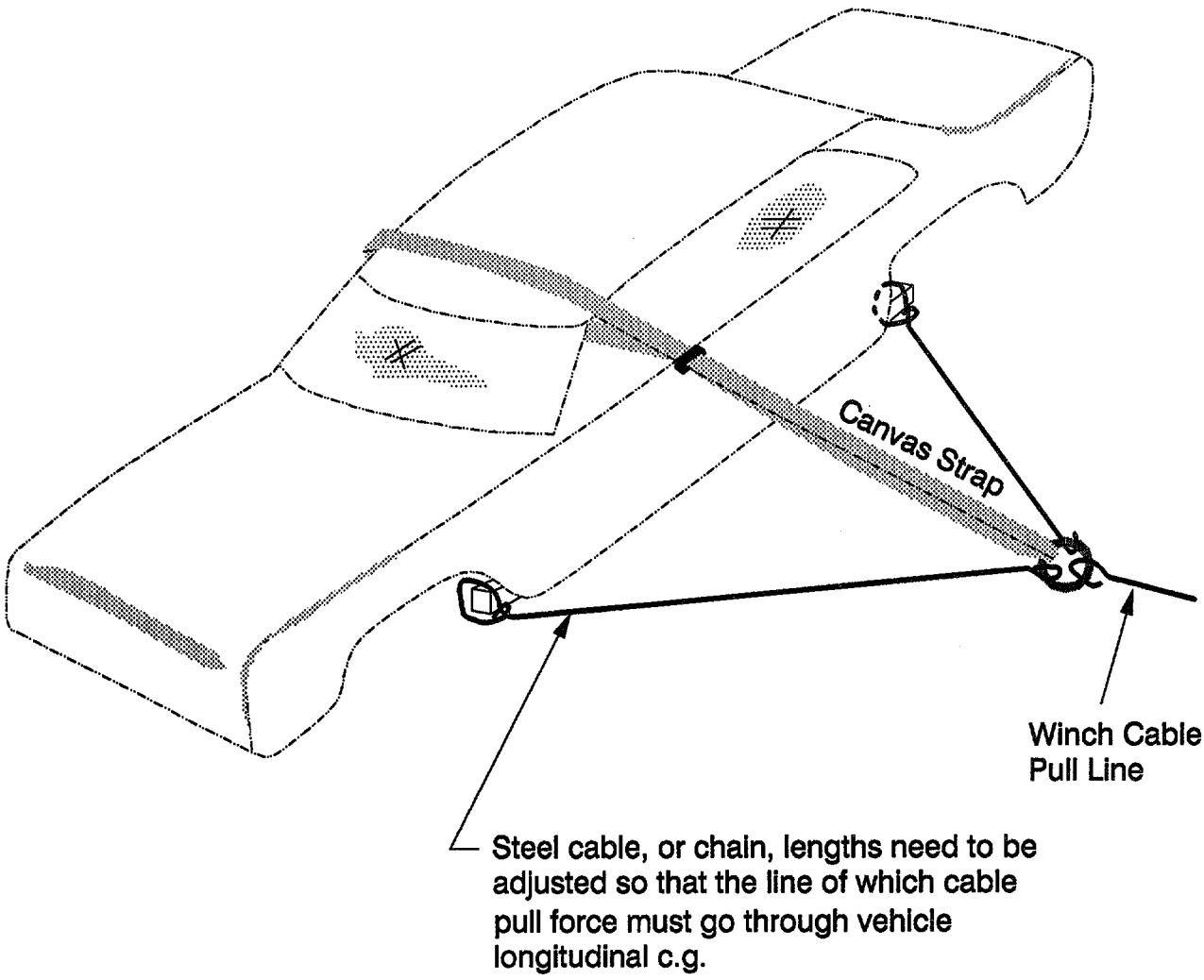
Canvas Strap
Winch Cable
Pull Line
Steel cable, or chain, lengths need to be adjusted so that the line of which cable pull force must go through vehicle longitudinal c.g.

STI VEHICLE TIP-OVER TEST SET-UP

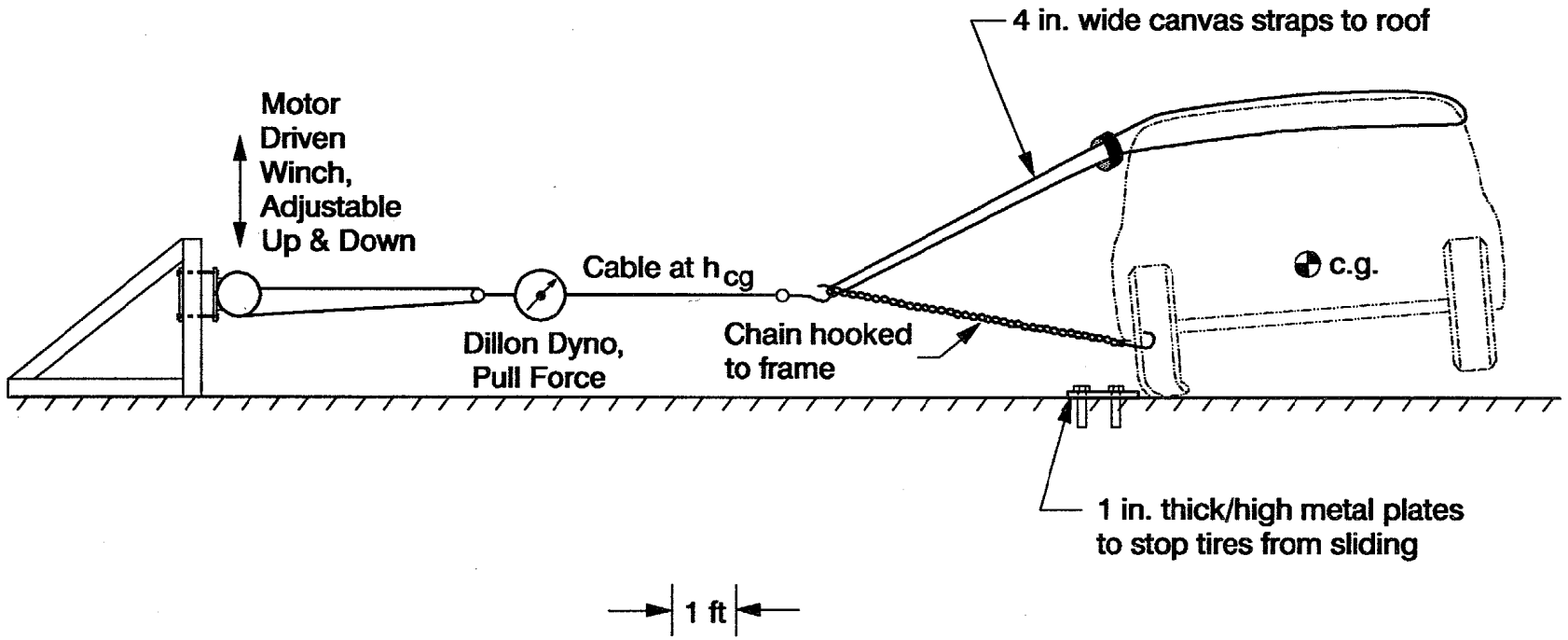

EXAMPLE CASE; CABLE IS TOO HIGH AT C.G. END

h_{cg} = Height of vehicle c.g. at each lift-up point
h_o = Line of action of F_p intersecting vehicle centerline
h_H = Height of cable where straps hook onto cable
h_w = Height of cable at winch end
Θ_c = Cable angle above horizontal
Y_T = Effective half track distance

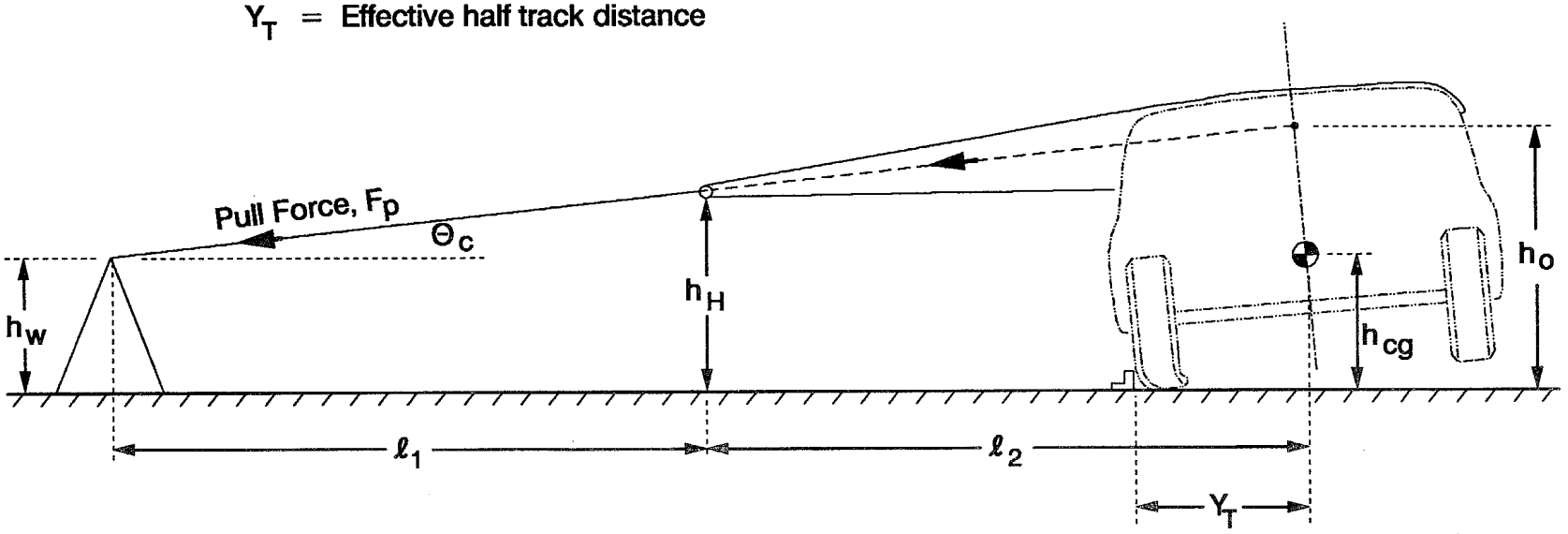

APPENDIX H

FIELD TEST AND COMPUTER SIMULATION VALIDATION DATA

APPENDIX H

FIELD TEST AND COMPUTER SIMULATION VALIDATION DATA

This appendix contains summary validation data for all twelve Phase 1 test vehicles. The validation consists of comparing field data and computer simulation data for comparable maneuvers for each test vehicle. The test maneuvers include the steady state turn circle, sinusoidal steer, and transient steer tests as described in Section V. Review of the data comparisons in Figures H-1 through H-12 shows generally good correspondence between vehicle test behavior and computer simulation response. Details for each of the maneuvering conditions are as follows.

A. STEADY STATE RESPONSE

Steady state response was determined with a constant radius turn circle maneuver with slowly increasing speed in order to measure steering, side slip and roll gradient properties as a function of lateral acceleration. The effect of tire side force saturation is evident in Figures H-1 through H-12 where the cornering acceleration reaches a limit. The field test data goes out to about 80-90% of the limit and shows good agreement over the measurement range. The steering angle results basically exhibit roll and compliance steer and side force saturation effects, while body slip angle relates to similar rear axle effects.

The low g slope of the steering angle versus lateral acceleration plots is basically determined by roll and compliance steer and the lateral load transfer distribution. The high g portion of the curve is given by tire saturation characteristics. Note that most vehicles have a rapidly increasing steering angle as they approach their corning limit and go into a limit understeer condition because the front axle side forces saturate. For these vehicles, the slip angle plots do not shown much indication of rear axle saturation near limit cornering conditions. Vehicles #23 and #34 are notable exceptions to this effect, however, and show indications of rear axle saturation without front axle saturation near the cornering limit.

The roll gradient response for all vehicles is virtually linear with respect to lateral acceleration.

B. DYNAMIC RESPONSE

The basic lateral/directional dynamic characteristics of the test vehicles and computer simulation were validated by taking describing functions of yaw rate, lateral acceleration and roll rate response to sinusoidal steering inputs. The simulation permits the specification of a sinusoidal steering input with increasing frequency throughout the run as discussed in Section VI. Fast Fourier transforms (FFT) were taken of the field test and computer simulation runs and compared with field test data as illustrated in Figures H-1 through H-12. Relatively good comparisons in response amplitude and phasing are noted for the directional and roll modes for all twelve Phase 1 field test vehicles. These data comparisons show that the computer simulation dynamics match those of the field test vehicles under low lateral acceleration dynamic conditions (i.e., less than 0.3 g's) where the tire side force characteristics are in their linear range.

The describing function data basically validate the combined effect of vehicle inertial dynamics and linear tire side force characteristics. The yaw rate to steering transfer functions are all quite consistent in the shape of the basically low pass response, although some vehicles, notably vehicles #10 and #34 show higher bandwidths. The lateral acceleration and roll rate to steering transfer functions show appreciable differences amongst vehicles. These differences are due to yaw/roll coupling effects, and should be explored further in future work. Larger transient inputs are needed to validate the limit performance capability of the computer simulation as discussed next.

C. TRANSIENT RESPONSE

The limit performance capability of the simulation was validated with large transient steering responses. The steering time profiles obtained in field test runs were used as inputs to the computer simulation and the subsequent time response of various variables were compared for each vehicle as shown in Figures H-1 through H-12. The transient test conditions represent maneuvering conditions up into the lateral acceleration regime of 0.8 g's which should encompass significant tire side force saturation. Reasonable matches are noted across vehicles and response variables for all twelve phase 1 field test vehicles.

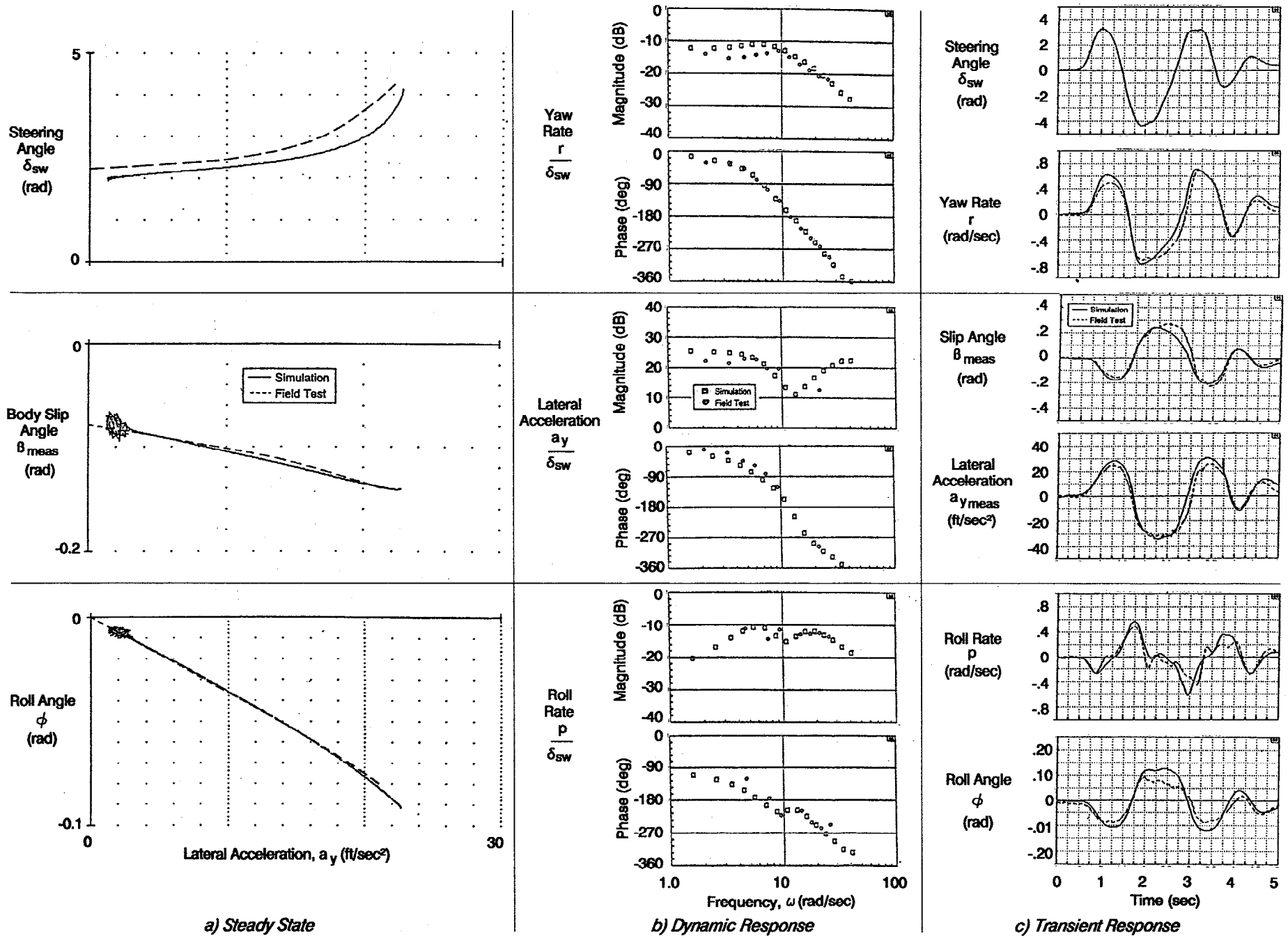

Figure H-1. Field Test and Computer Simulation Validation Data for Vehicle #1

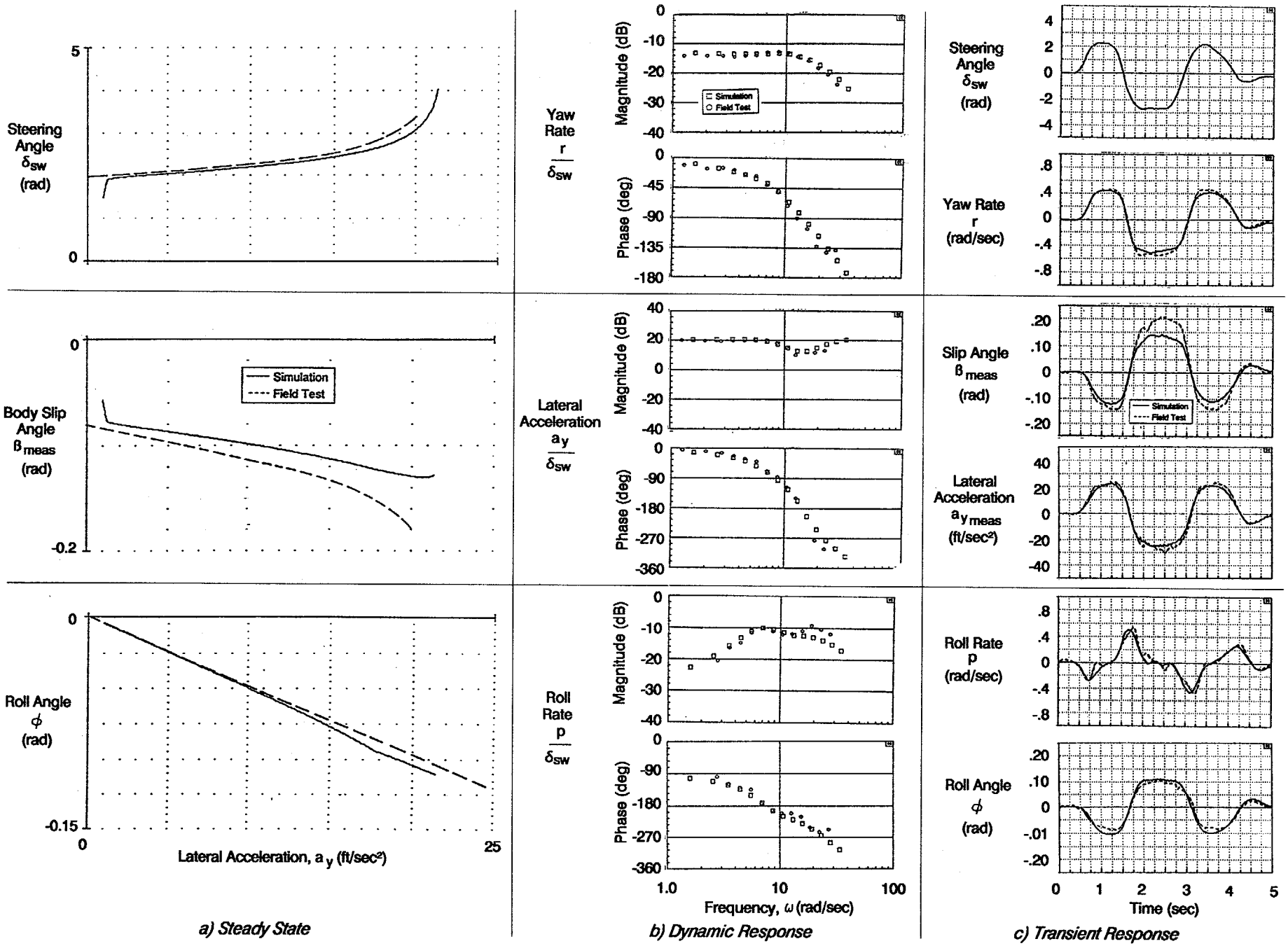

Figure H-2. Field Test and Computer Simulation Validation Data for Vehicle #6

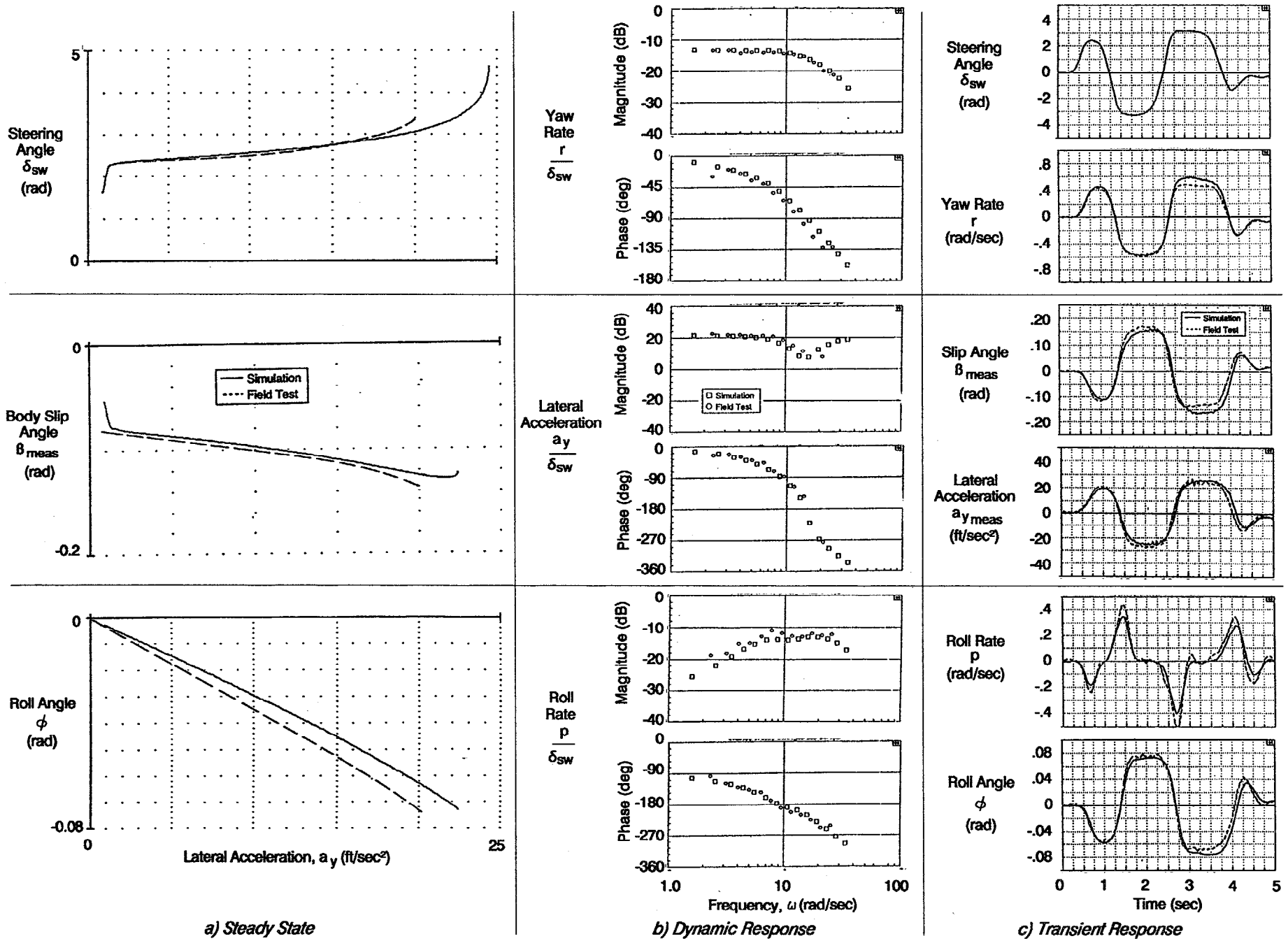

Figure H-3. Field Test and Computer Simulation Validation Data for Vehicle #8

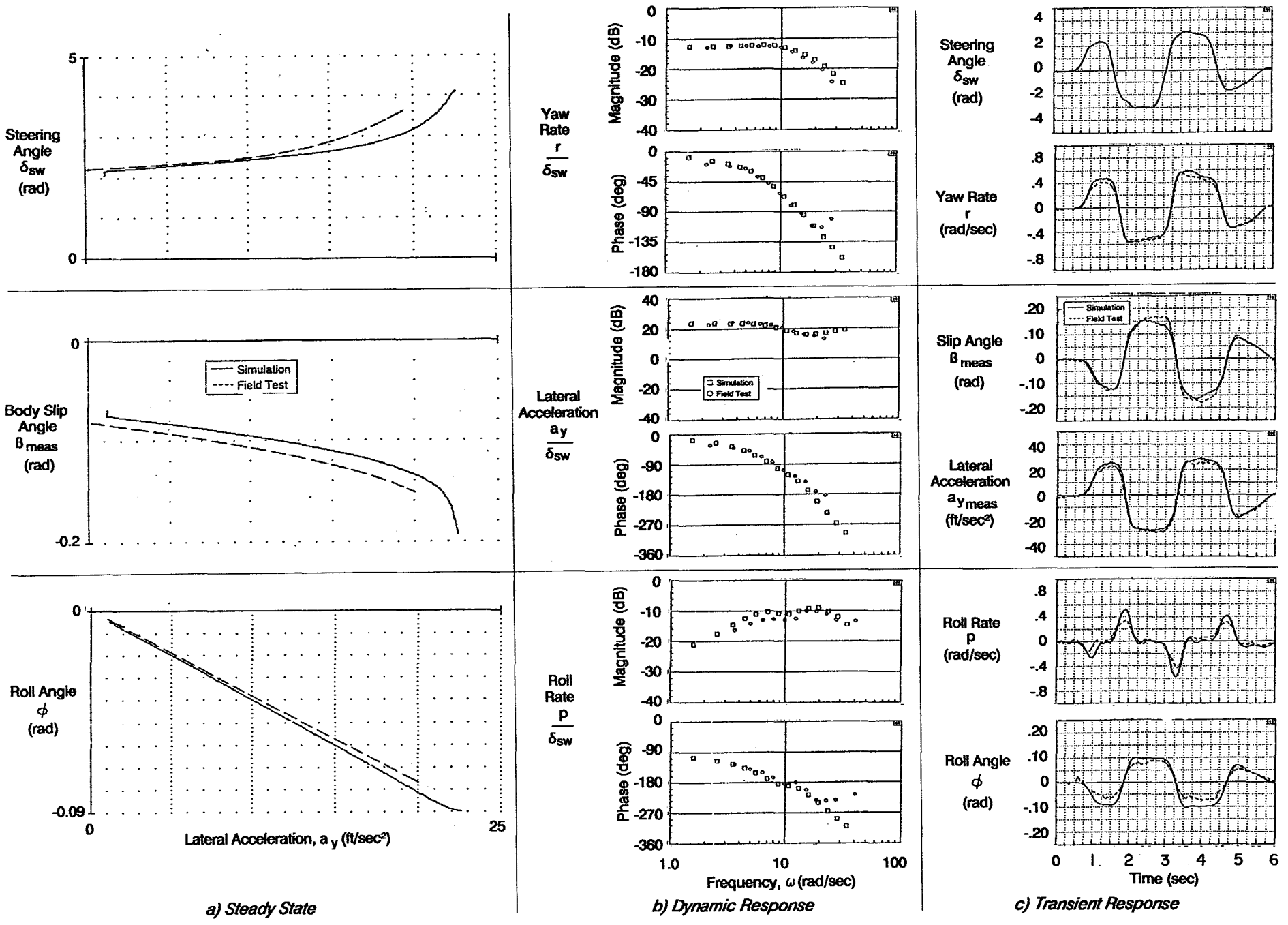

Figure H-4. Field Test and Computer Simulation Validation Data for Vehicle #10

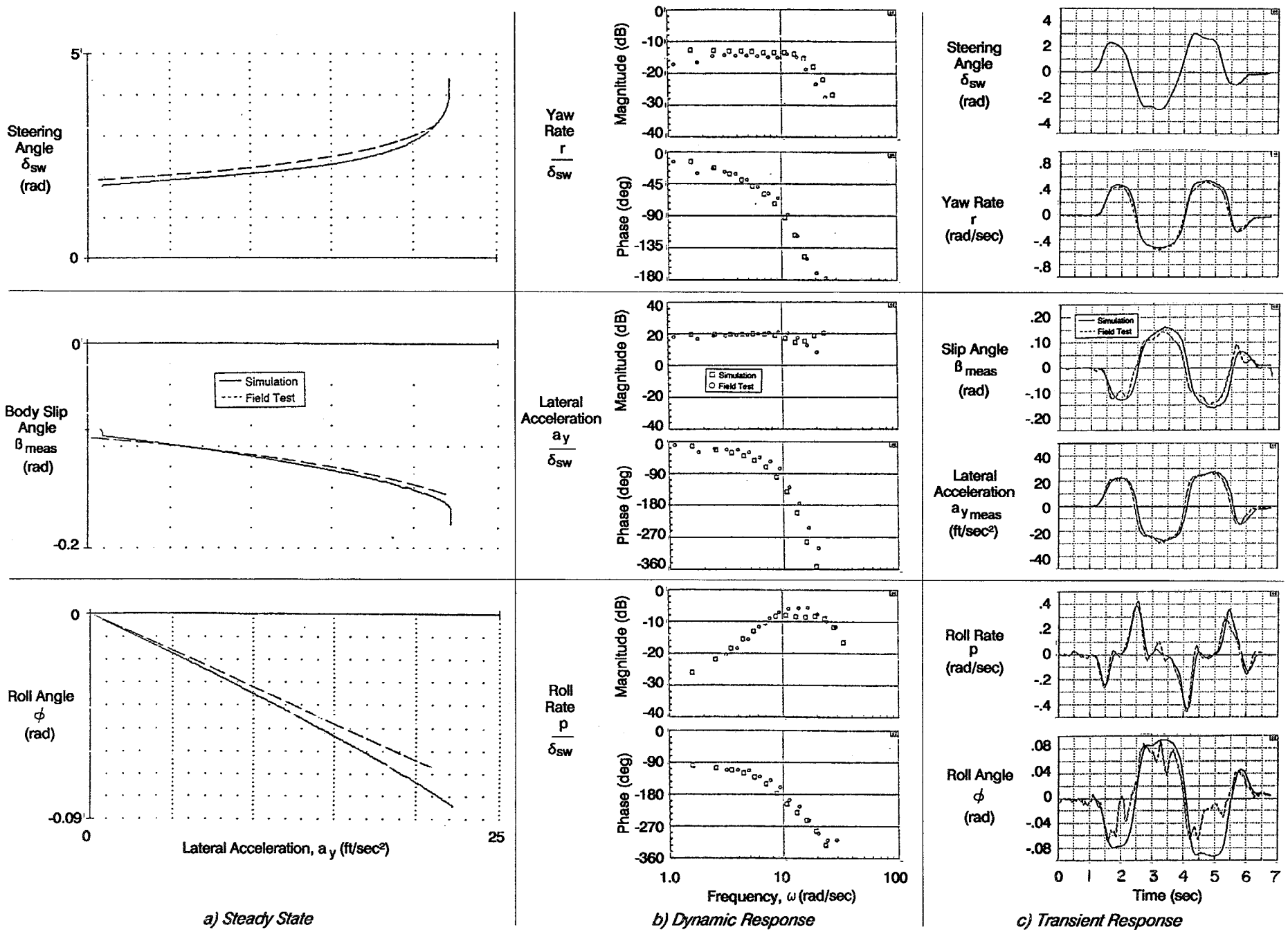

Figure H-5. Field Test and Computer Simulation Validation Data for Vehicle #16

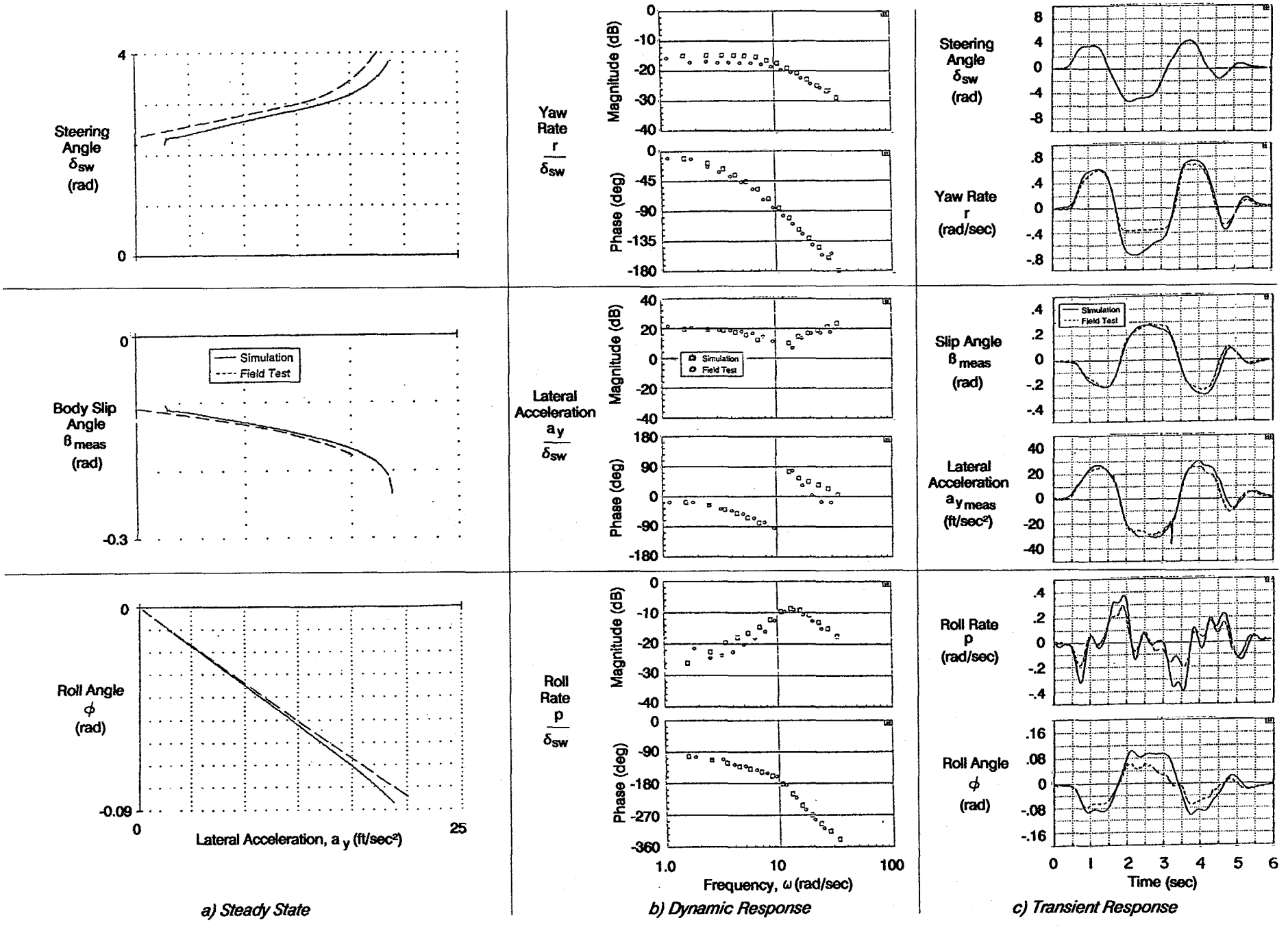

Figure H-6. Field Test and Computer Simulation Validation Data for Vehicle #17

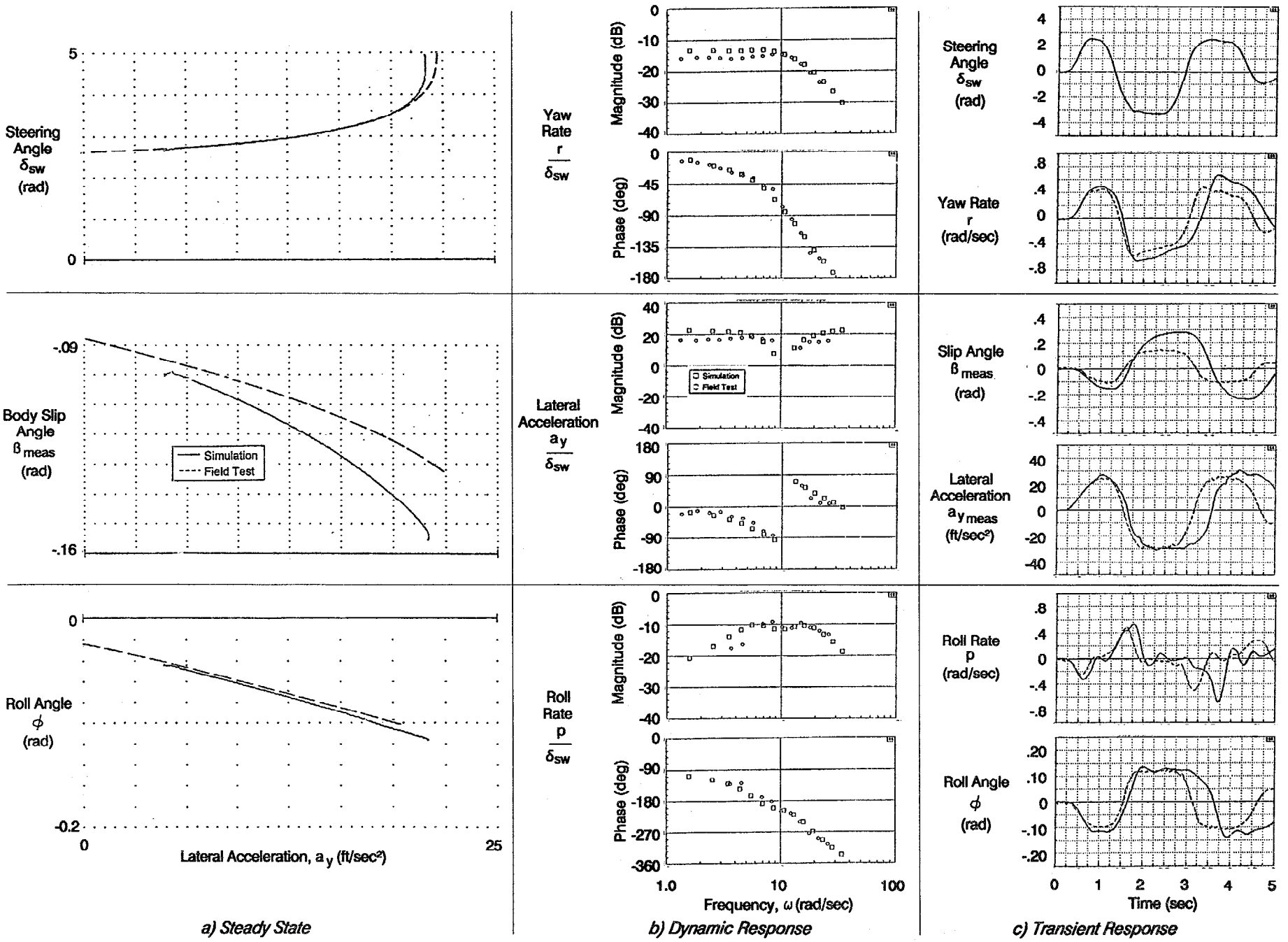

Figure H-7. Field Test and Computer Simulation Validation Data for Vehicle #18

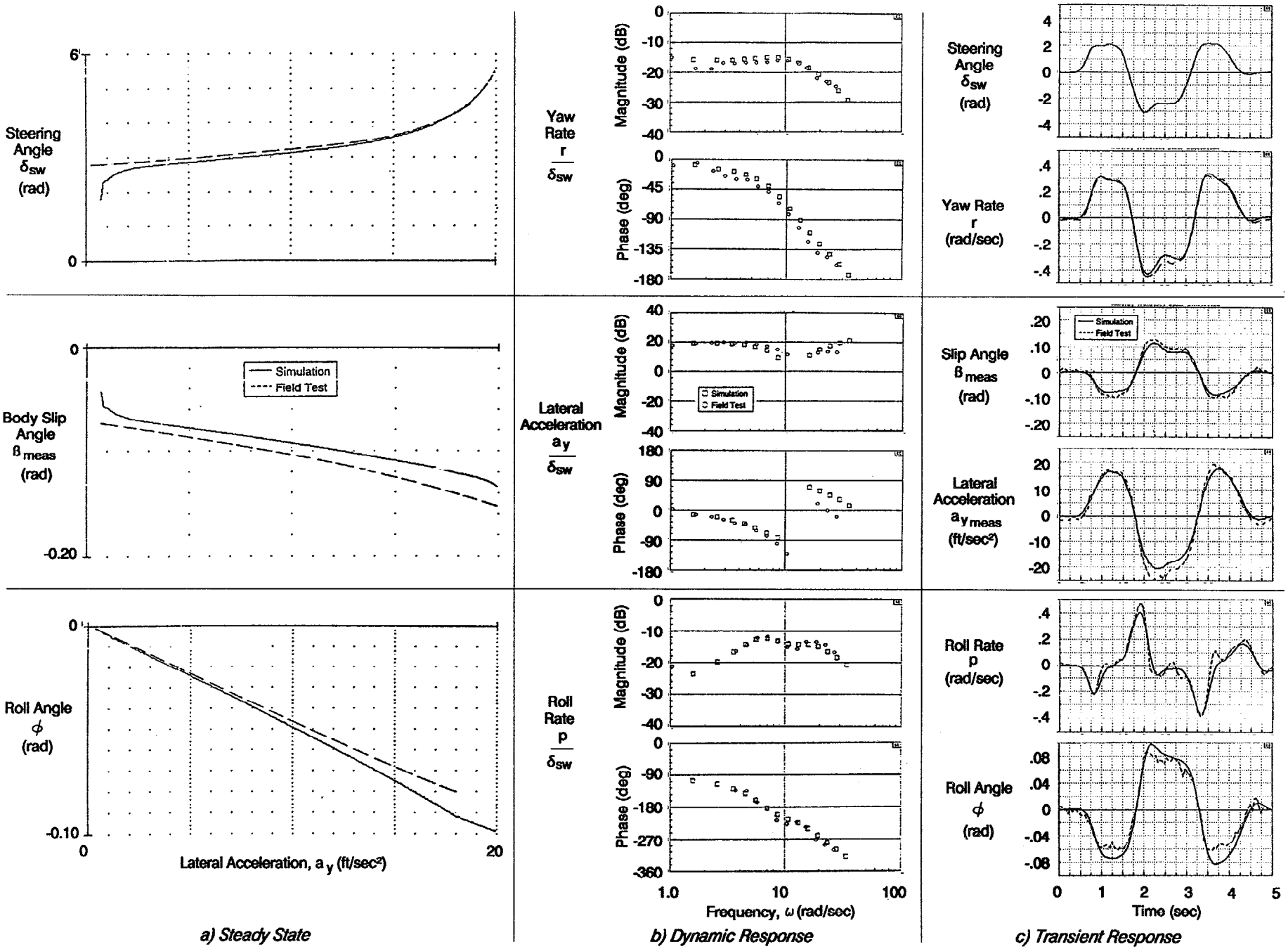

Figure H-8. Field Test and Computer Simulation Validation Data for Vehicle #19

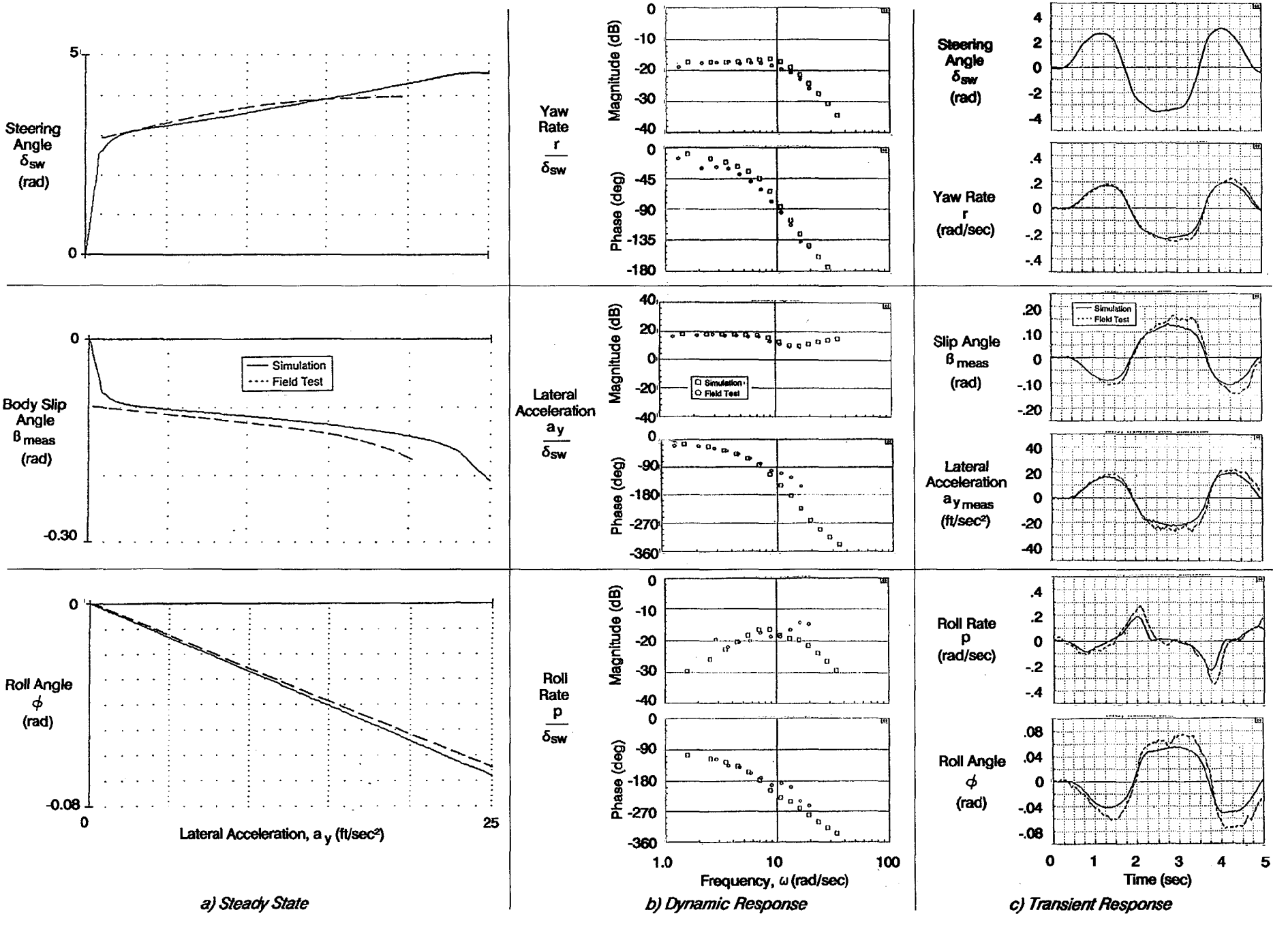

Figure H-9. Field Test and Computer Simulation Validation Data for Vehicle #23

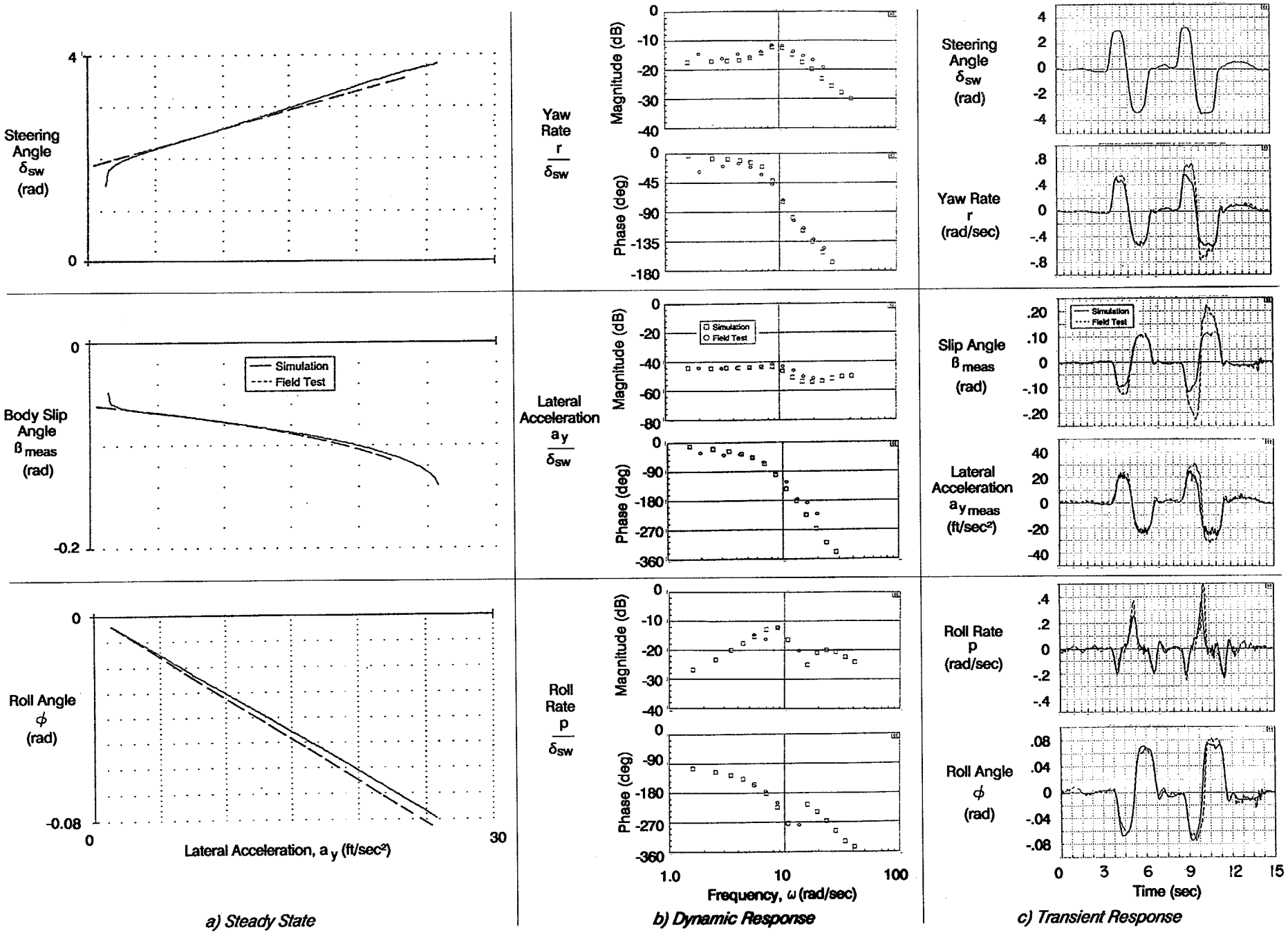

Figure H-10. Field Test and Computer Simulation Validation Data for Vehicle #34

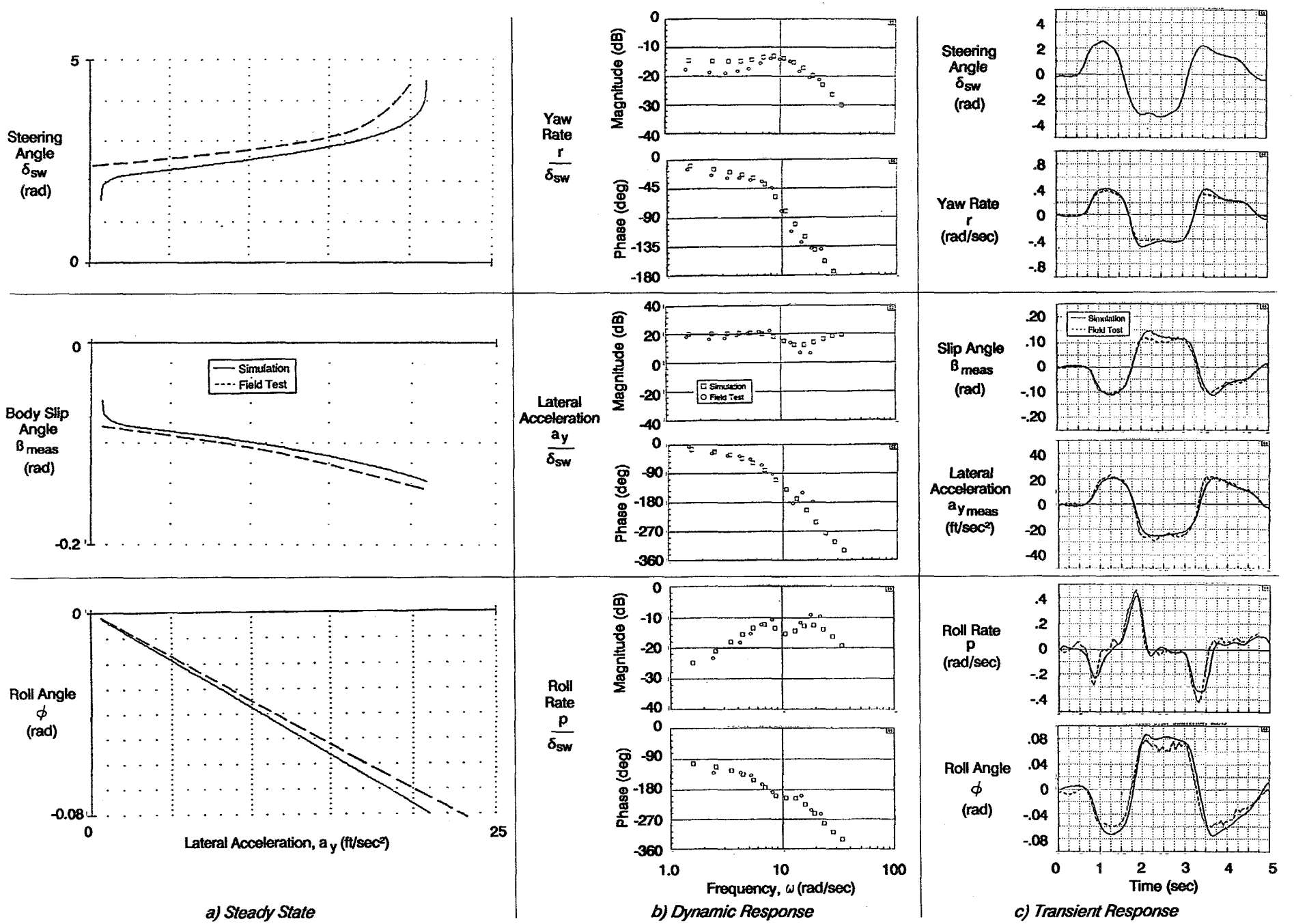

Figure H-11. Field Test and Computer Simulation Validation Data for Vehicle #37

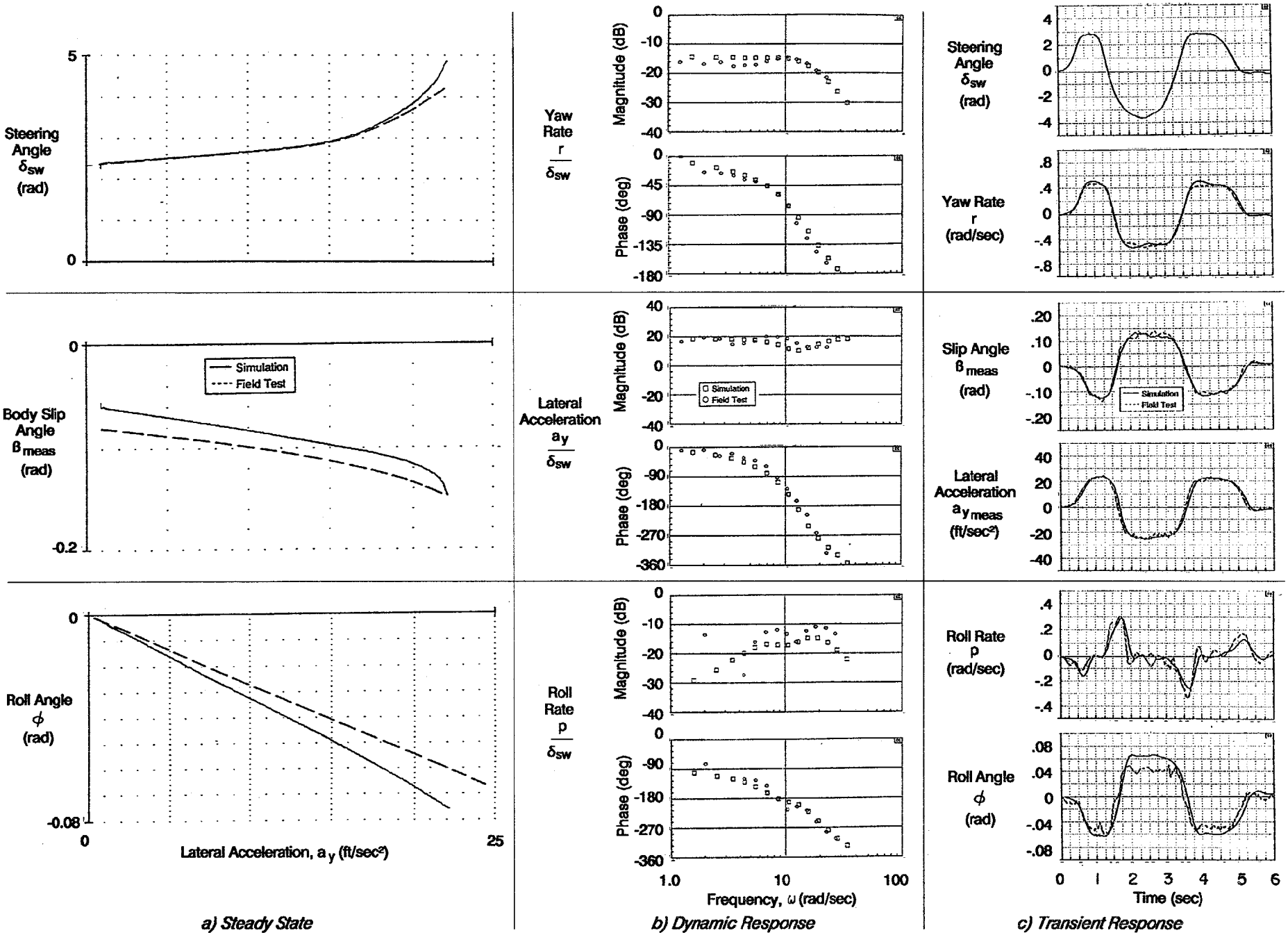

Figure H-12. Field Test and Computer Simulation Validation Data for Vehicle #40

☆U.S. GOVERNMENT PRINTING OFFICE: 1993-343-120-85842